Studies on the Chemical Modulation of Neuroprotective Agents Related to CR-6 Addressed to Improve the Delivery through the Blood-Brain Barrier

Laura Vázquez Jiménez

..

Studies on the Chemical Modulation of Neuroprotective Agents Related to CR-6 Addressed to Improve the Delivery through the Blood-Brain Barrier

LAURA VÁZQUEZ JIMÉNEZ

Programa de Doctorado en Química Orgánica

Dirigido por el Prof. Àngel Messeguer Peypoch y el Dr. Ciril Jimeno Mollet

Departamento de Química Biológica y Modelización Molecular, Instituto de Química Avanzada de Catalunya (IQAC-CSIC)

Departament de Química Orgànica, Universitat de Barcelona

Barcelona, septiembre de 2014

Memoria presentada por Laura Vázquez Jiménez para optar al título de Doctor en Química Orgánica por la Universidad de Barcelona.

Dirigida por:

Prof. Àngel Messguer Peypoch

Dr. Ciril Jimeno Mollet

Tutor:
Prof. Francisco López Calahorra

Barcelona, septiembre de 2014

Esta Tesis Doctoral no es el resultado del trabajo de una única persona, sino que de alguna forma u otra la contribución de muchas personas lo ha hecho posible. Por ello quiero agradecer el apoyo y soporte de toda esta gente que ha estado a mi lado durante estos años:

Primer de tot, vull agrair al Prof. Àngel Messeguer Peypoch, director d'aquesta Tesi Doctoral, que fa cinc anys em donés la oportunitat de formar part del seu grup d'investigació i de participar en aquest projecte amb el qual he patit i gaudit molt. Gràcies per donar-me ànims en moments de màxim nerviosisme, per a ajudar-me i guiar-me per poder continuar, i per felicitar-me quan calia.

També vull agrair al Dr. Ciril Jimeno Mollet que acceptés col·laborar amb el nostre projecte, i que, més tard, acceptés ser el codirector d'aquesta Tesi Doctoral. Moltes gràcies pels teus consells de com podia avançar quan jo no hi veia per on anar, i pels ànims i la teva positivitat.

To Prof. Romeo Cecchelli from Laboratoire de la Barriére Hémato-Encèphalique (LBHE) at Université d'Artois in Lens (France) for giving me the opportunity to do a short stay in his laboratory and to assay the synthesized compounds in *in vitro* models of BBB. Also, to Maxime Culot for his help during the first week, and also for his advises and guidelines in the biological area of the BBB. In addition, to all lab-mates (Anabelle, Aurore, Caroline and Melanie) for their support and help. But very especially, thanks to Emmanuel Sevin and Lucie Dehouck for their patience explaining me and helping me with the experiments, and the interpretation of the final results. Además, gracias Cristina Merino por ayudarme y ser mi compañera durante las primeras semanas de estancia.

Agradecer todo el tiempo dedicado a la Dra. María Miranda y la Dra. Inma Almansa de la Universidad Cardenal Herrera de Valencia durante los ensayos de la actividad antioxidante, y también, a las chicas del laboratorio Soledad, Laura y Tania. Un agradecimiento muy especial a la Dra. María Benlloch de la Universidad Católica de Valencia por alojarme en su casa y convertirse en una amiga en tan solo unos días.

Vull agrair a la Dra. Meritxell Teixidó el temps dedicat, les seves explicacions sobre els assajos *in vitro*, i els constants ànims. Gràcies per acceptar col·laborar amb nosaltres i per participar en aquest projecte.

Al Dr. Jordi Bujons vull agrair-li la seva participació, el seu ajut i el seu temps durant les anàlisis *in silico.*

Al Dr. Ignacio Alfonso por ayudarme en alguna ocasión con la química cuando yo ya no tenía ideas para continuar preparando alguno de los compuestos.

A toda la gente del laboratorio que ha pasado o que todavía continúan en él, quiero agradecer toda la ayuda recibida tanto a nivel profesional como a nivel personal. Muchas gracias a Glòria, Anna Morató, Natalia, Miquel, Fede y Dani. A los compañeros del laboratorio del Sur: Enrico, Jordi, Anna y Ángel, gracias por preguntar cómo me van las cosas e interesaros por mí. Joan gràcies per estar disposat a ajudar-me en tot moment i per venir al laboratori Nord a les tardes sense cap interès més que xerrar sobre com va tot. Inci thanks for your messages when you remember me and to be there when I need you. Maria gràcies

per pensar sempre en mi, per la teva energia i per les teves converses de temes diversos. Al laboratorio Norte le quiero dar las gracias de forma muy especial: sin ellos el camino hubiera sido muy diferente y aburrido. Maria Garrido moltes gràcies pel teu suport en el període final d'aquest Tesi. Muchas gracias Cristian por tus abrazos de osito cuando he estado un poco triste y por esos comentarios que nos hacen reír. Asun muchas gracias por tener una frase de ánimo y por sacarme una sonrisa a cada momento. Miri moltes gràcies per ensenyar-me a agafar el toro per les banyes i tirar endavant, i pels teus ànims en moments més fluixos. Esther muchas gracias por haber sido mi compañera de escritorio y de campana, por haberme enseñado tanto, por haberme apoyado y ayudado en todo momento, por esas largas charlas, y por hacerme a tocar con los pies en el suelo. Siempre me acordaré de todos vosotros y de los momentos tan especiales vividos: congresos, los momentos del café, las cenas, los bailes, las comidas en el italiano…. ¡¡Os voy a echar mucho de menos!!

Muchas gracias Anna Vázquez y Sandra por los años que he vivido a vuestro lado. Ambas me habéis ayudado mucho. Pese a que estéis tan lejos, siempre os tengo muy presentes. Habéis marcado un antes y un después en mi vida. Moltes gràcies Anna Soler per ser un suport incondicional tots aquests anys i per veure la llum quan jo anava totalment a les fosques. Gràcies per escoltar-me y per transmetre'm la teva positivitat.

Desde fuera del laboratorio también mucha gente ha hecho que las piezas encajaran y que todo rodara hacia adelante:

Quiero agradecer a todos mis amigos que desde la distancia han sabido apoyarme siempre y estar a mi lado, aunque no pudieran vivir ni entender mis angustias cuando una reacción no salía o mis alegrías cuando iba bien la cosa. En especial muchas gracias a Mercè, Tòni, Maribel y Eduard por escucharme y hacerme ver las cosas de una forma más sencilla.

Gracias a toda mi familia por soportarme y hacerme creer que puedo con todo y más cuando yo lo veo imposible y por felicitarme cuando una simple reacción me ha salido. Gracias por intentar entenderme cuando os explico lo que hago o a qué me dedico y entenderme. Gracias papá, mamá y Dani por vuestras palabras constantes de apoyo como que "eres la mejor" o "muy bien Laura, ya sabía que te saldría".

Finalmente, quiero agradecer a Jose, la persona que ha compartido el día a día en estos últimos cinco años, por soportar que trabajase hasta tarde y algún fin de semana, por aguantarme cada día cuando llego un poco más estresada. Muchas gracias por animarme en los momentos de derrumbe y por secar mis lágrimas y hacerme reír; gracias por estar a mi lado y quererme.

A toda esta gente, y muchos más que me dejo, miles de gracias por estar junto a mí.

Laura Vázquez Jiménez, septiembre 2014

"Well done is better than well said"

Benjamin Franklin

"Neither the wise man nor the brave man lies down on the tracks of history to wait for the train of the future to runo ver him"

Dwight D. Eisenhower

"Comprender las cosas que nos rodean es la mejor preparación para comprender el más allá"

Hipatia (aprox. 370-450)

A Jose

A mis padres y hermano

I. Introduction

I.1 OXIDATIVE STRESS, FREE RADICALS AND NEUROPROTECTION

I.1.1 Oxidative damage

Oxidative stress was originally defined as an imbalance between the high production of oxidant and highly reactive species (free radicals) and the low activity of endogenous antioxidant defenses that lead to tissue injury.[1] In 1985, Sies [2,3,4] defined the oxidative damage as 'a disturbance in the pro-oxidant/antioxidant balance in favor of the former, leading to potential damage'.

These free radicals are mainly generated from the O_2 uptake by the organism.

I.1.1.1 Oxygen and toxicity

Except for those organisms that have been adapted to live under anaerobic conditions, oxygen is used by all animals and plants to produce energy efficiently. $2 \cdot 10^9$ Years ago, molecular oxygen appeared in the Earth's atmosphere in significant amounts. Since then, organisms have developed endogenous mechanisms and a respiratory system to uptake and take profit of this energy source. However, due to the toxicity of this gas, neither aerobic animals nor plants can live in a high-oxygen concentrated atmosphere; the existent 21% of oxygen in the air is the maximal non-toxic quantity that an aerobic organism can tolerate.[5,6]

During the inhalation, the oxygen is uptaken into the organism to generate the adenosine triphosphate (ATP) in the electron transport chain (ETC), in mitochondria's membrane. The ETC involves the consumption of adenosine dinucleotide (ADP) that is converted to ATP; as well, this process generates H_2O and a small percentage of electrons that form the superoxide radical ($O_2^{\cdot-}$), as a by-product, together with O_2 (Figure 1.1). The production of ATP provides energy to the organism to power other cellular reaction such as cell division, metabolism, biosynthetic reactions and motility.[3,6]

[1] Sanvicens, N.; Gómez-Vicente, V.; Messeguer, A.; Cotter, T.G. *J. Neurochem.* **2006**, 1-13.
[2] Sies, H. In *Oxidative Stress*, Academic Press, London, **1985**, 1-8.
[3] Warner, D.S.; Sheng, H.; Batinić-Haberle, I. *J. Exp. Biol.* **2004**, *207*, 3221-3231.
[4] Miranda, M.; Muriach, M.; Almansa, I.; Arnal, E.; Messeguer, A.; Díaz-Llopis, M.; Romero, F.J.; Bosch-Morell, F. *Free Rad. Biol. Med.* **2007**, *43*, 1494-1498.
[5] Halliwell, B.; Gutteridge, J.M.C. *Free Radicals in Biology and Medicine, 2nd Ed.*, Clarendon Press, Oxford, **1989**.
[6] Halliwell, B. *Annu. Rev. Nutr.* **1996**, *16*, 33-50.

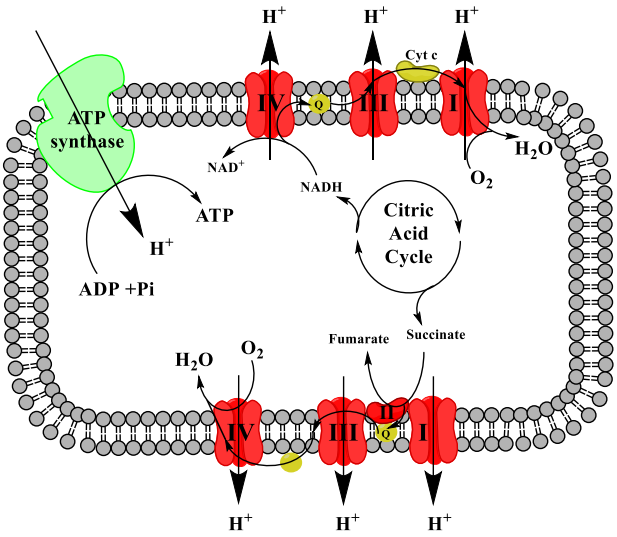

Figure 1.1. *Electron transport chain (ETC) in the mitochondria lipid bilayer.*

In 1954, Gerschman *et al.* proposed that the most damaging effects of oxygen could be attributed to the formation of free oxygen radicals. [6,7]

The ETC is the starting point of natural generation of free radicals in the body. However, there are other natural mechanisms that increase the concentration of oxidant species in the body.

I.1.1.2 Free Radicals

As it was defined by Halliwell and Gutteridge in 1989,[5] a free radical is 'any specie capable of having independent existence and contains one or more unpaired electrons'. Free radicals are divided in reactive oxygen and nitrogen species (ROS and RNS, respectively). ROS and RNS, in most cases, correspond to oxygen radicals, but also non-radicals. ROS and RNS are high reactive species that oxidize other molecules by forming, usually, new radical species. Although ROS and RNS cause the oxidative damage, they are generated *in vivo* to perform some cellular functions from host defense to neuronal signal transduction.[8]

The term ROS includes oxygen radicals such as superoxide ($O_2^{\cdot-}$), hydroxyl ($^{\cdot}OH$), peroxyl ($RO_2^{\cdot}$) and alkoxyl ($RO^{\cdot}$), as well as some non-radicals compounds that bear oxidizing properties such as hydrogen peroxide (H_2O_2), ozone (O_3), singlet oxygen ($^1O_2$) and hypochlorous acid (HOCl). RNS include nitric oxide radical ($NO^{\cdot}$), peroxinitrite anion ($ONOO^-$) and nitrogen dioxide radical ($NO_2^{\cdot}$). From all these reactive species, H_2O_2, $NO^{\cdot}$ and $O_2^{\cdot-}$ react quickly with very few molecules, whereas $^{\cdot}OH$, reacts quickly with almost any molecule. All other ROS and RNS have intermediate rates of reaction.[6] All these reactive species

[7] Gerschman, R. Gilbert, D.L., Nye, S.W., Dwyer, P., Fenn, W.O. *Science*, **1954**, *1119*, 623-626.
[8] Behl, C.; Moosmann, B. *Free Rad. Biol. Med.* **2002**, *33*, 182-191.

undergo the generation of the $^{\cdot}OH$ radical which, as $ONOO^{\cdot}$, $NO^{\cdot}$, $RO^{\cdot}$, $RO_2^{\cdot}$ and $NO_2^{\cdot}$, can react directly with a molecule. Actually, hydroxyl radical may be considered as most potent free radical.

Some chemical accidents that normally result in the organism produce also first superoxide radical, and then, it undergoes the formation of $^{\cdot}OH$. The respiration process, as mentioned before, and the auto-oxidation of some molecules with O_2 such as neurotransmitters dopamine and adrenaline,[3] carry out the generation of $O_2^{\cdot-}$. Indeed, it has been estimated that 1-3% of the molecular oxygen we breathe is being used to produce superoxide radical; it corresponds over 2 kg of $O_2^{\cdot-}$ per year.[6] A large proportion of generated superoxide is transformed *via* non-enzymatic or catalyzed by superoxide dismutase (SOD) to generate H_2O_2. As water, H_2O_2 compound can easily travel through membranes arriving at any part of the cell, where may cause toxicity.[6]

During the last century, other sources of *in vivo* generation of $^{\cdot}OH$ have been studied. The ETC, mentioned above, is one of the main sources of free radicals *in vivo*, but not the only one. Irradiation with γ- and X-ray promotes the generation of reactive $^{\cdot}OH$ from H_2O, which is highly abundant in the body. In less quantity, the ultraviolet light can break H_2O_2 by homolytic fission to undergo the generation of $^{\cdot}OH$ radical.[6]

In addition, the releasing of metal-ions by the oxidative stress may contribute to increase free radicals concentration. Iron and copper ions are normally sequestered in the body by proteins such as ferritin. In an oxidative stress and by the action of $O_2^{\cdot-}$ these metals can be released and take part in the generation of the radical $^{\cdot}OH$ by Fenton's reaction:[5,6]

$$O_2^{\cdot-} + Fe^{3+} \rightarrow Fe^{2+} + O_2$$
$$Fe^{2+} + H_2O_2 \rightarrow {}^{\cdot}OH + OH^- + Fe^{3+}$$

The peroxynitrite ion is generated by $NO^{\cdot}$ and $O_2^{\cdot-}$ reaction. This agent is also very reactive by itself or indirectly generating the $^{\cdot}OH$ radical at physiological pH 7.4. At this pH, the $ONOO^-$ is protonated (pK_a = 6.8) and the resulting peroxynitrous acid (ONOOH) is easily decomposed to give $^{\cdot}OH$ and $NO_2^{\cdot}$,[5,6] two highly reactive species:

$$NO^{\cdot} + O_2^{\cdot-} \rightarrow ONOO^-$$
$$ONOO^- \overset{pK_a = 6.8}{\rightleftharpoons} ONOOH \rightarrow {}^{\cdot}OH + NO_2^{\cdot}$$

Not only natural and/or unavoidable sources produce free radicals; there are several androgenic ones like fat-rich diet, smoke, alcohol and excessive breathing, between others, that generate these reactive species.

I.1.1.3 Damage from oxidative stress

Oxidative stress causes cellular damage and subsequent cell death, especially in organs like the brain, due to its high metabolic activity, high lipid concentration and low antioxidant defense

mechanisms. Hence, oxidative stress has been implicated in the etiology and progression of neurodegenerative diseases such as Parkinson's disease, Alzheimer's disease, atherosclerosis and stroke. In addition, apoptotic cell death linked to these neuronal diseases is mediated by free radicals generated during the oxidative stress. Regarding the relevant role of oxidative damage in the progression of these neurodegenerative disorders, the design of reactive species scavengers to protect cells and tissues has interest in pharmaceutical research.[1]

Oxidative damage induced by free radicals in the organism derives from the alteration of biomolecules such as DNA, proteins and lipids, for instance the oxidation and dimerization of nucleotides on purine and pyrimidine bases may end up in a mutation on DNA strands during the replication; the oxidation on proteins tertiary structure by hydroxylation of amino acids, for example, may destroy the structural protein and alter the function of enzymes.; lastly, oxidative damage may result in lipid peroxidation of polyunsaturated phospholipids that form the lipid cellular membrane leading to membrane dysfunction and cell lysis.[8] In healthy individuals, the presence of endogenous antioxidant systems counterbalance the production of such reactive species; but in an injured organ the accumulation of ROS and RNS is enhances.[9]

I.1.1.3.1 Disorders

As mentioned, damaging consequences of oxidative stress is involved in the etiology and progression of many neurodegenerative disorders[8] due to the high reactivity of free radicals generated in excess during the process. In present work, we are only centered in ischemia/reperfusion episode that results in stroke: [10]

- *Ischemia/Reperfusion and Stroke.*[5,9] Ischemia or hypoxia[11], which is the total or partial depriving of oxygen supply to a tissue, is considered the main cause of death in western society. During this traumatic event, the organ (normally, heart or brain) is damaged and, subsequently, it dyes; sensitive organs like brain are more susceptible to suffer an ischemia episode. If the period of ischemia is long enough, it can injure the tissue irreversibly; therefore, the reperfusion is provoked to save the organ. The reperfusion process is based on the restoration of blood supply and the oxygen and nutrients reintroduction. This beneficial process may cause negative effects in the brain tissue because of oxidative damage; the sudden and high oxygen concentration is followed by free radicals generation which induces the lipid peroxidation on the tissue and, ultimately, the total or partial loss of cerebral function.

[9] Jiménez-Altayó, F.; Caracuel, L.; Pérez-Asensio, F.J.; Martínez-Revelles, S.; Messeguer, A.; Planas, A.M.; Vila, E. *J. Pharmacol. Exp. Ther.* **2009**, *331*, 429-436.
[10] *Stroke*, or cardiovascular accidents, is the loss of brain function due to a disturbance in the blood supply caused by an ischemia episode.
[11] *Hypoxia* is the pathological condition where a region of the body is deprived of and adequate oxygen supply.

Nowadays, the most effective treatment to stroke in a post-ischemic brain is the recombinant tissue plasminogen activator (rtPA),[12] which is a serine protease that catalyzes the formation of plasmin from plasminogen and breakdown blood clots. Although the treatment with rtPA is effective for patient's administration within the 4-5 hours from the ischemic episode, it was an excess of mortality in patients within the first week of the event. On the other hand, most neuroprotective agents are not able to show beneficial effects in clinical trials II and III although they exhibited promising results in preclinical trials. It seems that the problem was the administration of the drug that in most cases required the co-administration an antithrombotic agent.

I.1.1.3.2 Lipid Peroxidation

Lipid peroxidation was defined as the oxidative deterioration of polyunsaturated lipids by the action of reactive species.[5,13] Oxygen-dependent deterioration, which leads to rancidity of fats and oils, has been recognized since the ancient time as a problem to storage some fat-rich foods. Furthermore, the relevance of lipid peroxidation in biological systems is consequence of the high amount of polyunsaturated fatty acids in cells membrane.[5,13]

The main constituents of biological membranes are lipids and proteins. Depending on the membrane functions, there are proteins in the surface, tightly attached, partially embedded or sometimes located in the interior or completely traversing the membrane. In animals, cell membrane consists mainly on phospholipids based on glycerol (like lecithin), but some membranes, such as plasma membranes, contain significant amounts of sphingolipids and the hydrophobic molecule cholesterol. In contrast, the organelle membrane, such as nuclei or mitochondria membranes, rarely contains sphingolipid or cholesterol.[5]

Phospholipids are amphipathic molecules with a polar and hydrophilic head and a fatty-acid side-chain (14-24 carbon atoms). This side-chain can contain one or more double bonds; lipids with double bonds exhibit higher viscosity. Thus, the membrane fluidity is due to the presence of unsaturated and polyunsaturated fatty-acid side-chains in membranes.[5]

In fatty acids, a C-H bond is weakened by the presence of an adjacent double bond; therefore, hydrogen atoms in an adjacent carbon to a double bond can be more easily abstracted by reactive species.[5,13] Since polyunsaturated lipids (with more than three double bonds in the fatty-acid side-chain) are more easily oxidized, the lipid bilayer of cell membrane is prone to be damaged by lipid peroxidation processes. Consequently, membrane fluidity, which is known to be essential for the proper function of the biological membrane, tends to be reduced.

Lipid peroxidation (Figure 1.2), as in other radical reactions, consists of three different stages: initiation, propagation and termination. Lipid peroxidation begins by the attack of an unsaturated lipid

[12] Amaro, S.; Chamorro, A. *Stroke* **2011**, *42*, 1495-1499.
[13] Devasagayam, T.P.A.; Boloor, K.K.; Ramasarma, T. *Indian J. Biochem. Biophys.* **2003**, *40*, 300-308.

(LH) by radical species, normally ·OH, that abstracts the hydrogen atom from a methylene group (-CH_2), leaving an unpaired electron on the carbon atom. The resultant carbon radical (·CH) may be stabilized by molecular rearrangement to produce a conjugated diene, or, more likely in aerobic atmosphere, it may react with an oxygen molecule forming lipid peroxyl radical (LOO·). These radicals are capable to abstract another hydrogen atom from another lipid molecule (LH) or from another susceptible part of the same lipid, giving rise lipid hydroxyperoxide (LOOH) or cyclic peroxide (LOOL), respectively. Another carbon radical (L·) generated goes on with the progression stage of the radical reaction. Radicals LOO· are unstable and, by acid hydrolysis or heating, break down to form degradation products such as maloaldehyde and nonenal that cause cytotoxicity, change in cell membrane permeability and cell death.[5,13]

The termination stage as well as the prevention of lipid peroxidation is carried out by using an antioxidant (AH) capable of donating a hydrogen atom to reduce the reactive radicals formed during the process.[13]

Noteworthy, lipid peroxidation can also be enzymatically or non-enzymatically activated by means of mixtures of Fe(II) and ascorbate or glutathione (GSH), or NADPH.[5]

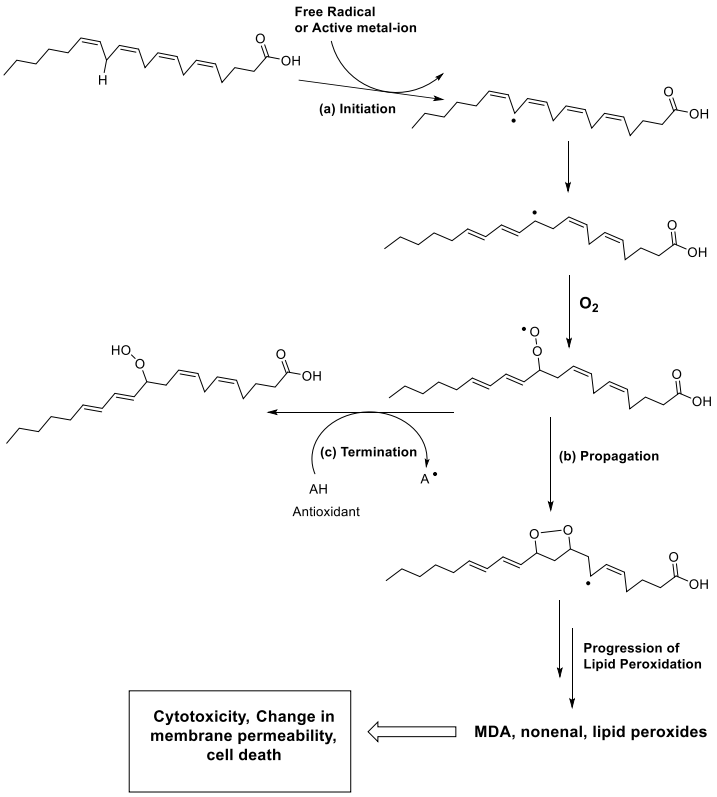

Figure 1.2. *Lipid peroxidation of polyunsaturated lipids located in the cellular membrane. In the initiation of the process and due to free radicals or active metal-ions or NADPH, a H· is abstracted from the lipid and a radical (L·) is formed. A lipid peroxide (LOO·) is generated by the oxidation of L· with O_2. The reaction ends with a hydrogen donator such as an antioxidant RH. If not, the lipid peroxidation undergo the decomposition of these intermediates leading to the formation of toxic aldehydes that can induce the breakdown of cell membrane, citotoxicity and cell death.*

I.1.2 Antioxidants

Enzymatic and non-enzymatic antioxidants keep the fine-tuned balance between the physiological ROS and RNS production and their detoxification in healthy individuals.[8] Catalases and peroxidases are known enzymatic endogenous systems to carry out the detoxification of some reactive species. Superoxide dismutase (SOD) is the enzyme that catalyzes the dismutation of $O_2^{\cdot-}$ to form H_2O_2 and O_2, thus reducing the deleterious effects of superoxide in the body.[5] Another important enzyme exerting antioxidant activity is glutathione peroxidase, which catalyzes the oxidation of glutathione (GSH) to its dimer GSSG at the expense of hydrogen peroxide. This enzyme requires selenium in the active site to perform the reduction of H_2O_2.[5,8] In the organism, there are also molecules generated *in vivo* that work as free radical scavengers: ascorbic acid, uric acid and glutathione.[5]

Nevertheless, it can occur that the concentration of these free radical scavengers (from enzymatic or other endogenous origins) in the body or incorporated by a healthy and antioxidant-rich diet, is not sufficient to reduce the overproduction of ROS and RNS. Furthermore, in an unhealthy situation, such as ischemia/reperfusion episode, the antioxidant defenses of the organ fail and reactive species are accumulated in the tissue. Therefore, antioxidant drugs to restore the normal balance between oxidative stress and detoxification process are required to reduce the potential, irreversible damage to the affected tissue. Hence, many researchers are working to design efficient antioxidant drugs.[8]

Different types of antioxidant action can be taken into consideration to develop new antioxidant pharmaceuticals:[8]

1. *Inhibition of radical formation*
2. *Direct chemical (non-enzymatic) scavenging of free radicals*
3. *Enzymatic detoxification of accumulating reactive species*
4. *Long-term support and induction of the cellular self-defense by the initiation of gene transcription*

Here, the focus of present work is put on chemical structures and compounds that have the potential activity to directly interact with ROS and RNS as mode of antioxidant action. Although their direct activity does not depend on endogenous cellular macromolecules (enzymes), these compounds are usually recycled by endogenous oxidoreductases, direct or indirectly *via* intracellular reducing compounds like ascorbate. The main direct scavengers are the chain-breaking antioxidants. Most prominent examples are phenols, which can be divided into two groups:[8]

- *Monophenols* are compounds with only one phenolic group. Tocopherols (Vitamin E), 17β-estradiol (estrogen), 5-hydroxytryptamine (serotonin) and derivatives of tyrosine are some examples.
- *Polyphenols*, in contrast, are those molecules with more than one phenolic group. Flavonoids, stilbenes, hydroquinones and resveratrol are polyphenols.

I.1.2.1 Vitamin E

There are several promising direct antioxidants that also have exhibited neuroprotection in *in vitro* assays, but vitamin E remains one of the most potent structures.[5] Vitamin E was first reported by Evans and Bishop in 1922.[5] Vitamin E is a natural antioxidant compound which includes a mixture of tocopherols and tocotrienols. Tocopherols hold a structure of chromanee and a saturated hydrocarbon side-chain at C_2 position, one of three controlled stereogenic centers of the molecule. Vitamin E is a mixture of four different tocopherols: α-, β-, γ- and δ-tocopherols (Figure 1.3), depending on the substitutions on the aromatic ring of the chromanee scaffold. α- and γ-Tocopherols are the most used tocopherols in the diet due to their high antioxidant potency.

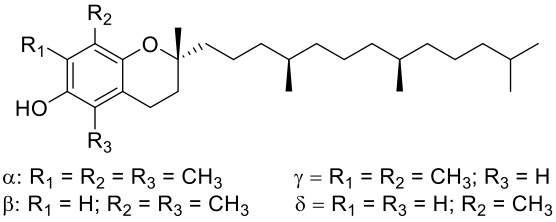

Figure 1.3. *Vitamin E is a mixture of α-, β-, γ- and δ-tocopherols, depending on the substitution on the aromatic ring of the chromanee moiety.*

The hydrogen atom of the phenol group in tocopherols is easily donated to a free radical, such as $^{\cdot}OH$ or $RO^{\cdot}$, to generate then another radical species stabilized by resonance.[14] In other way, γ-tocopherols has the activated C_5 aromatic position free and capable to interact with RNS such as $NO^{\cdot}$.[15]

However, the great pharmaceutical disadvantage of Vitamin E is its limitation to cross the blood-brain barrier (BBB). Hence, the identification and development of structures with better BBB permeation and an improved chain-breaking activity is on the interest of many research programs. Indeed, the permeability of BBB is one of the major hurdles of developing new neuroprotective antioxidants.

I.1.2.2 CR-6 as α- and γ-Tocopherol analogue

A few years ago, Irurre *et al*., working with precocenes, discovered a family of 2,2-dimethylchromenes that exhibited an inhibitory effect on lipid peroxidation once they were incubated with rat liver microsomes in the presence of NADPH. With the aim of finding a plausible mechanism which would rationalize that effect, further assays were contemplated.[16] Thus, the inhibitory effect on rat liver microsomal lipid peroxidation elicited by a series of 2,2-dimethylchromanees and chromenes structurally related to precocenes, was evaluated. From these experiments, CR-6, 3,4-dihydro-6-hydroxy-7-methoxy-2,2-dimethyl-1(*2H*)-benzopyran (Figure 1.4), appeared as the most potent antioxidant of that

[14] Burton, G. W.; Ingold, K.U. *Acc. Chem. Res.* **1986**, *19*, 164-201.
[15] Montoliu, C.; Sáez, R.; Yenes, S.; Messeguer, A.; Felipo, V. *Biochem. Pharmacol.* **1999**, *58*, 255-261.
[16] Irurre, J.; Casas, J.; Ramos, I.; Messeguer, A. *Bioorg. Med. Chem.* **1993**, *1*, 219-215.

series of compounds with an IC_{50} = 0.30 μM, even better than commercial antioxidants such as BHT (IC_{50} = 0.8 μM) and natural tocopherols.

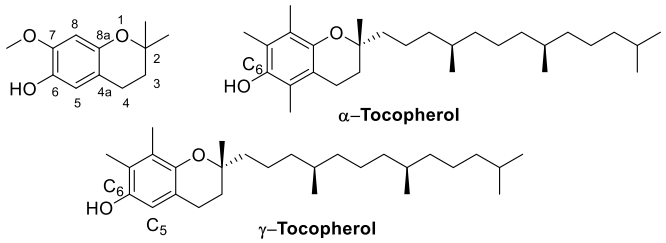

Figure 1.4. *From left to right, structures of CR-6 and natural tocopherols. The mixture of tocopherols is formed by four different tocopherols (α, β, γ and δ) depending on the substitutions on the aromatic moiety.*

The presence of a hydroxyl group at C_6 was the most important structural feature common to compounds, such as CR-6, eliciting the highest inhibitory activities in the above mentioned studies. From this point of view, that derivative could be considered as an α-tocopherol analogue. Generally, phenols have good antioxidant activities due to their ability to transfer the hydrogen atom to reactive radicals and form more stable structures (Figure 1.5). In 1986, Burton and Ingold demonstrated that the spatial arrangement between the hydroxyl group and the oxygen atom (in *para* position) of the 2,2-dialkylpyranyl moiety present in tocopherols permits an optimal stabilization of the phenoxyl radical by delocalization of the unpaired electron, which accounts for the high efficiency of CR-6 as free radical scavenger. [14]

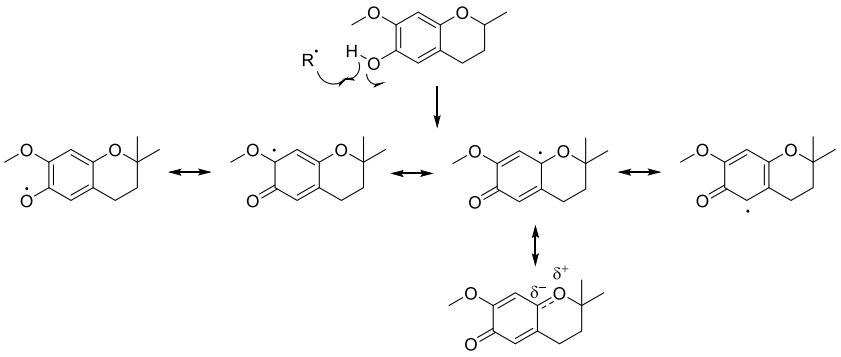

Figure 1.5. *Stabilization of phenoxyl CR-6 radical by resonance after neutralizing a free radical.*

Furthermore, the fact that CR-6 contains two non-substituted and highly activated aromatic positions (C_5 and C_8) led us to consider this antioxidant also as a specific γ-tocopherol analogue, particularly regarding its potential capacity to react with nitrating species such as NO or $ONOO^-$. Montoliu *et al*. performed some experiments that confirmed the regioselective nitration at C_5 position in CR-6 by nitrating species generated during oxidative stress processes (Figure 1.6).[15] The regioselectivity towards the 5-nitroderivative can be explained by the formation of a hydrogen bond between the phenolic

hydrogen and oxygen of the nitro group that stabilizes the transition state of this regioisomer. Even though C_8 position is also active, it is sterically hindered by methoxy group; therfore nitrating species prefer to react at C_5. With these experiments, Montoliu *et al.* demonstrated the neutralization of RNS by CR-6 antioxidant action.

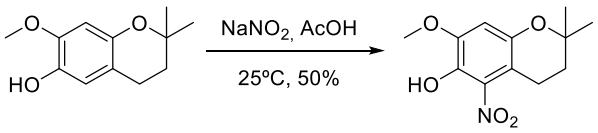

Scheme 1.6. *Experiments of nitration of CR-6. The reaction of CR-6 with nitric acid provided the oxidation of whole molecule; therefore milder conditions were applied. The aromatic electrophilic substitution of nitrous acid over the activated C_5 position followed by an oxidation afforded the 5-nitroderivative. With these antecedents, Montoliu et al. demonstrated the neutralization of RNS by CR-6 antioxidant action. These experiments were complemented with in vitro assays of cultures of neurons treated with CR-6 and glutamate and the extraction of 5-nitroderivative of CR-6.*[15]

I.1.2.3 CR-6 as Neuroprotectant and inhibitor of apoptosis

A few years later after developing CR-6 in the laboratory and, due to its antioxidant activity, the company Lipotec S.A. was interested in its potential commercialization and further investigations were planned. Currently, CR-6 is being commercialized as anti-aging ingredient in dermocosmetics and also it is in clinical trials phases II for cancer treatment by its encapsulation in liposomes and doxorubicin.

Furthermore, two collaborations were established with Dr. Anna Planas[17] from the IIBB-CSIC in Barcelona and Prof. Thomas Cotter[18] from University of Cork in Ireland, which enlightened novel potential applications for CR-6: as neuroprotectant in ischemia/reperfusion episodes and as inhibitor of apoptosis in eye diseases.

Ischemia/reperfusion reflects the interplay of different processes: transient ischemia that produces damage to the brain, and consequent reperfusion that exposes damaged tissue to re-establish blood flow, inducing an inflammatory response and excessive generation of Reactive Oxygen and Nitrogen Species (ROS and RNS, respectively). Experiments with CR-6 in ischemia/reperfusion processes in rat brains showed a complete prevention from $O^{\cdot-}_2$ and $ONOO^-$ formation.[9,17] These findings suggested that the treatment with CR-6 during reperfusion may reduce infarct size caused by cerebral ischemia through a mechanism that involves prevention of vessel hypertrophy and normalization of wall stress. Thus, CR-6 is a good antioxidant as neuroprotectant in ischemia/reperfusion episodes.

At that time, Cotter *et al*. demonstrated the use of CR-6 as a useful tool to reduce oxidative stress induced by apoptosis in 661W cells in ocular diseases. But, despite the fact of scavenging ROS species, CR-6 cannot prevent the activation of the caspase mediated mitochondrial pathway.[1,18]

[17] Pérez-Asensio, F.J.; de la Rosa, X.; Jiménez-Altayó, F.; Gorina, R.; Martínez, E.; Messeguer, A.; Vila, E.; Chamorro, A.; Planas, A.M. *J. Cerebr. Blood F. Met.* **2009**, *30*, 638-652.
[18] Sanvicens, N.; Gómez-Vicente, V.; Masip, I.; Messeguer, A.; Cotter, T.G. *J. Biol. Chem.* **2004**, *279*, 39268-39278.

Although from these findings it was derived that CR-6 penetrates into the brain, it was not sufficient to treat these diseases because of its low bioavailability through the blood-brain barrier.

I.2 BLOOD-BRAIN BARRIER

The very first experiments related to the presence of a barrier in the brain were attributed to Humphrey Ridley, in 1695. Ridley found evidences about the impermeability of the brain vasculature once a substance was injected into the blood circulation. However, pioneer experiments contributing to the discovery of the blood-brain barrier were performed by the physiologist Paul Elrich in 1885. Elrich observed that water-soluble Trypan dye injected in the blood flow of rats stained all the organs of the body with the exception of the brain and the spinal cord.[19,20] In 1900, Lewandowsky carrying out similar observations made up the term of 'blood-brain barrier' ('*Blurthirnschranke*') to define this barrier.[19,21] In 1913, Edwin Goldman, an Elrich's student, following Elrich's experiments by injecting the same dyes into the subarachnoid space, found that the brain was intensively stained but not the peripheral organs.[19,22] Therefore, Goldman assessed the existence of a barrier between the brain and the periphery. In 1933, Spatz postulated that an endothelial membrane was the responsible for the barrier function.[23] For many years the debate was on fire up to 1960 when the first observations by electron microscopy were carried out by Reese and Karnovsky (1967),[19,24] and Brightman and Reese (1969).[19,25] These authours found out that tight junctions connect adjacent capillary endothelial cells and seal the intercellular space. From these findings, the molecular structure of the barrier was identified and localized in the brain capillary endothelium.

I.2.1 Morphology and differences with other endothelial barriers

I.2.1.1 BBB and BCSFB

The brain is truly separated from the blood supply by two different barriers that control the way of endogenous and exogenous compounds: the blood-brain barrier (BBB) and the blood-cerebrospinal fluid barrier (BCSFB).[26,27,28] The BBB is the major barrier that regulates the entrance of active molecules from the blood circulation into the brain. The BBB is located at the level of brain

[19] Bradbury, M.W. *Exp. Physiol.* **1993**, *78*, 453-472.
[20] Ehrlich, P. *Verlag von August Hischwald* **1885**, 1-167.
[21] Lewandovsky, M. *Zeitschrift fur klinische Medizin* **1900**, *40*, 480-494.
[22] a) Goldmann, E.E. *Beiträge Zur Klinischen Chirurgie* **1909**, *64*, 192-265. b) Goldmann, E.E. *Beiträge Zur Physio-Pathologie des Plexus Chorioideus und der Hirnhäute*, Verlag de königlichen Akademie der Wissenschaften, **1913**, Berlin.
[23] Spatz, H. *Archiv. Für Phsychiatrie* **1933**, *101*, 267-358.
[24] Reese, T.S.; Karnovsky, M.J. *J. Cell Biol.* **1967**, *34*, 207-217.
[25] Brightman, M.W.; Reese, T.S. *J. Cell Biol.* **1969**, *40*, 648-677.
[26] Mykko Gynther's Thesis, *Blood-Brain Barrier transporters in CNS Drug Delivery*, **2010**, supervised by Prof. Veli-Matti Kosma and Proff. Hannele Turunen, in University of Eastern Finland, Kuopio.
[27] Pardridge, W.M. *Fluids Barriers CNS* **2011**, *8*, 1-4.
[28] Pavan, B.; Dalpiaz, A.; Ciliberti, N.; Biondi, C.; Manfredini, S.; Vertuani, S. *Molecules* **2008**, *13*, 1036-1065

capillaries and it is formed by different cell types: brain microvessel endothelial cells, pericytes, astrocytes and microglias. The brain microvessel endothelial cells (BMEC) have important morphological characteristics that restrict the passage of compounds from blood supply to the brain, such as the presence of tight junction between the cells, the absence of fenestration and a diminished pinocytic activity. In addition, BMEC expresses a variety of cytosolic and extracellular enzymes that participate in the restrictive capacity of the BBB.[26,27,28]

The BCSFB separates the blood from the cerebrospinal fluid (CSF) that circulates by the subarachnoid space around the brain (Figure 1.7). This barrier is located at the choroid plexus and is constituted by epithelial cells held together by tight junctions. The capillaries in the choroid plexus allow free movement of molecules *via* intracellular gaps and fenestrations (Figure 1.7).[26,27,28]

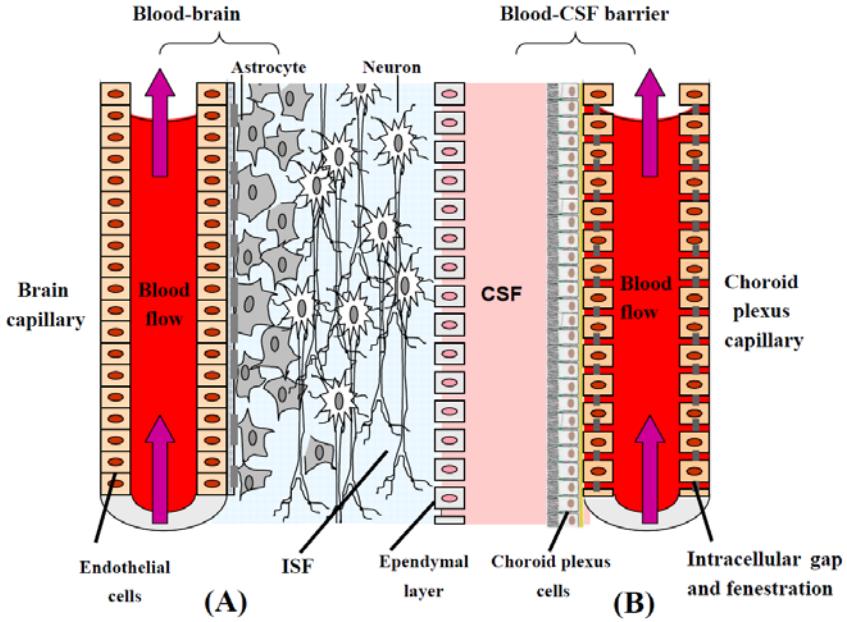

Figure 1.7. *Blood-Brain Barrier (BBB, (A)) and Blood-Cerebrospinal Fluid Barrier (BCSFCB, (B)). The BBB, which is a highly impermeable membrane, occupies the most part of the brain and spinal cord separating the brain from the blood supply. The BBB is formed by a base membrane and different cell types inside the interstitial fluid (ISF), such as endothelial cells joined by thigh junctions, astrocytes, pericytes and microglia. On the contrary, the BCSFB is more permeable with more fenestration and gaps that allow the penetration of molecules. The BCSFB is extended in a very small area that compromises the choroid plexus, where it is segregated the cerebrospinal fluid (CSF) through the brain. This fluid is surrounding all the brain as a protector layer. Figure from Pavan et al. publication.* [28]

The circumventricular organs (CVOs) correspond to those areas in CNS that lack a BBB, having fenestrated capillaries and allowing the free circulation of molecules between the blood and the surrounding interstitial fluid (ISF). However, the relative surface area of the permeable fenestrated capillaries of CVOs is 1:5000 compared to the tight capillaries of BBB; therefore, CVOs does not contribute significantly to the entrance of solutes into the brain.[26]

I.2.1.2 BBB morphology

- *Endothelial membranes.* The BBB is compromised by two different continuous layers of endothelial cells that separate the apical (blood side) and basolateral (brain side) sides of the brain capillary endothelium with a distance within 200-300 nm.[29] The endothelial cells that form the BBB differ from the endothelial cells in the periphery by having very small activity of pinocytosis and transcytosis, large number of mitochondria that provides energy to the barrier, and very tight junctions between overlapped cells.[26,29]

BBB endothelial membrane expresses several transporter proteins that are different in basolateral and apical sides: influx transporters (such as transporters of neutral amino acids, glucose, monocarboxylic acid, cationic amino acids and adenosine) and efflux pumps (such as P-glycoprotein and multidrug resistance associated proteins). In addition, cerebral endothelial cells express a variety of enzymes that create an enzymatic barrier. Hence, all this complex system protects the brain against the entrance of cytotoxic substances that may injure the organ, allowing the pass only to essential nutrients.[30]

- *Tight junctions* are large multiprotein complexes 50-100 times tighter than those encountered in peripheral endothelia.[31] These proteins fused all the endothelial cells between them and with the basal membrane, limiting the paracellular diffusion between the endothelial cells. In addition, tight junctions are the responsible of the polarization of endothelial cells and the differentiation of the apical and basolateral membranes or sides. Consequently, the electrical resistance in this barrier is higher (600-800 Ω/cm) than in other endothelia.[32,33]

- *The basal membrane* is a thin basement membrane that supports the basolateral surface of the endothelium.[34] The basal membrane surrounds the endothelial cells and the pericytes, and is in contact to the end-feet astrocytes. The basal membrane consists mainly on collagen fibers with a composition that provides mechanical support for cell attachment, separates adjacent tissue and may act as a barrier to the passage of macromolecules.[34,35]

- *Pericytes, Astrocytes and Microglia.* Straightaway of endothelial cells and basal membrane, in the ISF, there are the pericytes, the end-feet astrocytes and the microglia (Figure 1.7).[26]

Pericytes have an important role in the establishment and maintaining the phenotype of BBB; they are essential in the structural differentiation of brain endothelial cells and the formation of tight junctions. Several enzymes are expressed in cerebral pericytes acting as a second metabolic barrier.

[29] Pardridge, W.M. *Mol. Biotech.* **2005**, *30*, 57-69.
[30] Cecchelli, R.; Berezowski, V.; Lundquist, S.; Culot. M.; Renftel, M.; Dehouck, M.-P.; Fenart, L. *Nature* **2007**, *6*, 650-661.
[31] Abbott, N.J. *J.Anat*. **2000**, *200* (6), 629-638.
[32] Cecchelli, R.; Dehouck, B.; Descamps, L.; Fenart, L.; Buée-Scherrer, V.; Duhem, C.; Lundquist, S.; Rentfel, M.; Torpier, G.; Dehouck, M.P. *Adv. Drug Deliv. Rev.* **1999**, *36*, 165-178.
[33] Méresse, S. Dehouck, M.P.; Delorme, P.; Bensaïd, M.; Tauber, J.P.; Delbart, C.; Fruchart, J.C.; Cecchelli, R. *J. Neurochem.* **1989**, *55*, 1363-1371.
[34] Tilling, T.; Korte, D.; Hoheisel, D.; Galla, H.J. *Brain Res.* **1998**, *539*, 247-253.
[35] Hynes, R.O. *Cell* **1992**, *69*, 11-25.

Astrocytes are glial cells that envelope >99% of the BBB endothelium.[29] This large surface interaction suggests a good intercellular communication between astrocytes and endothelium, which is necessary for the differentiation of endothelial cells, and the formation and control of permeability in the BBB.[26]

Microglia is a class of glial cells present in the brain and spinal cord. They only constitute the 10-15% of glial cells in the brain and participate in the protection of brain matter.

This cellular environment is required for the physical, structural and metabolic properties of the BBB that play the role of selective permeation in the brain and protective interface of brain homeostasis.

I.2.3 Mechanisms of transport: paracellular and transcellular mechanisms

Regarding the complex system of capillary in the BBB, most of small-molecules and all of the large-molecules cannot cross this membrane unaided.[36,37] For this reason, there are only a few marketed drugs for brain disorders.

In last decades, to improve the permeability of drugs to treat cerebral diseases, medicinal chemists have been taking under consideration the typical mechanisms of penetration for nutrients and other essential molecules that enter into the brain. The different mechanisms of transport through this membrane can be divided into two groups: paracellular and transcellular transports. The paracellular way corresponds to the diffusion through the junction of endothelial cells. However, the presence of tight junctions between the endothelial cells restricts this pathway.[19,38,39] The transcellular way corresponds to any mechanisms of transport that cross within the endothelial cells, from apical to basolateral side. Transcellularly, molecules would be able to cross the BBB by passive diffusion through the lipid barrier, by facilitated diffusion or by some active system.[26] Figure 1.8 shows all paracellular and transcellular mechanisms of transport in the BBB.

[36] a) Pardridge, W.M. *J. Am. Soc. Exp. NeuroTher.* **2005**, *2*, 1-2. b) Pardridge, W.M. *Pharmaceut. Res.* **2007**, *24* (9), 1733-1744.
[37] Teixidó, M.; Zurita, E.; Malakoutikhah, M.; Tarragó, T.; Giralt, E. *J. Am. Chem. Soc.* **2007**, *129*, 11802-11813.
[38] Malakoutikhah, M.; Teixidó, M.; Giralt, E. *Angew. Chem. Int. Ed.* **2011**, *50*, 7998-8014.
[39] Tamai, I.; Tsuji, A. *J. Pharmaceut. Sci.* **2000**, *89* (11), 1371-1388.

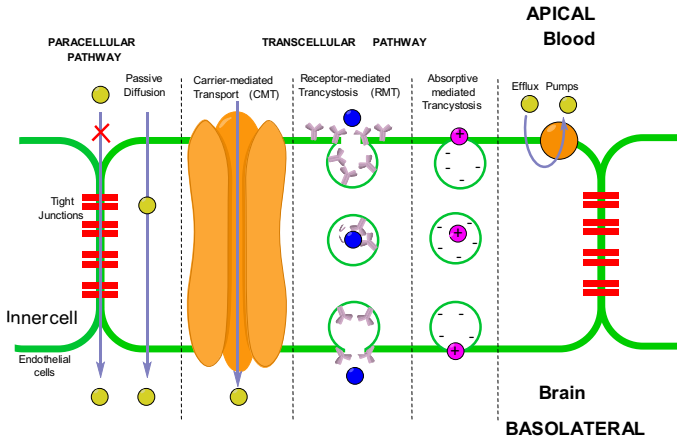

Figure 1.8. *Different mechanisms of transport through endothelial cell membranes: passive diffusion, carrier-mediated transport (CMT) and receptor-mediated transcytosis (RMT), absorptive-mediated trancystosis and active efflux (such as P-glycoprotein). The paracellular pathway is impeded by tight junctions.*

I.2.3.1 Passive diffusion

Passive diffusion is the most common mechanism of CNS drugs to be delivered through BBB and reach the brain. Passive diffusion involves an energy-independent transport of drug molecules that is proportional to the concentration gradient of solutes across the membrane. This kind of transport can occur by two different ways: paracellular (passive diffusion between the cells) or transcellular (passive diffusion through the cells) depending on the physicochemical properties of the solutes. As mentioned, since the paracellular diffusion is blocked by the very tight junctions that seal the endothelial cells, only solutes with specific physicochemical properties to penetrate through the endothelial cell membranes are able to cross the BBB *via* transcellular passive diffusion.[39] Hence, only few molecules are capable to cross spontaneously by passive diffusion the BBB.

Based on CNS marketed drugs, many authors have been suggested the physicochemical properties that a molecule should require to be diffused through the BBB.[26,28,40] In general, these compounds are lipophilic and have a molecular mass lower than 400 Da. Other physicochemical properties, such as cLogP, PSA, HBD and HBA,[40] have to be taken under consideration for the passive diffusion transport prediction. Regarding the physicochemical properties, medicinal chemists have developed *in silico* and *in vitro* models that provide information on transport by passive diffusion of small lipid-soluble tested compounds.[40] In summary, molecules without a passive diffusion do not cross the BBB or require aid to enter into the brain.

[40] a) Pajouhesh, H.; Lenz, G.R. *NeuroRx.* **2005**, *2* (4), 541-553. b) Hitchcock, S.A.; Pennington, L.D. *J. Med. Chem.* **2006**, *49* (26), 7559-7583. c) Lipinski, C.A.; Lombardo, F.; Dominy, B.W.; Feeney, P.J. *Adv. Drug Deliv. Rev.* **1997**, *23* (1-3), 3-25.

I.2.3.2 Carrier-mediated transport (CMT)

Carrier-mediated transport (CMT) is a facilitated diffusion by membrane proteins or carriers.[28] In this kind of transport may be divided into facilated diffusion and active influx. The first one does not require energy because the transport is directly proportional to the concentration gradient of the solutes transporters, but the second on require energy to transport essencial nutrients into the brain. There is recognition of the solute with a specific protein transporter in the apical membrane and it is delivered through the endothelial cell to reach the basolateral side where the solute is released. CMT contributes to the uptake of essential molecules and nutrients into the brain, such as monocarboxylates, hexoses, amines, amino acids, nucleosides, glutathione, small peptides, etc, which due to their hydrophilicity are not able to cross the BBB by passive diffusion.[36b,41]

The CMT BBB transporters may be unidirectional or bidirectional and also they can be expressed in the apical and/or basolateral sides of the endothelial cell membranes (Figure 1.9).

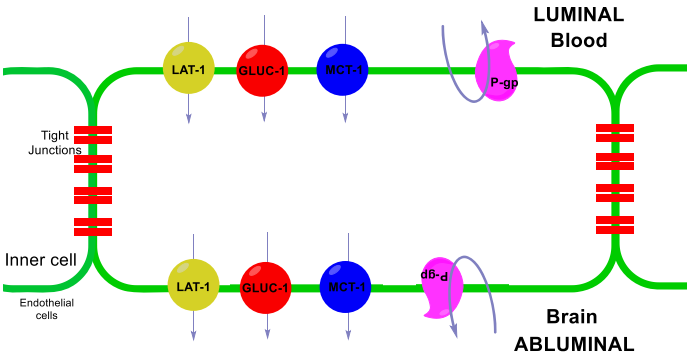

Figure 1.9. *Different CMT and efflux pump expressed in apical and basolateral endothelial cell membrane.*

- *Transport of amino acids.*[39,41,42,43,4444a] Essential amino acids are required in the brain because they are precursors for the synthesis of monoamine (serotonin, histamine, catecholamines), important co-factors and other neurotransmitters substances.[42] Hence, some specific mechanisms of transport have been documented to facilitate the delivery from the bloodstream to the brain. The transporters of amino acids have in general been classified depending on their functional traits, such as sodium dependence (energy requirements) and substrate specificity.[43]

Regarding the net charge of the substrates, the amino acids transporters are divided in anionic, cationic and neutral amino acids.[43] Amino acids such as phenylalanine, tyrosine and leucine are transported the large neutral amino acid transporter LAT-1, which is present in both sides (apical and basolateral) of endothelium and in other organs.

[41] Tsuji, A.; Tamai, I. *Adv. Drug. Deliv. Rev.* **1999**, *36*, 277-290.
[42] Tsuji, A. *J. Am. Soc. Exp. NeuroTher.* **2005**, *2*, 54-62.
[43] Hawkins, R.A.; O'kane, R.L.; Simpson, I.A.; Viña, J.R. *Am. Soc. Nutr.* **2006**, 218S-226S.
[44] a) Gynther, M.; Laine, K.; Ropponen, J.; Leppanen, J.; Mannila, A.; Nevalainen, T.; Savolainen, J.; Jarvinen, T.; Rautio, J. *J. Med. Chem.* **2008**, *51*, 932-936. b) Gynther, M.; Ropponen, J.; Laine, K.; Leppänen, J.; Haapakoski, P.; Peura, L.; Järvinen, T.; Rautio, J. *J. Med. Chem.* **2009**, *52*, 3348-3353.

An analysis of the LAT-1 substrates revealed their requirements: an amino group, a carboxyl group and a hydrophobic pocket site (Figure 1.9).

Furthermore, in less proportion, other systems are also present in the BBB: system y^+ mediates transport of cationic amino acids (lysine, arginine and ornithine); system A transports small neutral amino acids (proline, alanine and glycine); system β facilitates β-amino acids transport (taurine and β-alanine); system X^- allows the entrance to anionic amino acids (aspartic acid and glutamic); and others.[42,43] There are also specific systems for L-glutamate (system X_G^-) and L-glutamine transport (system n).[43]

Glutamate is the most abundant amino acid in the brain and the primary excitatory neurotransmitter of the CNS. To maintain the concentration of this amino acid into the extracellular brain fluid, an energy dependent transporter is required. Two of excitatory amino acid transporters (EAAT) family (EAAT-1 and -2) are expressed in the basolateral membrane of endothelium. In addition, some experiments confirmed the presence of facilitative transport system for glutamine (system n) and glutamate (system X_G^-) only in the apical membrane of the BBB. Furthermore, the enzyme glutaminase (that transforms the glutamine to glutamate), exists within the endothelial cell membranes. Therefore, the glutamate concentration inside the endothelial cells increases by two different mechanisms: glutamate transporter system X_G^- and the conversion of glutamine to glutamate by glutaminase. Hence, the EAAT allows the entrance of glutamate into the brain.

- *Transport of glucose*.[39,41,42,44b] D-Glucose is the main energy source of the brain, which consumes the 30% of total glucose in the body (Figure 1.9). Due to the hydrophilicity of the molecule, the uptake of glucose into the brain must be facilitated by a specific CMT.[26] The glucose transporter (GLUT-1) is present both in the apical and the basolateral membrane of BBB endothelium and exhibits the highest transport capacity of the brain CMT system.[28,41,42]

According to the GLUT-1 model published by Mueckler and Makepeace in 2008, a hydroxyl group at the carbon C_6 is required for the proper affinity with the transporter.[45] Some years later, Fernández *et al.*, synthesized several glycosyl derivatives of drugs like dopamine and tested the prodrug affinity to GLUT-1 in human erythrocytes.[46] They found that drugs were linked to GLUT-1 at positions C_1, C_3 and C_6. Moreover, the best affinity to transporter GLUT-1 was obtained for derivatives conjugated at C_6. Therefore, they concluded that the hydroxyl group at C_6 is likely the most potential functional group to which to attach the drug molecule in order to maintain the affinity of the glucose conjugate to transporter GLUT-1. Some years later, taking under consideration the previous studies, Gynther *et al.* demonstrated that GLUT-1 can be used to carry non-CNS drugs into the brain by conjugating the drug molecule to D-glucose with a bioreversible linkage such an amide or ester.[44b]

[45] Mueckler, M.; Makepeace, C. *J. Biol. Chem.* **2008**, *283*, 11550-11555.
[46] Fernández, C.; Nieto, O.; Rivas, E.; Montenegro, G.; Fontenla, J. A.; Fernández-Mayoralas, A. *Carbohydr. Res.* **2000**, *327*, 353-365.

- *Monocarboxylic acid transport system.*[28,41,42] Carboxylic acid compounds, such as lactic acid, are abundant in the brain and their distributions in brain are regulated by specific transporters present at the BBB. The monocarboxylate transporters (MCT) constitute a family of transporters that facilitate the entrance of metabolically relevant monocarboxylic acids, such as lactate, pyruvate and the ketone bodies acetoacetate and β-hydroxybutyrate, into the brain.[39]

Regarding the monocarboxylic acid transporter, in 2000, Tamai and Tsuji isolated the MCT1 and demonstrated its presence in both apical and basolateral membranes.[39] MCT1 works with pH gradient and it is the main responsible for the transport of relative small monocarboxylic acid through the brain. However, Tamai and Tsuji obtained evidence of an interaction of simvastatin acid and lovastatin acid, which are bigger monocarboxylic acids, to MCT1 in cultured brain capillary endothelial cells.[39]

I.2.3.3 Active influx

Regarding energy requirements (ATP or Na^+-dependent), some of the above explained transporters are active influx transporters although in this report have been classified as facilitated diffusion.[28]

I.2.3.3.1 Receptor-mediated transcytosis

Receptor-mediated transcytosis (RMT) facilitates the entrance or transport of large macromolecules such as antibodies, peptides or proteins, such as insulin and transferring, into the brain by a recognition and subsequent transcytosis process. RCMT is an endogenous large-molecule peptide transporter that operates parallelly to CMT. Transcytosis occurs once circulating ligand interacts with a specific receptor at the apical membrane of the endothelial cells. This receptor-ligand binding induces an endocytic event in the apical membrane that probably involves aggregation of receptor-ligand complexes and triggers the internalization of the solute in an endocytic vesicle containing the receptors and the attached protein molecules.[28,39,41,42]

Although the endocytotic activity in BBB endothelial cells is lower than in peripheral endothelial cells, the brain uptakes some large molecules by transcytosis.

- *Receptor of retinol and ocular barrier.*[47,48] Since it was discovered by Schnaudigel in 1913, the Brain-Retinal Barrier (BRB) has been widely studied.[49] In initial experiments, BRB was not stained after dye injection intravenously although peripheral tissues were. At that moment, BRB showed morphological similarities to BBB: endothelial polarized cellular membranes, restricting the transport of some drugs.

[47] a) Occhiutto, M.L.; Freitas, F.R.; Maranhao, R.C.; Costa, V.P. *Pharmaceut.* **2012**, *4*, 252-275. b) Kubo, Y.; Shimizu, Y.; Kusagawa, Y.; Akanuma, S.; Hosoya, K. *J. Pharm. Sci.* **2013**, *102* (9), 3332-3342.
[48] Maeda, A.; Golczak, M.; Chen, Y.; Okano, K.; Kohno, H.; Shiose, S.; Ishikawa, K.; Harte, W.; Palczewska, G.; Maeda, T.; Palczewski, K. *Nat. Chem. Biol.* **2012**, *8*, 170-178.
[49] Schnaudigel, O. *Graefes Arch. Clin. Exp. Ophthalmol.* **1913**, *86*, 93-105.

Hence, BRB presented similar transcellular transport mechanisms to BBB: passive diffusion, carrier- and receptor-mediated transports (CMT and RMT).

As in BBB, the transport from the blood to the photoreceptor side consists mainly of transport of nutrients such as glucose, ω3 fatty acids and retinal. For glucose transport, the GLUT-1 and 3 are present in both the apical and the basolateral membranes: GLUT-3 mediates the basic transport whereas GLUT-1 is responsible for an inducible glucose transport to adopt the glucose transport to different metabolic demands.[50] *Trans*-retinol is taken up from the bloodstream *via* a receptor-mediated process involving a serum-retinol-binding protein/transthyretin complex. Retinol is formed to all-*trans* retinyl ester and then enters directly into the visual cycle.[48]

I.2.3.4 Active efflux

Before 1992, investigations on CNS drug discovery were primarily focused on the influx mechanism from circulating blood into the brain. Since some findings demonstrated the presence of efflux pumps in the apical side of endothelium as a restriction of the accumulation of cytotoxic and/or lipophilic drugs, the concept of BBB changed.[39,41]

Active efflux transporters have a major impact on the drug systemic pharmacokinetics if the body.[51] The transcellular brain uptake of small lipophilic solutes is not as high as would be indicated by their lipophilicity.[28,39,41] Their lower brain uptake is often due to active efflux proteins such as P-glycoproteins (P-gp), Breast Cancer Resistance Protein (BCRP) and Multidrug Resistance Protein 2 (MRP-2) that remove solutes from endothelial cells into the bloodstream. These efflux pumps are present on one or both endothelial side membranes and it is known that several CNS drugs are their substrates; therefore, it give rises the restriction of the pass through BBB of these CNS drugs and their therapeutic effects.[30,51,52,53]

Although active efflux transporters are very important in the penetration of drugs into BBB, they are not discussed in more detail due to the fact that the scope of this Thesis is on the influx transporters.

I.2.4 Enzymatic metabolism

The enzymatic metabolism corresponds to the total or partial transformation of the solute or drug into a molecule with different structure, facilitating or restricting the entrance of some compounds into

[50] Kubo, Y.; Hosoya, K. *Diabetic Retinopathy, Chapter 5*, book edited by Prof. Mohammad Shamsul Ola, Intech, **2012**.
[51] Hitchcock, S.A. *J. Med. Chem.* **2012**, *55*, 4877-4895.
[52] Balimane, P.V.; Han, Y.H.; Chong, S. *Am. Ass. Pharmaceut. Sci. J.* **2006**, *8* (1), E1-E13.
[53] Deeken, J.F.; Löscher, W. *Clin. Cancer Res.* **2007**, *13* (6), 1663-1673.

the brain. In addition, the enzymatic metabolism is required for prodrugs that once they pass the BBB they are transformed into the active drug.[54]

γ-Glutamyltranspeptidase (γ-GT) is one of the main enzymes present inside of the endothelium and pericytes. This enzyme transforms the principal residue of γ-glutamyl of a donator peptide into an acceptor peptide.

The monoamines oxydases (MAO-A and MAO-B), from mitochondrial origin, are expressed in the brain endothelium. These enzymes facilitate the degradation of monoaminergie neutransmitters originated inside the brain, such as dopamine, serotonin, noradrenalin and adrenalin, to their precursors (5-hydroxytrytophan, 3,4-dihydroxyphenylalanine) from the periphery, with the aim of minimizing the release to the periphery. By this mechanism, L-DOPA, after being transported into the brain, is metabolized to the active dopamine.

Alkaline phosphatase represents another relevant enzyme in the BBB. This enzyme is involved in the hydrolysis of phosphorylated metabolites and controls the transport of phosphate ions and phosphate esters.

Moreover, the enzymes cytochrome p-450 family plays a detoxification role in the BBB.

Regarding all the hindrances that a molecule has to overtake to reach the brain, several mechanisms of administration have been studied for years.

I.2.5 Mechanisms of administration of drugs into the brain

Although effective neuroprotective drugs are available for the treatment of several brain disorders, most of them exhibit a limited application and fail in the clinical trials due to their lack of BBB permeation.[37,38,55] As mentioned in the previous section, drugs targeting the brain have to struggle with many impediments to reach the brain parenchymia. Therefore, only a few small lipophilic molecules are able to cross the BBB.[38]

Nowadays, some approaches are following to improve the uptake of the drug by going through BBB: temporarily opening of the BBB, administration of very high doses of the drug, directly injection of the drug in the spinal cord, co-administration of an efflux pump inhibitor, reversibly disruption of the BBB by focused ultrasounds and magnetic targeting using magnet nanoparticles, are some examples. However, all these approaches imply invasive techniques and cytotoxicity.[38] Other techniques that comprise the drug structure modification are also employed: to reduce the affinity to efflux pumps and to mimic a nutrient with a carrier transport. However, frequently these modifications may reduce the interaction of

[54] Bradbury, M.W. *Handbook of Experimental Pharmacology*, Vol. 103, Springer-Verlag Berlin Heidelberg, Germany, **1992**.
[55] Rasheed, A.; Theja, I.; Silparani, G.; Lavanya, Y.; Kumar, C.K.A. *J. Inn. Trends Pharmaceut. Sci.* **2010**, *1*(1), 9-18.

the drug with the receptor target once inside the brain parenchymia; thus, the therapeutic power decreases.[38]

Regarding these hurdles, the study of the conjugation of BBB transported compounds, such as essential nutrients, that act as a shuttle carrying a therapeutic drug, has emerged as an attractive alternative.[38]

I.2.5.1 BBB-shuttles

Thus, in this context, a BBB-shuttle is a molecule capable to cross the BBB by itself and play the role of carrying drugs that cannot pass through BBB by mentioned mechanisms. The strategy followed depends on the shuttle molecule:[38,55]

- *Passive diffusion.* In 2007, Teixidó *et al.* studied a library of diketopiperazines (DKP) N-PheMe-N-PheMe that aided to drugs targeting the brain by passive diffusion. These DKP were called BBB-shuttles.[37]

- *Chemical delivery system (CDC).* The system consists on the reduction of the shuttle dihydropyridine (T) coupled to the drug to pyridinium salt (T^+) in the brain. The lipophilicity of the drug increases and thus the adduct drug-T is distributed in the tissues, including the brain. An enzymatic oxidation of T to T^+ causes the "lock in" of drug-T^+ in the brain, in which an enzymatic cleavage leaves the drug freely of the T^+.[38,55]

- *Carrier-mediated transport (CMT).* As mentioned in the previous section, hydrophilic nutrients, such as amino acid and glucose, essentials for the functionality of the organ, are not able to cross the BBB by passive diffusion through lipid bilayer and use carrier-mediated mechanisms. These nutrients are capable to work as BBB-shuttles because they are specifically recognized by membrane proteins.[38,55]

- *Molecular Trojan Horses. E*ndogenous ligands with a specific receptor have the capacity to shuttle drugs into the brain.[28,38]

- *Colloidal carriers*. Nanoparticles and liposomes have been applied for the delivery of drugs encapsulated or attached superficially to the brain by invaginations. Specific antibodies or proteins can be attached to improve the recognition with proteins or antibodies in the BBB. These techniques reduce the toxicity of drugs like doxorubicin used for brain tumors.[38,55]

- *Peptide-vector-mediated strategy* employs proteins as delivery tool for targeting drugs to the brain. An advantage is the high affinity to receptors and selectivity for targeting drugs.[38,55]

In the present Thesis, the carrier-mediated strategy by the conjugation of some nutrients, such as amino acids or glucose, to CR-6 was followed to improve the neuroprotective ability of this compound.

II. Objectives

As mentioned in the Introduction, the oral or intravenous administration of a drug to treat neurodegenerative disorders or stroke is in most cases ineffective due to the hurdle of the BBB restriction for nearly all non-essential compounds. Nowadays, the treatment of these diseases is hard because the administration of the drug involves toxicity or disruption of BBB.

In recent years, new strategies to improve the BBB permeation have been developed. Teixidó *et al.* developed a new family of 2,5-diketopiperazines that conjugated to drugs let the delivery through BBB by passive diffusion.[37] Other authors, like Gynther *et al.* studied the efficiency of coupling drugs with essential amino acids or glucose that enter into the brain by a facilitated diffusion.[44] They called these new strategies BBB-shuttles.

Some years ago, CR-6 was developed as a potent antioxidant compound and moderate neuroprotectant. Following the previous work in our group, the main objective of the present Thesis is to improve the BBB permeability of CR-6.

From all the above antecedents, the specific Objectives of the present Doctoral Thesis were:

1. Design, synthesis and structural characterization of a small library of CR-6 analogues where the CR-6 scaffold would be coupled to a set of essential nutrients (such as amino acids), addressed to improve the ability of this antioxidant to cross the BBB barrier.

2. Evaluation of the antioxidant activity of this library of CR-6 analogues to ensure that the structural modifications have not altered the original activity of CR-6. This evaluation will be carried out using different standard protocols for measuring antioxidant activity.

3. Evaluation of the penetration capacity of the library components using *in silico* procedures and *in vitro* models of barriers.

4. Taking into account that the components of this library are racemates or diastereomeric mixtures, from all data collected from Objectives 2 and 3 select the best candidates to explore the resolution of those mixtures and determine the activity of isolated stereoisomers.

III. Synthesis of CR-6 analogues

III.1 SYNTHESIS OF CR-6 ANALOGUES

A Blood-Brain Barrier (BBB)-shuttle is able to transport a drug or pro-drug into the brain by passive or active diffusion. Thus, we envisaged the synthesis of a small library of CR-6-analogues coupled to putative BBB-shuttles that would carry the biologically active chromanee scaffold into the brain (Figure 3.1).

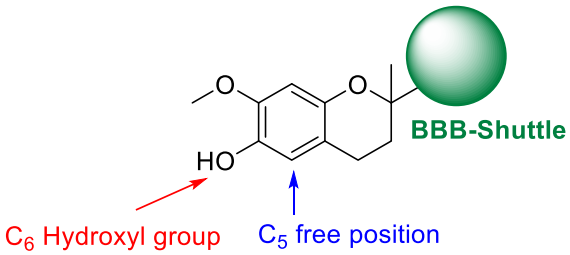

Figure 3.1. *General structure for CR-6-analogues in the designed small library. The active positions to neutralize ROS and RNS, phenolic hydroxyl at C_6 (in red) and free C_5 (in blue), are pointed out; the BBB-shuttle is in green.*

Specific transporters mediate the access of certain crucial molecules into the brain, such as glucose, amino acids and ions.[39,41,42] Other compounds or drugs are dependent on diffusion through the lipid bilayer of endothelial membranes, which requires that these compounds exhibit a certain degree of lipophilicity.[56] Thinking in the improvement of the passive and/or active diffusion of CR-6, compounds depicted in Figure 3.4 were designed. Most of these compounds introduce the variability into the CR-6 scaffold by an amide or peptide bond that connects CR-6-like scaffold with the BBB-shuttle.

These compounds were divided in three different families (Figure 3.2) depending on the similarities of BBB-shuttle structure and the pathway followed for their synthesis. Family 1 consists of CR6-carboxamide derivatives, and is composed by analogue **A** with a dopamine side chain; compounds derived from amino acid BBB-shuttles (**B**-**H**), which can be delivered through BBB by an active transporter; and the primary amide derivative **I**, which can get into the brain by passive diffusion. Family 2 consists of CR6-aminocarbonyl derivatives formed by the retinoic derivative **J** that could be introduced into the brain by a retinol receptor (Receptor Binding Protein acts as a transporter of retinol by blood circulation but also through some epithelial barriers such as BBB[57]); D-glucose, **K**, that could be actively delivered through BBB by the GLUT-1 mechanism; and the secondary amide **L** derivative that could be transported by passive diffusion. Finally, Family 3 contains free carboxylic acids, like **N**, or as an amino acid, **M**, which could be transported either by an active transporter or by passive diffusion to reach the brain.

[56] Van der Waterbeemd, H.; Camenisch, G.; Folkers, G.; Chretien, J.R.; Raevsky, O.A. *J. Drug Target.* **1998**, *6*, 151-165.
[57] Sun, H.; Kawaguchi, R. *Int. Rev. Cell Mol. Biol.* **2011**, *288*, 1-41.

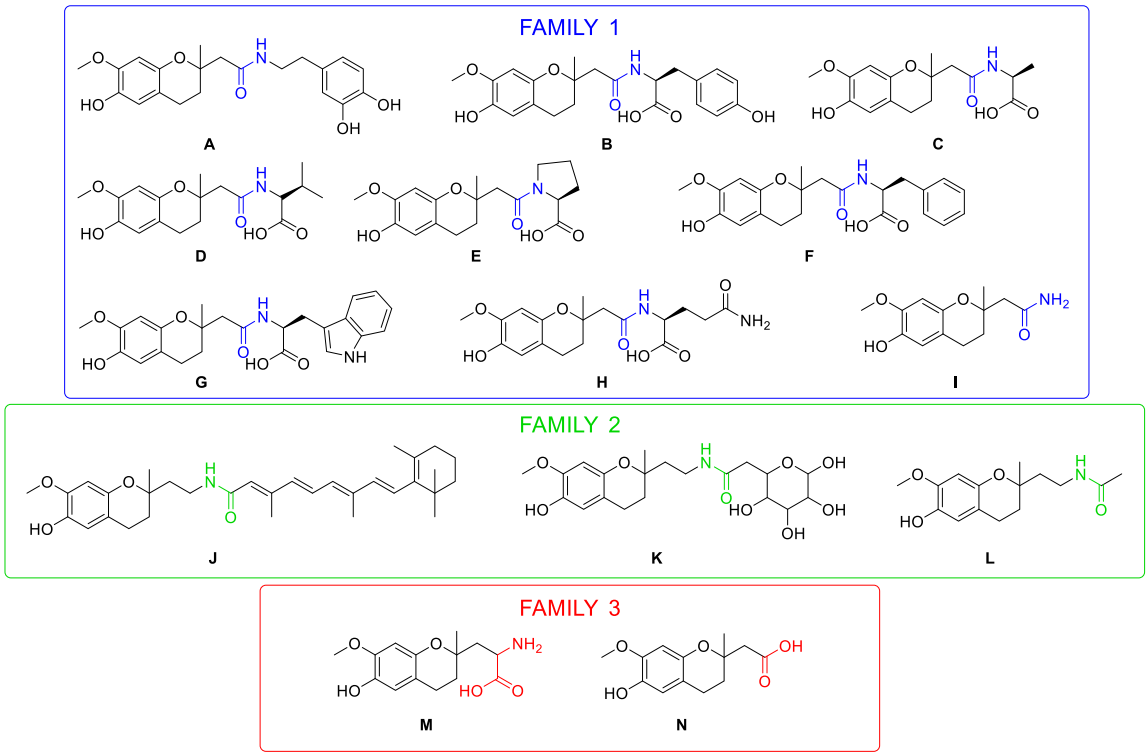

Figura 3.2. *Molecules designed as analogues of CR-6 to be delivered through the BBB. This library was divided into three different families depending on the BBB-shuttle structure and the synthetic pathway followed.*

III.1.1 Retrosynthesis

For the preparation of these compounds, two common key precursors, ester **III** and primary alcohol **VIII**, were first synthesized. The retrosynthetic pathway for the synthesis of a short library of CR-6-analogues, candidates to be BBB-neurotransporters, is shown in Scheme 3.1.

Compounds from Family 1 would come from the coupling reaction between acid **I** and an appropriate commercial amine **II**. By hydrolysis, acid **I** would be synthesized from ester **III**, one of the key precursors, which could come from a Horner-Wadsworth-Emmons reaction of hemiacetal **IV**, which in turn would be prepared from the hydrolysis of acetal **V**. Acetal **V** would come from the condensation of commercial hydroquinone and vinylketone in the presence of trimethyl orthoformate.

Compounds from Family 2 would be obtained from the coupling reaction between amine **VI** and different commercial acids **VII**. Amine **VI** would be prepared from primary alcohol **VIII**, which is the other key precursor in the synthetic pathway. Alcohol **VIII**, would be easily synthesized from the reduction of ester **III**.

In Family 3, the two compounds would be synthesized by different ways. **N** would come from the deprotection of acid **I**, and **M** would be obtained from aminonitrile **IX** after hydrolysis of the nitrile. The aminonitrile **IX** would be prepared from the aldehyde **X** by a Strecker reaction. Then, the aldehyde would be obtained from the oxidation of the primary alcohol **VIII**.

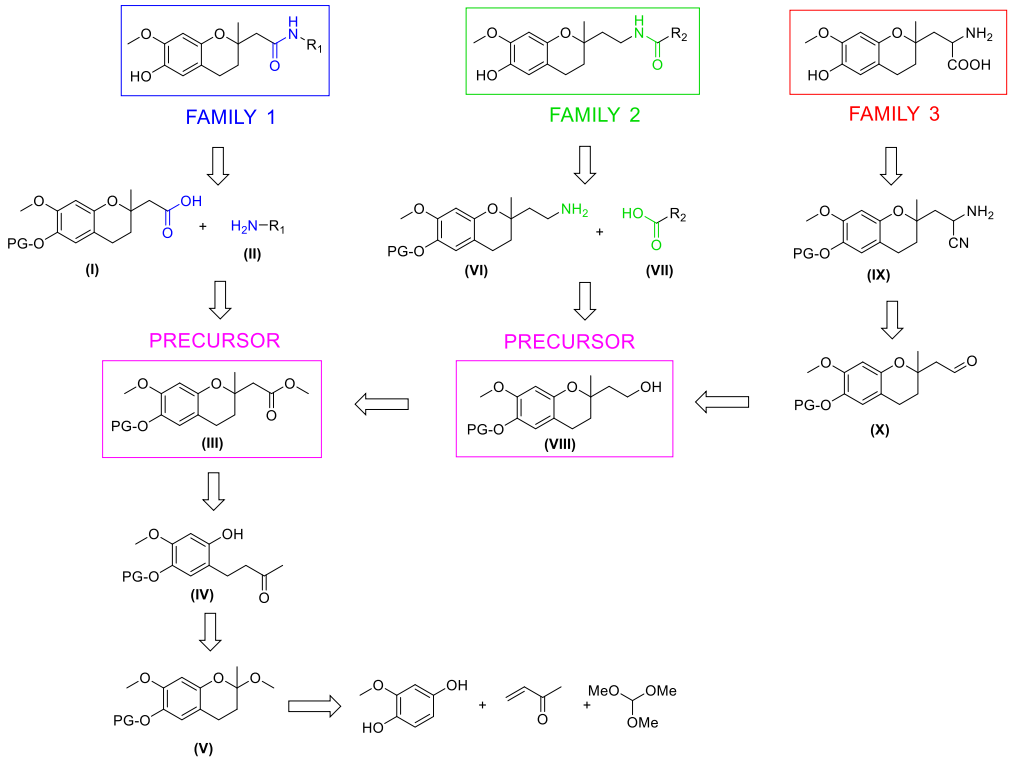

Scheme 3.1. *Retrosynthesis of all CR-6-analogues. Three families were synthesized from two common precursors* ***III*** *and* ***VIII****.* ***N*** *analogue was not considered in the retrosynthesis as a member of Family 3 because it is a precursor of Family 1. PG means Protecting Group.*

III.2 SYNTHESIS OF INTERMEDIATES 1 AND 2

The preparation of some of these derivatives was carried out with the support of the graduate student Martina Miceli from La Sapienza-University of Rome (Italy) that was in our laboratory for a short stay of four months with a Leonardo Program.

III.2.1 Synthesis of acetal 3

Acetal **3** was obtained in 80% yield after purification from the reaction of methoxyhydroquinone and methyl vinyl ketone in the presence of trimethyl orthoformate and sulphuric acid (Scheme 3.2).[58] As a by-product, hemiacetal **4** was also obtained due to the partial hydrolysis of the acetal, which could not be avoided after the neutralization of reaction crude during work-up.

[58] Scott, J.W.; Bizarro, F.T.; Parrish, D.R.; Saucy, G. *Helv. Chim. Acta* **1976**, *59*, 291-306.

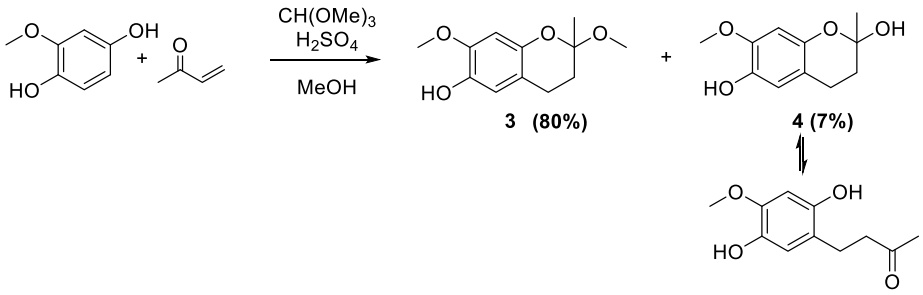

Scheme 3.2. *Reaction for the formation of the acetal* ***3****. During this reaction, the by-product* ***4*** *was also obtained.*

The reaction course for the formation of the acetal **3** and hemiacetal by-product **4** is shown in Scheme 3.3. It would start with the acetalization of the ketone in the presence of trimethyl orthoformate, followed by a nucleophilic attack over the double bond of this ketone intermediate. Finally, the acetalization of the phenolic hydroxyl would take place to close the ring.

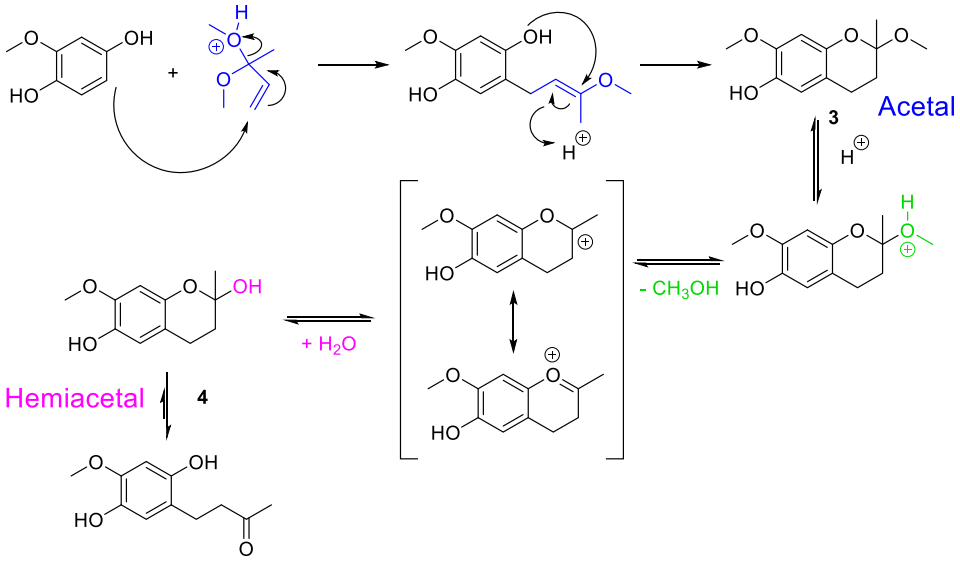

Scheme 3.3. *Proposed mechanism for the synthesis of acetal* ***3*** *and by-product hemiacetal* ***4****.*

The formation of these two compounds **3** and **4** was confirmed by HRMS and ^{1}H-NMR spectrum. The hemiacetal formed as a by-product was in equilibrium with the open form, a more stable compound. They were removed from the crude reaction mixture after purification by flash chromatography.

The ^{1}H-NMR spectrum for these two compounds is shown in Figure 3.5. In the upper one, the hemiacetal **4** appears as a mixture of two different species in equilibrium: open and closed form. In green, signals for the closed structure (in smaller proportion) are pointed out: methylene diasteriotopic protons H_4 and H_3 at 2.92, 2.60, 2.04 and 1.83 ppm, and, aromatic protons H_5 and H_8 at 6.64 and 6.38 ppm. On the other hand, characteristic protons for the open form are pointed out in yellow: aromatic protons H_5 and

H_8 at 6.56 and 6.53 ppm, protons H_4 and H_3 at 2.88 and 2.71 ppm, respectively, and proton for phenolic hydroxyl at 7.8 ppm.

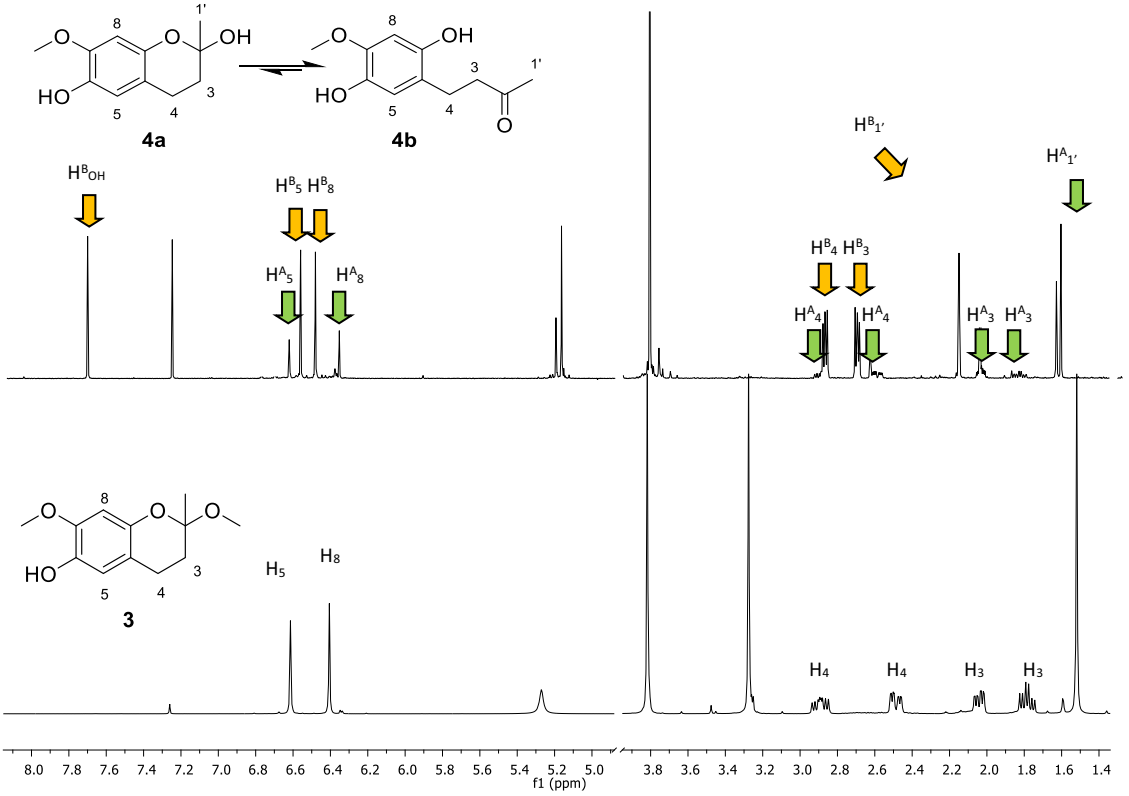

Figure 3.3. *^{1}H-NMR ($CDCl_3$, 400MHz) spectra for hemiacetal **4** (up) and acetal **3** (down). The open and closed forms of hemiacetal **4** are pointed out in green and yellow, respectively.*

In the second spectrum (Figure 3.3), acetal **3** is shown. As in the closed structure of hemiacetal **4**, diastereotopic protons H_3 and H_4 appear at 2.88, 2.49, 2.04 and 1.78 ppm.

Regarding the structure of bicycle 2,2-dialkylpyranyl moiety, CR-6 and the acetal **3** presented different spatial distribution that is reflected on the different ^{1}H-NMR (Figure 3.4). In the ^{1}H-NMR spectrum, diastereotopic hydrogen atoms from methylene groups of chromanee moiety in acetal **3** presented different chemical shifts and also a geminal coupling constant, $J_{geminal}$. This fact was explained for the pseudo-chair conformation in the 2,2-dialkylpyranyl moiety that allows pseudo-axial and pseudo-equatorial couplings between hydrogen atoms from two different methylene groups.

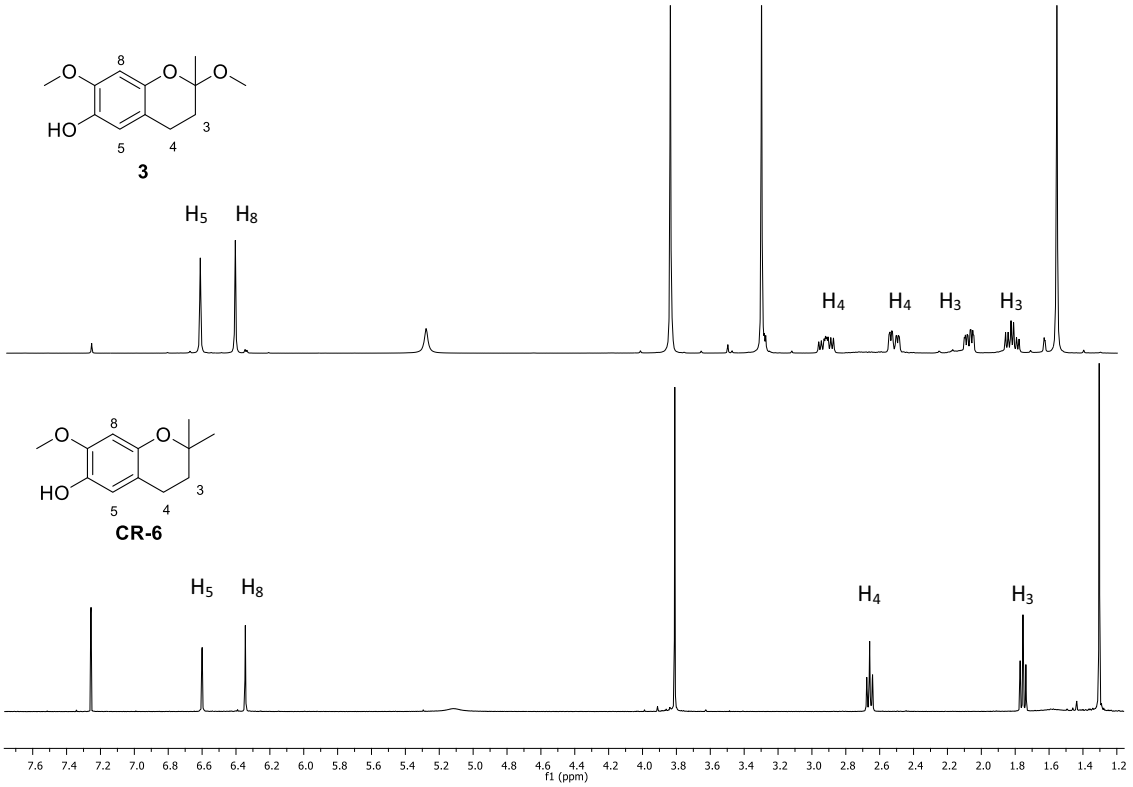

Figure 3.4. *Comparison of ^{1}H-NMR ($CDCl_3$, 400MHz) spectra for acetal **3** (up) and CR-6 (down) to illustrate the differences in the 2,2-dialkylpyranyl moiety.*

As distinctive structural features of acetal **3** in the ^{1}H-NMR spectrum, the hydrogen atoms H_3 and H_4 appeared at 1.78 and 2.04 ppm, and 2.49 and 2.89 ppm, respectively, as diastereotopic protons. The $J_{geminal}$ for protons H_3 was 6 Hz, different for H_4, 16 Hz, and the coupling constants for $J_{ax\text{-}ax}$ and $J_{eq\text{-}ax}$ were13 Hz, 6 Hz and 2 Hz, respectively (Figure 3.5).

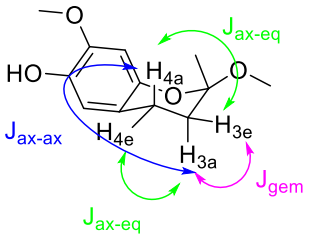

Figure 3.5. *Spatial distribution of 2,2-dialkylpyranyl moiety of acetal **3**. In this figure, the couplings between diasteriotopic protons H_3 and H_4 are pointed out in different colors: in green the axial-equatorial, in blue the axial-axial and in purple the geminal.*

III.2.2 Protection of phenol and hydrolysis of acetal

The phenolic hydroxyl is weakly acidic (pK_a around 10 - 11) and under high basic conditions a phenolate can be generated. This phenolate is stabilized by resonance and can give undesired side reactions (Scheme 3.5). For this reason, it was necessary to protect the phenol functionality in the next step of the synthetic pathway.

In Susana Yenes' thesis the *tert*-butyldimethylsilyl was used as protecting group.[59] Although this group was resistant to the acidic hydrolysis of the acetal and the following reaction to form the ester, it was removed during basic hydrolysis of the ester to generate the desired acid. Due to this reason, this protecting group was dismissed. Other protecting groups were taken into consideration, but benzyl ether protection was the best in terms of stability for the proposed synthetic pathway. Since hydrogenolysis is required for its cleavage, in principle no interference with the synthetic sequence was expected.

In this way, the synthesis of hemiacetal **5** was devised in two reactions in a one-pot procedure: first, the protection of phenol as benzyl ether and, second, the hydrolysis of the acetal under acid conditions.

The protection of the phenol hydroxyl (Scheme 3.4) was carried out using benzyl bromide and sodium hydride as base. In previous experiments, DMF was used as a solvent, but because of the difficulties to remove the solvent from the crude reaction mixture, it was replaced by THF. After 14 hours, the reaction was completed.

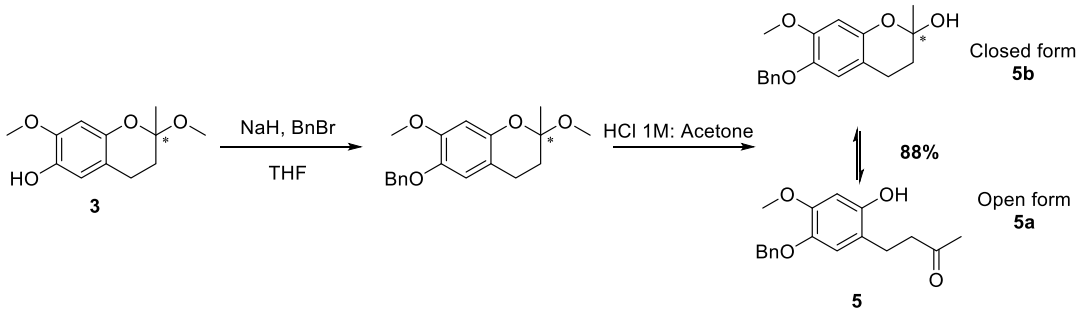

Scheme 3.4. Protection of phenol as benzyl ether and acid hydrolysis of the acetal in an one-pot reaction. The mixture in equilibrium of closed and open forms of hemiacetal **5** were obtained.

Specifically, the hydrolysis of the protected acetal was carried out by treatment of a solution of 1 M HCl followed by the same volume of acetone as co-solvent to facilitate the dissolution of the compound in aqueous phase. At that time, a change of color in the solution, from brown to yellowish, was observed. Finally, after 4 hours, hemiacetal **5** was obtained in 88% overall yield, after purification by flash chromatography.

[59] **Yenes Mínguez, S.** *Estudis sobre la preparació, reactivitat i biotransformació d'antioxidants fenòlics estructuralment relacionats amb els tocoferols*, **1999**, supervised by Prof. Àngel Messeguer Peypoch.

The mass at m/z = 301.1448 for $[M+H]^+$ confirmed the formation of this product. In addition, as distinctive structural features of benzyl protected CR-6 derivatives, in the ^{1}H-NMR spectrum, three multiplets within 7.48 to 7.27 ppm and singlets at 5.05 and 5.03 ppm showed the presence of the benzyl ether. Furthermore, by ^{1}H-NMR (Figure 3.6) we could identify the presence of two different species: the open (**5a**) and the closed (**5b**) form of 2,2-dialkylpyranyl ring in equilibrium in 3:1 ratio. Characteristic signals for these two different species demonstrated diasteriotopic methylenic hydrogens H_3 and H_4 in the closed form (at 2.87, 2.55, 2.03 and 1.87 – 1.76 ppm, respectively); and the same protons in the open form at 2.79 and 2.66 ppm. Also, peaks for protons H_5 and H_8 in both species were different (6.64 and 6.41 ppm for the open form, and 6.56 and 6.53 ppm for closed form). The signals in the ^{13}C-NMR spectrum for the ketone group at 212 ppm and, in the ^{1}H-NMR spectrum, the signal at 2.13 ppm for $H_{1'}$ confirmed the presence of the open form as major component of this equilibrium.

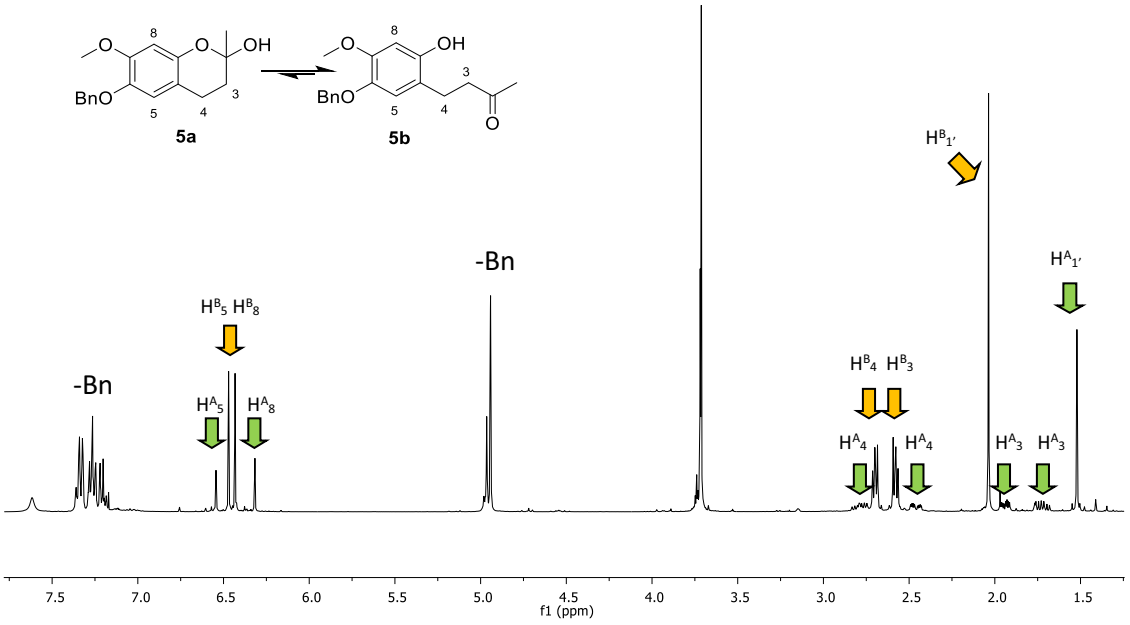

Figure 3.6. *^{1}H-NMR ($CDCl_3$, 400MHz) spectrum for the benzyl-protected hemiacetal **5**. The characteristic signals for benzyl protecting group are labelled. The equilibrium between the closed **5a** and open **5b** forms of hemiacetal **5** are pointed out in green and yellow, respectively.*

III.2.3 Tandem Horner-Wadsworth-Emmons olefination – Michael addition

The reaction of Horner-Wadsworth-Emmons (HWE) for the formation of a carbon-carbon bond was carried out for the synthesis of ester **1**. The nucleophilic attack over carbonyl group present in **5a** took place with trimethyl phosphonoacetate and sodium hydride as a non-nucleophilic base (Scheme 3.5).

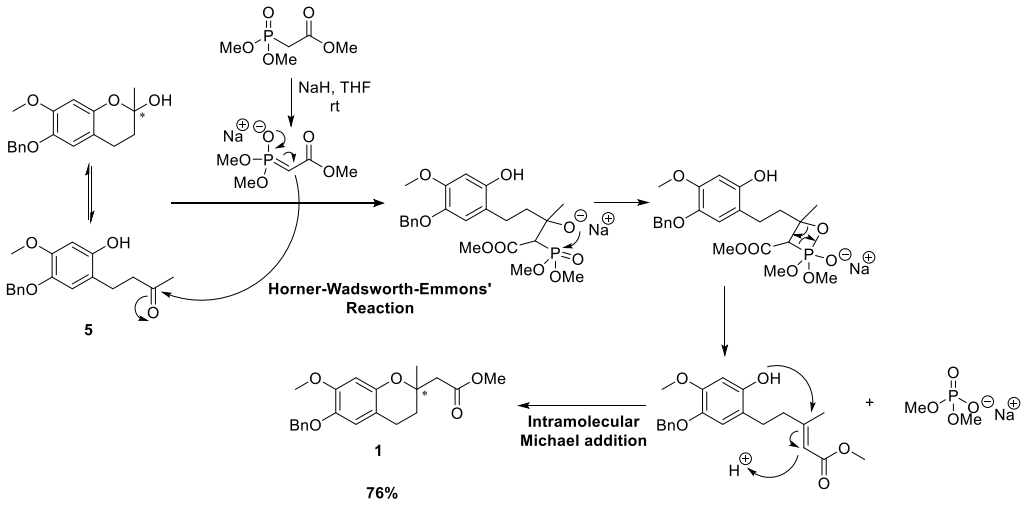

Scheme 3.5. *Horner-Wadsworth-Emmons and intramolecular Michael addition afforded the precursor ester* ***1****.*

First of all, the ylide was generated by the extraction of a methylene proton of trimethyl phosphonoacetate in the presence of sodium hydride during 1 hour at room temperature. Then, the hemiacetal **5** was added to the white suspension and the mixture was stirred for another 1 hour. Since the hemiacetal **5a** is the starting material in the HWE reaction, its consumption is the driving force to drive the equilibrium between **5a** and **5b** until the disappearance of the starting material. By heating the reaction from room temperature to reflux for 30 minutes, the conversion was completed, inducing first the nucleophilic attack of the ylide to the ketone, followed by the nucleophilic Michael addition-like of the phenolic hydroxyl to the double bond. Thus, the ester **1** was obtained with 76% of yield after purification by flash chromatography.

As distinctive structural features of compound **1**, the observation by NMR of a new peak at 3.75 ppm in the ^{1}H-NMR spectrum and at 170.89 ppm in the ^{13}C-NMR, which correspond to the ester group –COOMe, confirmed the presence of the ester. Other peaks in the ^{1}H-NMR changed from hemiacetal **5** to ester **1**: methylene protons H_4 and $H_{1'}$ appeared in the same multiplet at 2.60 ppm, and H_3 appeared as diastereotopic protons at 1.99 and 1.90 ppm. In addition, in the HRMS the mass m/z 357.1718 of $[M+H]^+$ confirmed the formation of the ester **1**, the first key precursor in the synthetic route.

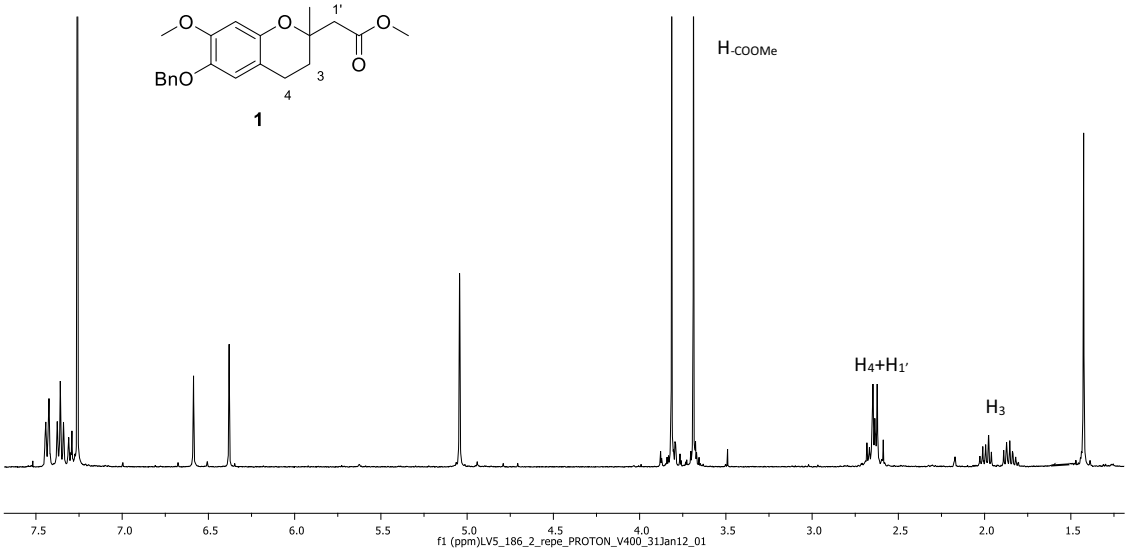

Figure 3.7. *^{1}H-NMR ($CDCl_3$, 400MHz) spectrum of precursor ester **1**.*

III.2.4 Reduction of ester 1

Primary alcohol **2**, the second key precursor in the proposed synthetic pathway, was obtained from the reduction of ester **1** by a standard protocol (Scheme 3.6).

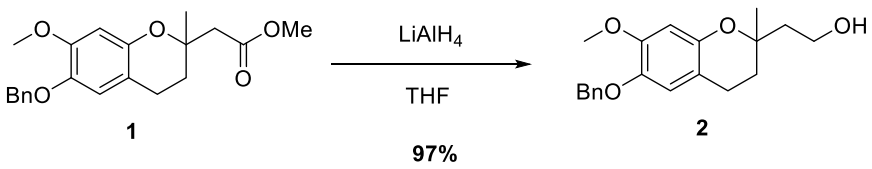

Scheme 3.6. *Reduction of the ester **1** with $LiAlH_4$ to give the primary alcohol **2**.*

For the reduction, lithium aluminium hydride was used. After 1 hour at room temperature, the alcohol **2** was obtained as a white solid at 97% yield without further purification.

As a distinctive structural feature of alcohol **2**, the absence of the –COOMe signal in ^{1}H- and ^{13}C-NMR confirmed the formation of the primary alcohol as the only product. In addition, in the HRMS, the signal at m/z = 329.1739 for $[M+H]^+$ evidenced the presence of **2**.

From these two precursors, **1** and **2**, all CR-6 analogues of the library were synthesized.

III.3 SYNTHESIS OF ANALOGUES IN FAMILY 1

III.3.1 Hydrolysis of ester 1

As explained in the retrosynthesis, section III.1.1, page 50, Family 1 was obtained from the coupling reaction of acid **6** and a commercial amine to form an amide or peptide bond.

Acid **6** was obtained after the hydrolysis of the ester precursor **1** under base conditions (Scheme 3.7), using a 4 M NaOH solution and dioxane as co-solvent. After 4 hours at reflux, acid **6** was obtained in 99% yield without further purification.

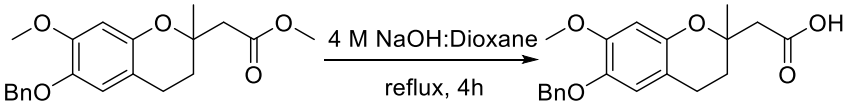

*Scheme 3.7. Hydrolysis of the ester **1** under basic conditions.*

As a distinctive structural feature for carboxylic acid **6**, in the ^{1}H-NMR spectrum, it was observed the absence of the signal -COOMe at 3.75 ppm. In addition, and different from alcohol **2**, in the HRMS the signal at m/z 343.1552 for $[M+H]^{+}$ evidenced the formation of the acid **6**.

III.3.2 Amides prepared by peptide coupling reactions

The amide functionality is a common feature in small or complex synthetic or natural molecules and plays an important role in the synthesis of drugs due to its great recognition by biological systems. Proteins might contain hundreds of amide bonds, and peptides and other pharmacological small molecules contain at least one amide bond.[60]

The amide or peptide bond formation consists of a condensation between a carboxylic acid and an amine. However, by mixing an amine and a carboxylic acid the stable salt is formed first, like in an acid-base reaction, which is in equilibrium with an unfavoured amide form (Scheme 3.8). For the final formation of the amide, high temperatures are required (around 180ºC), and, many times, it is quite incompatible with the presence of other functionalities in the reagents. Therefore, the activation of the acid by converting the –OH into a good leaving group (LG) prior to the treatment with the amine is necessary to increase the electrophilicity of the carbonyl group and favour the nucleophilic attack.[60c] Then, a good coupling agent needs to be able to cope with all these problems of reactivity in this reaction.

[60] a) Han, S.-Y.; Kim, Y.-A. *Tetrahedron* **2004**, *60*, 2447-2467. b) Motalbetti, C.A.G.N.; Falque, V. *Tetrahedron* **2005**, *61*, 10827-10852. c) Valeur, E.; Bradley, M. *Chem. Soc. Rev.* **2009**, *38*, 606-631. d) Joullié, M.M.; Lassen, K.M. *Arch. Org. Chem.* **2010**, *8*, 189-250.

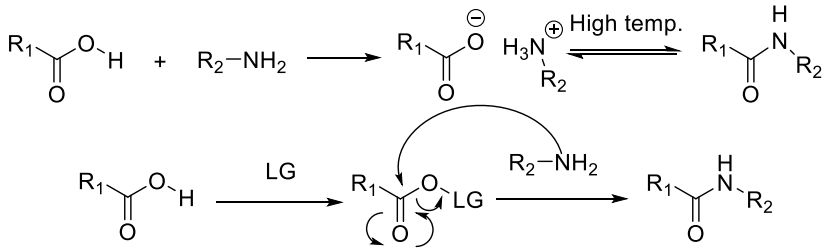

Scheme 3.8. Coupling reaction between an acid an amine without (up) and with (down) an activation of the acid feature (where LG represents the coupling agent). In the first reaction, in which a coupling agent is not used, high temperatures are required to form the final desired amide.

Within the last two decades, the conditions for the optimisation of this step have been widely studied. For example, avoiding racemisation and side-products, improving yields, or the final purification were among the most optimized issues. Thus, this reaction became a tool of choice to produce vast amounts of diverse compounds for the early discovery in pharmaceutical industry.[60]

The activation of carboxylic acid has been one of the most studied mechanisms to improve the results in the peptide coupling reaction. Carbonyl moieties can be activated as acyl halides, acyl azides, acylimidazoles, anhydrides, esters and so on. But the most used is the *in situ* generation of the acylating agent from the acid, by adding an activating or coupling agent (Scheme 3.8).

Carbodiimides are the cheapest and the most common coupling agent (Scheme 3.9). DCC, EDC and DIC are frequently used for amide bond formation (Table 3.1), although they have poor reactivity. In this reaction, the carbodiimide reacts with the carboxylic acid to form the *O*-acylisourea mixed anhydride (Scheme 3.9). This intermediate can then directly react with the amine to yield the desired amide and the related urea by-product, which acts as the driving-force of the reaction and it can be removed from the crude reaction mixture. The most useful carbodiimides and the way they can be eliminated are shown in Table 3.1.[60]

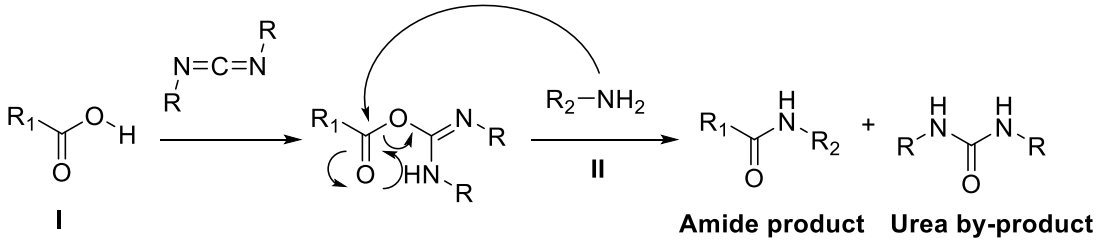

*Scheme 3.9. Coupling reaction between an acid **I** and an amine **II** using the carbodiimide reagents as coupling agents to acylate the carboxylic acid and improve its electrophilicity.*

***Table 3.1**. Comparison of most common carbodiimide coupling agents, the corresponding urea by-product and the way to purify the amide*.

Coupling agent	Structure	By-product urea	Elimination of by-product
DCC	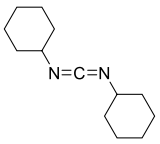	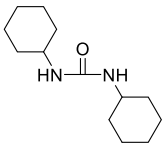	Urea by-product poorly soluble. Elimination by filtration
DIC	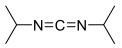	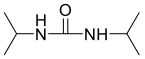	Urea by-product soluble in DCM. Elimination by DCM washes
EDC·HCl	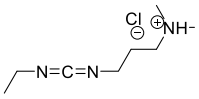	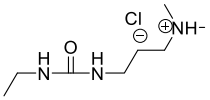	Urea by-product soluble in water. Elimination by aqueous washes

Taking into consideration the isolation of final amide, EDC is widely used because its water-soluble urea by-product elimination is easier than that of DIC or DCC.

At the same time, other side-reactions might occur during the coupling reaction. The racemization of the stereocenter is typical in peptide synthesis (Scheme 3.10). Under mild conditions, the oxazolone, which is formed from the intramolecular attack of a carbonyl group to another activated carbonyl group, may undergo the racemization. The generation of the *N*-acylurea by a transmutation from *O*-acylisourea is considered as another side-reaction. Fortunately, the racemization and the *N*-acylurea generation can be diminished by adding a nucleophile that reacts faster than competing acyltransfer, generating an intermediate still active enough to couple with the amine (Scheme 3.11).[60] Some examples of these nucleophiles are dimethylaminopyridine (DMAP) and 1-hydroxy-1*H*-benzotriazole (HOBt). Thus, these additives are widely used not only to avoid the racemization in a peptide synthesis, but to increase the reactivity (Scheme 3.11).

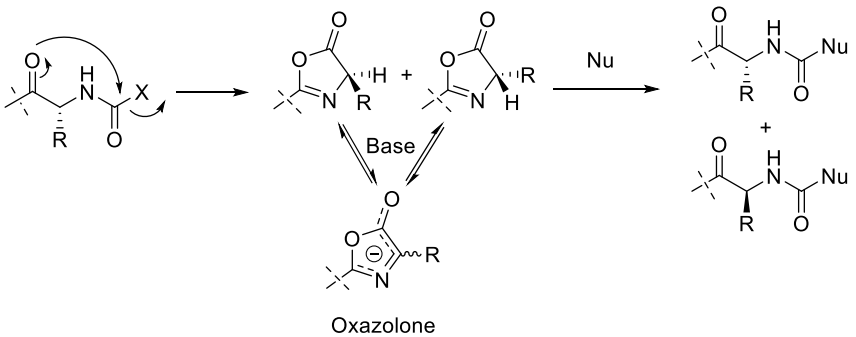

***Scheme 3.10.** Mechanism of racemization in peptide synthesis by the formation of an oxazolone intermediate.[60a]*

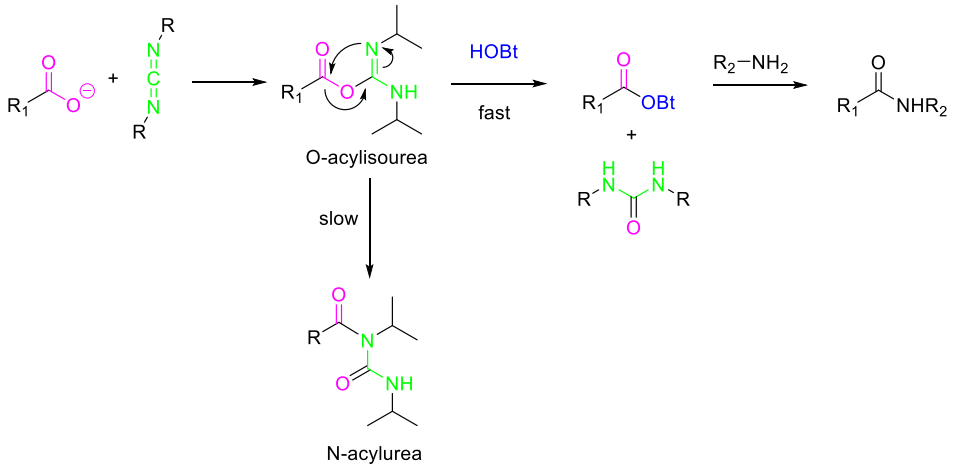

Scheme 3.11. *Generation of an N-acylurea is observed as by-product of the amide bond reaction. The addition of a nucleophile diminishes the side-products and increases the rate of reaction.*[60c]

*III.3.2.1 Synthesis of amides from Family 1 (Compounds **7**-**14**)*

The synthesis of molecules of family 1 was carried out by the coupling of acid **6** and different commercial amines. Taking into account the bibliography,[60] these reactions took place in parallel under standard conditions. The acid **6** was diluted with small amounts of CH_2Cl_2 and EDC·HCl as a coupling agent, HOBt as *N*-acylurea generation suppressor and DiPEA as non-nucleophilic base were added. The mixture was stirred for 30 minutes at room temperature to assure the formation of the activate intermediate, and following, the appropriate commercial amine (dopamine, L-tyrosine methyl ester, L-alanine methyl ester, L-valine methyl ester, L-proline benzyl ester, L-phenylalanine benzyl ester, L-tryptophan methyl ester and L-glutamine methyl ester), was added. Most of these amines have an amino acid moiety with the carboxylic acid protected as methyl or benzyl ester to reduce the likely interaction of –OH during the coupling reaction. All these reactions were completed after 20 to 48 hours (monitoring by HPLC in reverse phase).

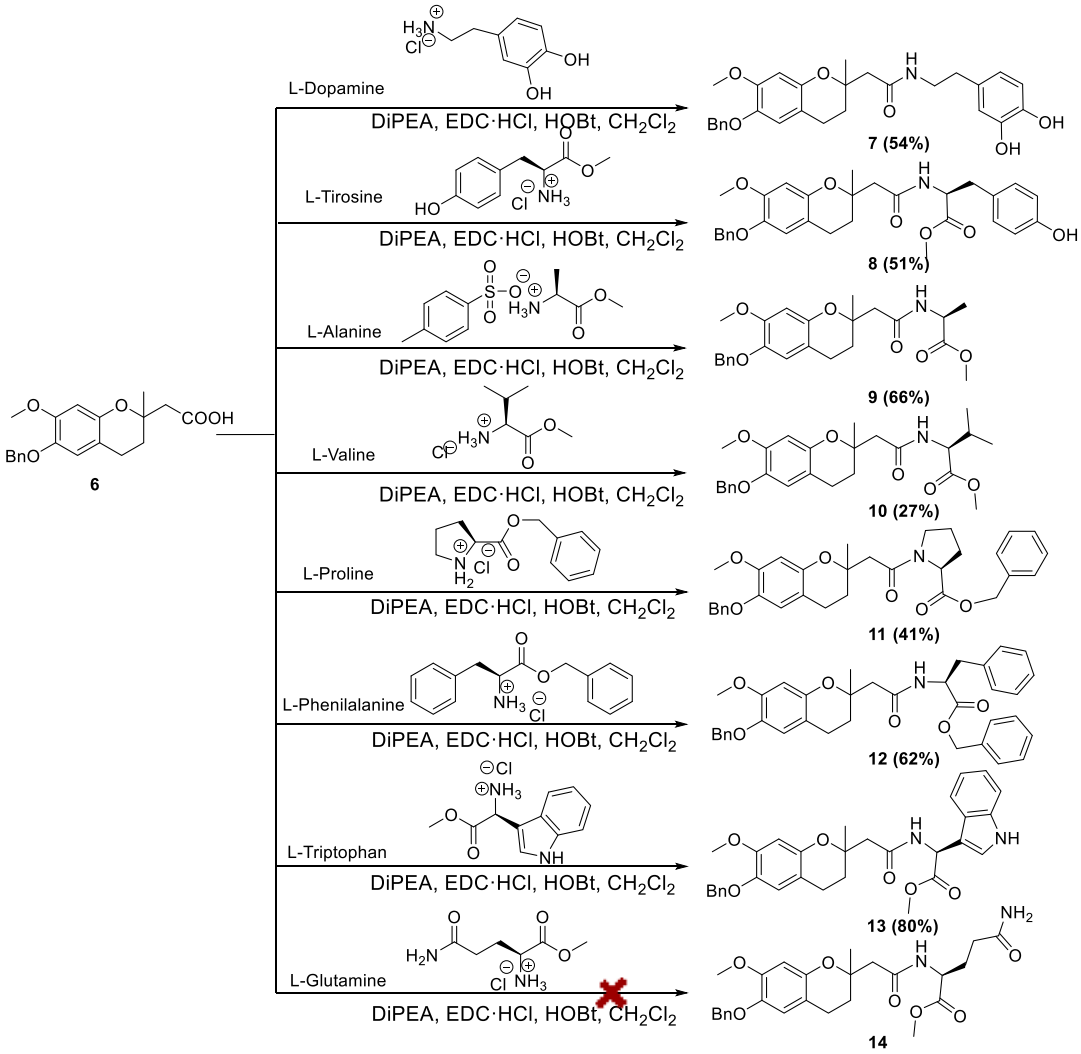

Schema 3.12. *The coupling reaction of acid* ***6*** *with different amines to form the desired amides* ***7-14****.*

The non-reacted EDC·HCl and urea by-product were washed away from the crude reaction mixture with HCl followed by neutralization with $NaHCO_3$. However, a subsequent purification in reverse phase was required to isolate amides **7-14** in variable but generally good yields (27-80% yield, Scheme 3.12), depending on the amine partner. An exception was L-glutamine that leads to a complex mixture of products; although the desired coupling product was detected by UPLC-MS, it could not be isolated.

*III.3.2.2 Improvements in the synthesis of the L-Glutamine derivative **14***

Following the above described methodology, derivative **14** was generated mixed with more impurities than in other reactions. Moreover, considerable amounts of starting material **6** were still present. One of these compounds was identified as intermediate **15** (Scheme 3.13), which was the result of the coupling between the acid and the carbodiimide coupling agent EDC (Scheme 3.13). The rest of species present in the crude reaction mixture could not be identified.

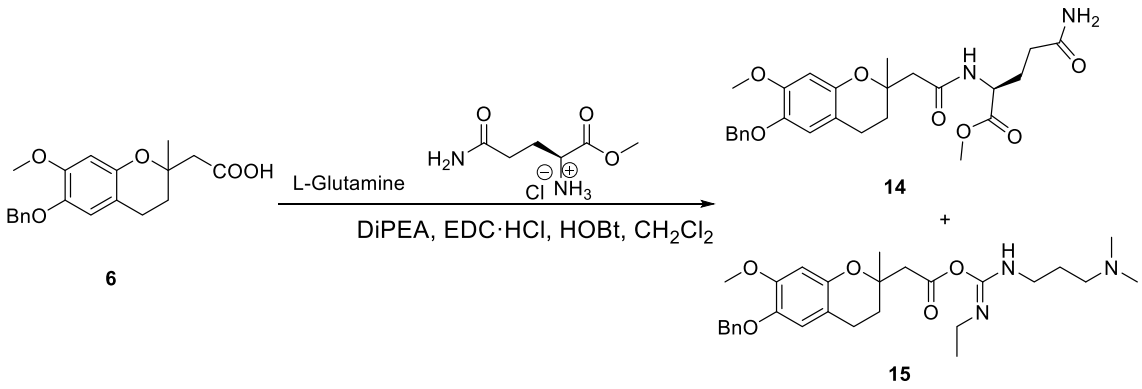

Scheme 3.13. Attempted synthesis of L-Glutamine derivative **14** using EDC·HCl and HOBt. The by-product **15** as major impurity.

According to this result, we decided to test other conditions. For instance, the use of other coupling agents, HATU,[60] DCC and EDC·HCl, with and without HOBt or DMAP, were tried with DiPEA as base and a small amount of CH_2Cl_2 (Scheme 3.14). Obtained results are shown in Table 3.2.

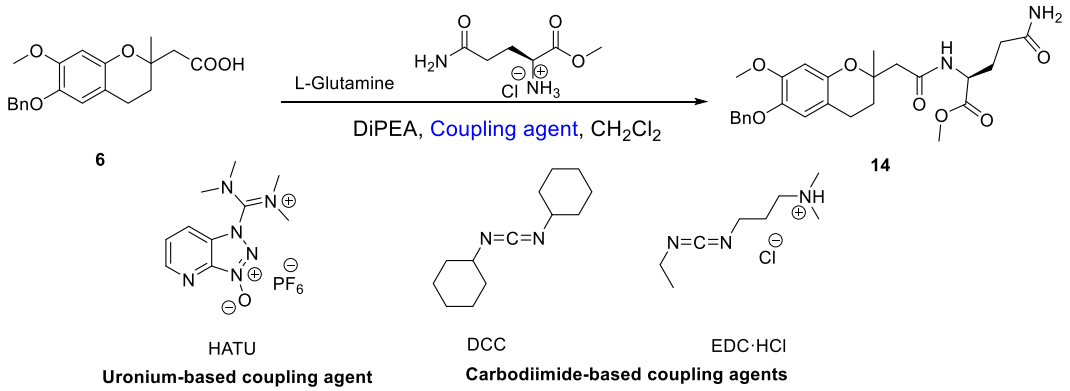

Scheme 3.14. *Test of different coupling reagents for the synthesis of L-Glutamine derivative* ***14****.*

In entry 1, EDC·HCl and HOBt were used for 20 hours at room temperature. Many impurities were observed and the reaction was discarded. In entry 2, we decided to change the coupling agent to a more reactive uronium salt, HATU, but the result was not different, even though the reaction was left reacting for 7 days. In entry 3, we repeated entry 1 conditions but without the additive HOBt, and, although the reaction time was increased from 20 to 48 hours, no improvement was observed. Although the desired compound was observed by HRMS and HPLC-UV in the crude reactions for entries 1, 2 and 3, we decided not to isolate the amide due to these negative results.

Table 3.2. *Conditions and results tested for improving the synthesis of L-Glutamine derivative* ***14****.*

Entries	Conditions				Yield (%)[a]
	Coupling Agent	Additive	Time (h)	T (ºC)	
1	EDC·HCl	HOBt	20	r.t.	*Not isolated*
2	HATU	-	168 (7 d)	r.t.	*Not isolated*
3	EDC·HCl	-	48	r.t.	*Not isolated*
4	DCC	-	48	r.t.	37
5	DCC	DMAP	48	30	40

[a] The yield was calculated for L-Glutamine derivative **14** only in cases where it was isolated from the crude reaction mixture.

Then, we changed the carbodiimide-like coupling agent to DCC. In entry 4, we tried the reaction without additive. After two days of reaction at room temperature, we isolated the L-glutamine derivative **14** in 37% yield after purification. Later on, we decided to try it with DMAP as additive (entry 5). After 48 hours heating at 30ºC, we obtained the desired derivate **14** in 40% yield. Therefore, using DCC, the addition of an additive did not improve the yield essentially, but fewer impurities were observed. The isolation of amide **14** in entries 4 and 5 was achieved by reverse phase chromatography after filtration of urea-precipitates. As a major advantage, when using DCC we observed smaller amounts of impurities than in the other experiments.

Finally, the L-glutamine derivative **14** (40% yield) was obtained using DCC, with catalytic amounts of DMAP in CH_2Cl_2 at 30ºC for 48 hours. Filtration and subsequent purification by chromatography in reverse phase were required to isolate the pure amide (Scheme 3.15).

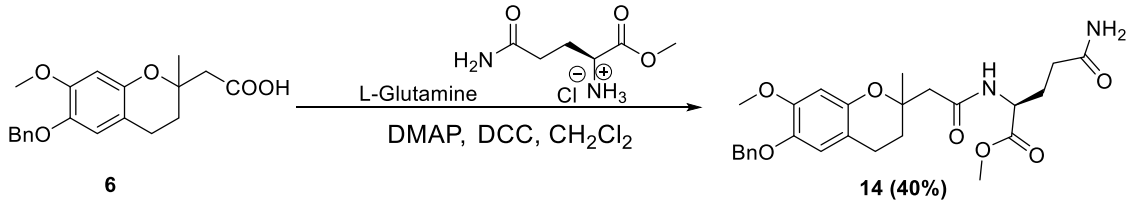

Scheme 3.15. *Synthesis of L-glutamine derivative* ***14*** *using DCC and DMAP.*

III.3.2.3 Preparation of primary amide functionality derivative ***16*** *synthesis*

The first approach for the synthesis of amide derivative **16** (Scheme 3.16) was the preparation of the acyl chloride intermediate from acid **6** following by an addition of NH_3. Thus, acid **6** was reacted with oxalyl chloride and catalytic amounts of DMF to get the acyl chloride **17**. After 20 hours of reaction at room temperature, an excess of 0.5 M NH_3 in dioxane was added. However, the generation of amide **16**

from acyl chloride did not take place efficiently. We attribute this result to a partial hydrolysis of the acyl chloride during the reaction or likely to its incomplete formation.

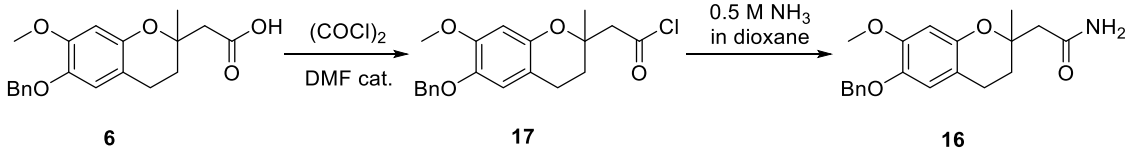

*Scheme 3.16. Synthesis of the terminal amide analogue **16** through the acyl chloride intermediate.*

Therefore, we decided to follow the same methodology described in section III.3.2.1, page 62. In this case, EDC was used as coupling agent and ammonia as nucleophile instead of a primary amine. Thus, the primary amide **16** was obtained from the acid **6** in 54% yield, after 24 hours reacting at room temperature and further chromatographic purification (Scheme 3.17).

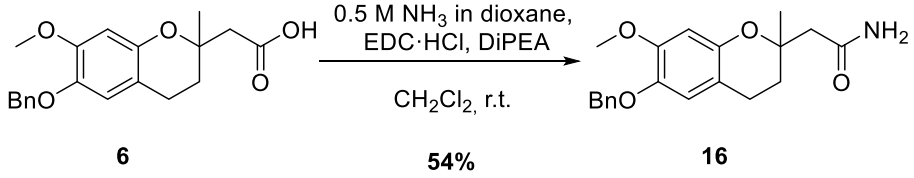

*Scheme 3.17. Synthesis of amide **16** following by a coupling reaction between acid **6** and ammonia.*

In general terms, a distinctive structural feature for compounds from **7**-**14** and **16**, the presence of the carbonyl of amide signal in the ^{13}C-NMR spectra at around 173 ppm was observed for all derivatives. Also, the formation of diastereomeric mixtures observed in the ^{1}H-NMR spectra for some of these derivatives evidenced the presence of the desired coupling product. In addition, the HRMS analysis for each product confirmed the success of the reaction to obtain compounds **7**-**14** and **16**.

Specifically, the ^{1}H-NMR spectrum of each compound was analysed to assure the purity of compounds **7**-**14** and **16**.

III.3.2.4 Deprotections

III.3.2.4.1 Basic hydrolysis of methyl ester

Methyl ester was removed in compounds **8** to **14** by hydrolysis under basic conditions. Thus, methyl ester derivatives were treated with aqueous 4 M NaOH and dioxane as co-solvent in a 1:1 v/v ratio for 15 hours at reflux (Scheme 3.18). The absence of proton signal of H_{COOCH3} in the ^{1}H-NMR spectrum within 3.7-3.6 ppm supported the formation of the acids in moderate to high yields (61-93%).

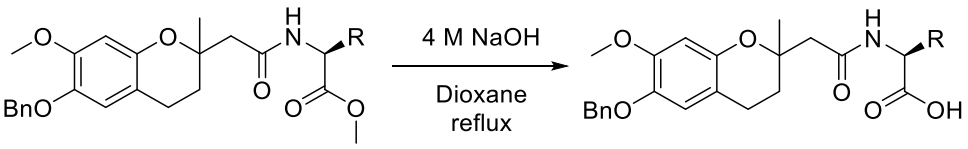

*Scheme 3.18. Deprotection of methyl ester in compounds from **8**, **9**, **10**, **13** and **14**.*

III.3.2.4.2 Hydrogenolysis

Phenols are unstable under basic conditions and light, forming the corresponding phenolate or phenoxyl radicals. For this reason, the benzyl ether deprotection should be the last step in the synthetic pathway to achieve the final products.

In the literature the hydrogenolysis appears as the best and cleanest way to remove a benzyl ether group using 10% w/w Pd/C as catalyst.[61,62] Thus, the amide dissolved in MeOH or EtOH, previously degassed with N_2, was added to a dispersion of Pd/C in the same solvent and submitted to 1 atmospheres of hydrogen for 6 hours at room temperature (Scheme 3.19). For amides **11** and **12**, the hydrogenolysis was not only used to deprotect the phenol but also the acid group. For this reason, the pressure of hydrogen used was higher, up to 2 atm.

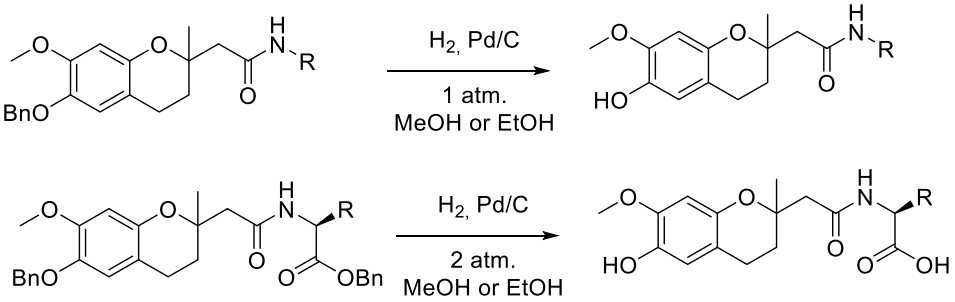

*Scheme 3.19. Deprotection of phenol and acid to obtain the final compounds: **A**-**I**.*

Comparing the HRMS analysis of experimental m/z for cation $[M+H]^+$ of pure products with their calculated values, we observed differences of 0.98 ppm for L-glutamine derivative **H**. Moreover, the comparison of ^{13}C-NMR spectra of compound **14** with **H** showed differences in carbonyl signals. In compound **14**, three doublet signals at 174.5, 172.5 and 170.5 ppm were observed. On the contrary, in derivative **H** the signals were at 176.5, 175.0 and 172.5 ppm. These differences were attributed to a hydrolysis of terminal amide of glutamine side chain during the hydrolysis of methyl ester under high basic conditions (Scheme 3.20). Therefore, the compound **H** is not L-glutamine analogue, if not L-glutamic acid derivative. However, for the purpose of the present Thesis both are good to improve the delivery through Blood-Brain Barrier (BBB).

[61] a) Hartung, W.H.; Simonoff, R. *Org. React.* **1953**, *7*, 263-326. b) Varma, R.S.; Chatterjee, A.K.; Varma, M. *Tetrahedron Lett.* **1993**, *34,* 4603-4606. c) Knuchsen, K.R.; Holden, J.; Ley, S.V.; Ladlow, M. *Adv. Synth. Catal.* **2007**, *349*, 535-538.
[62] Tran, V.H.; Hantharaj, R.; Roufogalis, B.D.-, Duke, C.C. *Eur. J. Org. Chem.* **2006**, 2970-2976.

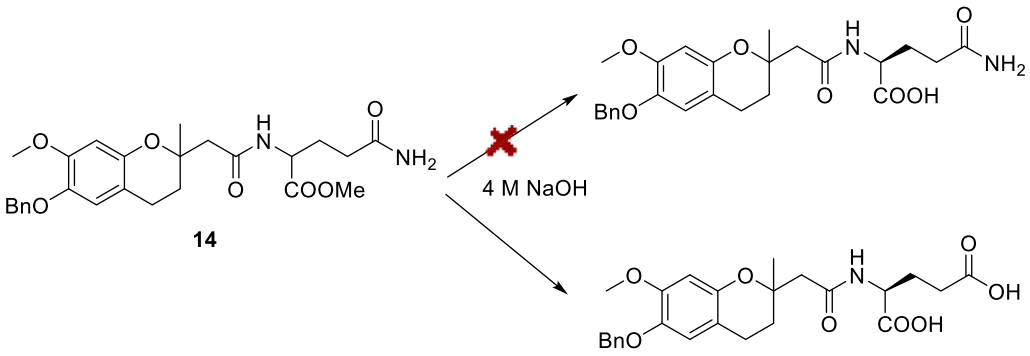

Scheme 3.20. *Hydrolysis of terminal amide of glutamine side chain under high basic conditions to form the glutamic acid derivative.*

The final derivatives **A-I** were obtained, in general, in high yields (50-99%), after the elimination of the Pd/C by filtering through Celite® and the evaporation of solvent under vacuum.

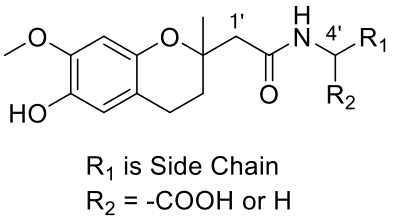

Figure 3.8. *Representation of protons considered in the analysis of Table 3.3.*

Table 3.3. *Distinctive structural feature signals for compounds **A-I** in the ^{1}H-NMR spectra and their m/z for cation $[M+H]^+$ in the corresponding HRMS spectra. R_2 and R_1 correspond to the variability on CR-6 scaffold.*

Derivative	*Distinctive ^{1}H-NMR signals (ppm)*	*$R_2 + R_1$*	*m/z for $[M+H]^+$ in HRMS*
A	6.68 – 6.64, 6.54, 3.41, 2.69 – 2.60, 2.46	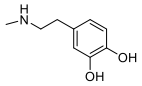	388.1768
B	7.10–7.05, 6.97–6.92, 6.72–6.66, 6.61–6.57, 4.68, 3.12, 2.93, 2.89, 2.69 – 2.39	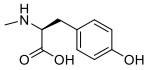	416.1730
C	4.59, 2.61, 1.51, 1.44		324.1458
D	4.57, 2.78 – 2.62, 2.36 – 2.19, 1.07, 1.03, 0.95		352.1763
E	4.67 – 4.61, 3.60, 3.55 – 3.43, 2.80 – 2.57, 2.50,2.11 – 1.83		350.1593
F	7.32 – 7.20, 7.13, 7.03, 4.91, 3.31 – 3.19, 3.15, 3.01, 2.72 – 2.39	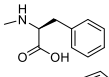	400.1766
G	7.57, 7.50, 7.36 – 7.27, 7.14, 7.07, 6.98, 4.85 – 4.76, 3.41 – 3.36, 3.35, 3.26, 3.17, 2.64 – 2.36	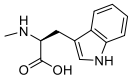	439.1864
H	4.51 – 4.40, 2.62 – 2.42, 2.42 – 2-34, 2.25 – 2.14, 2.00 – 1.88	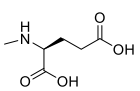	382.1521
I	6.28, 5.77, 2.76 – 2.44		252.1207

All compounds in Family 1 were characterized by ^{1}H- and ^{13}C-NMR. The signal at around 173 ppm in ^{13}C-NMR demonstrated the presence of the amide. The mass spectrum for each compound also confirmed they had been obtained. In Table 3.3 all distinctive structural feature signals in the ^{1}H-NMR spectra (for protons $H_{1'}$, $H_{4'}$ and side chain, Figure 3.8) for each compound **A**-**H** and their m/z value for $[M+H]^+$ are shown.

III.4 SYNTHESIS OF FAMILY 2 ANALOGUES

Amino derivatives from glucose and retinol were not commercially available, but their carboxylic acid forms were. For this reason, derivatives from Family 2 were synthesized by a coupling reaction between amine **18** and the required carboxylix acid.

III.4.1 Initial approaches for the synthesis of amine 18

III.4.1.1 Reductive amination of an aldehyde

Reductive amination of carbonyl compounds is a very important and powerful tool to target the synthesis of structurally diverse primary, secondary and tertiary amines. The sequence proceeds through the formation of an imine or iminium intermediate from the reaction of a carbonyl compound with NH_3, a primary or secondary amine, followed by an *in situ* reduction to an amine of higher order (Scheme 3.21).[63]

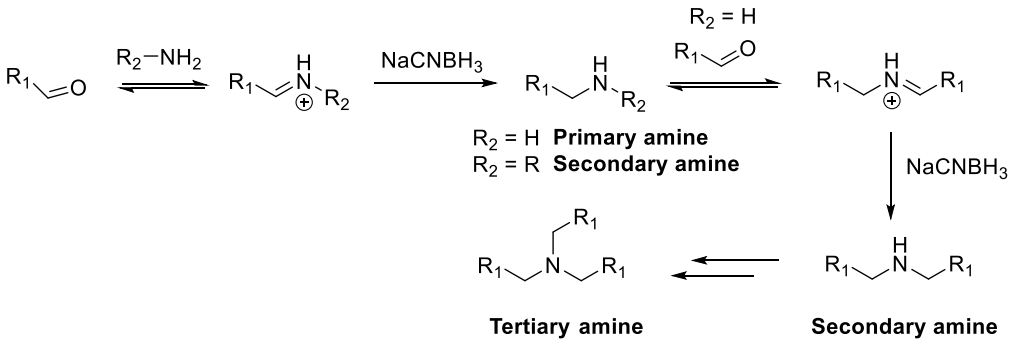

Scheme 3.21*. Reductive amination reaction for the synthesis of primary, secondary and tertiary amines.*

*III.4.1.1.1 Synthesis of aldehyde **19***

First of all, the required aldehyde **19** was obtained in 99% yield from primary alcohol **2** following an oxidation with 2-iodoxybenzoic acid (IBX) in EtOAc at reflux for 4 hours (Scheme 3.22).

[63] Miriyala, B.; Bhattacharyya, S.; Williamson, J.S. *Tetrahedon* **2004**, *60*, 1463-1471.

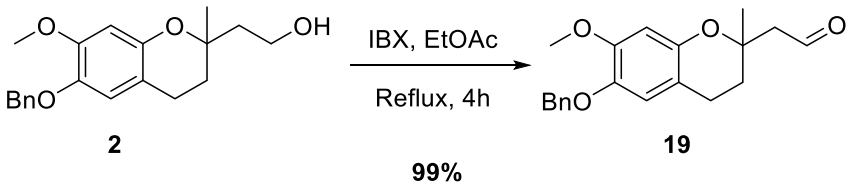

2 **19**

99%

*Scheme 3.22. Synthesis of aldehyde **19** from primary alcohol **2** by oxidation with IBX reagent.*

As distinctive structural features for aldehyde **19**, it can be mentioned the signal of –CHO at 9.90 ppm in the ^{1}H-NMR spectrum and at around 201 ppm in the ^{13}C-NMR spectrum. In addition, the molecular mass at m/z 327.1596 for $[M+H]^+$ in HRMS confirmed the presence of aldehyde **19**.

III.4.1.1.2 Attempts of preparation of amine 18 through reductive amination.

Catalytic hydrogenation is commonly used to reduce *in situ* formed imines but there are several incompatible functional groups that can be reduced as well, such as nitro, cyano, C-C multiple bonds, and protecting groups like benzyl ether.[63] Among the borohydride reagents, sodium cyanoborohydride and sodium triacetoxyborohydride have found significant applications as reducing reagents.[63,64] However, these reagents are limited sometimes in scope. Many of the reported protocols for reductive amination work well for the preparation of tertiary amines, but, in many cases, the synthesis of primary and secondary amines are compromised by over-alkylation reactions.[63] This is consequence of the increased reactivity of the primary amine product compared to ammonia. Traditionally, protecting groups have been used when preparing primary amines *via* metal hydride reductive amination, but the incorporation of a protecting group in a synthetic route has a number of disadvantages: it increases the steps in the sequence, it decreases in atom-economy and sometimes it can affect on the orthogonality and the reactivity. As a solution, some methodologies have been described to prepare primary amines from ketones, but in many cases, these reactions do not work with aldehydes.[65b]

A few years ago, a reduction developed by Vasella *et al.* was described for the formation of alkenylamines from halo-glycoside precursor in a two-step reaction. It involved the over-night reflux of a suspension of Zn, NH_4OAc in excess, NH_3, $NaCNBH_3$ and the iodo-sugar as aldehyde precursor in ethanol, to form exclusively the primary amine. Following this methodology, in a more recent work, Dangerfield *et al.*[65] explored the direct reductive amination of several unprotected aldehydes. In this case, Zn was not used. These authors found a methodology to synthesize the primary amines from the unprotected aldehydes with moderate to high yields.

[64] a) Khan, S.N.; Bae, S.-Y.; Kim, H.-S. *Tetrahedron Lett.* **2005**, *46*, 7675-7678. b) Xu, Y.; Wang, Z.; Tian, Z.-Q.; Li, Y.; Shaw, S.J. *Chem. Med. Chem.* **2006**, *1*, 1063-1065. c) Kato, H.; Shibata, I.; Yasaka, Y.; Tsunoi, S.; Yasuda, M.; Baba, A. *Chem. Commun.* **2006**, 4189-4192.

[65] a) Dangerfield, E.M.; Timmer, M.S.M.; Stocker, B.L. *Org. Lett.* **2009**, *11*, 535-538. b) Dangerfield, E.M.; Plunkett, C.H.; Win-Mason, A.L.; Stocker, B.L.; Timmer, M.S.M. *J. Org. Chem*. **2010**, *75*, 5470-5471.

Following this methodology, aldehyde **19** was reacted with sodium cyanoborhydride, a saturated solution of ammonium acetate in ethanol and a solution of 30% NH_3 (Scheme 3.23). After 20 hours stirring at room temperature, the reaction was not completed. Therefore, it was heated to 85ºC for 2.5 hours, but although the conversion was complete, the dialkylated product was formed. The peaks in HPLC reverse phase and the mass at m/z 328.19 and 638.35 were evidences of these results.

Then, the order of addition of the reagents was changed to favour the formation of the primary amine. Therefore, the imine formation was monitored by ^{1}H-NMR (disappearance of the –CHO signal of aldehyde **19** at 9.9 ppm and appearance of the imine signal (NH=CH-) at 7.5 ppm). At this point, the reducing agent $NaCNBH_3$ was added, but, again, in all cases, the dialkylated product was obtained (Scheme 3.23).

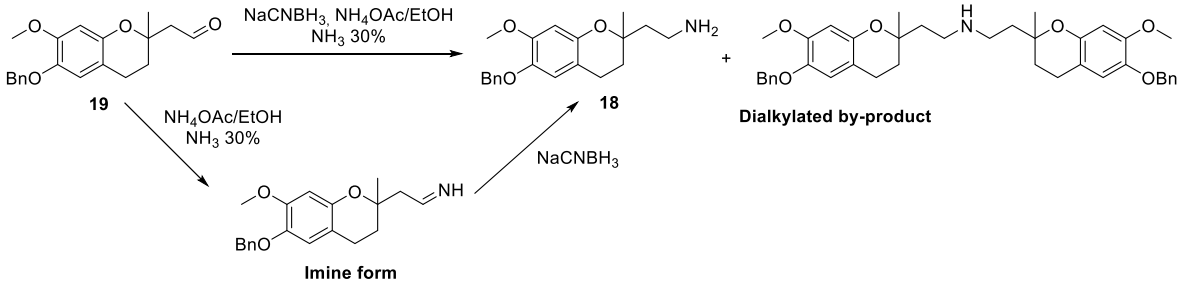

Scheme 3.23. *Attempts of the synthesis of amine **18** from the aldehyde **19** by reductive amination.*

From these experiments, we decided to change the methodology to prepare amine **18**.

III.4.1.2 Attempts to use a carbamate as intermediate for the synthesis of amine 18

The formation of the primary amine **18** by Dangerfield's modification of Vasella's reduction from unprotected aldehydes did not work for aldehyde **19**. Therefore, other reactions were taken into consideration. In 2008, Lehmann *et al*., following a recent report by Dube and Scolte to furnish the desired primary amine in good yields and purity, carried out some studies for the formation of a methyl carbamate from an aldehyde in the presence of a silane and trifluoroacetic acid (TFA), and the subsequent deprotection by hydrolysis under basic conditions. In spite of its efficacy, the only drawback of this method was the relatively long reaction times required to achieve the conversion (one or two days for the synthesis of the simple primary amines). The rapid one-pot microwave-assisted methodology developed by Lehmann *et al.,* afforded a simple and general protocol for parallel synthesis of several primary amines (Scheme 3.24).[66]

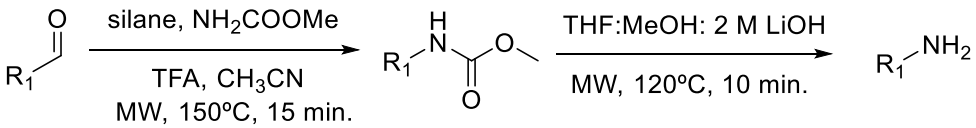

Scheme 3.24. *General synthesis of a primary amine via a carbamate intermediate using microwave activation.*

[66] Lehmann, F.; Scobie, M. *Synthesis* **2008**, *11*, 1679-1681.

Lehmann *et al.* tested several silanes and optimized the reaction using a one-pot microwave-assisted methodology.[66] They found that triethylsilane, triisopropylsilane, trichlorosilane and *tert*-butyldimethylsilane (TBDMSH) afforded the desired carbamate in the presence of TFA at 150ºC for 15 minutes under microwave irradiation. The basic hydrolysis, with 2 M LiOH in the microwave reactor at 120ºC, led to the primary amine in good yields and without further purifications.

The above methodology was applied to the formation of amine **18** using the triethylsilane as reducing agent, but, unfortunately it did not work. In our case, the synthesis of the carbamate intermediate and the hydrolysis were carried out in two separate reactions. The carbamate was isolated in 53% yield after purification. However, after attempting the carbamate deprotection process, the starting material was always recovered (Scheme 3.25). Alternatively, *tert*-butyl aminofluoride (TBAF),[67] was also tested for the deprotection of the carbamate, but it was also unsuccessful.

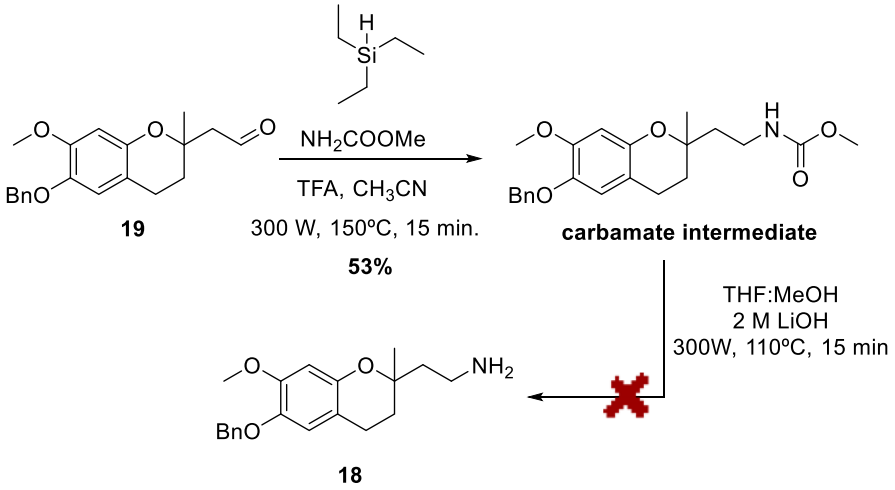

Scheme 3.25. *Synthesis of primary amine **18** from aldehyde **19** via carbamate intermediate.*

III.4.2 Synthesis of amine 18

As mentioned before, the reductive amination of the aldehyde **19** in order to get the primary amine **18** did not take place. Thereafter, we decided to change the starting point and return to the primary alcohol **2**. In this way, the amine would come from reduction of an azide which would be formed by nucleophilic substitution of an alcohol-derivative with a good *O*-leaving group (Scheme 3.26).

[67] Jacquemard, U.; Bénéteau, V.; Lefoix, M.; Routier, S.; Mérour, J.-Y., Coudert, G. *Tetrahedron*, **2004**, *60*, 10039-10047.

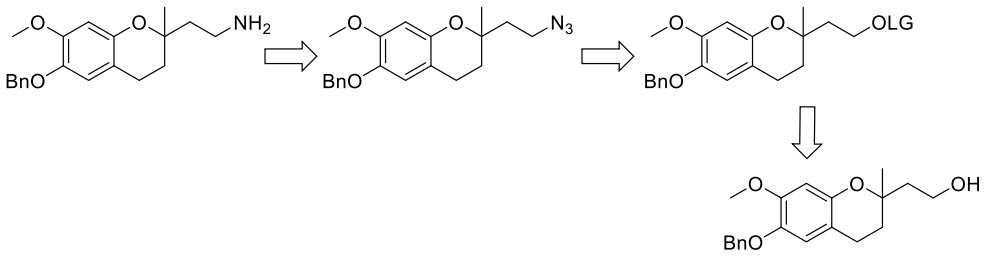

Scheme 3.26. *Retrosynthesis for an alternative formation of amine* ***18****.*

III.4.2.1 Synthesis of tosylate ***20***

An easy way to introduce a good leaving group in a primary alcohol is through the tosyl derivative. Thus, following the standard protocol, TsCl (previously purified to remove the residual *p*-toluenesulfonic acid) and pyridine were added to a solution of the primary alcohol **2** in a small amount of CH_2Cl_2. The reaction was stirred for 5 hours at room temperature to afford the tosyl-intermediate **20** in 83% yield after purification (Scheme 3.27).

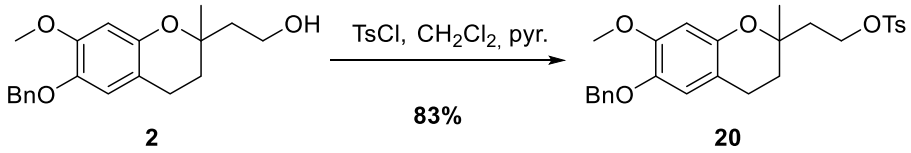

Scheme 3.27. *Synthesis of tosyl-intermediate* ***20****.*

The formation of compound **20** in high purity was evidenced in the ^{1}H-NMR spectrum by the presence of aromatic signals at 7.82-7.74, 7.39 ppm and a sharp singlet at 2.43 ppm (Me group), as distinctive structural features of the tosyl group (Figure 3.9). In addition, in the HRMS the mass at m/z 483.1775 for $[M+H]^+$ confirmed that we had intermediate **20**.

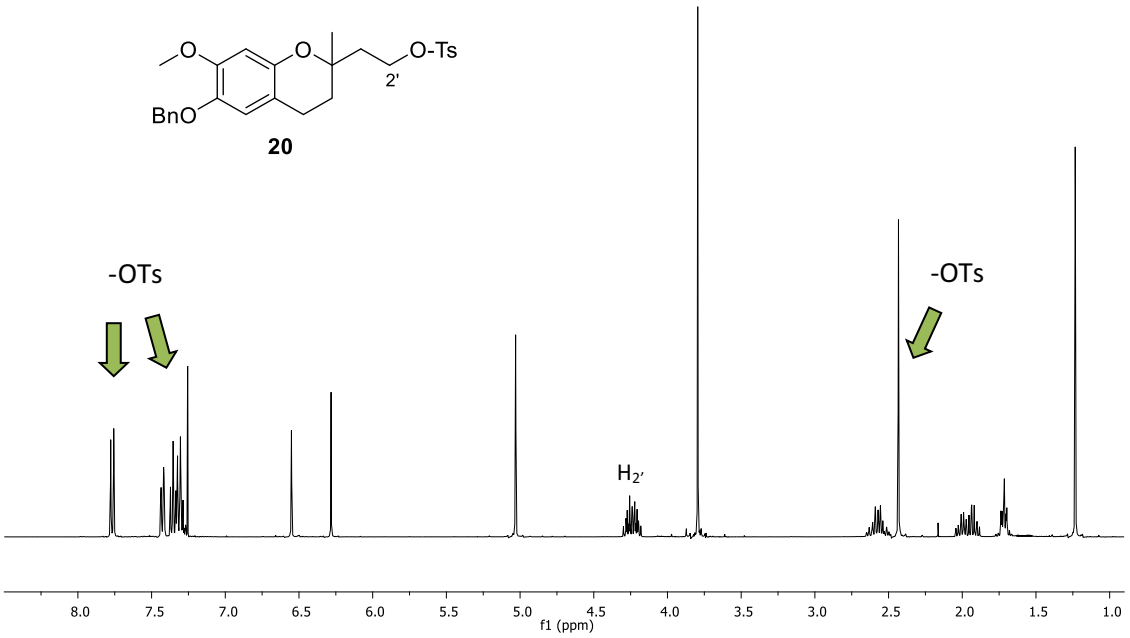

Figure 3.9. *^{1}H-NMR ($CDCl_3$, 400MHz) spectrum for tosylate derivative* ***20****.*

III.4.2.2 Synthesis of azide ***21***

The synthesis of the azide also took place following a standard procedure. Sodium azide was added to a solution of intermediate **20** in DMF and the mixture was stirred overnight at room temperature. Then, azide **21** was obtained as a pure product in 90% yield after eliminating the tosyl residue acid with water washes and the DMF by heating under vacuum (Scheme 3.28).

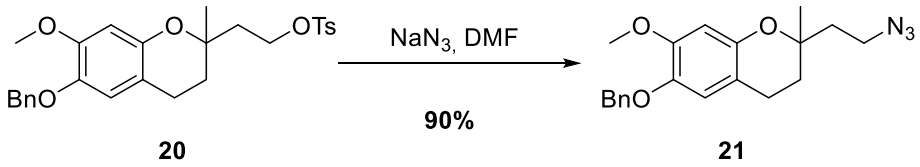

Scheme 3.28. *Synthesis of azide intermediate* ***21****.*

As distinctive structural features for azide intermediate **21**, it can be mentioned in the ^{1}H-NMR spectrum (Figure 3.10), the absence of the tosyl signals and the shift of the $H_{2'}$ signal from 4.24 ppm to 3.47 ppm that assured the absence of TsO- group. Moreover, in FTIR spectrum, the characteristic peak at 2097 cm^{-1} for the azide group evidenced the formation of azide **21** (Figure 3.11). In addition, by HRMS analysis, the mass m/z 354.1793 for $[M+H]^+$ confirmed the formation of desired compound.

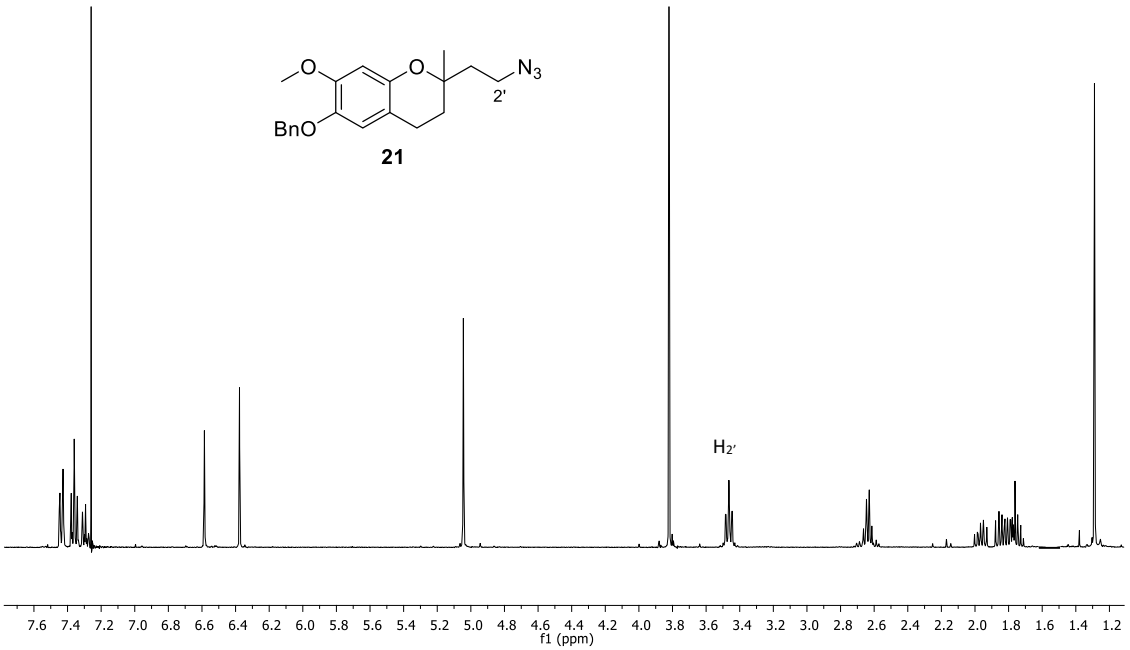

Figure 3.10. *^{1}H-NMR ($CDCl_3$, 400MHz) spectrum for azide derivative **21**.*

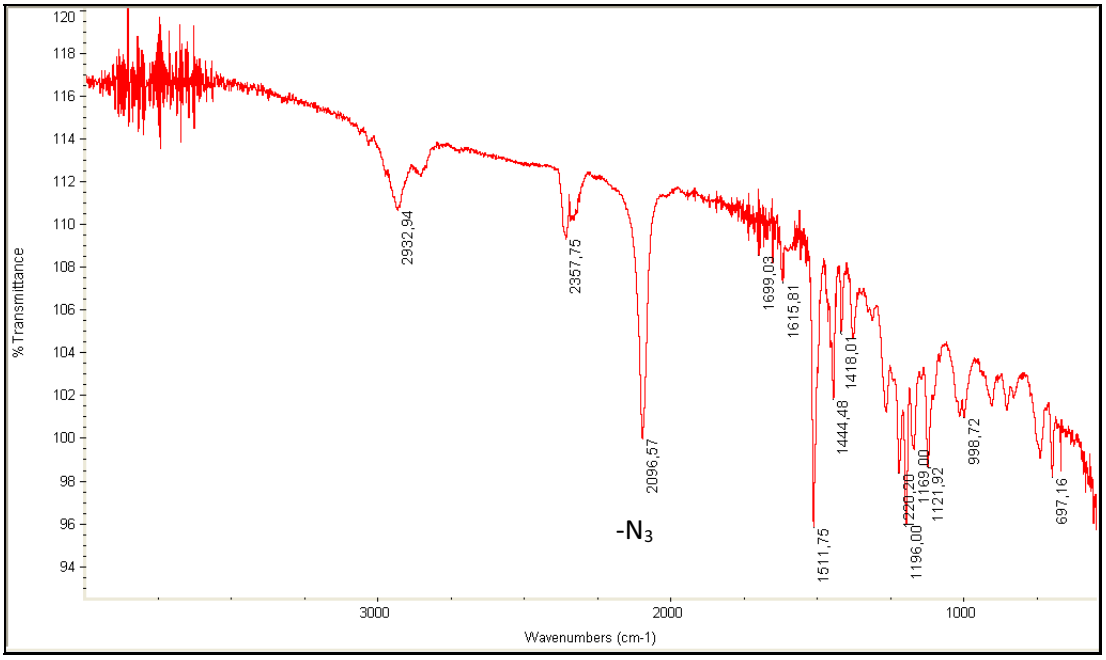

Figura 3.11. *FTIR spectrum for azide derivative **21**. The signal at 2096.57 cm^{-1} corresponds to the azide group.*

III.4.2.3. Reduction of azide to amine

III.4.2.3.1 Staudinger reaction

One of the most common and cleanest ways to reduce the azide is the Staudinger reaction. This reaction is a well-known and useful reaction in organic and biological chemistry to transform

azides into primary or secondary amines using phosphines as reducing agents under mild conditions. The mechanism of this reaction was proposed by Quan Tian *et al.*[68] and Lin *et al.*[69] (Scheme 3.29).

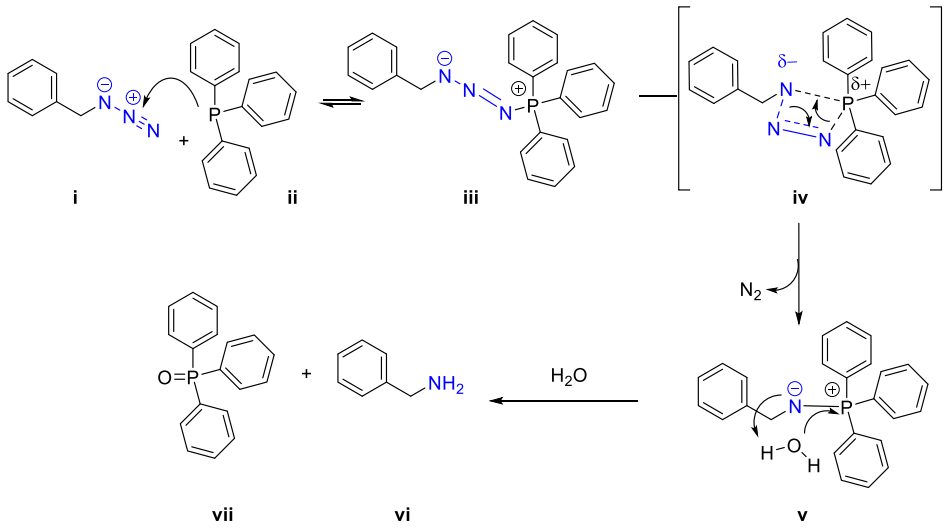

Scheme 3.29. *Mechanism of Staudinger reaction as proposed by Tian et al.[68] and Lin et al.[69]*

The mechanistic studies of the classical reaction between triphenylphosphine (PPh_3, **i**) and benzyl azide (**ii**) suggest that the lone pair electrons of phosphine **ii** attacks the terminal nitrogen atom of the azide **i** to yield the linear phosphazide intermediate **iii**. This intermediate can undergo intramolecular rearrangement *via* four-membered ring transition state (**iv**) to obtain a second intermediate, azaylide **v**, by concomitant loss of N_2. In the presence of water, azaylides **v** undergoes hydrolysis to form amine **vi** and phosphine oxide **vii** as a by-product (Scheme 3.29). In this reaction, the solvent polarity, the phosphine and the quantity of water are very important for a good performance of the conversion to achieve the desired primary amine.

Following this method, we synthesized primary amine **18** in good yield (82%). The phosphine PPh_3 was added to a solution of azide **21** in anhydrous THF and the mixture was stirred for 18 hours at room temperature to assure the formation of the azaylide intermediate and the loss of nitrogen. Then, water was added to hydrolyze the intermediate and form the desired primary amine **18**, which was isolated after purification by flash chromatograohy (Scheme 3.30).

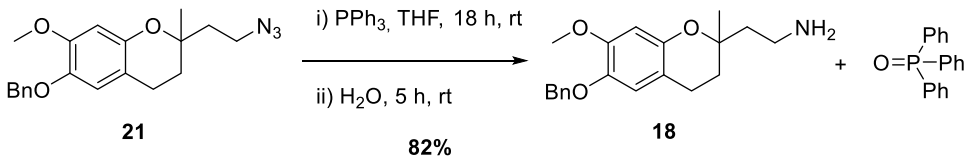

Scheme 3.30. *Synthesis of primary amine **18** with high yield following the Staudinger reaction.*

[68] Tian, W.Q.; Wang, Y.A. *J. Org. Chem.* **2004**, *69*, 4299-4308.
[69] Lin, F.L.; Hoyt, H.M.; Van Halbeek, H.; Bergman, R.G.; Bertozzi, C.R. *J. Am. Chem. Soc.* **2005**, *127*, 2686-2695.

As distinctive structural features of amine derivative **18**, it can be mentioned in the ^{1}H-NMR spectrum the appearance of exchangeable singlets corresponding to NH at 2.88 ppm and the change in the signal of $H_{2'}$ from 3.47 ppm in compound **21** to 2.62 ppm in amine **18**. In the ^{13}C-NMR spectrum, the decrease in chemical shift of the $C_{2'}$ from 46.6 ppm in **21** to 36.7 ppm in **18**, and also, in the FTIR spectrum, the absence of the peak at 2097 cm^{-1} evidenced the presence of amine **18**. In addition, in the HRMS the mass of $[M+H]^+$ at m/z 328.1908 confirmed the formation of amine derivative.

III.4.3. Coupling reactions for the synthesis of Family 2

The synthesis of amine **18** allowed us to prepare the derivatives of glucose and retinol by the coupling reaction explained in section III.3.2, page 59.

III.4.3.1 Retinol derivative J

Retinoic acid is an unsaturated molecule with high level of conjugation. In the presence of hydrogen and Pd/C the double bonds could be reduced. Therefore, the deprotection of the phenol of the amine **18** by hydrogenolysis was required before the coupling reaction. Deprotection of the amine **18** took place following the same procedure as explained before, in section III.3.2.4.2 page 67, for the rest of the compounds. By hydrogenolysis at 1 atmosphere and using Pd/C as catalyst the deprotection of the benzyl ether took place (58% yield). Subsequent coupling with retinoic acid using EDC·HCl as coupling agent in the presence of DIPEA as base was carried out. The retinoic derivative **J** was obtained in 38% yield after purification by flash chromatography on silicagel (Scheme 3.31).

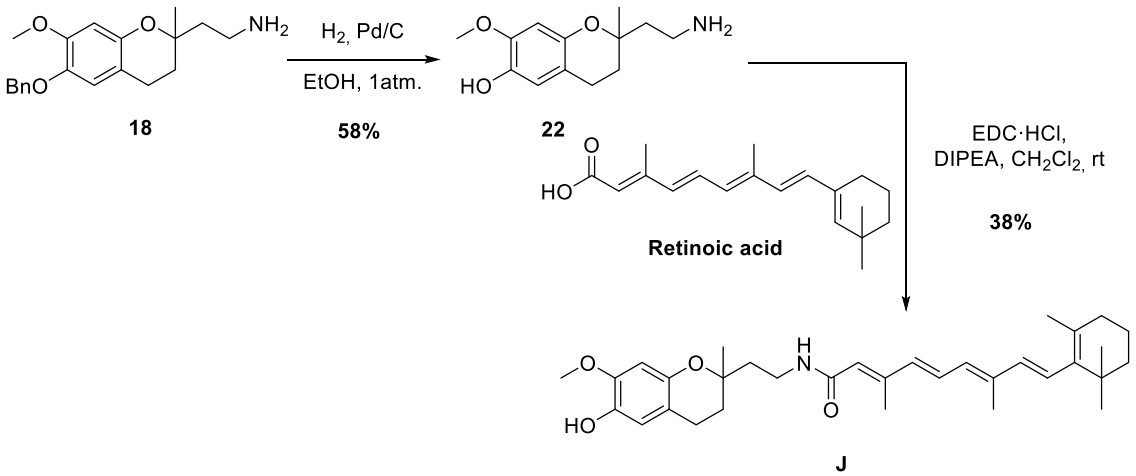

Scheme 3.31. *Synthesis of derivative **J** from the amine **18**.*

In this reaction, the nucleophile HOBt was not used because in previous experiments using this reagent, EDC·HCl and DIPEA in CH_2Cl_2, the yield of the reaction was lower.

The formation of the deprotected amine **22** was assured by NMR. As a distinctive structural feature, the absence of aromatic signals of –OBn in the ^{1}H- and ^{13}C-NMR spectra evidenced the formation of compound **22**. In addition, in the HRMS the mass corresponding to $[M+H]^+$ at m/z 238.1421 confirmed the loss of the benzyl protection. In the ^{1}H-NMR spectrum, the typical signals for protons in a conjugated unsaturated systems appeared within 6-7 ppm. Moreover, the signals for $–CH_3$ groups at 2.30, 2.01, 1.72 and 1.05 ppm evidenced the presence of final compound **J**. In HRMS, the mass at m/z 520.3414 for $[M+H]^+$ confirmed the presence of retinol derivative **J**.

*III.4.3.2 D-Glucose derivative **K***

Former experiments in couplings between D-gluconic acid and amine **18** following the method explained in section III.3.2.1 page 62, showed the negative interaction of free hydroxyl groups from the glucose ring in the reaction. Therefore, a good protecting group for secondary hydroxyl groups of D-gluconic acid was required. Several protecting groups like benzyl or acetal derivatives were envisaged. The benzyl moiety was thought initially as a good possibility because all benzyl groups, including the protected phenol, would be deprotected at the same time without affecting the number of steps of the synthetic pathway. However, during the benzyl protection the carboxylic acid could be protected as ester as well, which was out of our interest. We thought that the acyl protecting group could be a better option because it could protect the secondary alcohols and transform the carboxylic acid group into an anhydride, a good leaving group, at the same time.

Following a report in the literature,[70] D-gluconic acid was protected with acetic anhydride in the presence of iodine to afford the mixed anhydride 1,2,3,4-tetra-O-acetyl-D-methylglucopyranuronyl acetate **23a** in 96% (Scheme 3.34). The loss of the carboxylic acid group by the formation of the anhydride took place simultaneously. In this way, the coupling reaction between an amine and anhydride is more favourable than with an acid, and it does not require coupling agents to proceed.

Thus, amine **18** reacted with anhydride **23a** to form the desired amide **23** in 55% yield after purification by reverse phase chromatography (Scheme 3.32).

[70] El-Nezhawy, A.; Adly, F.G.; Eweas, A.F.; Hanna, A.G.; El-Kholy, Y.M.; El-Sayed, S.H.; El-Naggar, T.B.A. *Archiv. Pharm. Chem. Life Sci.* **2011**, *344*, 648-646.

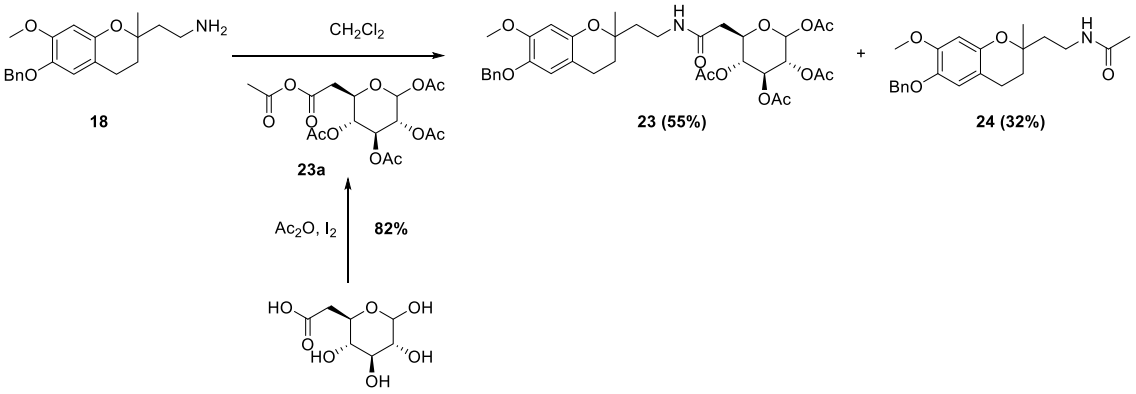

Scheme 3.32. *Synthesis of amide **23** from amine **18**.*

As distinctive structural features of compound **23**, in the ^{13}C-NMR spectrum nine signals between 170.05 and 168.9 ppm represented eight carbonyl moieties for –OAc (likely related to the α/β diastereomers of the anomeric carbon of glucose) and one carbonyl for the amide group. Moreover, four signals between 21.0 and 20.0 ppm and, in the ^{1}H-NMR spectrum (Figure 3.12), signals at 2.14 and 1.99 ppm corresponded to the methyl group of –OAc. In addition, in the HRMS the mass at m/z 686.2770 corresponding to $[M+H]^+$ confirmed that compound **23** was isolated.

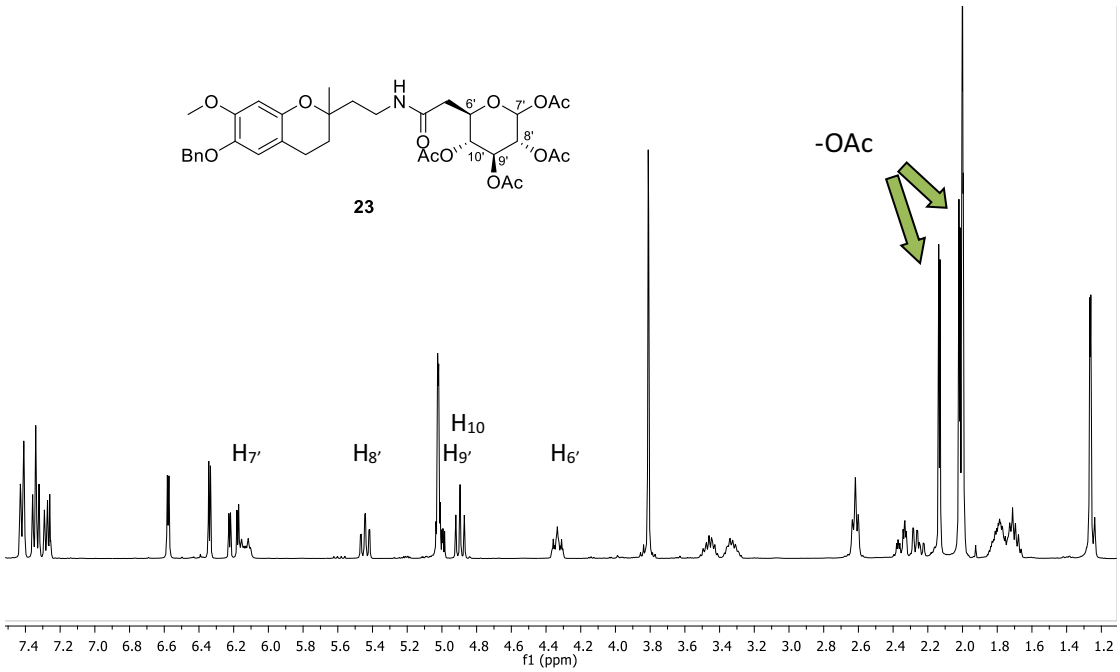

Figure 3.12. *^{1}H-NMR ($CDCl_3$, 400 MHz) spectrum for compound **23**. The characteristic protons for the glucose moiety ($H_{6'}$, $H_{7'}$, $H_{8'}$, $H_{9'}$ and $H_{10'}$) and the –OAc protecting group are pointed out.*

As shown in Scheme 3.34, the acetyl derivative **24** appeared as by-product in the synthesis of amide **23** in a 1.5:1 (**23**:**24**) ratio, taking into consideration that **23** is a mixture of four diasteriomers. Thus, the

nucleophilic primary amine **18** could attack by two different ways: first, to the desired carbonyl (A) to form amide **23**, and, second, it could also attack to the other carbonyl in the mixed anhydride (B) to form the acetyl derivative **24** (Scheme 3.33). Compound **24** was obtained in 32% yield, after the chromatographic purification.

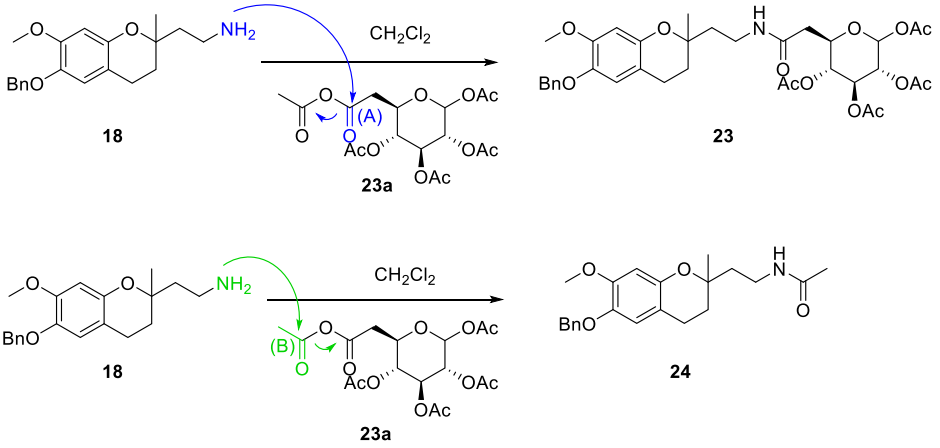

Scheme 3.33. *Two different pathways for the reaction of the amine **18** in the presence of **23a** intermediate.*

III.4.3.2.1 Deprotection of glucose derivative 23

If phenol was free, the molecule would not be stable under basic conditions. For this reason, before deprotecting the phenol by hydrogenolysis, acetyl groups from protected glucose should be removed. Accordingly, a saponification step was carried out. Following a standard methodology, the O-acetyl protection of amide **23** was reacted with a solution of sodium methoxide (MeONa) in MeOH for 5 hours at room temperature. The addition of acidic resin Amberlite 120 was necessary to stop the reaction (Scheme 3.34).

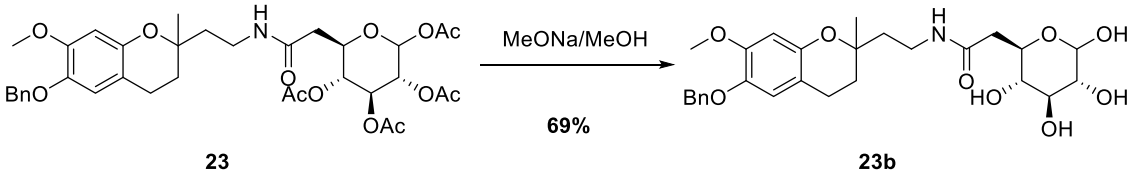

Scheme 3.34. *Removing the acetyl groups by saponification.*

In the ^{1}H-NMR spectrum of **23b**, the absence of signals of acetyl protons (CH_3 as singlets) within 2.14 – 1.99 ppm evidenced the success of the deprotection step. Therefore, the deprotection of benzyl ether to phenol was carried out. Previous experiments showed that the hydrogenolysis of OH-glucose derivative at 1 atmosphere of hydrogen did not work after 24 hours at room temperature. Indeed, 2 atmospheres of

hydrogen and 7.5 hours of reaction, in presence of 10% w/w Pd/C, were required to afford the final product **K** in 67% yield (Scheme 3.35).

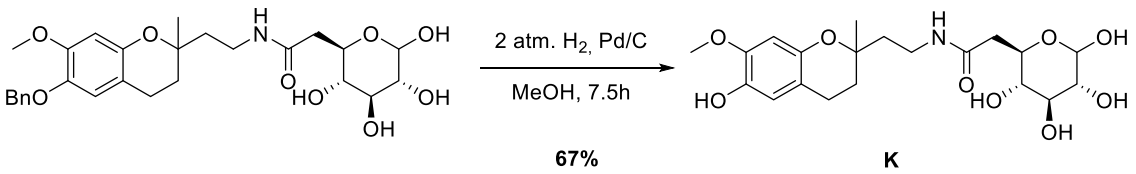

Scheme 3.35. *Deprotection of phenol to obtain the final derivative **K**.*

As distinctive structural features of the compound **K**, it was observed in the ^{1}H-NMR spectrum the change of chemical shift of protons CH in the glucose moiety from the compound protected **23** to final derivative **K**, and the absence of aromatic protons of –OBn and the signals within 2.16-1.98 ppm corresponding to –OAc. In addition, in the HRMS the mass at m/z 428.1902 for $[M+H]^{+}$ confirmed the formation of compound **K**.

*III.4.3.3 Acetyl derivative **L***

Although the acetyl derivative **24** could be obtained as a by-product of the coupling reaction between the amine **18** and D-glucose anhydride, (see page 78), we were interested in its preparation and, therefore, improved procedures for its synthesis were investigated. Thus, to a cold solution of the amine **18** dissolved in a small amount of CH_2Cl_2 it was added acetyl chloride and triethylamine, NEt_3. The mixture was stirred for 24 hours at room temperature to furnish the acetyl derivative **24** in 66% yield (Scheme 3.36), after purification by flash chromatography.

The formation of derivative **24** from amine **18** was assured by NMR (Figure 3.13). As distinctive structural features, it can be mentioned, in the ^{1}H-NMR spectrum, the presence of singlet exchangeable for NH at 5.98 ppm, the increase of chemical shift for $H_{2'}$ from 2.62 to 3.52 and 3.64 ppm, and the appearance of a singlet at 1.93 ppm corresponding to methyl group ($H_{5'}$). In addition, in the HRMS the mass at m/z 370.2048 corresponding to catión $[M+H]^{+}$ confirmed the formation of derivative amide **24**.

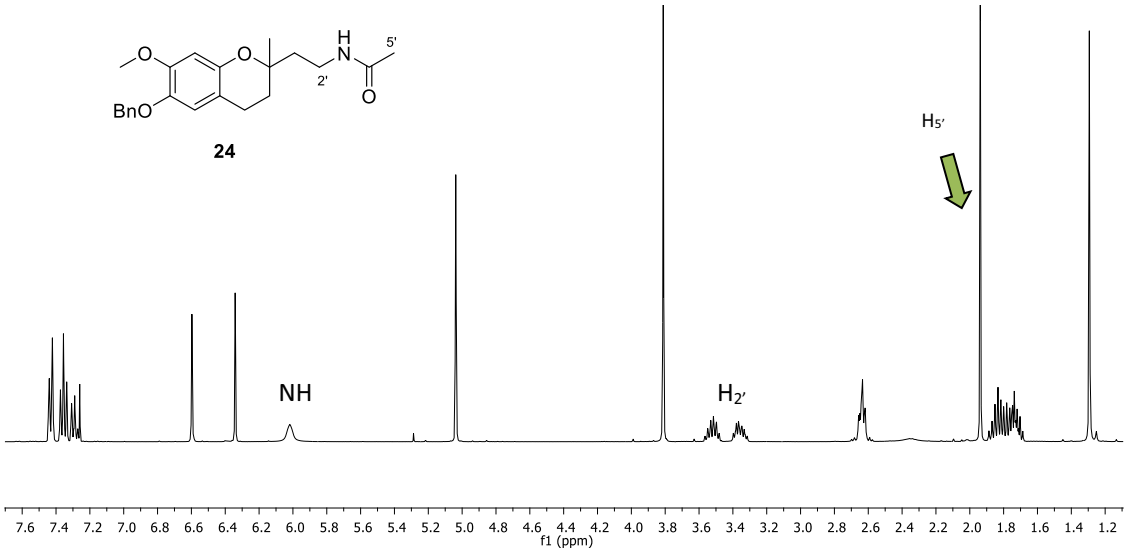

Figure 3.13. *^{1}H-NMR ($CDCl_3$, 400 MHz) spectrum for compound **24**. Signals of NH, $H_{2'}$ and $H_{5'}$ are structurally distinctive of **24**.*

Afterwards, compound **24** was hydrogenated under 1 atmosphere of hydrogen in the presence of 10% w/w Pd/C to deprotect the benzyl ether. Thus, the final product **L** was obtained in 95% yield, after filtering through Celite® (Scheme 3.36).

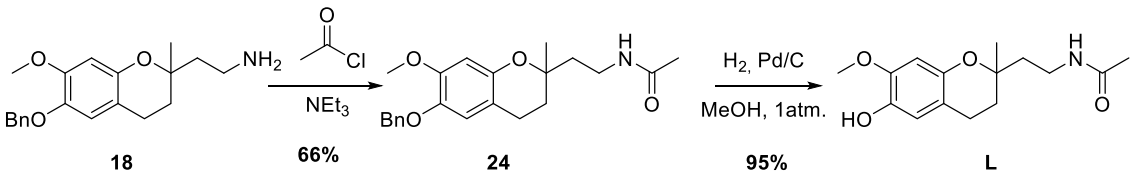

Scheme 3.36. *Synthesis of acetyl derivative **L** from amine **18**.*

As distinctive structural features of compound **L**, it can be mentioned the signal at 1.88 ppm corresponding to the methyl group of the acetyl moiety in the ^{1}H-NMR spectrum and the signal at 169.71 ppm for acetyl carbonyl in the ^{13}C-NMR spectrum. Moreover, the absence of peaks from –OBn group evidenced the compound **L**. In addition, in the HRMS the mass at m/z 280.1517 for $[M+H]^+$ confirmed the formation of derivative **L**.

III.5 SYNTHESIS OF ANALOGUES IN FAMILY 3

Family 3 consists of only two compounds: **M** and **N**. The synthesis of derivative **N** came from the hydrogenolysis of acid **6**, whose synthesis was commented in section III.3.1 in page 59. Thus, in this section, only the synthesis of derivative **M** is explained. These two compounds are quite different from the rest of derivatives due to the fact that they are free carboxylic acids and do not have an amide bond.

III.5.1. Synthesis of amino acid derivative M

III.5.1.1 Strecker reaction

The Strecker reactionis the typical way for preparing α-aminonitriles, which are versatile intermediates for the preparation of α-amino acids *via* a final hydrolysis of the nitrile group.[71] The reaction takes place through the addition of cyanide to an imine. This reaction starts with the *in situ* generation of hydrogen cyanide from equimolar amounts of cyanide salts, like sodium cyanide, and ammonium chloride. Simultaneously, ammonia condensates with an aldehyde group present in the starting material to form an imine (Scheme 3.37). This condensation starts with the protonation of the aldehyde in acid media and subsequent nucleophilic attack of ammonia. A reorganization of protons and the loss of water yields the imine. A subsequent nucleophilic attack of cyanide to the electrophilic carbon of the imine gives the α-aminonitrile. During this process several equilibria take place, and the amount of water in the reaction media must be controlled to avoid the reversal of the reaction to the starting material by hydrolysis of the imine. For this reason, molecular sieves or magnesium sulfate are used as additives (Scheme 3.37).

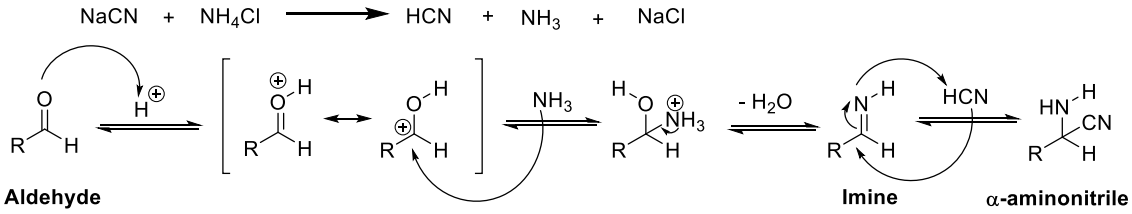

Scheme 3.37. *Strecker reaction's mechanism.*

In particular, the method of Keuthe *et al.*, for the synthesis of α-amino acids *via* Strecker reaction, was followed to synthesize the aminonitrile **25**.[71e] Accordingly, a solution of aldehyde **19** (section III.4.1.1.1 in page 69), in anhydrous methanol, was added to a cold mixture of 0.5 equivalents of dry magnesium sulfate, 0.5 equivalents of ammonium chloride, 1 equivalent of sodium cyanide and a solution in excess of 7 M NH_3 in MeOH. After 3-4 hours at 30ºC, the α-aminonitrile **25** was isolated in 96% yield after purification as a 1:1 mixture of diastereomers (Scheme 3.38).

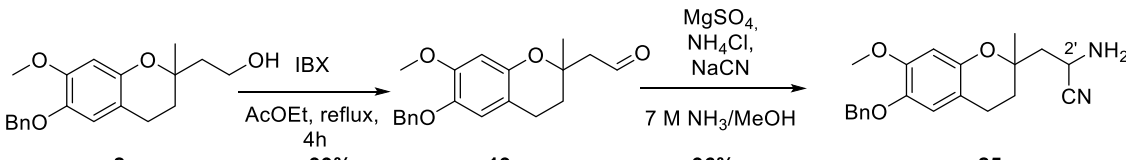

Scheme 3.38. *Synthesis of aldehyde **19** and aminonitrile **25**.*

[71] a) Duthaler, R.O. *Tetrahedron* **1994**, *50*, 1539-1650. b) Vincent, S.P.; Schleyer, A.; Wong, Ch.-H. *J. Org. Chem.* **2000**, *65*, 4440-4443. c) Yadov, J.S.; Reddy, B.V.S.; Eeshwaraiah, B.; Srinivas, M. *Tetrahedron* **2004**, *60*, 1767-1771. d) Cativiela, C.; Díaz-de-Villegas, M.D *Tetrahedron Asymmtr.* **2007**, *18*, 569-623. e) Kuethe, J.T.; Gauthier, D.R., Jr.; Beutner, G.L. *J. Org. Chem.* **2007**, *72*, 7469-7472. f) Pérez-Fuentes, Y.; Taylos, J.E.; Tickell, D.A.; Mahon, M.F.; Bull, S.D.; James, T.D. *J. Org. Chem.* **2011**, *76*, 6038-6047.

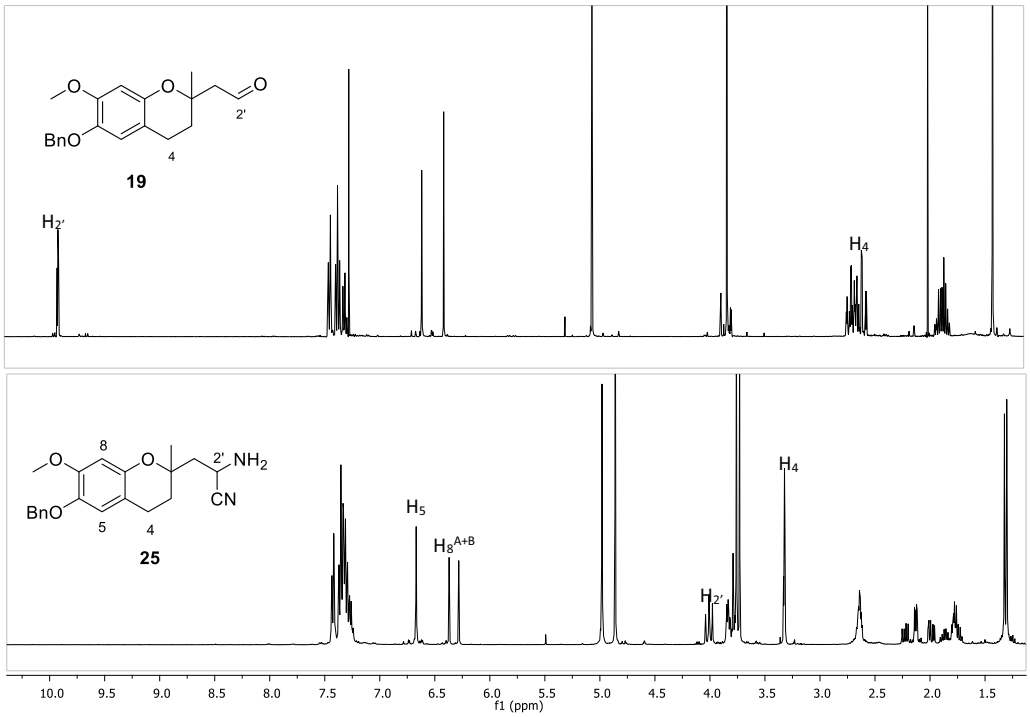

Figure 3.14. *^{1}H-NMR ($CDCl_3$, 400 MHz) spectra for compounds **18** (up) and **25** (down). For compound **18**, the signal of aldehyde group ($H_{2'}$) is a characteristic structural feature. For compound **25**, the appearance of diastereomeric mixture is observed. Moreover, the characteristic signals $H_{2'}$ and H_4, that changed from compound **18**, are pointed out.*

As a distinctive features of 25 it can be observed, in the ^{1}H-NMR spectrum, the signals at 4.01 and 3.97 ppm corresponding to proton $H_{2'}$ (anomeric CH) for both diastereomers and, in ^{13}C-NMR, at 122.6 ppm for the nitrile group. In addition, the observed mass m/z at 353.1882 ppm corresponding to $[M+H]^+$ in HRMS confirmed the presence of desired compound **25**. In Figure 3.13, the FTIR of aminonitrile **24** is shown. The peaks at 2208 cm^{-1} and 3321 cm^{-1} evidenced the formation of the aminonitrile moiety (Figure 3.12).

*III.5.1.2 Hydrolysis of nitrile **25***

The synthesis of the α-amino acid from α-aminonitrile **25** required the hydrolysis of nitrile group to carboxylic acid.[71d,f] Preliminary experiments were carried out under acidic conditions.[71d,f] A solution of 6 M HCl was added to a solution of aminonitrile **25** in acetone and the mixture was heated under reflux. Monitoring this reaction by reverse phase HPLC, we could observe a complex mixture of different species.

Accordingly, we decided to perform the reaction under basic conditions. A solution of 1M NaOH was added to the same volume of the aminonitrile **25** in dioxane and the mixture was stirred under reflux for 17 hours (Scheme 3.39). Monitoring the reaction by reverse phase HPLC, we observed the disappearance of the peak at 10.1 minutes and the appearance of a band at 9.9 minutes. In spite of the small difference in retention time, the formation of amino acid **26** could be assured by HRMS (m/z 372.17 for $[M+H]^+$).

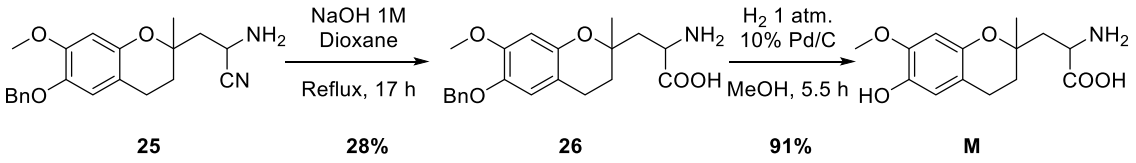

Scheme 3.39. *Synthesis of amino acid* ***25*** *and further deprotection of the benzyl ether to yield the derivative amino acid* ***M****.*

The amino acid **26** was obtained in 28% yield after a reverse phase chromatographic purification of the crude reaction mixture. With the aim of improving the yield of this reaction, the isolation of amino acid **26** was attempted by ion exchange chromatography using acid Amberlite 120 or Dowex 50 resins. Unfortunately the yield could not be improved.

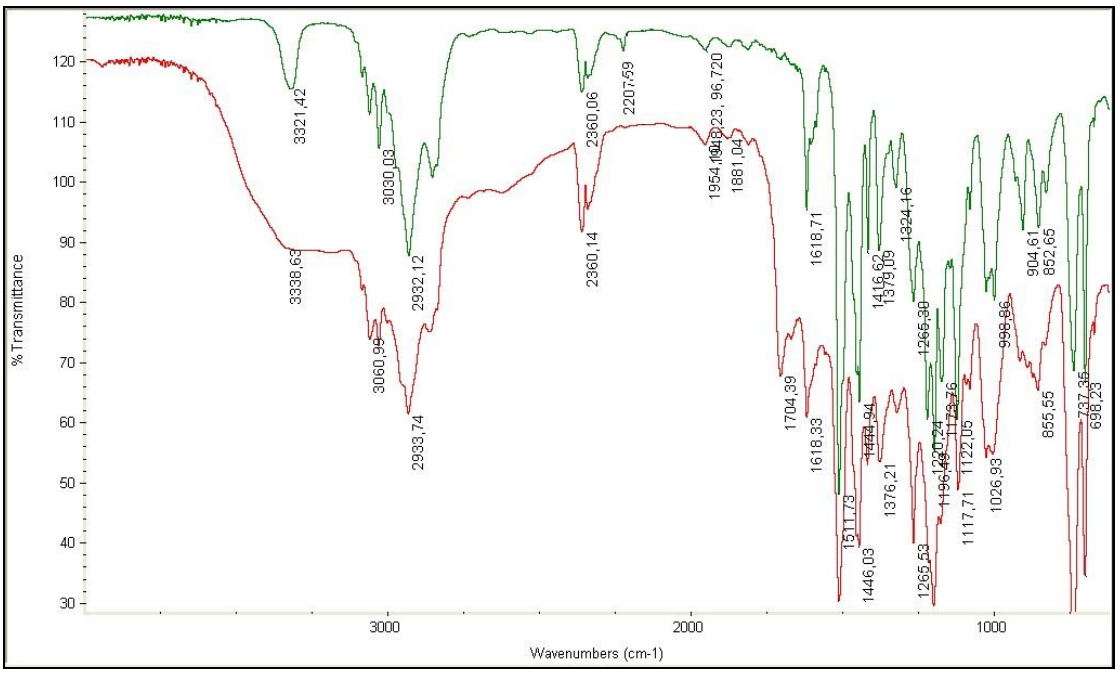

Figure 3.15. *FTIR for aminonitrile* ***25*** *(in green) and amino acid* ***26*** *(in red). For* ***25****, peaks at 2208 cm^{-1} and 3321 cm^{-1} evidenced the nitrile and the amino group, respectively. For* ***26****, peaks at 1704 cm^{-1} and 3339 cm^{-1} demonstrated the acid group (the carbonyl and the hydroxyl groups, respectively) in amino acid* ***26****.*

There were not many differences between the ^{1}H-NMR of aminonitrile **25** and that of amino acid **26**, but in the ^{13}C-NMR spectrum the presence of signals at 151.65 and 151.61 ppm for the carboxylic acid of two diasteriomers (versus 122.6 ppm for the nitrile) confirmed the formation of **26**. In addition, in the HRMS, the mass at m/z 372.1737 corresponding to $[M+H]^+$ also demonstrated the formation of the amino acid **26**. In Figure 3.14, the FTIR spectrum for the aminonitrile intermediate **25** and the amino acid **26** are compared. Signals at 1704 cm^{-1} and a broad band at 3339 cm^{-1} evidenced as well the formation of the carboxylic acid moiety (Figure 3.15).

After its isolation, the amino acid **26** was submitted to hydrogenolysis under 1 atmosphere of hydrogen in the presence of 10% w/w Pd/C for 5.5 hours at room temperature to yield the final amino acid derivative **M** in 91% yield, after filtration through Celite® (Scheme 3.39).

As distinctive features of **M** it can be mentioned the absence of aromatic signals of –OBn in ^{1}H- and ^{13}C-NMR spectra, and the decrease of mass to m/z 282.1326 (for $[M+H]^+$) in HRMS.

*III.5.1.3 Deprotection of benzyl ether for acid **6**. Synthesis of acid derivative **N***

Following the standard protocol explained in section III.3.2.4.2 page 67 for the deprotection of benzyl ether, acid **6** in EtOH was submitted to hydrogenolysis under 1 atmosphere of hydrogen in presence of 10% w/w Pd/C for 4 hours to yield acid **N** in 99% yield (Scheme 3.40).

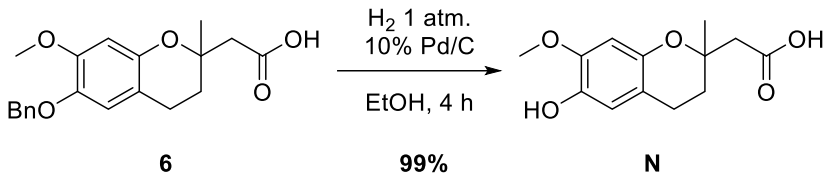

Scheme 3.40. *Synthesis of acid derivative **N**.*

The elimination of the benzyl group was demonstrated by the absence of the absorptions of –OBn within 7.41 to 7.25 ppm and the singlet of methylene group at 5.03 ppm. In addition, in the HRMS the mass at m/z 343.1552 corresponded to the cation $[M+H]^+$ of the desired product **N**.

III.6 STEREOSELECTIVITY FEATURES OF THE NEW ANTIOXIDANT COMPOUNDS

III.6.1 Biological importance of stereochemistry

Stereoisomers are those compounds that only differ from each other in the 3D geometry or spatial distribution of their atoms. Compounds with at least a chiral center, normally a carbon with four different substituents, have different non-superimposable stereoisomers. This difference can look like subtle and irrelevant, but due to its abundance in nature, and most important, in biological systems such as human body, molecules with a particular, well defined stereochemistry are recognized by receptors or enzymes to have a specific biological activity. These differences have indeed sweeping implications. Whilst one stereoisomer may have positive effects, the other one may be negative. For this reason, it is very important to know which stereoisomer of a drug is involved on the biological activity.

In biological systems, receptors and enzymes are considered as high-chiral macromolecules. Hence, a specific-chiral substrate is bound to the binding side of these macromolecules. A standard model of differentiation between stereoisomers in the recognition of a binding site is shown in Figure 3.16. While one stereoisomer of a chiral compound has the right 3D-shape to bind the target protein receptor, the other one does not, being ineffective for the described therapeutic target.

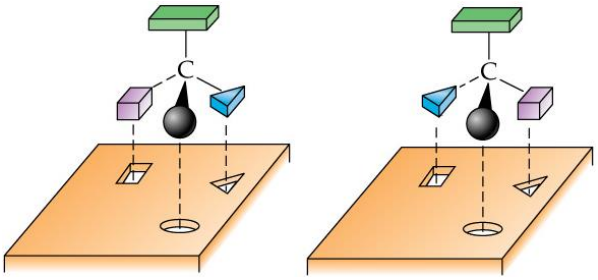

Figure 3.16. *Recognition of a chiral substrate by an enzyme or receptor in a biological system. On the left, the chiral substrate matches perfectly with the receptor, but on the right there is a mismatch.*

There are many stereoisomeric drugs involved on the biological activity. That is why the separation of their stereoisomers becomes an important issue. A famous example is Thalidomide, a drug used during the 1950s to suppress morning sickness on pregnant women. The drug was prescribed as a racemic mixture, but, unfortunately, only one stereoisomer was active for the specified effect while the other turned out to be a powerful theratogenic responsible for many birth defects. Moreover, the importance of chirality in biological systems is extended to more than just drugs. Only biological molecules, like amino acids and carbohydrates, with a certain stereochemistry, can be found in living organisms, and this fact determines the subsequent stereochemical interactions with other chiral molecules.

The chiral dihydrobenzopyran (chromanee) moiety is the core of numerous natural products and synthetic analogues showing an extensive array of biological activities. As mentioned, the most well-known chiral chromanees are the tocopherol family (vitamin E), serving as a natural lipophilic antioxidant and radical scavenger. Tocopherols possess a chromanee moiety and a terpenoid-side chain leading to a 6-chromaneol framework with a (*R*) stereogenic center at C_2 and two (*R*) configured stereocenters at the side chain. Recent studies have shown that (*2S*)-configured tocopherols have no antioxidant effect in biological systems because they are not accepted as a substrate by the *R*-tocopherol transfer protein (TTP), responsible for the transport of vitamin E into the tissue. On the other hand, the configuration of the stereogenic centers in the side chain seems to have no influence on the antioxidant activity. Thus, (*R,R,R*)-α-Tocopherol is the biologically most active member of the vitamin E family, capturing highly reactive free radicals formed in the body as by-products of natural or non-natural metabolism.

CR-6 does not present any chiral center in the molecule because the C_2 is substituted by two methyl groups. However, as in tocopherols, new CR-6 analogues present in this study have at least a chiral center

at C_2 and thus compounds have been obtained as racemic mixtures of two enantiomers. Some derivatives have other chiral centers in the side-chain, but these present a specific configuration arising from the enantiopure reagent (acid or amine) used in the coupling reaction (between the acid **6** and an amine or the amine **18** and an acid). As happened with tocopherols, different antioxidant and/or BBB-penetrating activity could be shown by different C_2 enantiomers. Therefore, the preparation of the different enantiopure stereoisomers synthesized as CR-6 analogues and the study of their activity would be very interesting.

From the synthetic point of view, we thought in resolving or separating the enantiomers of a common precursor for all the families of compounds. In a second step, the most active CR-6 analogues would be prepared stereoselectively from the (*R*) and (*S*)-precursor. The following studies outline our preliminary results on the first step.

III.6.2 Resolution of enantiomers by diastereomeric salt fomation

The separation of enantiomers of ester **1**, a common precursor for all new compounds, was studied. Initially, the racemic mixture of this ester was analyzed by chiral HPLC (Chiracel OD column with 250 x 4.6 mm ID, isocratic 9:1 of hexane:isopropyl alcohol) and the resulting chromatogram is shown in Figure 3.17. Peaks at 10.8 and 13.8 minutes correspond to enantiomer A and enantiomer B

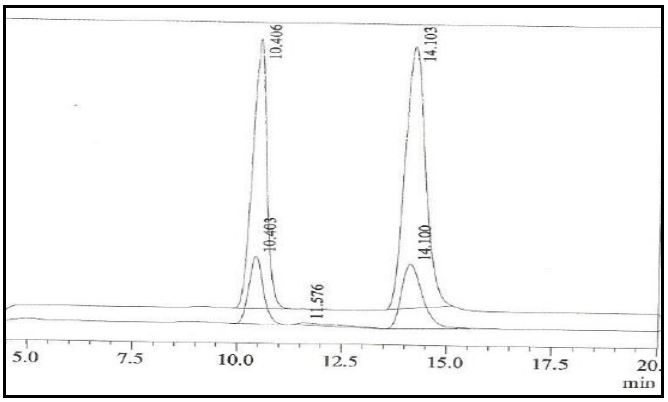

*Figure 3.17. Chromatogram of ester **1** in chiral-phase HPLC (Chiralcel OD column).*

Pig Liver Esterease (PLE)[72] was used as a first approach to hydrolyze stereoselectively one enantiomer of the ester to the corresponding acid by means of a kinetic resolution (Figure 3.18). Some experiments were carried out using PLE in tBuOH(10%):H_2O and ACN:PBS (pH = 8) as solvent, but in no case the stereoselective hydrolysis took place. We assumed that the chiral center was too far from the ester moiety to promote any stereoselective recognition at C_2 by the lipase.

[72] a) Fadel, A.; Vandromme, L. *Tetrahedron Asymmetr.* **1999**, *10*, 1153-1162. b) Arzel, P.; Freida, V.; weber, P.; Fadel, A. *Tetrahedron Asymmetr.* **1999**, *10*, 3877-3881.

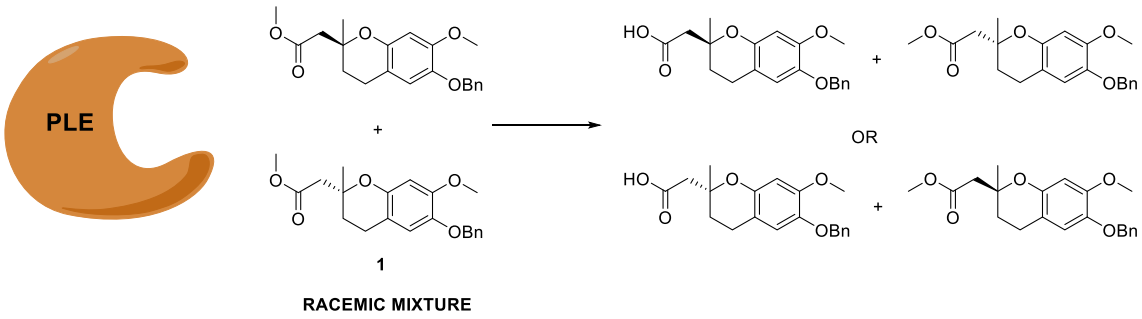

Figure 3.18. *Attempted stereoselective kinetic resolution of ester* ***1*** *by PLE lipases. Only one of the enantiomers from the racemic mixture of ester* ***1*** *is able to be hydrolyzed to the corresponding acid by the esterase PLE in a stereoselective way.*

Afterwards, other methodologies were taken into consideration, such as the formation of diastereomeric salts to separate enantiomers. Electrostatic interactions between the racemic acid **6** and an enantiopure amine can promote a preferential crystallization of one diastereomeric salt while the other one would remain in solution.

In 2010, He *et al.*[73] investigated the factors that influence on the efficient resolution by different solubility between diastereomeric salts. They further investigated the characteristic differences between the thermodynamic properties and crystal structures of the pair of diastereomeric salts by using (*R*)-α-phenylethylamine ((*R*)-PEA, **27**) as resolving agent. The less soluble salt was much more stable than the more soluble salt. Examining the crystals, they found that both salts presented similar infinite hydrogen-bonding network perpendicular to *c*-axis in which ammonium cations and carboxylate anions form columnar hydrogen-bonding around a two-fold screw axis. However, the packaging between hydrogen-bonding layers in two diastereomeric salts was significantly different. The less soluble salt showed a very planar boundary surface among the hydrophobic layers, which enhanced the salt stability by Van der Waals interactions, whilst the more soluble did not. So, they suggested that Van der Waals interactions were the responsible for the differentiation in salt solubility. He and coworkers studied different factors that affect to the resolution effectiveness: solvent, molar ratio between acid and resolving agent, volume of solvent and temperature of filtration. The best results with **27** as resolving agent appeared using 1 equivalent of **27** in 95% EtOH (120 mL 95% EtOH/0.1 mol acid) and filtrating at 20ºC.

For our investigations, other references were taken into consideration. Scott *et al.*, in 1976, found another experimental procedure for the enantiomeric resolution of *rac.*-(6-hydroxy-2,5,7,8-tetramethyl-chromane-2-yl)acetic acid, structurally similar to the acid **6** by using also **27** as resolving agent but, in this case, in THF as solvent. [58]

[73] He, Q.; Peng, Y.-F.; Rohani, S. *Chirality* **2010**, *22*, 16-23.

Table 3.4 shows the results for the enantiomeric resolution of acid **6** by using the resolving agent **27** in 95% EtOH (entries 1, 2 and 3) and in THF (entries 4 and 5). Evaluating all the results from the resolution of acid **6** with amine **27**, only the assay in THF at room temperature for 60 minutes led to a 40% ee, and 89% yield. This result was not considered sufficient and we decided to explore other enantiopure amines (Scheme 3.41).

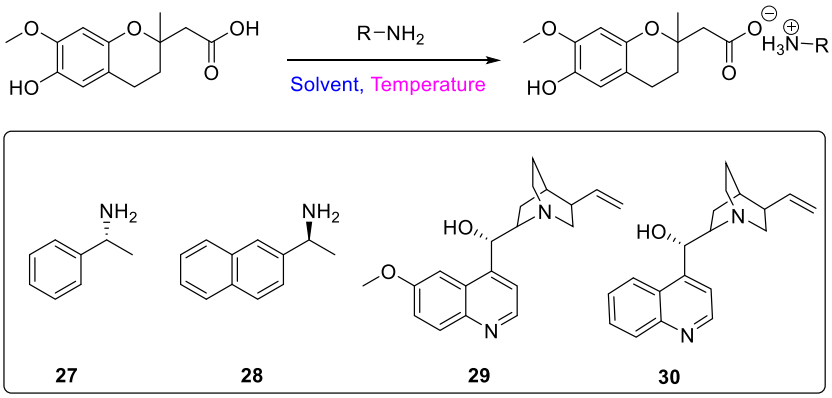

Scheme 3.41. *Diastereomeric resolution of salts from the acid* ***6*** *and an enantiopure amine.*

Table 3.4. *Results for diastereomeric resultion assay of the acid* ***6*** *with different enantiopure amines.*

Entry	Resolving Agent	Molar ratio (eq.)	Solvent	[Acid] (M)	ee (%)[a,b]	Temperature (ºC)/Time (min.)
1	27	1	95% EtOH	0.83	-	72ºC/15 min.; cooled to 15ºC and r.t./60 min
2				0.87	-	
3			EtOH abs.	0.34	-	85ºC/20 min
4		1.1	THF	0.20	-	r.t./60 min
5				0.20	20	22ºC/60 min
6				0.19	40	r.t./60 min
7	28	1		0.20	-	r.t./180 min
8				0.17	-	r.t./60 min
9		1.1		0.20	39	
10	29	1		0.17	-	
11	30	1.1		0.18	-	
12		1		0.09	-	r.t./60 min + heat and cool

[a] After the resolution of diasteriomeric salts, the formation of the ester using BF_3/MeOH at reflux for 20-30 minutes took place (yields around 90%). The ee (%), calculated by HPLC, was only measured for compounds that crystallized as diastereomeric salts or those that were transformed to the enantiopure ester.

[b] Values of ee(%) for the ester obtained after resolving the acid **6**. ee (%) = enantiomeric resolution = % peak area of majoritary diastereomer - % peak area of minoritary diastereomer.

From the data using **27** as resolving agent, we speculated that π-stacking interactions between the phenyl group of **27** and the chromanee moiety or also benzyl protecting group may promote the package of the molecule, thus stabilizing or crystallizing preferentially one diastereomer salt (Figure 3.19). Then, we decided to change to amine **28** which has a bigger naphthyl group. In these experiments (entries 7, 8 and 9), we tried the best conditions from assays with **27**: THF as solvent and at room temperature for 60

minutes. With 1.1 equivalents of resolving agent (entry 9), we obtained a white solid in 39% ee, essentially the same result as for 2-phenylethylamine 27 (entry 6).

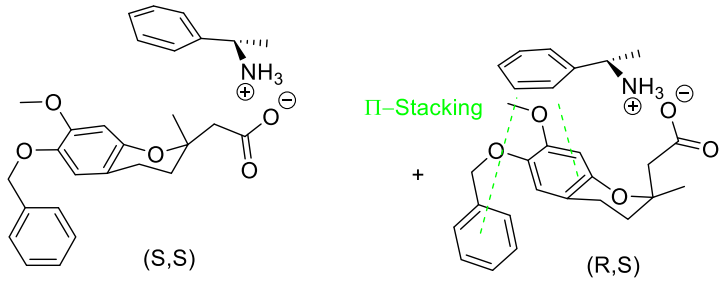

Figure 3.19. *π-Stacking interactions may help in the preferential crystallization of one diastereomer.*

In order to improve the results with **27** and **28**, we changed to more complex chiral amines[74]: quinine **29** and cinchonine **30**, typically used in diastereomeric resolution of salts. Unfortunately, neither **29** nor **30** appeared as good resolving agents for acid **6** in the described conditions, (entries 10, 11 and 12). Amines **29** and **30** had problems of solubility and even though solvent was replaced by DCM, no satisfactory results could be obtained. At this point, taking profit of some analytical and preparative chromatography columns available in our department, we explored the chromatographic separation of enantiomers of ester **1**.

III.6.3 Separation of enantiomers by chiral chromatography

Nowadays, HPLC is recognized as a powerful tool for the production of enantiomerically pure compounds at a preparative scale. In order to perform the physical separation of the enantiomers by preparative HPLC, different chiral chromatography columns were studied. Among the chiral stationary phases available, polysaccharide-based ones are particularly useful because they combine excellent chiral recognition properties with high loading capacity. In recent years, columns of this type in which the chiral selector is covalently bonded to the silica matrix have become commercially available. Interesting examples are Chiralpak IA, IB, IC and ID columns, which contain, respectively, tris(3,5-dimethylphenylcarbamate) of amylose, tris(3,5-dimethylphenylcarbamate) of cellulose, tris(3,5-dichlorophenylcarbamate) of cellulose and tris(3-chlorophenylcarbamate) of amylose. These immobilized phases retain the advantages of coated polysaccharide-based phases while being compatible with a variety of organic solvents, a feature of value for preparative-scale resolution.

The HPLC resolution of racemic mixture ester **1** was first examined at the analytical level using 250 x 4.6 mm Chiralpak IA, IB, IC and ID columns, and the typical Chiralcel OD column, which has a cellulose tris(3,5-dimethylphenylcarbamate) selector coated to silica-gel support,. Complete baseline separation of

[74] Rodríguez-Docampo, Z.; Quigley, C.; Tallon, S.; Connon, S.J. *J. Org. Chem.* **2012**, *77*, 2407-2414.

peaks was observed on the first four stationary phases tested (OD, IA, IB, and IC) eluting with isocratic 90:10 n-hexane/2-propanol at 1 mL/min. Results of capacity (k'), selectivity (α) and resolution (R_S) factors are shown in Table 3.5.

Table 3.5. *Selected chromatographic date for the analytical HPLC resolution of ester* ***1*** *on Chiralpak IA, IB, IC, ID and Chiralcel OD columns.*[a]

Column	t_M (min.)	t_1 (min.)	t_2 (min.)	k'_1	k'_2	α	R_S
Chiralcel OD	3.1	10.4	14.1	2.3	3.5	1.52	21.8
Chiralpak IA	3.5	11.1	13.8	2.2	2.9	1.32	24.5
Chiralpak IB	3.3	7.6	9.2	1.3	1.8	1.39	14.5
Chiralpak IC	3.9	13.5	14.7	2.5	2.8	1.12	11.8
Chiralpak ID	3.4	15.8	16.1	3.1	3.1	1	-[b]

[a] Column size: 250 x 4.6 mm ID; flow rate: 1.0 mL/min; UV detection at 290 and 254 nm. The chromatographic parameters k' (capacity factor for each enantiomer), α (selectivity) and R_S (resolution) are defined as follows:

$$k' = \frac{t_R - t_0}{t_0}; \alpha = \frac{k'_2}{k'_1}; R_S = 1.18\frac{t_2 - t_1}{w_2 - w_1}$$

where subscript 1 and 2 refer to the first and the second eluted enantiomer, t_R and t_0 represent their retention times (R = 1, 2) and for a non-retained compound (dead time), in minutes; and w_1 and w_2 denote their half-height peak widths, in minutes.

[b] Peaks using this chiral column were not totally separated.

The best selectivity factor was attained with the Chiralcel OD column (α = 1.52 and R_s = 21.8, Figure 3.19). However, the higher resolution of Chiralpak IA column (R_s=24.5) make it more suitable for a preparative resolution of the enantiomers of ester **1** (Figure 3.20).

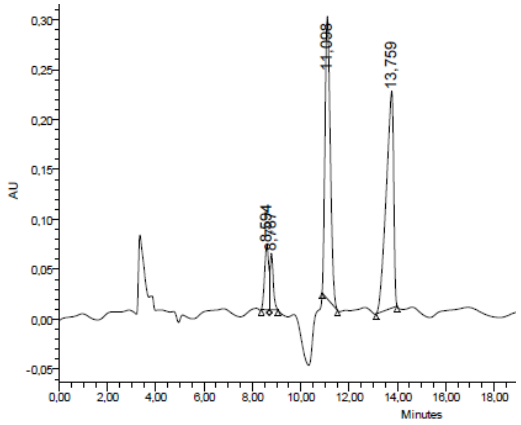

Figure 3.20. *Chromatogram of ester* ***1*** *in a normal phase system using Chiralpak IA column and an isocratic elution 90:10 hexane:isopropyl alcohol for 30 minutes. The peaks at 11.1 and 13.8 minutes correspond to two enantiomers of a racemic mixture of ester* ***1****. As the Chiralpak IA column have the best resolution (R_s = 24.5) and good selectivity factor (α = 1.32), comparing to Chiralcel OD column (Figure 3.19), it would be a good option to separate these two enantiomers.*

From these experiments, future work will contemplate the enantiomerically separation, by chromatographic devices, of the most potent compounds among **A**-**N** in the evaluation of their capacity to pass the Blood-Brain Barrier (BBB) using available BBB-models.

Fourteen CR-6 analogues (A-N) have been synthesized in a short synthetic route to improve the BBB bioavailability by coupling the CR-6 scaffold to different essential nutrients to the brain or retina (amino acids, glucose, retinol, etc.). The synthetic pathway coursed through the formation of peptidic bond with acid 6 and commercial amines, and amine 18 and commercial acids. In addition, the peptidic bond formation was studied by a coupling reaction with different coupling agents and conditions, and by different ways. Hence, the couplings of CR-6 scaffold with essential nutrients to the brain and retina were performed in moderate to high yields. Furthermore, the formation of the amine intermediate **18** was studied with different reactions, and in the end, the Staudinger reaction was the most clearest and efficient route.

Regarding the stereogenic center at C_2, the stereoselective preparation of compounds has been studied. The chiral chromatographic separation of ester **1**, as a key intermediate for all CR-6 analogues, was evaluated. Thus, the two enantiomers were efficiently separated in most of the columns tested. Overall, taking under consideration selectivity (α) and resolution (Rs) factors, column Chiralpak IA was selected as the best one for the enantiomeric separation of ester **1**.

IV. Evaluation of Antioxidant capacity

IV.1 ANTIOXIDANT CAPACITY

IV.1.1 Methodologies to evaluate the antioxidant capacity of a compound

In the last decades, there has been an increasing interest on antioxidants, particularly in those intended to prevent the presumed deleterious effects of free radicals in the human body and on deteriorating fats and other constituents of foodstuffs. For this reason, there has been an increasing interest in the use of methods for estimating the efficiency of such substances as antioxidants.[75] These methods have evolved from chemical assays with lipids substrates to more complex assays to measure the antioxidant capacity in fluids and biological samples.[76] Antioxidant effectiveness is measured by monitoring the inhibition of an oxidation process of a suitable substrate by chemical, instrumental or sensory methods.[76]

Table 4.1. *Some methodologies for the evaluation of antioxidant substrates in fluids and biological systems.*

TEST	Name	Measurement
ABTS[77]	2,2'-Azino-bis(3-ethylbenzthiazoline-6-sulfonic acid)	Inhibition of the initiation of oxidation
DPPH[78,79]	2,2-Diphenyl-1-picryl-hydrazyl	Analyses of the ability to reduce this radical cation
FRAP[78]	Ferric reducing ability of plasma	Uses the metal ion to produce oxidation and analyses the ability to reduce Fe^{3+}
ORAC[78,80]	Oxygen radical absorbance capacity	Measures the inhibition of fluorescence due to the oxidation by peroxyradicals
TRAP	Radical-trapping antioxidant capacity	Analyses the delay in oxidation. Compares the ability of an antioxidant to scavenge the $ABTS^{+}$ cation with that elicited by Trolox
TBARS[81]	2-Thiobarbituric acid	A indirect fluorometric screening test of total oxidative stress
DCFH-DA[82]	Dichlorofluorescein diacetate	Analyses the ability of an antioxidant to inhibit the oxidation of DCF inside the cell
Lipid assay	Linoleic acid	Measures the ration of the rate differences in the generation of double bonds in the presence or absence of antioxidants

The most used antioxidant tests can be classified into two groups. Depending on what they evaluate, there are some assays to evaluate the lipid peroxidation process, in which a lipid or lipoprotein substrate is oxidized and the inhibition of this process is measured, and other assays to measure the free radical scavenging ability.[76]

[75] Molyneux, P. *Songklanakarin J. Sci. Tech.*, **2004**, *26*, 211-219.
[76] Sánchez-Moreno, C. *Food Scientif. Technol. Int.,* **2002**, *8*, 121-137.
[77] Re, R.; Pellegrini, N.; Proteggente, A.; Pannala, A.; Yang, M.; Rice-Evans, C. *Free Rad. Biol. Med.* **1999**, *26*, 1231-1237.
[78] Aruoma, O. I. *Mut. Res.* **2003**, *523-524*, 9-20.
[79] a) Blois, M.S. *Nature*, **1958**, *181*, 1199-1200. b) Brand-Williams, W.; Cuvelier, M.E.; Berset, C. *Lebensm.-Wiss. u.-Technol.* **1995**, *28*, 25-30.
[80] Prior, R.L.; Cao, G. *Free rad. Biol. Med.* **1999***, 27*, 1173-1181.
[81] Kulisic, T.; Radonic, A.; Katalinic, V.; Milos, M. *Food Chem.* **2004**, *85*, 633-640.
[82] Liu, R.H.; Finley, J. *J. Agric. Food Chem.* **2005**, *53*, 4311-4314.

However, there is a widespread agreement that the different methodologies for the evaluation of antioxidant potential can lead to different results.[76,83] For this reason, it is advisable to use complementary methodologies to determine the antioxidant capacity of a substrate.

Two different antioxidant assays were applied complementarily for the evaluation of the antioxidant capacity of new antioxidant compounds **A**, **B**, **C**, **D**, **E**, **F**, **G**, **H**, **I**, **J**, **K**, **L**, **M** and **N**: the DPPH (2,2-diphenyl-1-picrylhydrazyl) assay and the cellular DCFH-DA assay. The first one is used due to its simplicity, speed and sensitivity.[84] The second assay is an assay that evaluates the antioxidant capacity in cells and takes into account the cell membrane permeability of test compounds.

The electron paramagnetic resonance (EPR) technique, where the inhibition of the hydroxyl (OH·) radical generated by a Fenton's reaction is evaluated, was also used to measure the radical scavenging capacity of CR-6, but not for the rest of antioxidants synthesized. Therefore, this technique is not described in the present work.

IV.2 FREE RADICAL SCAVENGING ASSAY: THE DPPH ASSAY

IV.2.1 A brief introduction

The DPPH assay is based on the measurement of the scavenging capacity of antioxidants towards a free stable radical 1,1-diphenyl-2-picrylhydrazyl (DPPH·). It was first developed by Blois in 1958 to determine the antioxidant activity by using a free stable radical.[79a] Regarding this procedure, other authors such as Molyneux or Sánchez-Moreno have improved the features of this assay.[75,76]

DPPH· is characterized as a very stable free radical by the delocalization of the unpaired electron over the whole molecule. Hence, two molecules of DPPH· do not dimerize, like most other free radicals do. This delocalization also gives rise to a deep violet colour characterized by an absorption maximum between 515 and 528 nm in alcohol solution (methanol or ethanol). When a solution of DPPH· is mixed with a molecule that can donate easily a hydrogen atom, like an antioxidant compound, the DPPH· molecule is reduced to the corresponding hydrazine. The resulting solution then loses the violet color and the absorbance decays, giving rise to a residual pale yellow color due to the picryl group still present in the compound (Scheme 4.1).[85]

[83] Buenger, J.; Ackermann, H.; Jentzsch, A.; Mehling, A.; Pfitzner, I.; Reiffen, K.-A.; Scheroeder, K.-R.; Wollenweber, U. *Int. J. Cosm. Sci.*, **2006**, *28*, 135-146.
[84] Magalhães, L.M.; Segundo, M.A.; Reis, S. Lima, J.L.F.C. *Anal. Chim. Acta* **2006**, *558*, 310-318.
[85] a) Contreras-Guzmán, E.S.; Strong, F.C. *J. Ass. Off. Anal. Chem.* **1982**, *65*, 1215-1222. b) Kedare, S.B.; Singh, R.P. *J. Food Sci. Technol.* **2011**, *48*, 412-422.

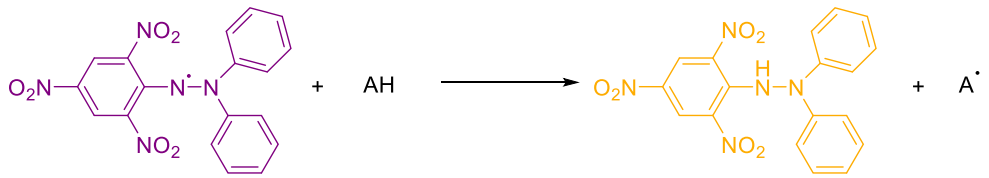

Oxidized form of DPPH
Intense violet colour
$\lambda_{máx.}$ 515 - 520 nm

Reduced form of DPPH
Pale yellow colour
No absorbance

Scheme 4.1. *A deep violet solution of DPPH· in alcoholic solvent reacts with a hydrogen atom donor AH to give rise to a pale yellow solution characteristic of the reduced species.*

The decrease of the absorbance can be monitored spectrophotometrically at a fixed wavelength at different concentrations of antioxidant. Following Lambert-Beer's law, the relationship between the absorbance and the antioxidant concentration must be linear up to reach the plateau or the steady state. At this point, no more DPPH· can be reduced in spite of the antioxidant concentration present in the sample.

Since the radical compound DPPH· is stable and does not need to be generated, the DPPH assay is a rapid, simple, inexpensive and widely used method to measure the ability of compounds that act as free radical scavengers or hydrogen atom donors, and also to evaluate antioxidant activity of food. This assay has been successfully used for investigating the antioxidant properties of many different foods like wheat grain and bran, vegetables, conjugated linoleic acids, herbs, etc. The assay can be performed in different solvent systems including ethanol, aqueous acetone, methanol, aqueous alcohol and benzene.[86] Also, it can be used to examine both hydrophilic and lipophilic antioxidants.[87] Therefore, it is a convenient method for assessing the antioxidant assay of a variety of compounds like cysteine, glutathione, ascorbic acid, tocopherol and polyhydroxyl aromatic compounds.[76,88] Moreover, the DPPH assay can be performed in the presence of complex samples and it allows the evaluation of weak antioxidants.[89]

However, this assay has some limitations. Since DPPH· is a long-lived nitrogen radical, there are kinetic differences in the hydrogen atom transfer reaction that occurs between antioxidants and highly reactive peroxyl radicals involved in lipid peroxidation compared with those between antioxidants and DPPH. Thus, antioxidants that react rapidly with peroxyl radicals may react slowly or may even be inert in front of DPPH·.

[86] a) Yu, L.L. *J. Agric. Food Chem.* **2001**, *49,* 3452-3456. b)Parry, J.; Su, L.; Luther, M.; Zhou, K.Q.; Yuraweez, M.P.; Wittaker, P.; Yu, L.L. *J. Agric. Food Chem.* **2005**, *53*, 566-573.
[87] Prior, R.L.; Wu, X.; Schaich, K. *J. Agric. Food Chem.* **2005**, *53*, 4290-4302.
[88] Masahiro, N.; Masahiro, K.; Minemitsur, N.; Akio, K.; Yoshimi, N. *Chem. Pharm. Bull*. **2005**, *53*, 714-716.
[89] Pakrash, A. *Med. Lab. Anal. Prog.* **2001**, *19*, 1-6.

IV.2.2 Improvements of the DPPH assay

IV.2.2.1 Reaction vessel

For 1-cm pathlength spectrophotometer cuvettes with a maximum working volume of 4 mL, the common practice in which 0.1 mL of antioxidant compound solution at a given concentration is mixed up with 3.9 mL of DPPH stock solution, or viceversa, reduces the accuracy of the method. Molyneux and co-workers[75] showed that for an optimal accuracy of the experiment, 2 mL of antioxidant compound must be mixed with 2 mL of DPPH solution.[75] On the other hand, cheap plastic "disposable" cuvettes can be used since they are not attacked by the solvents normally used in this assay (methanol or ethanol). Actually, performing the assay in ethanol or methanol, similar results are obtained. The use of other solvents could cause erratic values due to the different extent of the reduction.

IV.2.2.2 Reagents concentration and stability

Taking into account the normal practice in spectrophotometry, the initial DPPH· concentration in the cuvette must be selected to give absorbance values lower than 1.0. Thus, an initial concentration of DPPH· in the cuvette should be 50 to 100 μM. The antioxidant concentration may be initially selected from a wide range to scan the titration plot.[75] In solution, DPPH· is not stable to light or to oxygen, losing from 2 to 4% of absorbance every week. Therefore, it is recommended to use a fresh solution, protected from light and in an inert atmosphere.

IV.2.2.3 Reaction time

In the original method, a reaction time of 30 minutes was recommended, but shorter times (5 or 10 minutes) have been used in recent publications. Molyneux[75] recommended to reach the completion or steady state (plateau) of the reaction.

IV.2.3 Evaluation of radical scavenging for new antioxidant compounds A, B, C, D, E, F, G, H, I, J, K, L, M and N.

Following the DPPH assay using the protocol improved by Molyneux and co-workers,[75] the antioxidant capacity of the new antioxidant compounds **A**-**N** was evaluated.

IV.2.3.1 Calibration curve

First of all, the working $\lambda_{max.}$ was determined. A stock solution of 250 µM DPPH· in methanol was scanned spectrophotometrically from 400 to 700 nm. This scan is depicted in Figure 4.1 and shows the maximum point at 515 nm.

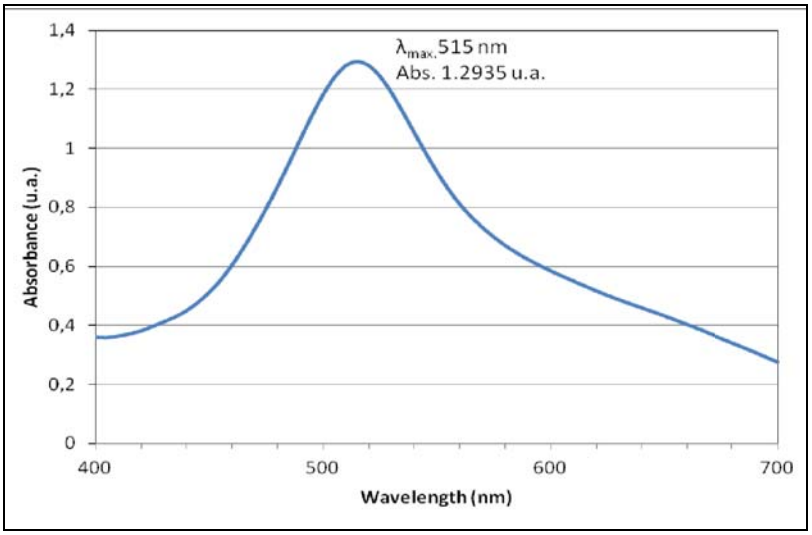

Figure 4.1. *Measurement of $\lambda_{max.}$ by scanning a solution of 250 µM of DPPH· radical in methanol from 400 to 700 nm.*

To evaluate the linearity of the monitored method at a 515 nm, eleven solutions at different concentrations from 0 to 110 µM were prepared in methanol from the stock 250 µM solution. From the calibration curve, the square's correlation coefficient R^2 = 0.9986 confirmed the Lambert-Beer's law expected profile. From these values, the regression line A = 0.0103[DPPH·] – 0.011 was derived.

IV.2.3.2 Kinetics in the reaction of DPPH with Trolox and CR-6 as antioxidant agents

Few years ago, Sánchez-Moreno and co-workers[76] proposed to represent the antioxidant efficiency versus the reaction time instead of using the antioxidant concentration. Although these representations were not linear, they are useful to extract kinetic information about the antioxidant reaction course. Then, from the analyses of several natural compounds they were able to classify the kinetic behaviour of antioxidants in three different categories: rapid for reaction times below 5 minutes, intermediates for periods between 5 and 30 minutes and slow for over 30 minutes. Accordingly, the kinetics of antioxidants CR-6 and Trolox were studied to estimate the reaction time values needed for tocopherol-like compounds to complete the scavenging of DPPH·.

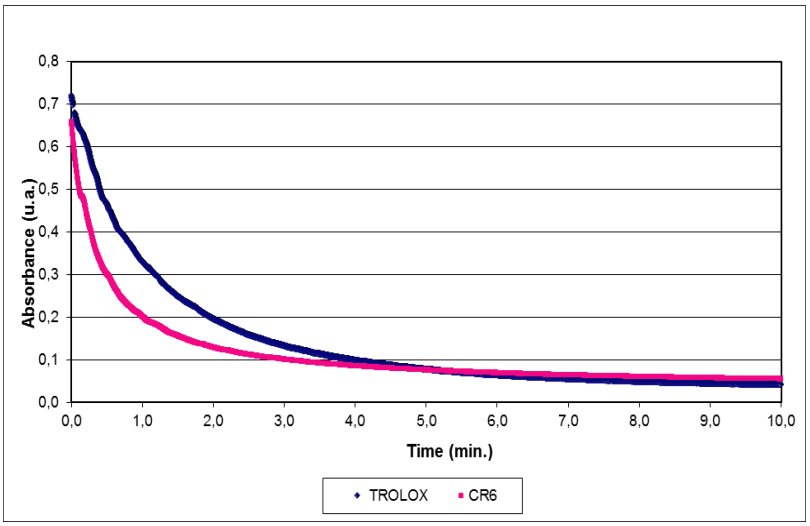

Figure 4.2. *Reaction course profiles of reference antioxidant compounds Trolox (in blue) and CR-6 (in purple) in front of DPPH·.*

Experimentally, 2 mL of 120 µM Trolox or CR-6 were mixed at time 0 with 2 mL of 160 µM DPPH· and the absorbance was measured up to 1 hour. After this period, it was observed that Trolox or CR-6 had intermediate kinetics, since they arrived at the steady state before 10 minutes of reaction (Figure 4.2). Nevertheless, keeping in mind that kinetics depends on the tested substrate, to assure that all new antioxidant compounds would reach the plateau, the DPPH assay was performed for 1 hour.

IV.2.3.3 Evaluation of the antioxidant capacity of Trolox and CR-6: rIC$_{50}$ and other parameters

The initial compounds to be evaluated were Trolox and CR-6, well-known antioxidants bearing a tocopherol-like structure. For comparison purposes, they were used as positive controls during the antioxidant evaluation of the newly synthesized products.

First, a wide range of CR-6 and Trolox concentrations was evaluated. From a stock solution of 200 µM of Trolox or CR-6 in degassed methanol, 2 mL-solutions at final concentration from 0 to 110 µM into 4 mL were prepared. Then, rapidly, 2 mL of stock solution 140 µM of DPPH· were added to each one (70 µM DPPH final concentration).[75,76,85b] The reaction took place for 60 minutes under stirring at room temperature in the absence of light. Then, the absorbance was measured at 515 nm.

The exact concentration of working DPPH· was calculated from the absorbance response at 515 nm of the initial solution in the absence of antioxidant (Trolox or CR-6) and using the above calibration curve. The scavenging percentage or inhibition (I%) of DPPH· was calculated from the absorbance using the following expression:

$$I(\%) = \left(\frac{A_0 - A_t}{A_0}\right) \cdot 100$$

where A_0 and A_t represent the absorbance in the absence of antioxidant and at a given antioxidant concentration, respectively, after 60 minutes of reaction. The plot of I(%) versus the mol ratio of reagents (mol of antioxidant/mol of DPPH·)[79b] presented a linear response until the plateau is reached, that is, when the inhibition reached its maximum.

Figure 4.3 shows the linear section of plotting the inhibition percentage results versus the molar ratio of reagents (mol of antioxidant/mol of DPPH·). From the adjusted regression line, the predicted relative IC_{50}[90] (rIC_{50}, the half inhibitory concentration in terms of mol of antioxidant/mol of DPPH) was estimated replacing the ŷ-value[91] by 50. The rIC_{50} values for Trolox and CR-6 were 0.23 and 0.22 mol antioxidant/mol DPPH·, respectively.

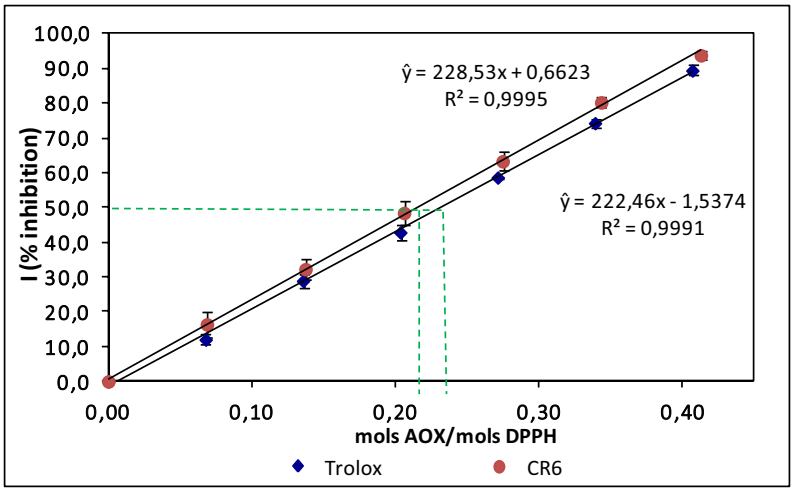

Figure 4.3. *Results of the DPPH assay for antioxidants Trolox and CR-6. In green, the rIC_{50} for Trolox and CR-6 are defined. The estimated calibration curve for the lineal section are shown.*

For the sake of clarity, sometimes it is more useful to discuss in terms of antiradical power (ARP = $1/rIC_{50}$). Thus, the larger the ARP value, the more efficient is the antioxidant.[79b]

In addition, the stoichiometry and the number of DPPH· molecules reduced were calculated to observe the reactivity of the antioxidant compound in the presence of a free radical like DPPH·.[79b] The stoichiometry was obtained by multiplying the rIC_{50} of each antioxidant by two, to give the quantity of antioxidant that is needed to reduce 100% of the DPPH· (as rIC_{100}). The inverse of stoichiometry corresponds to the number of DPPH· molecules that were reduced by one molecule of antioxidant. These results for Trolox, CR-6 and δ-tocopherol[79b] are presented in Table 4.2 for comparison purposes. Since the antioxidant capacity depends on the ease of a compound to donate a H· radical to a free radical, similar results for these three tocopherol-like antioxidants would be expected (Table 4.2).

[90] rIC_{50} represents the relative predicted x-value for ŷ = 50 into the adjusted regression line expressed in mol of antioxidant/mol of DPPH·.
[91] ŷ-value corresponds to y-value from the estimated regression line for an specific x-value.

Table 4.2. *Results obtained for antioxidants Trolox, CR-6 and δ-tocopherol in the DPPH assay.*

Antioxidant	rIC_{50} (mols AOX/mols DPPH)	ARP	Stoichiometry value	Number DPPH reduced
Trolox	0.23	4.31	0.46	2.16
CR-6	0.22	4.63	0.43	2.31
δ-Tocopherol[79b]	0.25	4.00	0.50	2

According to these data, the stochiometry value around 0.5 means that for each molecule of antioxidant, two molecules of DPPH· are reduced. However, these compounds have only one phenolic hydroxyl group available. Some authors have explained this fact by the reaction's mechanism for tocopherol-like antioxidants. In 2003, Khanduja and Bhardwaj proposed a mechanism based on two different steps.[92] In the first step, one molecule of DPPH· and the phenolic hydrogen from tocopherol react to give the reduced DPPH-H and the tocopheroxyl radical (Scheme 4.2). Then, in a second step, due to the delocalization of the electron around the antioxidant molecule, the reaction of the tocopheroxyl radical intermediate with another molecule of DPPH· takes place and yields the tocopherolquinone. Hence, two molecules of DPPH· are reduced to DPPH-H by only one molecule of tocopherol consumed (Scheme 4.2). From the results obtained in our case, we suggest that Trolox and CR-6 follow the same reaction course.

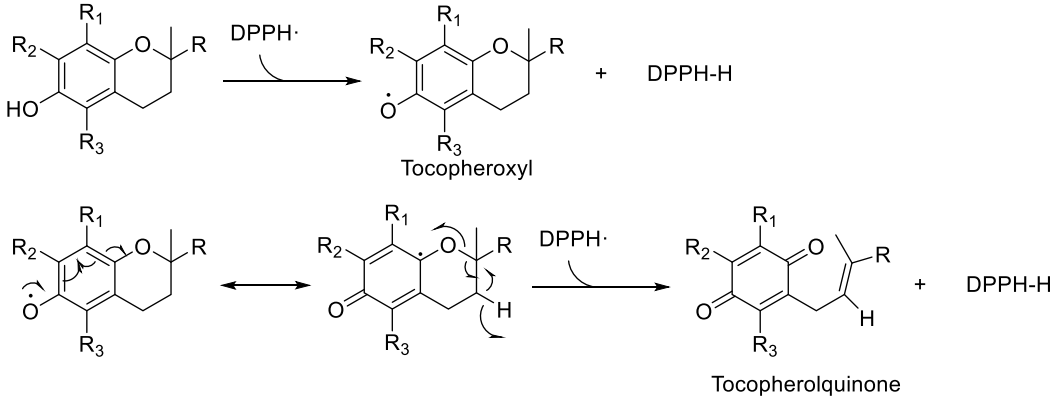

Scheme 4.2. *Reaction course between tocopherol and free radical DPPH· explained by the reduction of two molecules of DPPH· per molecule of antioxidant, to give finally tocopherolquinone as by-product.*[92]

IV.2.3.4 Evaluation of the antioxidant capacity using $logIC_{50}$

Even though the above results provided useful information about the process of neutralization of free radicals, the IC_{50} was also calculated in terms of concentration in order to know the half maximal inhibitory concentration required to scavenge the DPPH· radical. Thus, the representation of %Inhibition, calculated above, versus the log[antioxidant] was carried out. Using the software GraphPad Prism 5 for Windows[93], the $logIC_{50}$[94] for Trolox and CR-6 were determined by adjusting the results to a nonlinear

[92] Khanduja, K.L.; Bhardwaj, A. *Indian J. Biochem. Biophys.* **2003**, *40*, 416-422.
[93] *GraphPad Prism Software. Inc, 5.0*; San Diego, CA 92121, **2007**.
[94] The $logIC_{50}$ from GraphPad Prism 5 calculation corresponds to the inflexion point of the nonlinear sigmoidal fitted curve from the given results. The results were expressed in terms of $logIC_{50}$ due to the symmetric character of the

sigmoidal curve (log[inhibitor] vs response) (Figure 4.4). The bottom and top plateau were constrained to 0 and 100. The $logIC_{50}$ and the 95% Confidence Interval for Trolox were 1.196 and (1.172; 1.220), and for CR-6 were 1.15 and (1.124; 1.176).

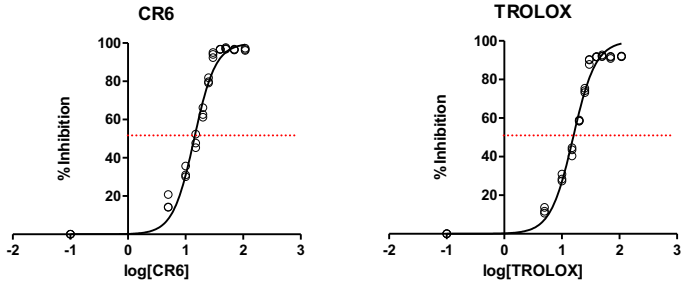

Figure 4.4. *Percentage of inhibition versus log[Antioxidant] nonlinear sigmoidal adjusted curve; leading to the $logIC_{50}$ value for the antioxidant.*

The sigmoidal equation for the estimated curve employing GraphPad Prism 5[93] for Windows followed the expression:

$$Y = Bottom + \frac{(Top - Bottom)}{1 + 10^{(\log ec50 - X)Hillslope}}$$

where *Bottom* and *Top* values correspond to y-value for inferior and superior plateau values (0 and 100, respectively), *Logec50* represents the x-value when y-value is the inflexion point between the *Bottom* and the *Top*, and *Hillslope* is the slope of the curve between the *Bottom* and the *Top*.

*IV.2.3.5 Evaluation of test compounds **A**, **B**, **C**, **D**, **E**, **F**, **G**, **H**, **I**, **J**, **K**, **L**, **M** and **N***

IV.2.3.5.1 Evaluation of the antioxidant mechanism

The evaluation of the antioxidant capacity of the new antioxidant compounds **A**-**N** by the scavenging of the free radical DPPH· was performed following the same procedure explained above for Trolox and CR-6 controls. In this case, the linear section of the response was that desired; therefore, only final concentrations from 0 to 30 μM of antioxidant were assayed.

Figure 4.5 and Tables 4.3 and 4.4 shows all the results for compounds **A**-**N**.

value compared to IC_{50} and because the x-value was expressed in log[antioxidant]. Ultimately, to understand better all these results, they were transformed to IC_{50}.

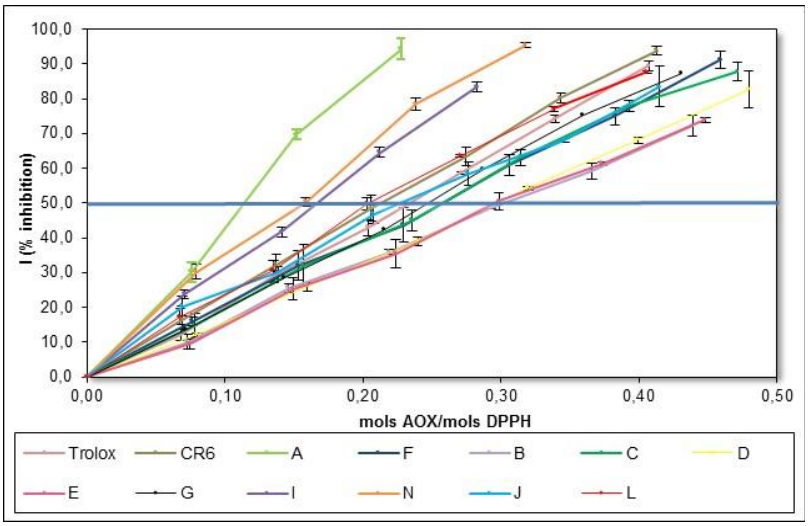

Figure 4.5. *Comparison of the scavenging activity of DPPH· between test compounds* ***A-N*** *and positive controls, Trolox and CR-6. The blue line points out the 50% of inhibition.*

According to the graph, most of test compounds reached a ratio of mol (or stoichiometry) around 0.5 (mol antioxidant/mol DPPH·) close at 100% of inhibition of DPPH·, as observed for Trolox, CR-6 and δ-tocopherol.

In Table 4.3, an estimated linear regression line from curves plotted in Figure 4.5 and their coefficient of determination R^2 for all test compounds are shown to demonstrate the linear relationship between the absorbance signal and antioxidant concentration, and the low variability of ŷ.

Table 4.3. *Estimated linear regression line for new CR-6-analogues* ***A-N*** *in the DPPH assay.*

Antioxidant	Regression line	n[a]	R^2
Trolox	ŷ = – 1.5374 + 222.46x	21	0.999
CR-6	ŷ = 0.6623 + 228.53x	21	0.999
A	ŷ = 0.1716 + 424.96x	12	0.993
N	ŷ = 3.0598 + 300.87x	15	0.992
I	ŷ = 1.1949 + 293.51x	15	0.998
L	ŷ = 0.8757 + 229.34x	18	0.997
K	ŷ = 3.7628 + 213.29x	21	0.990
M	ŷ = – 0.1921 + 221.43x	21	0.986
G	ŷ = – 0.8155 + 206.92x	20	0.999
J	ŷ = 2.1985 + 192.21x	21	0.997
F	ŷ = 0.4991 + 196.12x	21	0.999
H	ŷ = 1.8797 + 191.21x	21	0.996
C	ŷ = 0.7367 + 191.13x	21	0.997
D	ŷ = – 1.3043 + 173.47x	21	0.999
E	ŷ = – 1.0417 + 167.68x	21	0.998
B	ŷ = – 0.2655 + 164.71x	20	0.998

[a] n is the sample size

Table 4.4. *Antioxidant capacity in the DPPH assay for CR-6-analogues* ***A-N****.*

Antioxidant	rIC_{50} (mols AOX/mols DPPH)	ARP	Stoichiometry	Number DPPH reduced
TROLOX	0.22	4.63	0.43	2.32
CR-6	0.23	4.32	0.46	2.16
A	0.12	8.53	0.23	4.26
N	0.16	6.41	0.31	3.20
I	0.17	5.98	0.33	2.99
L	0.21	4.67	0.43	2.33
K	0.22	4.61	0.43	2.31
M	0.23	4.41	0.45	2.21
G	0.25	4.07	0.49	2.04
J	0.25	4.02	0.50	2.01
F	0.25	3.96	0.51	1.98
H	0.25	3.97	0.50	1.99
C	0.26	3.88	0.52	1.94
D	0.30	3.29	0.59	1.69
E	0.30	3.29	0.61	1.64
B	0.31	3.28	0.61	1.64

From these data, the rIC_{50} in terms of mol of antioxidant/mol of DPPH· was estimated. Then, the ARP, the stoichiometry and the number of DPPH· reduced also were calculated. All these results are shown in Table 4.4, compared with Trolox and CR-6 controls. These results are shown in descending order of antioxidant capacity, depending on the slope of their regression line. Thus, all new antioxidant compounds **A**-**N** presented rIC_{50} from 0.12 to 0.31 mols of antioxidant/mols of DPPH·. These results suggested that all of them have similar mechanism of reaction to those of references Trolox and CR-6, consuming from 2 to 4 molecules of DPPH· by molecule of antioxidant. Nevertheless, it seems that molecules **A**, **N** and **L** also progress through a complementary mechanism to consume 1 or 2 molecules of DPPH· more.

It is remarkable the high antioxidant capacity or ARP elicited by compounds **A**, **I** and **N**, even better than references. In case of **A**, which consumed 4 molecules of DPPH· by molecule of antioxidant, the presence of three hydroxyl groups in the molecule could be the responsible for the higher antioxidant capacity. Compounds **I** and **N**, which have similar structure to CR-6 differing only on a terminal amide in **I** and a terminal acid in **N**, consumed 3 molecules of DPPH·. Thus, the less hindered the molecules, the more active they are. Also, the carbonyl group at position $C_{2'}$ may contribute to conjugate the spare electron around the molecule and then facilitate the donation of a second hydrogen atom to another DPPH· molecule (Scheme 4.3). In contrast, looking at the antioxidant capacity of **L**, in which the carbonyl of the amide is one carbon atom distant from $C_{2'}$, $C_{3'}$, the resulting radical could be less stabilized than in **I** (Table 4.4).

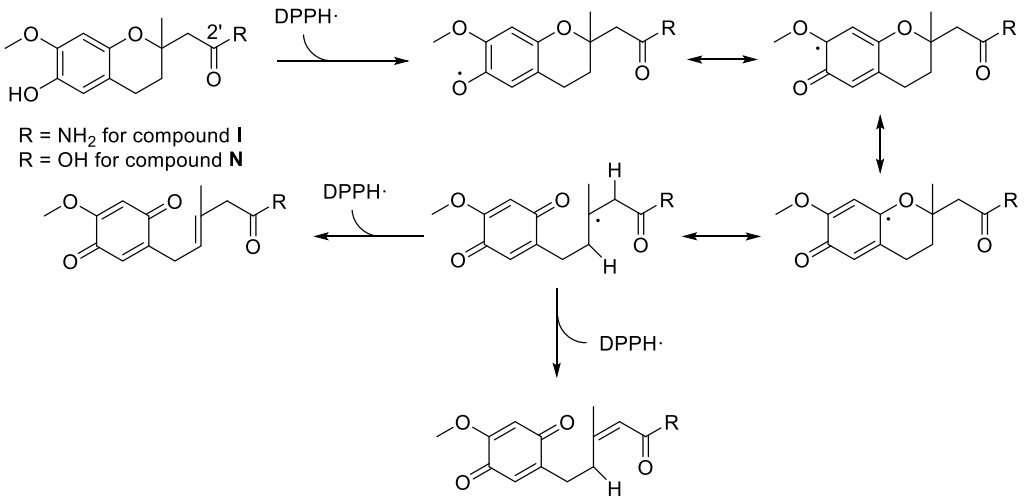

Scheme 4.3. *Proposed explanation for the higher antioxidant capacity of compounds* ***I*** *and* ***N****.*

Surprisingly, compound **B** which has two phenolic hydrogens is the least active of whole collection of compounds.

IV.2.3.5.2 Evaluation of the antioxidant capacity using logIC$_{50}$

From the plot of %Inhibition versus log[antioxidant], the logIC$_{50}$ were calculated for compounds **A**-**N** by using the GraphPad Prism 5 for Windows.[93] The results are shown on Table 4.5, and the representations, in which nonlinear sigmoidal curves were adjusted to the respective results, are shown in Figure 4.6.

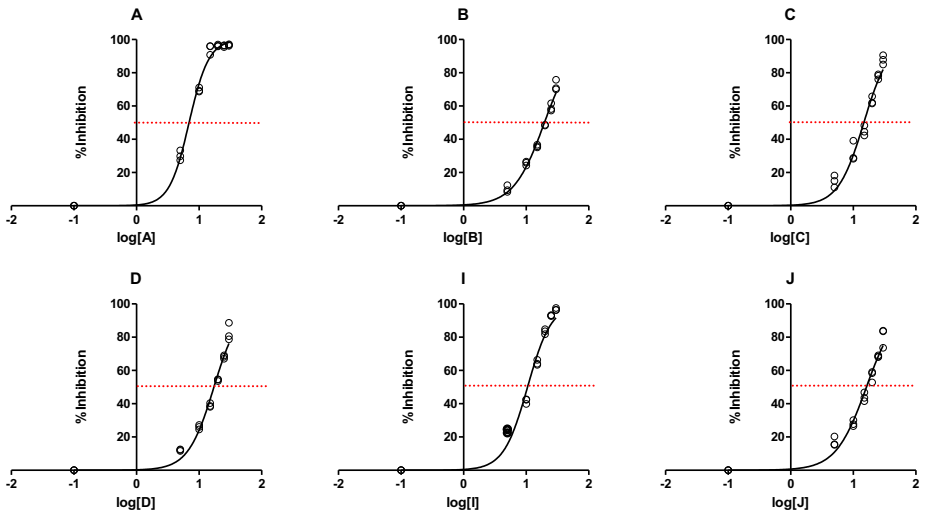

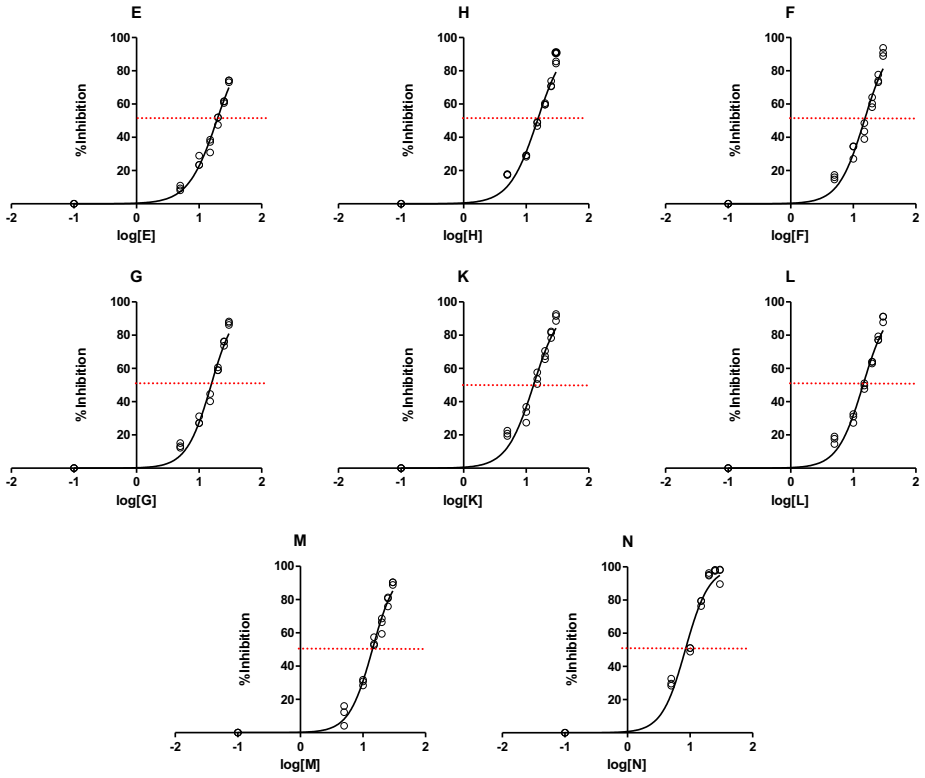

Figure 4.6. Representation of percentage of Inhibition versus log[Antioxidant] for all tested samples in the DPPH assay. Determination of logIC_{50} was carried out by GraphPad Prism 5,[93] for Windows software. The spotted red line points out the 50% of inhibition.

From the adjustment of the results for triplicates into a nonlinear sigmoidal curve (%Inhibition vs log[antioxidant]), the logIC_{50} values for test compounds were obtained using GraphPad Prism 5 for Windows.[93] These values, the IC_{50}[95] and their respective 95% Confidence Interval are shown in Table 4.5. The results are in ascending order of IC_{50}.

Comparing all these data with the rIC_{50} obtained in Table 4.4, page 107, the test compounds and the references can be ordered by their antioxidant capacity as follows: **A** > **N** > **I** > **K** > **M** = **Trolox** > **L** > **C** > **F** > **H** > **G** > **CR-6** > **J** > **D** > **E** > **B**.

Taking into account these results, it was assumed that the new antioxidant agents have a similar antioxidant capacity as those elicited by Trolox and CR-6 for neutralizing free radicals like DPPH·. Thus, the structure modification carried out at C_2 in all CR-6 analogues did not modify their antioxidant capacity in comparison with CR-6 as measured by the DPPH assay. These results were as anticipated. In any case, to assure that the antioxidant capacity is or is not significantly different from CR-6 a statistical approach was used.

[95] IC_{50} is the half maximal inhibitory concentration in terms of μM.

Table 4.5. *Comparison of the IC_{50} (μM) values for test compounds **A-N** and references Trolox and CR-6.*

Antioxidant[a]	IC_{50} (μM)	95% Confidence Interval of IC_{50}	$logIC_{50}$	95% Confidence Interval of $logIC_{50}$
TROLOX	14.1	(14.87; 16.59)	1.196	(1.172;1.220)
CR-6	15.7	(13.30; 15.00)	1.150	(1.124; 1.176)
A	6.9	(6.621; 7.245)	0.840	(0.820; 0.859)
N	8.4	(7.629; 9.265)	0.925	(0.903; 0.945)
I	10.5	(9.741; 11.35)	1.022	(0.988; 1.054)
K	13.1	(12.17; 14.10)	1.117	(1.085; 1.490)
M	14.1	(13.46; 14.83)	1.150	(1.129; 1.171)
L	14.3	(13.46; 15.21)	1.156	(1.130; 1.780)
C	14.7	(13.81; 15.71)	1.168	(1.140; 1.196)
F	14.9	(13.81; 16.18)	1.175	(1.140; 1.208)
H	15.0	(14.13; 16.01)	1.177	(1.150-1.204)
G	15.5	(14.67; 16.49)	1.192	(1.188; 1.194)
J	16.2	(15.26; 17.21)	1.210	(1.183; 1.235)
D	17.3	(16.39; 18.18)	1.237	(1.215; 1.259)
E	19.1	(18.39; 19.93)	1.282	(1.265; 1.299)
B	19.6	(18.76; 20.40)	1.291	(1.273; 1.309)

[a] The compounds **A**-**N** are ordered from high to low antioxidant activity.

IV.2.3.6 Statistical comparison of new antioxidants and Trolox with CR-6

All statistical experiments presented in this work were carried out with the assistance of María José Bleda Hernández from the *Synthesis and Biomedical Applications of Peptides' group* of the *Department of Biomedical Chemistry* in our institute.

Thus, results for synthesized new antioxidants and Trolox were compared with CR-6's results using three different statistical methods because there is no statistical method reliable enough to give statistically differences between results from different antioxidant compounds. Differences were statistically significant at $\alpha = 0.05$ level.

1) Comparison of the sigmoidal estimated curves (%Inhibition vs log[antioxidant]) of CR-6 with each of the new test compounds using the **F-test**: [93,96,97] the sum of square (SS) for compounds separately was compared with SS for the combination of both compounds, using GraphPad Prism 5[93] and Microsoft Excel.

2) **T-test**[93,98,99] compares only one point of the sigmoidal estimated curve, the $logIC_{50}$, of CR-6 with each of the new test compounds considering the standard deviation (SD) and the sample size (n), using STATA 12.0 software.

[96] Ratkowsky, D. A. *Handbook of nonlinear regression models*. Dekker: New York, **1990**.
[97] Motulsky, H.J. *Prism 5 Statistics Guide*, GraphPad Software Inc., San Diego CA, **2007**. www.graphpad.com.
[98] Gosset, W. S. *"Student's" Collected Papers*. London: Biometrika Office, University College, **1943**.
[99] StataCorp. Stata: Release 12. Statistical Software. College Station, TX: StataCorp LP, **2011**.

3) Estimation of a regression line using the linear part of sigmoidal estimated curve for CR-6 and the new test compound. Comparison of estimated regression lines using a **Wald's test**,[99,100,101] employing the margins and contrast commands of STATA 12.0 software.

Initially, with the F-test the sigmoidal curves for CR-6 and a synthesized antioxidant (**A**, **B**, **C**, **D**, **E**, **F**, **G**, **H**, **I**, **J**, **K**, **L**, **M** and **N**) or Trolox were compared. This test is very sensitive to small variance changes in the curve; therefore, it is easy to determine significant differences. However, using this method, **I** was the only compound that showed non-significant differences with CR-6 to reduce free radicals.

Alternatively to this test, two less sensitive methods were used in order to establish differences between CR-6 and new antioxidants and Trolox. In the t-test, results were different. Compounds **C**, **F**, **H**, **K**, **L** and **M** had no significant differences with CR-6 ($p \geq 0.05$). The rest of compounds had significant differences ($p \leq 0.05$): **A**, **I** and **N** had positive differences since they were better antioxidants than CR-6; in contrast, compounds **B**, **D**, **E**, **G**, **J** and Trolox showed negative and significant differences due to their lower antioxidant capacity.

In Figure 4.7, $logIC_{50}$ and its 95% Confidence Interval are plotted in decreasing order of antioxidant activity for antioxidants **A**-**N**. Compounds delimited in orange and in green presented significant differences from CR-6 ($p \leq 0.05$). In red, the $logIC_{50}$ of CR-6 and its 95% Confidence Interval is defined. The orange group represents those compounds with less antioxidant capability than CR-6, while those delimited by green are more active (Figure 4.7).

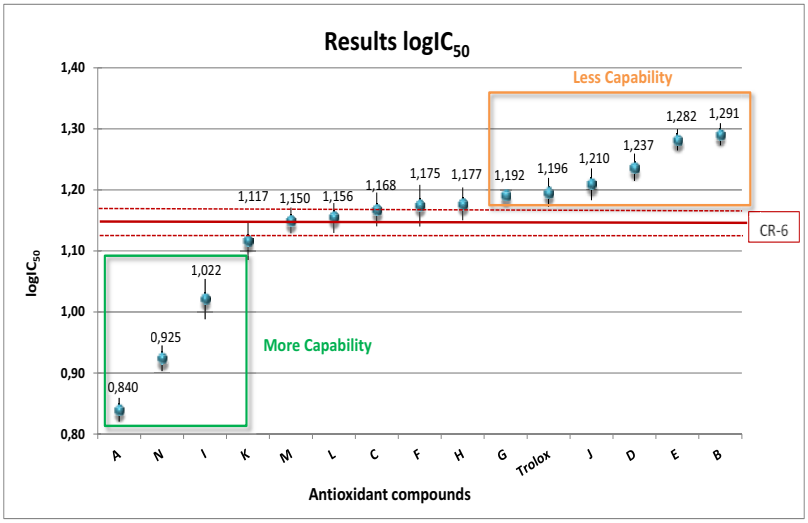

Figure 4.7. *$logIC_{50}$ and its 95% Confidence Interval in DPPH assay for each compound. The red lines represent de $logIC_{50}$ for CR-6 and its 95% Confidence Interval.*

[100] Kuehl, R. O. *Design of Experiments: Statistical Principles of Research Design and Analysis.* 2nd ed. Belmont, CA: Duxbury, **2000**.
[101] Coster, D. *Contrast*, *Encyclopedia of Biostatistics*, ed. P. Armitage and T. Colton, 2, 1153-1157. Chichester, UK: Wiley, **2005**.

By employing the third method, the t-test results were confirmed. Only compounds **C**, **F** and **H**, which had no significant differences from CR-6 in t-test, appeared as statistically significant different ($p \leq 0.05$) from CR-6 and less active.

In Figure 4.8, the contrast results from Wald's test for test compounds are represented from the weakest to the strongest antioxidant. The contrast stands for the difference from reference CR-6 and tested antioxidant. Negative values mean that test antioxidant is less active than CR-6 in this assay, while positive means they are more active. As it is shown (Figure 4.8), only two compounds, **L** and **M**, presented no significant differences ($p \leq 0.05$). Then, compounds delimited by orange are less active than CR-6 and those delimited by green are more active (Figure 4.8).

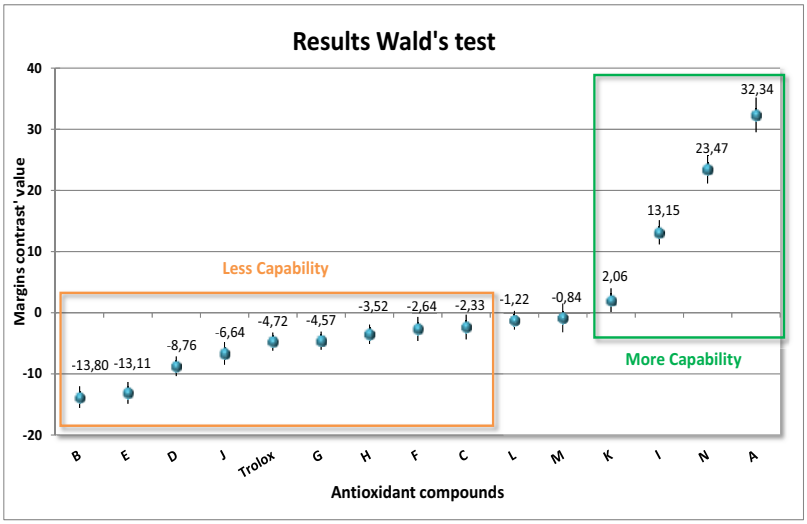

Figure 4.8. *Differences on means for each new antioxidant and CR-6 using the information of estimated linear regression. Wald's test results.*

In principle, the DPPH assay reflects the capacity to donate the phenolic hydrogen atom. Thus, the antioxidant activity results only depend on the chromane moiety, and the introduction of additional structural motifs in the molecule at C_2 should not have a significant effect on that capacity. However, some differences have been observed. From the statistical analysis, there are some new antioxidants that could be considered different from CR-6. But from a structural point of view, these differences are not so relevant. Taking into account the number of DPPH· molecules reduced by molecule of antioxidant (Table 4.4 in page 107), a chemical criteria was established: all compounds with a $\log IC_{50}$ different than 1.12 – 1.21 (13.2 µM < IC_{50} < 16.2 µM) in t-test and a difference higher than 8 units in Wald's test were consider chemically different from CR-6. According to these criteria, compounds **A**, **I** and **N** are different and more active than CR-6 because they are able to reduce from 3 to 4 molecules of free radical while CR-6 is able to reduce only 2. Nonetheless, compounds **B**, **D** and **E** are different and less active than CR-6 due to the fact that they only reduced around 1.7-1.6 molecules of DPPH·. The rest of compounds (**C**, **F**, **G**, **H**, **J**, **K**, **L**, **M**, **N** and Trolox) had then similar antioxidant capacity than CR-6 in DPPH assay.

IV.3 CELLULAR ANTIOXIDANT ACTIVITY

Animal and human models are the best way to measure the antioxidant capacity of a compound, but these models are expensive and time-consuming, and not suitable for initial antioxidant screening in foods and dietary supplements.[102] Even though there are widely useful chemical antioxidant capacity assays, as mentioned in section IV.1.1, page 97, their ability to predict *in vivo* activity is questioned for a number of reasons. None of them takes into account the bioavailability of antioxidants into the cell or the organism, the uptake of the antioxidant compound and the structural alteration due to metabolism.[103,104] Moreover, most of them are performed in non-physiological pH and temperature. Thus, the development of reliable and quantifiable cell culture antioxidant assays, which could be cost-effective, relatively fast and address some issues of uptake, distribution and metabolism, have been widely studied.[105]

IV.3.1 A brief introduction to the Cellular Antioxidant Activity (CAA) assay

The Cellular Antioxidant Activity (CAA) assay uses the ability of ROS and RNS, generated during the lipid peroxidation process, to induce the formation of a fluorescent oxidative stress indicator in cell culture. At different concentrations of antioxidant agent, the inhibition of fluorescent oxidative stress could be monitored and the activity of this antioxidant evaluated.

Initially, the Andreae method[106] employed the fluorescent compound 6-methyl-7-hydroxy-1,2-benzopyrone (Scopoletin) as an indicator to determine the oxidant hydrogen peroxide (H_2O_2) in ultramicro amounts in the presence of peroxidases (a group of enzymes that catalyze the reduction of reactive species generated during the oxidative damage process). Scopoletin was oxidized for the action of H_2O_2 to a non-fluorescence species and the decrease of the signal was monitored at different concentrations of peroxidase. Although this method was extremely sensitive, it was based on the decrease of fluorescence. Then, high concentration of fluorescent molecule was required to detect accurately signal differences.

The leucofluorescein derivatives are a class of compounds more useful to solve this issue. In 1965, Keston and Brandt[107] reported the use of dichlorofluorescein (DCFH), a leucoderivative, to measure H_2O_2 levels. 2,7'-Dichlorofluorescein diacetate (DCFH-DA) was first activated by the alkali removal of diacetated moiety, to give DCFH. In the presence of an oxidant agent such as H_2O_2, DCFH is oxidized to dichlorofluorescein (DCF), a flourescent compound that can be easily detected. By the action of an

[102] Liu, R.H.; Finley, J. *J. Agric. Food Chem.* **2005**, *53*, 4311-4314.
[103] Frankel, E.N.; Meyer, A.S. *J. Sci. Food Agric.* **2000**, *80*, 1925-1941.
[104] Liu, R.H. *J. Nutr.* **2004**, *134*, 3479S-3485S.
[105] Wolfe, K.L.; Liu, R.H. *J. Agric. Food Chem.* **2007**, *55*, 8896-8907.
[106] Andreae, W.A. *Nature,* **1952**, *170*, 83-84.
[107] Keston, A.S.; Brandt, R. *Anal. Biochem.* **1965**, *11*, 1-5.

antioxidant, like peroxidases, the fluorescence decreases; thus, in this case, the concentration of oxidant is proportional to the fluorescent signal.

In 2007, Wolfe and Liu[105] reported the use of DCFH as indicator of lipid peroxidation in cells HepG2 (human hepatocarcinoma cells), and the evaluation of antioxidant agents, foods or dietary supplements (gallic acid, quercetin, kaempherol, myricetin, caffeic acid, luteolin, ascorbic acid, catechin and epigallocatechin gallate) in a more biological environment. Figure 4.9 shows the biological processes that take place inside the cell. Cells are first pre-treated with the antioxidant compound and DCFH-DA. The antioxidant binds to the cell membrane or passes through the membrane to enter into the cell. Non-polar DCFH-DA diffuses also into the cell and, then, DA moiety is cleaved by cellular esterases to generate a more polar molecule, DCFH, which is retained inside the cell. Cells were then treated with an oxidant compound, 2,2'-azo-bis-amidinopropane (ABAP), which is able to be diffused into the cells. The generation of reactive species (ROS and RNS) in or out the cells attacked the lipids in the cell membrane producing more radicals in a radical cascade and, then, oxidizing the intracellular DCFH to fluorescent DCF. The use of an antioxidant prevents the oxidation of DCFH and membrane lipids, by reducing the formation of reactive species and, thus, the fluorescent signal decreases. Therefore, the intracellular fluorescence of DCF can be used as indicator of overall oxidative stress in cells and to evaluate the antioxidant compounds.

Figure 4
DCFH-D
in the
pre

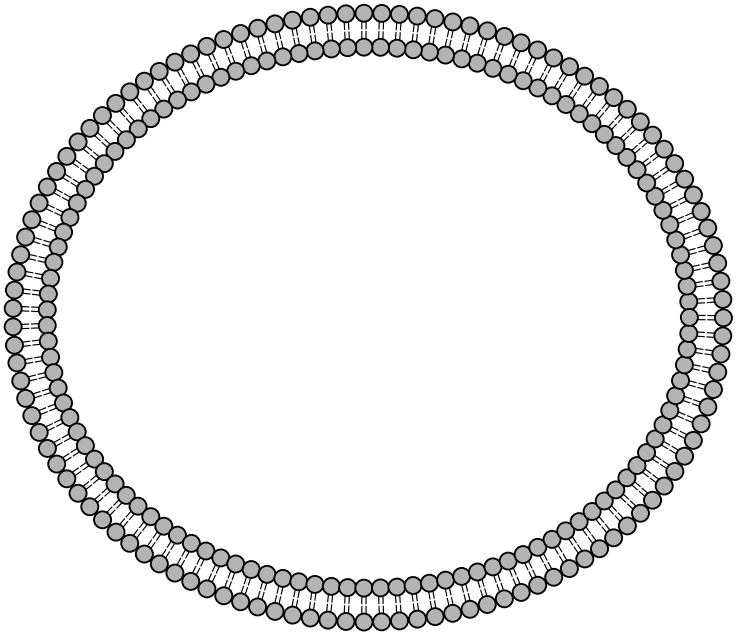

There are few potential problems with the use of DCFH in this assay. One of them is the exposure of DCFH-loaded cells to light. DCFH is photosensitive and can be autooxidized to DCF by light exposure. This fact can interfere in the antioxidant assay due to an overestimation of the fluorescence signal and the increase of variability in the assay. Many studies have used fluorescent microscopy with DCFH-DA for the quantification of oxidative stress in cells. Using a microscope in the experiment, the time control of light exposure is long when trying to locate and focus cells. In 1999, Wang and Joseph[108] proposed to use a fluorescent 96-well microplate reader that permitted the evaluation of a large amount of data with low variability. Finally, in Wolve and Liu work,[105] they used ABAP as inductor of peroxyl radical in cells, but other strong oxidants like H_2O_2, 2,2'-azobios(2-amidinopropane) dihydrochloride (AAPH), SIN-1 (3-morpholinosydnonimine as NO and superoxide generator) and SNP (Sodium Nitro Prusside as NO generator) could be also employed.[108]

IV.3.2 CAA assay for new synthesized antioxidant compounds A-N using MDA-MB-231 and MDA-MB-468 cell lines

The cell antioxidant activity of new antioxidant compounds **A**-**N** was evaluated using two different cell lines: MDA-MB-231 and MDA-MB-468 from a human breast adenocarcinoma.[109,110] This assay was performed by Dra. María Garrido Martínez from our group in the *Department of Biological Chemistry and Molecular Modelling*.

IV.3.2.1 Determination of oxidant concentration

According to Wolfe and Liu work,[105] previous experiments with T98 cell line from human caucasian glioblastoma were considered to select the right oxidant reagent (Figure 4.10). From these experiments, it was demonstrated that, at lower concentrations, H_2O_2 had higher response of fluorescence, and oxidizes better DCFH to DCF into the cell, compared to other oxidants like ABAP. In the figure shown below we can observe that while ABAP arrived at a stationary state at 600 µM, H_2O_2 arrived at higher levels of fluorescence at 62.5 µM and then the fluorescence dropped down to a stationary state twice lower than the maximum. Therefore, H_2O_2 was selected for our experiments.

[108] Wang, H.; Joseph, J.A. *Free Rad. Biol. Med.* **1999**, *27*, 612-616.
[109] Sofi, M.S.; Sateesh, M.K.; Bashir, M.; Harish, G.; Lakshmeedha, T.R.; Vedashree, S.; Vedamurthy, A.B. *Cytotechnol.* **2013**, *65*, 407-417.
[110] Ling, L.-U.; Tan, K.-B.; Chiu, G.N.C. *Cell Death Dis.* **2011**, *2*, 1-12.

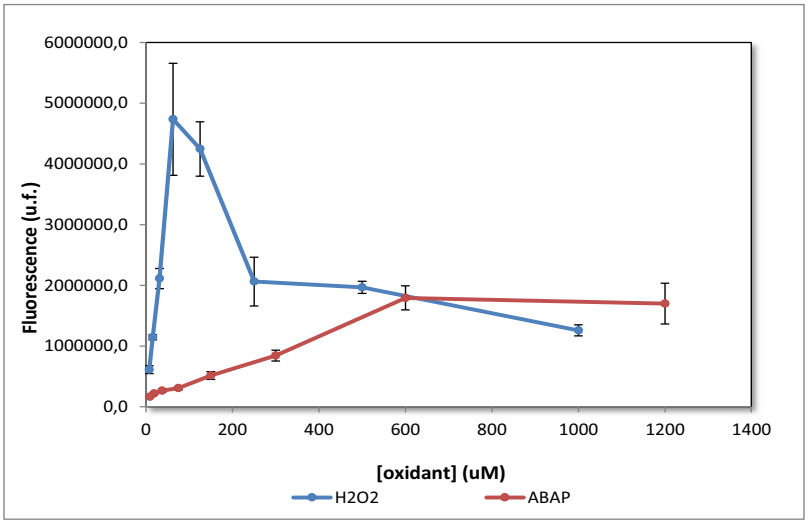

Figure 4.10. *Plot of the fluorescence versus the concentration of oxidant reagent for H_2O_2 (in blue) and ABAP (in red) in T98 cell line.*

To optimize the assays, the concentration of H_2O_2 for the CAA assay in MDA-MB-231 and MDA-MB-468 cell lines was determined. In a 96-well plate, 60 000 cells/well were seeded from a suspension in culture media (Dubelco's Modified Eagle Medium, DMEM, supplemented with 10% v/v Foetal Bovine Serum, FBS, and 100 ng/mL of penicillin and streptomycin). Then, the plate was incubated overnight at 37ºC in 5% CO_2 and humidified atmosphere. After the removal of the culture media, a solution of 25 µM DCFH-DA was added in each well, and the plate was incubated for one additional hour. During this time, DCFH-DA, taking advantage of its low polarity, entered into the cell and DA was removed for the action of cellular esterases. Thus, after the removal of all media in wells, a solution of 1000 µM H_2O_2 in EBSS (Eagle's Balance Salt Solution) was added by triplicate in the first row of the plate. In subsequent rows, the concentration of oxidant was diluted by half arriving close to 0 µM in the last row. After 1 hour of incubation, the fluorescence of DCF was measured at $\lambda_{emission}$= 530 nm and $\lambda_{excitaticon}$= 425 nm. These results are shown in Figure 4.11. Controls and blanks were measured at the same time: positive control corresponded to a solution of DCFH-DA with H_2O_2 and blanks to EBSS and DCFH-DA only.

As explained above, the fluorescence of DCF in presence of H_2O_2 increased to a maximal response at 125 µM and then decreased at higher concentrations. Hence, a solution of 125 µM H_2O_2 was selected for further experiments. In addition, Figure 4.11 shows the different fluorescence response for both cell lines. MDA-MB-231 cells had nearly double intensity signal than MDA-MB-468 cells with maximum of 1475 and 836 u.f. (units of fluorescence), respectively, at 125 µM H_2O_2. These differences might come from the different morphology or the different induction of oxidative stress between the two cell lines.

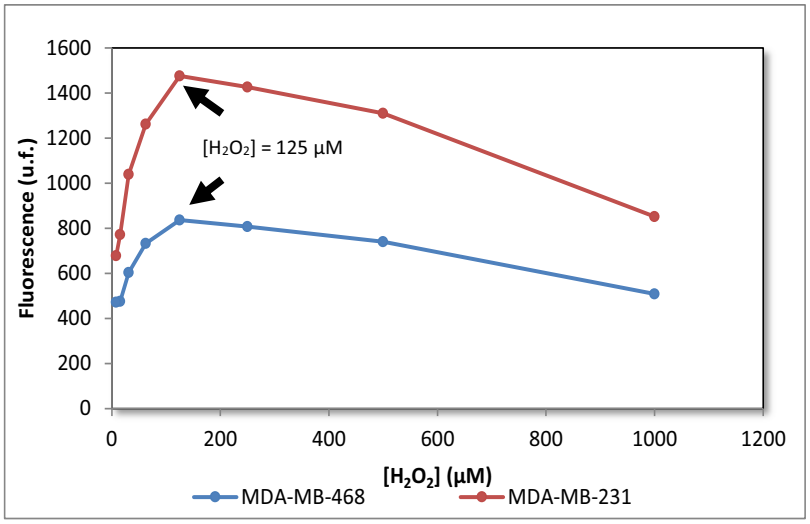

Figure 4.11. *Determination of maximal concentration of H_2O_2 in the assay using MDA-MB-231 and MDA-MB-468 cell lines. For both cell lines, the maximal concentration of H_2O_2 was 125 µM.*

*IV.3.2.2 Evaluation of the cell antioxidant activity of compounds **A**-**N***

IV.3.2.2.1 Evaluation of the antioxidant activity at a given concentration of antioxidant

The antioxidant activity of synthesized antioxidants (from **A**-**N**) was evaluated at a fixed concentration of 50 µM in the two different cell lines (MDA-MB-231 and MDA-MB-468), and results were compared to commercial reference Resveratrol, and tocopherol-like derivatives Trolox and CR-6. Thus, in a 96-well plate 60000 cells/well were seeded from a suspension in culture media. The plate was incubated overnight at 37ºC in 5% CO_2 and humidified atmosphere. Then, the media was removed and 100 µL of 50 µM antioxidant (from **A** to **N**) in culture media were added by triplicate in presence of 25 µM DCFH-DA. After 1 hour, it was assumed that the antioxidant compound and DCFH-DA reached the interior of the cell; then, the media was removed and a solution of 125 µM of H_2O_2 in EBSS was added in each well. The plate was incubated for 1 more hour. After this time, the fluorescence was measure at $\lambda_{emission}$= 530 nm and $\lambda_{excitation}$= 425 nm. Results obtained are shown in Figure 4.12. Controls and blanks were measured at the same time, also by triplicate: positive control for a solution of DCFH-DA with H_2O_2 and blanks for EBSS and DCFH-DA only.

Less fluorescent signal corresponds to less generation of DCF by the oxidation of DCFH; therefore, it means less production of oxidative species due to a higher capacity of antioxidant. CR-6 and Trolox, which were used as tocopherol-like references, exhibited better antioxidant activities than resveratrol (RV) in both cell lines. As in Figure 4.12, the new antioxidant compounds presented similar activity for both cell types. Compounds **J** and **G** had higher fluorescence signals than controls, that is, lower antioxidant activity. The fluorescence for assayed compounds, Trolox and CR-6 was around the same value in both cell lines, but RV exhibited less response in MDA-MB-468 cells than in MDA-MB-231. In any case, all compounds, except **J** and **G**, showed good antioxidant activities at 50 µM compared to references.

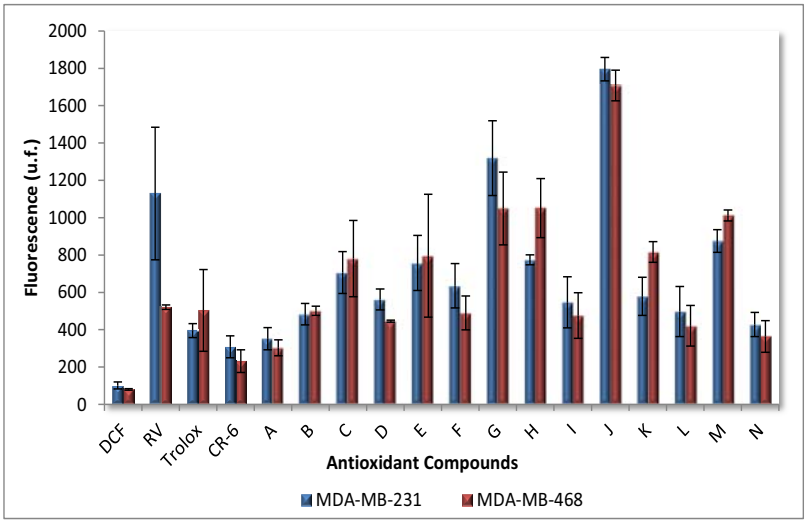

Figure 4.12. *Antioxidant activity of compounds **A**-**N** (50 µM) in the CAA assay. In blue the results for test compounds **A**-**N** in MDA-MB-231 cells and in red for MDA-MB-468 cells.*

Due to the fact that the activity of Trolox and CR-6 was better than resveratrol, it was decided not to use this compound as control in the next experiments.

IV.3.2.2.2 Percentage of oxidant species production for test antioxidant compounds

Since all new compounds showed good activities at 50 µM in both cell lines, the evaluation at a lower concentration was carried out. Taking into account the experiment explained above, all new antioxidant compounds, Trolox and CR-6 were assayed at fixed concentrations of 10 and 50 µM, by triplicate, with the two mentioned MDA-MB-231 and MDA-MB-468 cell lines. Results obtained are shown in Figure 4.13 and 4.14.

In Figures 4.13 and 4.14, the results are presented as percentage of oxidant species (OS) production which is related to the oxidation process of DCFH to DCF and also to the activity of the antioxidant. This parameter was helpful to understand the antioxidant potential of new compounds in a cellular assay by reducing the initial concentration of OS. Hence, better antioxidants would give smaller fluorescence signal and smaller OS-production (%) because it would reduce the quantity of OS in the cell and subsequently the oxidation process of DCFH. Thus, OS-production (%)was calculated by the following expression:[105]

$$OS-production(\%)=\frac{F_{tested}}{F_{control}}\cdot 100$$

where F_{tested} and $F_{control}$ represent the fluorescence for test compounds at a fixed concentration and positive control (DCFH-DA with H_2O_2 in absence of antioxidant), respectively.

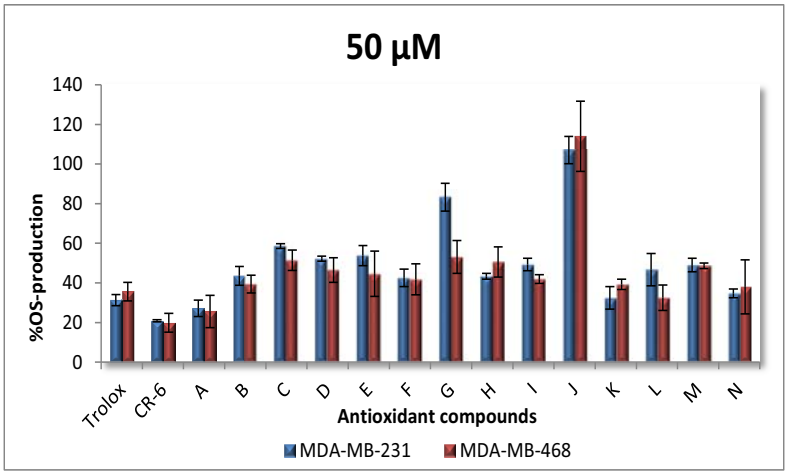

*Figure 4.13. CAA assay for 50 µM of antioxidant compound **A**-**N** at using MDA-MB-231 and MDA-MB-468 cells. Results for Trolox and CR-6 are also shown for comparative purposes.*

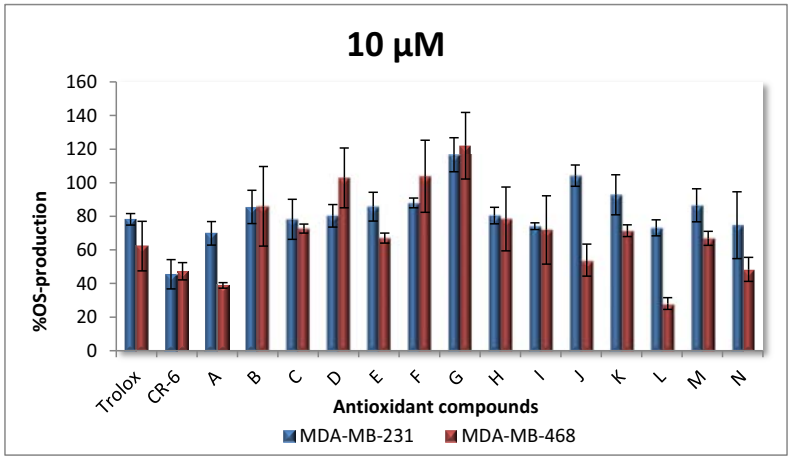

*Figure 4.14. CAA assay for 10 µM of antioxidant compound **A**-**N** at using MDA-MB-231 and MDA-MB-468 cells. Results for Trolox and CR-6 are also shown for comparative purposes.*

According to the results at 50 µM concentration (Table 4.6), most CR-6 analogues exhibited similar antioxidant activities for both cell lines, but none of them showed an antioxidant activity compared to CR-6 (with an OS-production of 19-18%). In the experiments with MDA-MB-468 cells, derivatives **A**, **B**, **F**, **I**, **K**, **L** and **N** presented activities close to Trolox (32% OS-production) from 23 to 39% OS-production. Even though derivatives **C**, **D**, **E**, **G**, **H** and **M** showed less antioxidant activities than references; they did not present high values of OS-production (from 40 to 51%). Finally, compound **J** exhibited no inhibition of OS generation.

Table 4.6. *OS-production (%) for the CAA assay of test compounds **A**-**N** at 10 and 50 µM.*

Antioxidant	OS-production (%)			
	MBA-MD-231		MBA-MD-468	
	10 µM	50 µM	10 µM	50 µM
TROLOX	78	28	56	32
CR-6	46	19	42	18
A	70	24	35	23
B	86	39	89	35
C	78	53	65	46
D	80	47	92	42
E	86	41	76	40
F	88	38	93	38
G	117	75	110	48
H	74	40	78	51
I	74	44	54	38
J	104	109	113	102
K	85	30	71	39
L	73	42	59	29
M	80	45	67	49
N	75	31	43	28

In general, for MDA-MB-231 cells all test compounds demonstrated similar results than in MDA-MB-468 cell line. Derivatives **G** and **L** decreased the capacity to reduce the OS to nearly the double compared to MDA-MB-468 (from 75 to 48% and from 42 to 29%, respectively), showing less antioxidant activity in MDA-MB-231. On the other hand, it is important to point out that derivative **A** was the most active compound in both cell lines.

Regarding the results at 10 µM of antioxidant (Table 4.6) and, as expected, all compounds showed less antioxidant activity than in experiments at 50 µM. For MDA-MB-468 cells, compound **A** exhibited again the best antioxidant activity with only 35% OS-production, in that case better than CR-6 (42%). Only derivative **N** (43% of OS-production) showed comparable results to CR-6. Compounds **I** and **L** displayed an antioxidant activity around 50% (54 and 59%, respectively), which were similar to Trolox (56%). The other compounds displayed a lower activity showing OS-production higher than 60%. At this concentration, **G** and **L** did not elicit antioxidant activity.

In experiments with MDA-MB-231 cells, the activities were still lower. None of the assayed compounds exhibited less than 60% of OS-production and only the reference CR-6 arrived to 46%. However, compounds **A**, **C**, **H**, **I**, **K**, **L**, **M** and **N** showed an OS-production similar to Trolox (78%) from 70 to 85%. As occurred with MDA-MB-468, **G** and **J** did not present any antioxidant activity.

*IV.3.2.2.3 Quantification of the cell antioxidant activity for **A**-**N** compounds*

We have observed that the oxidation of DCFH using H_2O_2 as oxidant reagent was inhibited by antioxidant compounds in a dose-dependent manner. In the above experiments, it was shown that all synthesized antioxidant compounds, except **G** and **J**, had antioxidant activities comparable

with Trolox, CR-6 and resveratrol. Then, to calculate the $logIC_{50}$[95], using GraphPad Prism 5 for Windows,[93] for CAA assay in cell lines MDA-MB-231 and MDA-MB-468, the dose-response nonlinear sigmoidal curves, %OS-production versus log[antioxidant] (from 0 to 100 μM), were plotted (Figure 4.15 for MDA-MB-231 and 4.16 for MDA-MB-468). It was assumed that in some cases the estimated sigmoidal curve was not perfect. However, the $logIC_{50}$ was considered as a good parameter to compare the new test antioxidant compounds. As it can be observed in Figures 4.15 and 4.16, if the concentration range was increased to higher concentrations, the sigmoidal curve in some cases would be completed.

On the other hand, to know the half-maximal inhibitory concentration, the IC_{50} (μM) was obtained. Three values are shown in Tables 4.7 and 4.8 and expressed as triplicates.

Table 4.7. *Results of test antioxidant compounds* ***A-N*** *in the CAA assay using the MDA-MB-231 cell line.*

Antioxidant[a]	IC_{50}(μM)	95% Confidence Interval IC_{50}	$logIC_{50}$	95% Confidence Interval $logIC_{50}$
Trolox	11.61	(10.07; 13.40)	1.065	(1.003; 1.127)
CR-6	4.54	(4.02; 5.13)	0.657	(0.604; 0.710)
A	7.73	(6.46; 9.27)	0.888	(0.810; 0.967)
L	8.41	(7.14; 9.91)	0.925	(0.854; 0.996)
N	9.16	(7.66; 10.96)	0.962	(0.884; 1.040)
I	13.50	(11.85; 15.38)	1.133	(1.074; 1.187)
F	16.40	(12.79; 21.04)	1.215	(1.107; 1.323)
E	21.52	(17.91; 25.88)	1.333	(1.253; 1.413)
B	22.08	(19.05; 25.53)	1.344	(1.280; 1.407)
C	22.89	(19.36; 27.04)	1.360	(1.287; 1.432)
K	36.06	(29.58; 44.06)	1.557	(1.471; 1.644)
H	39.71	(33.65; 46.88)	1.599	(1.527; 1.671)
M	46.58	(37.76; 57.41)	1.668	(1.577; 1.759)
G	66.30	(58.75; 74.82)	1.822	(1.769; 1.874)
D	89.09[b]	(77.80; 102.09)	1.950	(1.891; 2.009)
J	*no inhibition*	-	-	-

[a] The test compounds **A-N** are ordered from the strongest to the weakest antioxidant.
[b] The experiment for this molecule was repeated to discard likely mistakes, but the negative result was confirmed.

Table 4.8. *Results of test antioxidant compounds* ***A-N*** *in the CAA using the MDA-MB-468 cell line.*

Antioxidant[a]	IC_{50}(μM)	95% Confidence Interval IC_{50}	$logIC_{50}$	95% Confidence Interval $logIC_{50}$
Trolox	11.69	(9.79; 14.66)	1.078	(0.991; 1.166)
CR-6	4.34	(3.47; 5.45)	0.638	(0.540; 0.736)
A	3.64	(2.88; 4.60)	0.561	(0.459; 0.663)
F	6.20	(4.92; 7.83)	0.793	(0.692; 0.894)
N	10.73	(6.59; 14.76)	1.031	(0.819; 1.169)
L	12.52	(10.69; 14.69)	1.098	(1.029; 1.167)
D	13.47	(10.74; 16.90)	1.129	(1.031; 1.228)
B	13.54	(10.96; 16.71)	1.132	(1.040; 1.223)
E	19.46	(15.38; 24.60)	1.289	(1.187; 1.391)
I	19.93	(16.29; 24.38)	1.299	(1.212; 1.387)
C	23.87	(18.45; 30.90)	1.378	(1.266; 1.490)
K	32.45	(24.10; 43.65)	1.511	(1.382; 1.640)
M	48.93	(33.96; 70.47)	1.690	(1.531; 1.848)
H	61.12	(45.50; 82.04)	1.786	(1.658; 1.914)
G	87.73	(72.95; 105.44)	1.943	(1.863; 2.023)
J	*no inhibition*	-	-	-

[a] The test compounds **A-N** are ordered from the strongest to the weakest antioxidant.

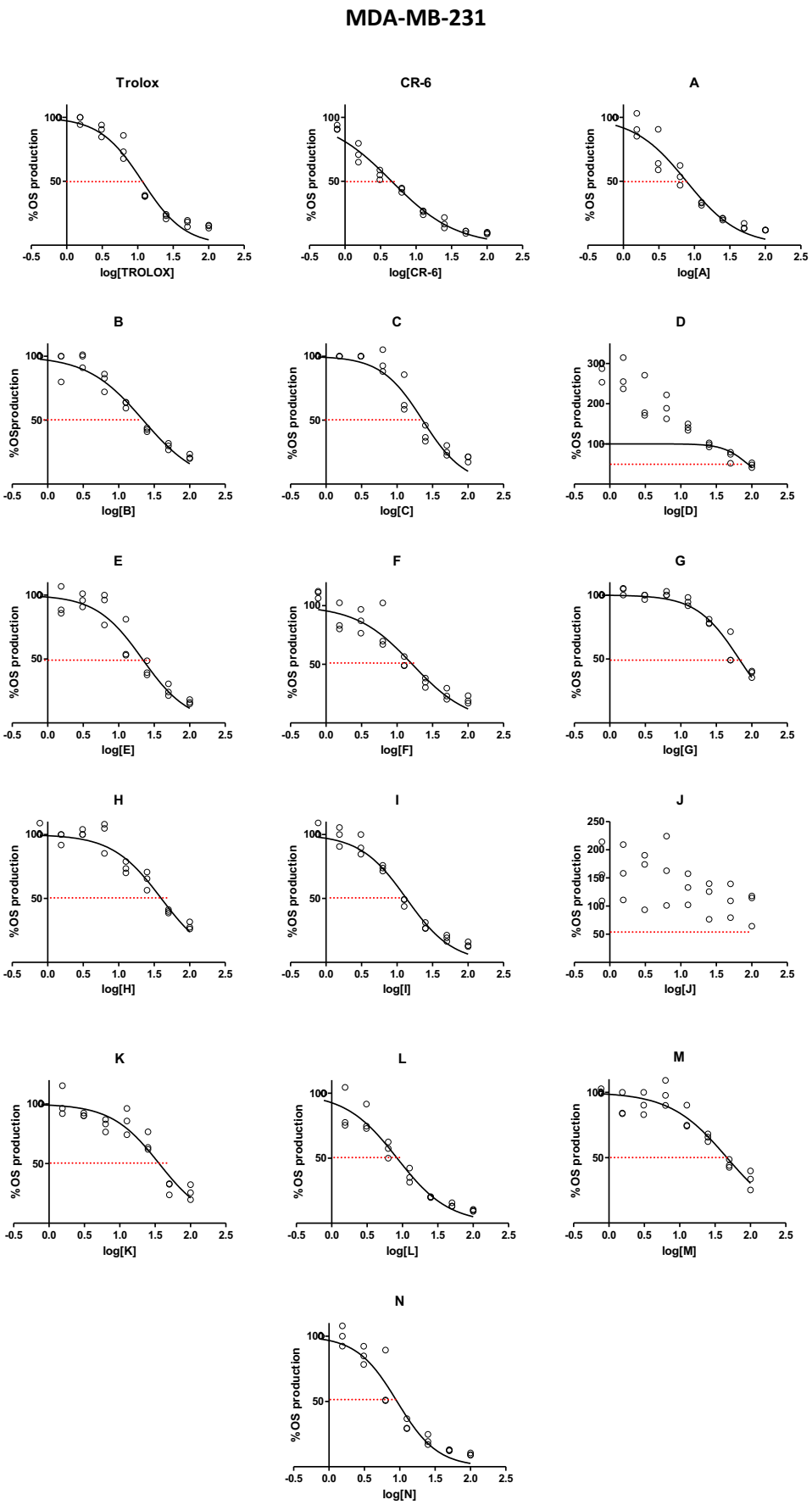

Figure 4.15. *Plot of %ROS versus log[Antioxidant] for MDA-MB-231 cell line. The IC_{50} value was determined with GraphPad Prism 5 for Windows. The red line indicates the 50% of OS-production.*

According to data derived from MDA-MB-231 cell line (Table 4.7), compounds **A**, **L** and **N** were the most effective antioxidants, although the values obtained differed from CR-6 activity. However, their activity and the activity of compounds **F** and **I** could be compared to that of Trolox. **G** and **D** presented the lowest antioxidant activity of that group of compounds. **J** had not inhibition of the oxidative stress, and its $logIC_{50}$ could not be calculated. Considering the overall data, the antioxidant activity of test compounds for MDA-MB-231 cell line could be ordered as: **CR-6** > **A** > **L** > **N** > **Trolox** > **I** > **F** > **E** > **B** > **C** > **K** > **H** > **M** > **G** > **D**.

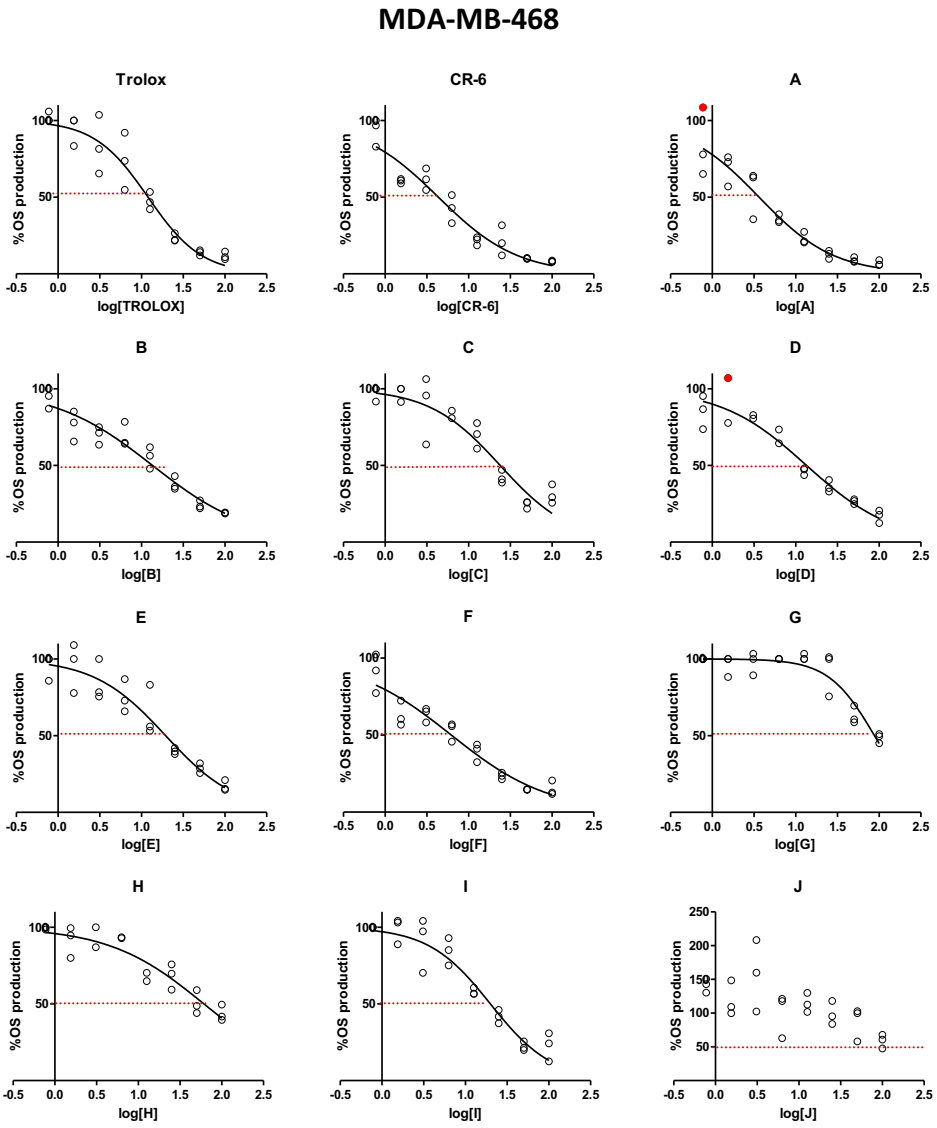

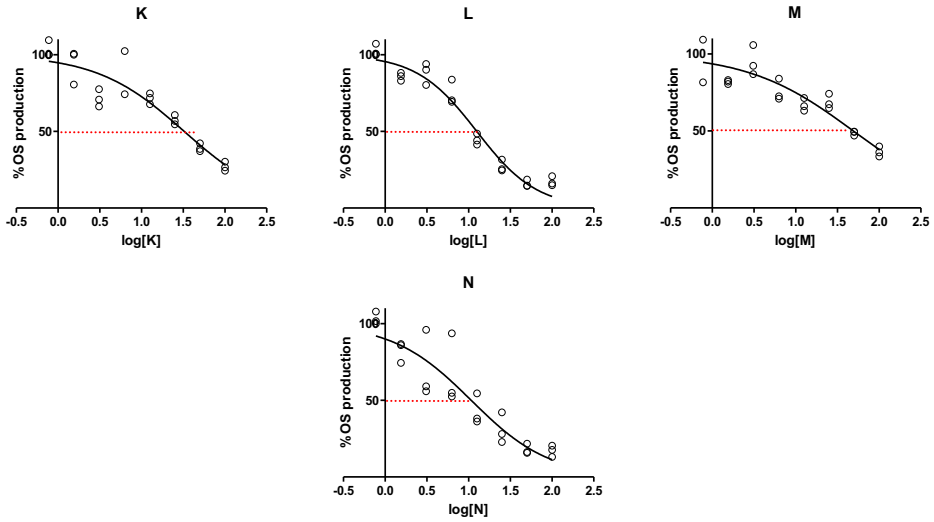

Figure 4.16. *Plot of %ROS versus log[Antioxidant] for MDA-MB-468 cell line. The IC_{50} value was determined with GraphPad Prism 5 for Windows. Red points correspond to the outliers when nonlinear sigmoidal curve is adjusted. The red line indicates the 50% of OS-production.*

For experiments with MDA-MB-468 cells (Table 4.8), slight differences in the antioxidant efficiency from results with MDA-MB-231 were observed. Derivatives **A** and **E** showed the best antioxidant activities, comparable to that of CR-6, and they were better than with MDA-MB-231 cell line. Compounds **B** and **D** also presented better antioxidant activities in the experiments with MDA-MB-468. However, compounds **C**, **E**, **K, M** and **N** exhibited the same antioxidant activity for both cell lines, and **G**, **H**, **I** and **L** had higher logIC_{50}. As in the other cell lines, derivative **J** did not shown inhibition of the production of oxidant species and its logIC_{50} could not be calculated. Therefore, the antioxidant activity for assayed compounds for MDA-MB-468 cell line could be ordered as: **A** > **CR-6** > **F** > **N** > **Trolox** > **L** > **D** > **B** > **E** > **I** > **C** > **K** > **M** > **H** > **G**. Surprisingly, while all compounds maintained more or less the same logIC_{50} for both cell lines, compound **D** presented a big difference among the respective values. The experiments for this compound were repeated, but there was no change on the results obtained. It is worth noting that compound **B**, which was the worst antioxidant of the series in the DPPH assay, appeared as a moderate antioxidant agent in CAA assay.

*IV.3.2.3 Statistical comparison of the activity of compounds **A**-**N** and Trolox with CR-6 in the cellular assay using MDA-MB-231 and MDA-MB-468 cell lines*

Similarly to the statistical comparison carried out on the DPPH results (in section IV.2.3.6, page 110), the results of the CAA assay of compounds **A**-**N**, and Trolox were compared to CR-6 for both MDA-MB-231 and MDA-MB-468 cell lines.

In CAA, the different morphology of the two cell lines used and the different permeation of the molecules (or reagents, like H_2O_2 or DCFH-DA) through the lipidic bilayer membrane are relevant for the final antioxidant activity. Furthermore, not only the chromane moiety and the phenolic hydrogen atom

are implicated in the activity, as occurred in the DPPH assay. In CAA, the whole structure of the compound and its physicochemical properties (lipophilicity) or the presence of a specific mechanism of transport in the membrane can exert some influence. Large, highly hydrophilic, and lipophilic compounds can have problems to penetrate through the cellular membrane and to reach the cytosol, where all biochemical processes of the assay take place. In addition, the different cell types can operate with different enzymes that metabolize some of the compounds into molecules of unpredictable activity. Taken together, they can present differences on their behaviour in the CAA assay (Figure 4.9, page 114).

Thus, the three statistical methods explained in section IV.2.3.4, page 104, were also followed in this case. For MDA-MB-231 cells, as expected looking at $logIC_{50}$-values, significant differences ($p \leq 0.05$) were found using the three statistical methods:[93,96,97,98,99,100,101] All new antioxidant compounds and Trolox appeared as significantly poorer antioxidants than CR-6. Results for the t-test, which compared the $logIC_{50}$ of test compounds with $logIC_{50}$ of CR-6, and for Wald's test, that compared the estimated regression lines, are shown in Figures 4.17 and 4.18 respectively.

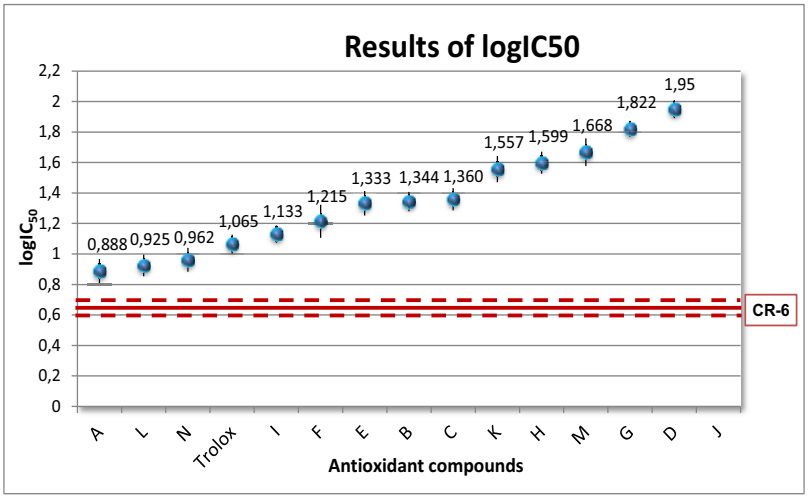

Figure 4.17. *$LogIC_{50}$ Statistical comparison of CR-6 with test compounds for MDA-MB-231 cells by using t-test in STATA 12.0. Red lines are the $logIC_{50}$ and its 95% Confidence Interval for CR-6.*

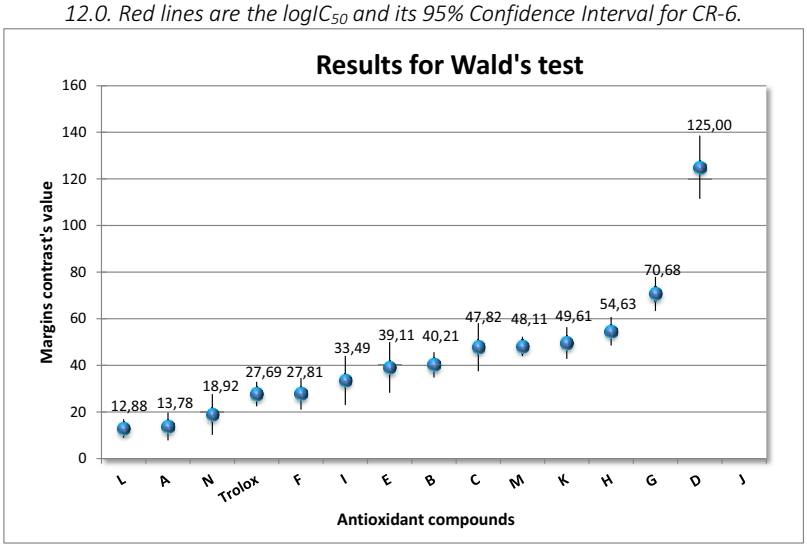

Figure 4.18. *Statistical comparison of regression line from linear part of adjusted sigmoidal curve (%Inhibition vs log[Antioxidant]) for MDA-MB-231 cells by a Wald's test in STATA 12.0.*

These results suggest that CR-6 has better penetration across the cell membrane or its interaction with enzymes that could metabolize the antioxidant is less effective. Compounds **D** and **G** showed the worst activity of the group. Compound **J** did not elicit inhibition, probably due to its large size and high lipophilicity, and exhibit problems to reach the cytosol.

The results for MDA-MB-468 cells (t-test and Wald's test results) are shown in Figures 4.19 and 4.20. In this case, compound **A** was the only antioxidant assayed that exhibited significant similarities ($p \geq 0.05$) better than CR-6. In case of compound **F**, although the inferior limit of confidence interval overlapped the superior limit of $logIC_{50}$ of CR-6, it did not show significant similarities with CR-6 (Figure 4.19).

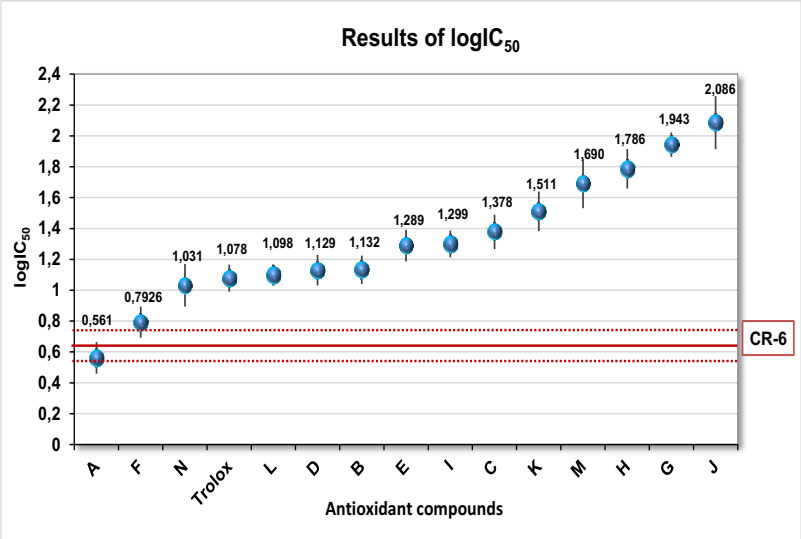

Figure 4.19. *$LogIC_{50}$ Statistical comparison of CR-6 with test compounds for MDA-MB-468 cells by using the t-test in STATA 12.0. Red lines are the $logIC_{50}$ and its 95% Confidence Interval for CR-6.*

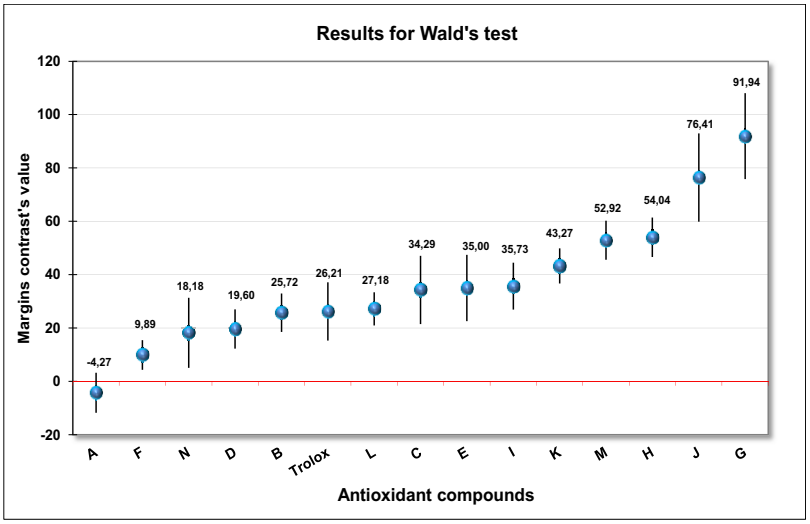

Figure 4.20. *Statistical comparison of regression line from linear part of adjusted sigmoidal curve (%Inhibition vs log[Antioxidant]) for MDA-MB-468 cells by a Wald's test in STATA 12.0.*

On the other hand, it is accepted that both cell lines have different membrane morphology, which could cause different mechanisms of transport of the molecules for penetrating inside the cell. Then, for

example, compound **D**, being the worst antioxidant compound in MDA-MB-231 cell line, was a good one in MDA-MB-468 cells. Other cases showed no differences (**C**, **K**, **M**, **N**, and **Trolox** and **CR-6**), suggesting that these molecules are not affected by the different membrane morphology or metabolizing enzyme profile. It could be that these compounds are delivered to the cytosol by passive diffusion.

From another point of view, most test compounds exhibited differences from CR-6 in the CAA for MDA-MB-231 and MDA-MB-468 cell lines. However, these differencies are not so relevant regarding the chemical structure of tested compounds. Thus, only compounds with $\log IC_{50} > 1.2$ (IC_{50} = 15.8 µM, the double value of $\log IC_{50}$ for CR-6 ($\log IC_{50}$ 0.638; IC_{50} = 4.35 µM), were really different from CR-6. In consequence, only compounds such as **Trolox**, **A**, **B**, **D**, **F**, **L** and **N** were considered similar to CR-6 for MDA-MB-468 cells, and **Trolox**, **A**, **I**, **L** and **N** for experiments with MDA-MB-231 cells.

To sum up, with the exception of compound **J**, the insertion of residues ay C_2 in CR-6 scaffold did not affect significantly the antioxidant activity. Even in some cases (for example, compound **A**), the antioxidant activity was higher than the exhibited by CR-6. These results gave us confidence to test the ability of these new CR-6 derivatives to cross the Blood-Brain-Barrier (BBB) using different models.

V. Evaluation of permeability through Blood-Brain Barrier models

V.1 STRUCTURAL PREDICTION

The previous data on *in vivo* treatments with CR-6,[1,9,18] which indicated that this compound can pass through the blood-brain barrier (BBB) although in minimum amount, suggested that this crossing might be by a passive diffusion transport.

All antecedents mentioned previously and structural features suggest that new test antioxidants (**A**-**N**) might use different mechanisms of transport to enter into the brain parenchymia (Table 5.1).

Table 5.1. *Prediction of mechanisms of transport for all new CR-6-analogues.*

ANTIOXIDANT	Mechanism of transport
A	Passive Diffusion
B	LAT-1 or MCT1
D	LAT-1 or MCT1
C	LAT-1 or MCT1
E	LAT-1 or MCT1
F	LAT-1 or MCT1
G	LAT-1 or MCT1
H	X_G^-
I	Passive diffusion
J	RMT for retinal
K	GLUT-1
L	Passive diffusion
M	Passive diffusion or LAT-1
N	Passive diffusion or MCT1

The acid carboxylic group or the amido-acid moiety of compounds **B** to **G** would be delivered through a CMT of monocarboxylic acids or of amino acids such as MCT1 or LAT-1, respectively. Compound **H** would be transported thanks to glutamate transporter X_{G^-} that recognizes the two carboxylic acids of the molecule. Compound **J** would enter into the brain by receptor-mediated transcytosis. Compound **K** could be recognized for GLUT-1 due to its similarity to D-glucose. Compounds **I**, **L**, **M** and **N** would not be recognized by any specific protein, but their physicochemical properties might be suitable to be delivered by transcellular passive diffusion. In case of **A**, the presence of the chromanee moiety would help to be diffused through endothelial cells. However, compounds **M** and **N**, bearing the amino acid and carboxylic acid groups, might be also recognized by LAT-1 or MCT1.

At this point, *in silico* and *in vitro* models were performed to study the transport through the BBB of the new CR-6 analogues and compared them with references Trolox and CR-6.

V.2 *IN SILICO* ANALYSIS

In general terms, drugs can be divided into CNS and non-CNS drugs depending on the ability to be transported through the blood-brain barrier (BBB).[111] Our overall goal was to use the tocopherol-scaffold to generate a short library of compounds capable of being delivered through BBB and improve the CR-6 neuroprotective activity. These CNS candidates must be optimized for CNS physicochemical properties and ADME (Absorption, Distribution, Metabolism and Excretion) requirements. Although the evaluation of properties is critical when the CNS is the target, useful *in silico* guidelines were performed to make decisions for a successful drug development.[112]

V.2.1 Relevant physicochemical properties for CNS and non-CNS drugs

For many years, a large number of reports have attempted to establish the physicochemical properties of CNS drugs that are crucial for the BBB penetration. More than 100 years ago, some authors started to connect the lipophilic character of simple neutral organic compounds with a narcotic activity.[113] At the end of the last century, other authors have discussed the necessity of a hydrophobic-hydrophilic equilibrium and an optimal logP (octanol-water partition coefficient) for drugs that penetrate or are precluded from penetrating the brain.[114]

In 1997, Lipinski established the well-known rule of five (RO5) that described the drug-likeness from a database of clinical candidates, CNS and non-CNS targeted, in phase II trials or even more advanced.[40c,115] This rule defined endpoints for four physicochemical properties that described the most orally administered active drugs in humans: the molecular weight, MW < 500 Da; the lipophilicity, logP or the calculated 1-octanol-water partition coefficient, ClogP < 5; the number of hydrogen bond donor (-OH and –NH present in the molecule), HBD < 5; and the number of hydrogen bond acceptor (O and N present in the molecule), HBA < 10. These parameters described fundamental attributes for a drug associated with aqueous solubility and intestinal permeability, which are key factors for the first step of oral bioavailability.

Over the years, scientists formulated various guidelines as a tool for medicinal chemists in the drug design based on the most valuable physicochemical properties.[116] It was also noted that efflux pumps (such as P-gp), present not only in the BBB but in other membrane barriers, such as the intestinal, contributes to the poor uptake of some compounds. Related to this, in 2002, Mahar Doan *et al.* studied

[111] Ghose, A. K.; Herberts, T.; Hudkins, R.L.; Dorsey, B.D.; Mallamo, J.P. *ACS Chem. Neurosci.* **2012**, *3* (1), 50-68.
[112] Lowe, J.T.; Lee IV, M.D.; Akella, L.B.; Davoine, E.; Donckele, E.J.; Durak, L.; Duvall, J.R.; Gerard, B.; Holson, E.B.; Joliton, A.; Kesavan, S.; Lemercier, B.C.; Liu, H.; Marié, J.-C.; Mulrooney, C.; Muncipinto, G.; Welzel-O'Shea, M.; Panko, L.M.; Rowley, A.; Suh, B.-C.; Thomas, M.; Wagner, F.F.; Wei, J.; Foley, M.A.; Marcaurelle, L.A. *J. Org. Chem.* **2010**, *77*, 7187-7211.
[113] a) Overton, E. *Z. Phys. Chem.* **1897**, *22*, 198-209. b) Meyer, H. *Arch. Exp. Pathol. Pharmakol.* **1899**, *42*, 109-118.
[114] Hansch, C.; Björkroth, J.P.; Leo, A. *J. Pharm. Sci.* **1987**, *76*, 663-687.
[115] Lipinski, C.A. *Drug Discovery Today: Technol.* **2004**, *1*, 337-341.
[116] Van de Waterbeemd, H.; Camenisch, G.; Folkers, G.; Chretien, J.R.; Raevsky, O.A. *J. Drug Targeting*, **1998**, *6*, 151-165.

the passive permeability, the P-gp-mediated efflux and 18 physicochemical properties for marketed CNS and non-CNS drugs.[117] They concluded that CNS-drug set exhibited fewer hydrogen bond donors (HBD), fewer positive charges, higher lipophilicity (represented by logP), smaller polar surface areas (PSA) and reduced flexibility than non-CNS drugs. Later on, in 2007, Manallack studied the pK_a distribution as another important attribute for the bioavailability of CNS and non-CNS drugs in human, concluding that pK_a values should be restrained between 6 and 10.5 in case of CNS drugs.[118]

In 2008, Hughes *et al.*, examining physicochemical drug properties associated with *in vivo* toxicology outcomes, confirmed that toxicity was increased for highly lipophilic (ClogP > 3) and low polar (topological polar surface area, TPSA < 75 $Å^2$) compounds.[119] These two factors could provide to medicinal chemists the safety and the probability of succeeding in a particular chemical space. On the contrary, the brain permeability, crucial in the design of new CNS drugs, can be improved by the modification of new compounds towards ClogP < 3 and TPSA > 75 $Å^2$ area. However, the application of these cutoffs would be significantly restrictive and would lead to undue hardship in the discovery of CNS drugs. Consequently, the identification of strategies to balance these attributes is important to success in both brain penetration and safety perspectives.

Furthermore, medicinal chemists have modified the molecule lipophilicity with the aim of improving simultaneously multiple ADME and safety attributes. However, in 2010, Wager *et al.* pointed out that the variation of a single parameter may fail.[120] Hence, in order to achieve the optimum balance of ADME and safety characteristics, multiple physicochemical properties of a molecule should be modified.

Also in 2010, Wager *et al.* reported the analysis of the physicochemical properties, the *in vitro* ADME attributes, the binding efficacies and the *in vitro* safety assay data associated to 119 CNS marketed drugs and 108 CNS candidates to identify the most favourable CNS property space.[121] They generated a significant amount of data that may lead to a successful set of CNS drug candidates. From these data, they established a multiparameter called CNS MPO which is based on six fundamental physicochemical properties. They also studied the alignment of CNS MPO desirability score for CNS drugs, candidates and a large diverse set of proprietary Pfizer compounds with the desired *in vitro* ADME and safety attributes.

[117] Mahar Doan, K.M.; Humphreys, J.E.; Webster, L.O.; Wring, S.A.; Shampine, L.J.; Serabjit-Singh, C.J.; Adkinson, K.K.; Polli, J.W. *J. Pharmacol. Exp. Ther.* **2002**, *303*, 1029-1037.
[118] Manallack, D.T. *Perspect. Med. Chem.* **2007**, *1*, 25-38.
[119] Hughes, J.D.; Blagg, J.; Price, D.A.; Bailey, S.; DeCrescenzo, G.A.; Devraj, R.V.; Ellsworth, E.; Fobian, Y.M.; Gibbs, M.E.; Gilles, R.W.; Greene, N.; Huang, E.; Krieger-Burke, T.; Loesel, J.; Wager, T.; Whiteley, L.; Zhang, Y. *Bioorg. Med. Chem. Lett.* **2008**, *18*, 4872-4875.
[120] Wager, T.T.; Hou, X.; Verhoest, P.R.; Villalobos, A. *ACS Chem. Neurosci.* **2010**, *1*, 435-449.
[121] Wager, T.T., Chandrasekaran, R.Y.; Hou, X.; Troutman, M.D.; Verhoest, P.R., Villalobos, A.; Will, Y. *ACS Chem. Neurosci.* **2010**, *1*, 420-434.

V.2.2 *In silico* analysis by multiparameter optimization methods

V.2.2.1 Multiparameter description and desirability functions

Multiparameter optimization methods are commonly used to assess and balance the effects of several variables which are weighted based on their importance to the overall objective. Harrington was the first to introduce the concept of "desirability function" as the transformation of several attributes into dimensionless scales which were arithmetically or geometrically combined into a single score. [122] Wager *et al.* applied a variant of Harrington's optimization method which involved the summation of individual components to build up a combined desirability score.[120]

Figure 5.1 shows two different desirability functions. A monotonic function (Figure 5.1, A)) is defined by two inflexion points: a desirability region for $x \leq x_1$ and an undesirability region for $x > x_2$; and a linear transformation between the two inflexion points, for $x_1 < x \leq x_2$. A hump function (Figure 5.1, B)) is defined by two undesirable regions and one desirable region, with two linear transformations in between. *x*-Variable (x_1, x_2 and x) is formed by the components of the selected property that delimited the desirability areas. The resultant desirability score (*y*-value) has a number from 0.0 to 1.0 for each region: 1.0, for components in desirable region; 0.0, for components in undesirable region; and a number between 0.0 and 1.0, which is the $\hat{y}$-value estimated from a regression line, for those in the linear transformation area delimited between the two inflexion points. The *y*-value corresponds to the transformation of the components or attributes and is called T0.

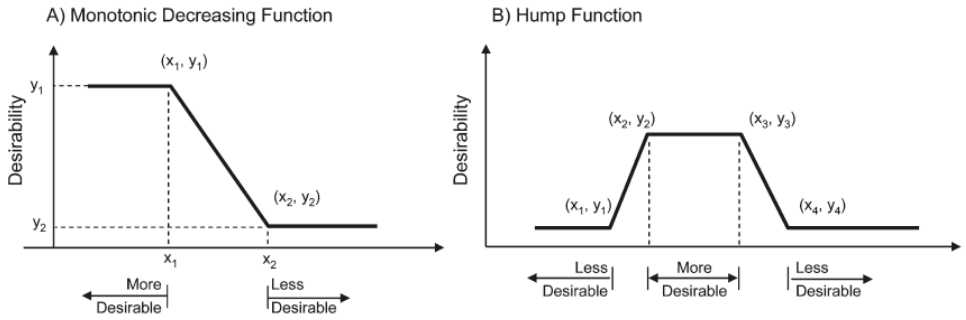

Figure 5.1. Monotonic Decreasing Function (A) and Hump Function (B) for the calculation of CNS MPO scores. These two functions are extracted from Wager et al.[120]

The overall desirability function is the sum of all transformed components (T0) – the summation represents a way to reduce the severe penalty if the desirability score of one parameter is outside the desired limits, comparing to a multiplication in which the final score would be at or near zero. An example to clarify the concept is commented below.

[122] Harrington, E. C., Jr. *Ind. Qual. Control*, **1965**, *21*, 494-498.

V.2.2.2 CNS MPO and the alignment to ADME and safety attributes

The CNS MPO score was built up using six fundamental physicochemical properties commonly employed in the design of compounds to address specific ADME and safety issues: ClogP, ClogD, MW, TPSA, HBD and pK_a. From the analysis of 119 marketed CNS drugs and 108 CNS candidates to identify the most favorable CNS property space, Wager *et al.* set up the desirable range for each physicochemical property (Table 5.2).[120] On that account, for a better understanding for each data a value from 0.0 to 1.0 was ascribed for weighting the transformed values (T0) of the desirability functions. The plot of T0 for each drug or candidate resulted on a monotonic decreasing function for ClogP, ClogD, MW, HDB and pK_a properties, and a hump function for TPSA property. As an example, for a CNS drug with ClogP ≤ 3 a T0 = 1.0 was assigned. If the ClogP was > 5, the T0 would be 0.0; and for a ClogP between 3 and 5, the desirability value would be obtained from the regression line delimited between the desirability and non-desirability area. The same principle was followed with the other properties (Table 5.2). Thus, the CNS MPO score was obtained from the summation of all T0 for each physicochemical property, obtaining a value from 0.0 to 6.0.

***Table 5.2**. The CNS MPO properties, functions, weights, value range and parameter range. The desirable range for each physicochemical property was set up by Wager et al. from the analysis of 119 marketed CNS drugs and 108 CNS candidates to identify the most favorable CNS property space.[120]*

Properties	Transformation T0	Weight	Desirable range (T0 = 1.0)	Non-desirable range (T0 = 0.0)
ClogD	Monotonic decreasing	1.0	ClogD ≤ 2	ClogD > 4
ClogP	Monotonic decreasing	1.0	ClogP ≤ 3	ClogP > 5
TPSA	Hump function	1.0	40 < TPSA ≤ 90	TPSA ≤ 20; TPSA > 120
MW	Monotonic decreasing	1.0	MW ≤ 360	MW > 500
HBD	Monotonic decreasing	1.0	HBD ≤ 0.5	HBD > 3.5
pK_a	Monotonic decreasing	1.0	pK_a ≤ 8	pK_a > 10

A CNS MPO algorithm was established to guide medicinal chemists in the way of high-throughput (HT) trials or the evaluation of chemical matters without carrying out *in vitro* assays. Hence, Wager *et al.* evaluated the alignment of drug-like ADME and safety characteristics with the desirable CNS MPO (> 5).[121] From the analysis of the compounds set, they compared the distribution of the CNS MPO with four drug-like ADME and safety end points: (a) high passive apparent permeability, P_{app} (low for $P_{app} \leq 2.5$, medium for $2.5 < P_{app} \leq 10$, and high for $P_{app} > 10 \cdot 10^{-6}$ cm/s); (b) low P-gp efflux liability, ER (low P-gp liability for ER ≤ 2.5); (c) high metabolic stability, $CL_{int,u}$ (low clearance for $CL_{int,u} \leq 100$ and high clearance for $CL_{int,u}$ > 100 mL/(min·kg)); and (d) low general toxicity, THLE Cv (low cell viability for THLE Cv ≤ 100 μM and high cell viability THLE Cv > 100 μM). These analyses showed that higher CNS MPO desirability score enhances the probability of identifying compounds in the drug and candidate sets bearing drug-like ADME and safety attributes.

Conclusively, the CNS MPO algorithm does increases the probability of identifying compounds with the desired *in vitro* ADME and safety attributes from a large and diverse set, reinforcing the potent general utility of this tool beyond the CNS area. In many cases, if the hard cutoffs had been applied for one or some physicochemical properties, numerous compounds would have been eliminated, resulting in a lost opportunity for new drugs. CNS MPO enables more physicochemical flexibility and expands design space whereas it enhances the probability to identify a compound with drug-like properties and accelerate the discovery of new medicines.

V.2.2.3 CNS MPO for new test antioxidant compounds

The *in silico* analysis with the CNS MPO algorithm calculation was performed with the assistance of Dr. Jordi Bujons Vila from *Department of Biological Chemistry and Molecular Modelling* in our institute. The CNS MPO score was calculated for the new antioxidant compounds (**A**-**N**), Trolox and CR-6 to predict if they could be considered as good CNS candidates by passive diffusion through BBB before performing the corresponding *in vitro* assays.

Following Wager report, calculated physicochemical properties for test compounds (Trolox, CR-6 and new antioxidants from **A** to **N**) were obtained using standard commercial packages (Table 5.3):[120] Chemdraw for ClogP, ACD/Laboratories for pK_a and ClogD at pH 7.4, and for calculation of TPSA, the protocol reported by Ertl *et al.* were used (calculations for TPSA are in Supporting Information CD).[123] Regarding these calculations, the transformed values (T0) of desirability functions for the selected six physicochemical properties (ClogP, ClogD, MW, TPSA, HBD and pK_a) were weighted assigning a value from 0.0 to 1.0 depending if they were in a desirable or undesirable range of the cutoffs (Table 5.2, page 135). Table 5.3 shows the T0 values obtained for assayed compounds. The values of the six physicochemical properties for all these compounds are shown in the Supporting Information section (CD). The CNS MPO value was estimated from the summation of these six T0 from the physicochemical properties. Taking into account the CNS MPO drug-like values (≥ 5), conclusions about the prediction on ADME and safety attributes for test compounds were extracted.

Considering all the CNS MPO data, no one of the tested compounds, neither Trolox nor CR-6, exhibited a value > 4.5 (Table 5.3); thus, and concerning passive diffusion, these results predicted low ADME and safety attributes *in vivo* for assayed compounds as CNS candidates and oral drugs. Trolox and **N** showed the best results (CNS MPO = 4.5) although they are a bit lower than results expected for a good drug-like candidate (CNS MPO > 5) from Wager *et al.* analysis. CR-6, **E**, **I** and **K** derivatives scored from 4 to 4.5; compounds **C**, **D**, **F** and **M** were between 3 and 4; and the rest (**A**, **B**, **G**, **H** and **J**) showed CNS MPO score lower than 3.

[123] Erlt, P.; Rohde, B.; Selzer, P. *J. Med. Chem.* **2000**, *43*, 3714-3717.

Remarkably, the CNS MPO scoring was in general negatively impacted by three physicochemical properties which were far from those desired and they did not adjusted to drug-like attributes. All test antioxidant compounds, including references Trolox and CR-6, were systematically characterized by a highly basic pK_a (pk_a > 10.5) due to the phenolic hydroxyl group (pKa = 10.6 – 12.6). In addition, the vast majority feature many HBD (> 3.5) and high TPSA (> 90 $Å^2$) values. On the contrary, the lipophilicity, expressed as ClogP and ClogD, and the MW were positively scored for the CNS MPO algorithm.

Table 5.3. *T0 for the studied physicochemical properties and CNS MPO values for new test antioxidant compounds.*

Antioxidant	T0_MW	T0_TPSA	T0_pK_a	T0_HBD	T0_ClogD	T0_ClogP	CNS MPO[a]
Trolox	1.0	1.0	0.0	0.51	1.0	0.96	4.5
CR-6	1.0	0.90	0.0	0.84	0.49	1.0	4.3
N	1.0	1.0	0.0	0.51	1.0	1.0	4.5
L	1.0	1.0	0.0	0.51	0.78	1.0	4.3
I	1.0	1.0	0.0	0.18	1.0	1.0	4.2
E	1.0	0.50	0.0	0.50	1.0	1.0	4.0
C	1.0	0.50	0.0	0.17	1.0	1.0	3.7
D	1.0	0.50	0.0	0.17	1.0	1.0	3.7
M	1.0	0.60	0.0	0.0	1.0	1.0	3.6
F	0.77	0.50	0.0	0.18	1.0	0.85	3.3
H	0.90	0.0	0.0	0.0	1.0	1.0	2.9
A	0.86	0.40	0.0	0.0	0.61	1.0	2.9
B	0.66	0.0	0.0	0.0	1.0	1.0	2.7
G	0.50	0.10	0.0	0.0	1.0	0.86	2.5
K	0.58	0.0	0.0	0.0	1.0	1.0	2.6
J	0.0	1.0	0.0	0.50	0.0	0.0	1.5

[a] Test compounds were in decreasing order of CNS MPO values.

In any case, it should be asserted that the CNS MPO algorithm should be considered as a predicting tool for ADME and safety attributes, and *in vivo* BBB passive diffusion. Nevertheless, some molecules could not follow it. In consequence, although predictions for our compounds by these *in silico* CNS MPO algorithm were negative, molecules with a CNS MPO ≤ 5 may exhibit positive ADME and safety properties, and be a CNS candidate, as Wager *et al.* demonstrated.[121] Thus, other experiments might be taken under consideration. For this reason, we considered that experimental *in vitro* assays to measure BBB permeability and gastrointestinal absorption should be carried out.

V.3 *IN VITRO* ASSAYS TO PREDICT *IN VIVO* BBB PERMEABILITY AND GASTROINTESTINAL ABSORPTION

Several high-throughput screening (HTS) cell-based assays have been developed to assess the *in vivo* BBB permeability, including primary brain microvessel endothelial cells (rat, bovine, porcine, human), immortalized brain endothelial cell lines (such as MBEC), non-cerebral origin cell lines (such as MDR1-MDCK and Caco-2) and non-cellular assays (PAMPA).[52] A large number of studies have demonstrated

good correlations between these *in vitro* HTS models and the *in vivo* BBB permeability assays. The permeability of new chemical entities is routinely screened in early stages of drug research. The comparison of various *in vitro* models for the prediction of human absorption as well as brain penetration of these compounds is a requisite for the evaluation of new candidates.

V.3.1 Caco-2 cellular assay

Caco-2 cellular assay has been traditional used to evaluate the oral drug absorption of new drugs to assess the permeability in the gastrointestinal tract through the mucosa membrane. However, due to transport similarities of Caco-2 cells with BBB such as the expression of efflux pumps and influx active and passive mechanisms of transport, this assay has been also applied as an *in vitro* model in BBB permeability studies of new chemical CNS candidates. Hence, from the comparison of Caco-2 results with an in vitro BBB model assay, more conclusions can be extracted.

Actually, Caco-2 cellular assay is used to evaluate the oral absorption and predict the permeation of new antioxidant compounds across gastrointestinal barrier.

V.3.1.1 Absorption of drugs into the blood circulation

In initial states of drug discovery, the screening of ADME characteristics and toxicity of new chemical entities carried out in parallel to pharmacological efficacy provide the selection of superior drug candidates with better quality for further developments. Sufficient intestinal absorption of orally administered drugs from the gastrointestinal tract to the blood circulation is one of the prerequisites for a successful oral drug therapy. Intestinal drug absorption depends on the dissolution rate, the solubility and the permeability through intestinal wall.[124]

The drug absorption barrier in intestine track is formed by polarized intestinal epithelium cells called enterocytes. In the intestinal membrane, the enterocyte cells are separated only by tight junctions and, due to its polarization, two different sides, apical and basolateral, can be distinguished. Therefore, drug absorption across the intestinal membrane is a complex multi-pathway process, as shown in Figure 5.2, similar to BBB transport system.[125]

[124] Himanshu, R.; Jakir, P.; Pradnya, H.; Suneel, P.; Rahul, S. *J. Drug Delivery Therapeut.* **2013**, *3* (3), 20-29.

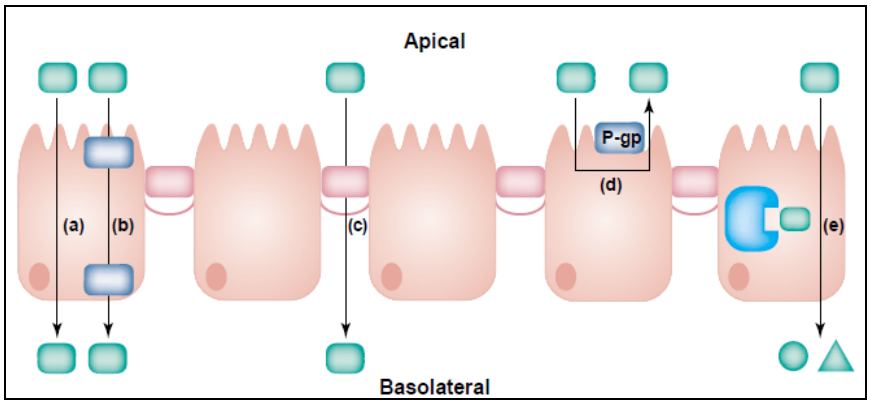

Figure 5.2. *Different pathways for the intestinal absorption of a compound. Mechanisms that are involved in the intestinal absorption of a compound:* ***(a)*** *transcellular passive permeability,* ***(b)*** *carrier-mediated transport, and* ***(c)*** *paracellular passive permeability. However, there are also mechanisms that prevent that absorption:* ***(d)*** *P-gp efflux pump and* ***(e)*** *metabolic enzymes in the cells that might metabolize the compound. Figure extracted from Balimane et al.*[125]

Passive absorption occurs most commonly through the cell membrane of enterocytes (transcellular route, Figure 5.2a) preferentially for hydrophobic molecules or *via* the tight junctions (paracellular route, Figure 5.2c) for hydrophilic compounds. Carrier-mediated absorption and receptor-mediated trancystosis could also play a role in active influx transport (Figure 5.2b). Various efflux transporters, such as P-gp, BCRP and MRP-2, are also functional, mainly, in the apical side of cell membrane, limiting the permeability of compounds into the systemic circulation (Figure 5.2d). Finally, a barrier of intestinal enzymes could metabolize the drugs, modifying moieties that can facilitate or impede in the penetration (Figure 5.2e).[125]

Drug absorption primarily occurs in the small intestine, where the pH varies from acid to neutral and slightly basic. In the upper small intestine where pH is likely to be more acid, weakly acid drugs, primarily as unionized form, present a dominant passive transcellular pathway permeation route. In contrast, weakly basic drugs will be mostly in the form of ionized species, and consequently the passive transcellular route plays a minor role.[125] Lipophilicity plays also a major role in passive transcellular diffusion of drug candidates across endocytic membrane. More hydrosoluble drugs may be easily excreted by the urine and more lipophilic drugs may have problems to arrive to blood circulation. Therefore, a good drug candidate must have an equilibrium between lipohilicity and water solubility for being absorbed by passive diffusion.[52]

In the last decades, highly accurate, low-cost, and HTS techniques that can provide fast and reliable data on the development of drug candidate characteristics have been studied.[126] The most popular HTS tool to predict the *in vivo* gastrointestinal drug absorption in humans are the *in vitro* cell-based models such as Caco-2 and Mardin-Darby Canine Kidney (MDCK) assays.[127] In the present Thesis, Caco-2 cellular assay was selected to evaluate the gastrointestinal absorption of new antioxidant CR-6-analogues, and

[125] Balimane, P.V.; Chong, S. *Drug Dicov. Today.* **2005**, *10* (5), 335-343.
[126] Balimane, P.V.; Patel, K.; Marino, A.; Chong, S. *Eur. J. Pharmaceut. Biopharmaceut.* **2004**, *58*, 99-105.
[127] Behrens, I.; Kissel. T. *Eur. J. Pharmaceut. Sci.* **2003**, *19*, 433-442.

references Trolox and CR-6. As mentioned before, this technique would be complementary in the study of the BBB permeation.

V.3.1.2 Caco-2 cellular assay technique

The Caco-2 cells are derived from human colorectal adenocarcinoma cell line and exhibit morphological as well as functional similarities to intestinal enterocytes.[128] In culture, Caco-2 cells form monolayers and spontaneously enterocytic differentiation and polarization with well-established tight junctions between cells. Apparent Caco-2 permeability measured from the apical to basolateral direction (A→B) is frequently useful in predicting drug absorption.[129] Also Caco-2 cellular assay is widely used to evaluate the drug candidate interaction with the efflux pumps such as P-gp and BCRP expressed in this kind of cells. In addition, Caco-2 cells also houses several drug metabolizing enzymes comparable with those presented in intestine cells and thus this assay provides a complementary information from drug metabolism.[130]

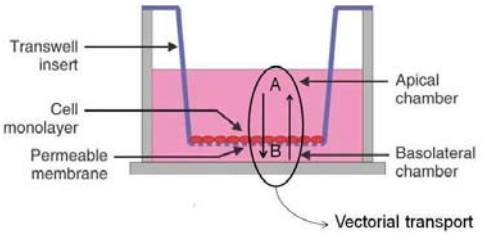

Figure 5.3. Experimental procedure of the Caco-2 assay. Apical and basolateral compartments are separated by a polarized-Caco-2 cell-monolayer membrane coated over an inert filter or permeable membrane. The vectorial transport experiments from A to B and from B to A are studied.

From an experimental point of view, cells are grown for at least 21 days to form differentiated monolayers on a porous permeable filter as it is illustrated in Figure 5.3. This period is required for the cells to form the tight junctions, the cell polarity and a high expression of drug efflux mechanisms and enzymes. The filter consists of an inert material such as polycarbonate with diameter pore of 0.4 µm that avoid cell migration from the apical to basolateral side. For transport experiments, test compounds are typically added to the donor side of the monolayer, and the occurrence in the receiver compartment is analyzed by mass spectrometry. The rate of drug transport is usually expressed as the apparent permeability coefficient (P_{app}, in 10^{-6} cm/s), by assuming that the system is a single barrier.[131]

$$P_{app} = \frac{dQ}{dt}\frac{1}{A \cdot C_0}$$

[128] Bohets, H.; Annaert, P.; Mannens, G.; Van Beijsterveldt, L.; Anciaux, K.; Verboven, P.; Meuldermans, W.; Lavrijsen, K. *Curr. Top. Med. Chem.* **2001**, *1* (5), 367-383.
[129] a) Pade, V.; Stavchansky, S. *J. Pharm. Sci.* **1998**, *87* (12), 1604-1607. b) Thomas, S.; Brightman, F.; Gill, H.; Lee, S.; Pufong, B. *J. Pharm. Sci.* **2008**, *97* (10), 4557-4574.
[130] Cummins, C.L.; Mangravite, L.M.; Benet, L.Z. *Pharm. Res.* **2001**, *18* (8), 1102-1109.
[131] Lundquist, S.; Renftel, M.; Brillault, J.; Fenart, L.; Cecchelli, R.; Dehouck, M.P. *Pharm. Res.* **2002**, *19* (7), 976-981.

where *dQ/dt* is the transport rate (nmol/s), C_0 is the initial concentration (μM) in the donor compartment and *A* is the surface area of the monolayer (0.33 cm^2 for 24-well Transwell microplates from Costar).

Usually, another purpose of transport studies in Caco-2 cell monolayer is to ascertain whether the test compound is a substrate of the efflux pumps, especially P-gp, which is the most expressed in intestinal and cerebral barriers. The efflux pump interaction is measured by the efflux ratio (ER) factor which corresponds to the ratio between permeability from the basolateral to the apical (B→A) compartment and vice versa direction (A→B):

$$ER = \frac{P_{app(B\rightarrow A)}}{P_{app(A\rightarrow B)}}$$

where $P_{app(B\rightarrow A)}$ and $P_{app(A\rightarrow B)}$ (in units of 10^{-6} cm/s) correspond to apparent permeability from basolateral to apical (from basolateral to apical) transport direction and vice versa, respectively. Broadly speaking, a value of $ER \leq 2.5$ suggests that the test candidate is not an efflux pump substrate.[117,120] Therefore, by using the Caco-2 assay three different transport mechanisms can be observed depending on the interpretation of the results: passive diffusion, active and facilitated influx and active efflux pump transports.

*V.3.1.3 Caco-2 cellular assay for new antioxidant compounds **A**-**N***

The absorption of new antioxidant compounds **A**, **B**, **C**, **D**, **E**, **F**, **G**, **I**, **J**, **L** and **N**, Trolox and CR-6 was evaluated by using the Caco-2 cellular assay. Compounds **H**, **K** and **M** were not available at the time of performing this experiment and they were not evaluated. This assay was performed in the *Laboratoire de la Barrière Hémato-Encéphalique* at the *Université d'Artois (Lens, France)* under the supervision of Prof. Romeo Cecchelli and Dr. Maxime Culot, and the assistance of Emmanuel Sevin, during a short stay of three months.

V.3.1.3.1 Prediction of gastrointestinal in vivo absorptive activity by Caco-2 cellular assay

Caco-2 cells were seeded into cell HTS 24-well plates with 0.4 μm polycarbonate membrane inserts at 75 000 cell/well in 0.4 mL of complete medium[132] in every apical compartment and 24 mL in shared basolateral compartment (in HTS 24-well plates the basolateral compartment for the incubation of cells is shared for all 24 wells). The cells were incubated in humidified atmosphere with 5% CO_2 for 21 days at 37ºC (Figure 5.4), changing the complete medium every two days.

[132] Complete medium is composed by Dubelco's Modified Eagle's Medium DMEM, high glucose with L-glutamine supplemented with 10% of Fetal Calf/Bovine Serum, 1% non-essential amino acids and 1% of penicillin and streptomycin solution

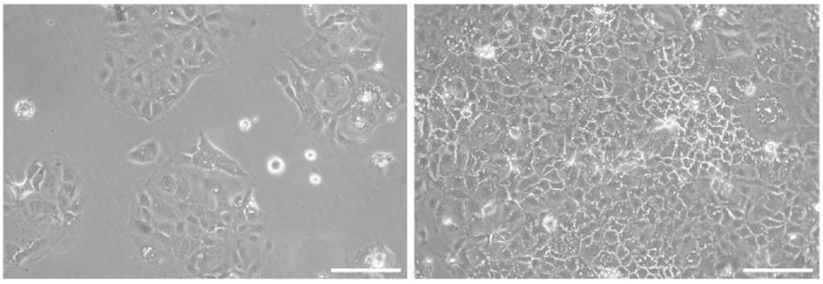

Figure 5.4. *Caco-2 cells imaging by microscope before reaching the monolayer (left) and after 21 days of incubation (right).*

After three weeks, the cells reached the full differentiation of cell monolayer and they were ready for the transport experiments (Figure 5.4). Stock solutions at 10 mM of all compounds were prepared in DMSO and they were diluted to reach the working concentration of 25 µM in Ringer-HEPES' buffer (RH, 0.25% of DMSO). For sample **J**, the addition of 12.5 µL of DMSO and the ultrasonic bath were required to favor the total dissolution of the compound. Before the transport experiments, the pH on cells was equilibrated at 7.4 using RH and the temperature of all sample solutions was adjusted at 37ºC.

For A→B transport experiments, 0.2 mL of sample solution were placed on the apical side of cells and 0.8 mL of RH buffer solution on the basolateral side. The 24-well plate was placed on a circular stirrer for 60 minutes at 37ºC. Then, aliquots on the donor (apical) and the acceptor (basolateral) compartments were analyzed by UPLC-MS, in the *Servei d'Espectrometria de Masses* of our institute. For B→A transport experiments, 0.8 mL of sample solution were placed by triplicate on the basolateral side of cells and 0.2 mL of RH buffer solution on the apical side. Following the above experimental procedure, after 60 minutes, the donor (basolateral) and acceptor (apical) compartments were analyzed by UPLC-MS.

In the resulting chromatogram, the mass of the resulting cation $[M+H]^+$ for each compound was integrated and the areas under the curve were applied in the following expression for the calculation of P_{app} (10^{-6} cm/s) in both experiments, A→B and vice versa:

$$P_{app}(cm/s) = \frac{J}{A \cdot C_0}$$

where J is the rate of appearance of the compound in the receiver compartment (C_t/t, where C_t is the concentration at time t and t is 60 minutes of experiment), C_0 is the initial concentration of the solute in the donor chamber and A, the surface area of the filter (0.33 cm^2).[131] The ER factor was also calculated for each test compound as explained above. Table 5.4 shows the results obtained for experiments A→B and B→A, the ER factor and the interpretation of these results regarding the efflux pump interaction.

Table 5.4. *Results for absorption experiments in Caco-2 cell-monolayer assay of test compounds.*

Antioxidant	$P_{app(A\rightarrow B)}$ ($\cdot 10^{-6}$ cm/s)	$P_{app(B\rightarrow A)}$ ($\cdot 10^{-6}$ cm/s)	ER	Interpretation
Trolox	0	0	0	*No penetration*
CR-6	*Not detected*	*Not detected*	-	*Not detected*
A	*Not detected*	*Not detected.*	-	*Not detected*
B	27.6[a]	0	0	*No efflux*
C	0	0	0	*No penetration*
D	10.9±2.9	0	0	*No efflux*
E	3.4±0.6	0	0	*No efflux*
F	2.3[a]	0	0	*No efflux*
G	0	3.2±3.1	-	*Efflux*
H	*Not analyzed*	*Not analyzed*	-	*Not analyzed*
I	330±69.6	123±41.1	0.37	*No efflux*
J	62.1±39.1	3.1±0.2	0.05	*No efflux*
K	*Not analyzed*	*Not analyzed*	-	*Not analyzed*
L	449 [a]	120 [a]	0.27	*No efflux*
M	*Not analyzed*	*Not analyzed*	-	*Not analyzed.*
N	*Not detected*	*Not detected*	-	*Not detected*

[a] The results are expressed as mean±SD of triplicates, but for compounds **B**, **F** and **L** the SD was not calculated because only one replicate was possible to take into account.

Analyzing the results of efflux pump substrate, compounds **G**, **I**, **J** and **L** exhibited an apparent permeability from B→A different from 0; therefore, they exhibited an interaction with efflux pumps. However, only compound **G** exhibited an interaction with efflux pumps (EF ≥ 2.5) because P_{app}(B→A) was different from 0 and P_{app}(A→B) was equal to 0, even though it was not possible the calculation of ER factor. In contrast, looking at the influx transport, **I**, **J** and **L** showed higher values of P_{app}(A→B) than the vice versa transport direction and very low ER factors. Conclusively, only compound **G** can be considered as an efflux pump substrate.

Unfortunately, compounds CR-6, **A** and **N** could not be detected by UPLC-MS at the biological concentration assayed (25 µM or lower). Trolox and compound **C** did not present a transport means across the Caco-2 monolayer. A possibility is that they are hydrophilic enough to penetrate through membrane or have been metabolized.

In Table 5.5, the general cutoffs for *in vitro* P_{app} values from the Caco-2 assay are related to the predicted percentage of *in vivo* oral absorption, extracted from Readycell® kit assay.

Table 5.5. *General cutoffs for P_{app} in vitro Caco-2 assay extracted from a Readycell® and the correlation with the in vivo oral absorptive prediction.*

In vitro P_{app} values	Range of predicted *in vivo* absorption
$P_{app} \leq 10^{-6}$ cm/s	LOW (0-20%)
10^{-6} cm/s < $P_{app} \leq 10 \cdot 10^{-6}$ cm/s	MEDIUM (20-70%)
$P_{app} > 10 \cdot 10^{-6}$ cm/s	HIGH (70-100%)

In order to deduce the prediction of *in vivo* oral absorption in humans for test compounds, the results obtained in Table 5.4 were compared with the *in vitro/in vivo* relation studies from Readycell® kit assay (Table 5.5). According to the data from *in vitro* Caco-2 assay, compounds **B**, **D**, **I**, **J** and **L** might have high *in vivo* permeation due to their high P_{app}(A→B) values; these compounds are likely to have an 70 to 100% *in vivo* oral absorption. Compounds **E** and **F**, with P_{app}(A→B) between 10·and $1 \cdot 10^{-6}$ cm/s, might present medium (20-70%) permeability across intestine endocytic membrane. Finally, Trolox, and compounds **C** and **G** showed P_{app}(A→B) equal to 0, then they might be poor (0-20%) orally absorbed. These predictions of *in vivo* permeability across the intestine to blood circulation might correspond to a paracellular or transcellular influx transport.

The *%Recovery*[133] or Mass balance can be a useful tool to interpret the Caco-2 data. If the recovery is low, this may indicate problems with solubility, binding of the compounds to plastic devices such as plate, metabolism of compounds by cellular enzymes or accumulation of the compound inside the lipidic bilayer or polycarbonate filter.

For experiment A→B, all compounds presented recoveries from 40-60%, except **C** and **F** that had more than 80%. This fact pointed out that while the vast majority of compounds were attached to cells, plastic or filter or metabolized, **C** and **F** were less attached. In contrast, for experiments B→A, only compounds **G** and **I** showed recoveries from 40-60% whereas the rest had more than 90%. Conclusively, the vast majority of compounds might be attached to or metabolized by cells.

During these experiments, problems with the detection of compounds by UPLC-MS at biological concentration (lower than 25 µM) did not let us to compare the test compound's results with the reference CR-6. Salt concentration in the samples from the buffer solution and the low capacity of some compounds to be ionized might be the responsible for these detection problems.

On the other hand, Caco-2 provides more information than only the prediction of *in vivo* absorption across gastrointestinal barrier. Caco-2 cells monolayer presents many characteristics that BBB expressed, giving preliminary understandings about BBB permeation of test compounds, such as efflux pumps interaction or toxicity. Thus, despite Caco-2 assay provided a prediction of *in vivo* absorption of the new antioxidant compounds in humans, this assay only differentiates between an influx or efflux transport not between active or passive mechanisms. For this reason, complementary assays were attempted.

V.3.2 Parallel Artificial Membrane Permeability Assay (PAMPA)

Although Caco-2 assay is widely used, the demand for a higher throughput, reduced cost, and increased predictability in drug discovery arose discussion on some drawbacks of this method. These limitations include the long time (21 days) of cell culture for full cell differentiation, low throughput,

[133] *%Recovery* = [Final acceptor compartment amount (nmol)/Initial donor compartment amount(nmol)]· 100

variable expression of transporters and metabolizing proteins, requirement of liquid chromatography/mass spectrometry (LC/MS) system for the quantification, difficulties in the interpretation of results among others.[134] These points have been partially improved by reducing culture time from 21 to 3-10 days and moving from 24- to 96-well plates.[126,135] But, taking into account that 80-95% of commercial drugs are absorbed primarily by passive diffusion, there is strong interest in a quicker and cheaper permeability assay that provides direct data on the passive diffusion mechanism.[134]

Taking profit of this situation, other methodologies to measure the drug absorption were developed. Kansy *et al.* introduced in 1998 a new technique called Parallel Artificial Membrane Permeability Assay (PAMPA).[136] This technique involves no cell culture and therefore only passive diffusion is tested; no other transport mechanisms are involved and the interpretation of the results is easier. Moreover, PAMPA is performed in a 96-well plate and can be rapidly quantified by UV. In addition, higher concentrations of test compounds can be used because there are not transporters that easily may be saturated.[126]

For the sake of clarify, PAMPA and Caco-2 assay characteristics and differences are shown in the Table 5.6.

Table 5.6. *Comparison between PAMPA and Caco-2 assay characteristics.*

Characteristic	PAMPA	Caco-2
Membrane Composition	Phospholipid in alkane	Caco-2 cell monolayer
Permeability Mechanisms	Passive diffusion	Passive diffusion Active transport Active efflux Paracellular
Metabolism	No	Yes
Maximum throughput per instrument	650 compounds/week (three plates/day in duplicate)	50 compounds per week (two plates/day in duplicate in both directions A→B and vice versa)
Resources	Robot, plate washer, UV reader	Cell culture lab, robot, HPLC or LC/MS

Nevertheless, Kansy *et al.* and Avdeef *et al.* have demonstrated that PAMPA and Caco-2 have similar correlation to human absorption; consequently, so they are the most useful assays to predict oral absorption *in vivo*.[136,137] In addition, they can be also used to evaluate the permeability of new candidates in other kind of tissues different from gastrointestinal barrier, such as BBB.

[134] Kerns, E.H.; Di, L.; Petusky, S.; Farris, M.; Ley, R.; Jupp, P. *J. Pharm. Sci.* **2004**, *93* (6), 1440-1453.
[135] Sevin, E.; Dehouck, L.; Fabulas-da Costa, A.; Cecchelli, R.; Dehouck, M.P.; Lundquist, S.; Culot, M. *J. Pharmacol. Toxicol. Methods*, **2013**, *68*, 334-339.
[136] Kansy, M.; Senner, F., Gubernator, K. *J. Med. Chem.* **1998**, *41*, 1007-1010.
[137] Avdeef, A. *Eur. J. Pharm. Sci.* **2001**, *14*, 271-280.

V.3.2.1 An introduction to PAMPA

Since it was introduced by Kansy *et al.* to evaluate the oral absorption of drugs, several reports have been published to illustrate the general applicability of this model as a HTS permeability tool.[136] PAMPA model involves a hydrophobic inert filter material coated with a mixture of lecithin/phospholipids dissolved in an inert organic solvent to create an artificial lipid membrane barrier and mimic the intestinal epithelium, and other barriers such as BBB. The rate of permeation across the membrane barrier correlates satisfactorily with the extent of drug permeability in humans.

PAMPA is a HTS, non-cell-based permeability model that provides estimations of the passive transcellular permeability through a lipid barrier. Due to the lack of any functional drug transporters and paracellular pores, it is an inappropriate model for compounds that are absorbed *via* transporter- and pore-mediated processes. Thus, one of the main limitations of this model is the underestimation of the absorption of compounds that are actively absorbed. Despite this limitation, owing of its HTS capability and less labor-intense with similar predictability, PAMPA can be applied in primary permeability screenings at early drug discovery stages.[52]

V.3.2.1.1 Lipid composition: PAMPA and PAMPA-BBB

Traditionally, PAMPA model uses polar lipids for the study of gastrointestinal membrane permeation such as Polar Membrane Lipid (PML). Furthermore, the assay has been optimized to mimic permeation through several biological membranes, such as PAMPA-BBB for brain penetration, PAMPA-skin for skin permeation, and PAMPA-DS for intestinal absorption. The use of one or another PAMPA model depends on the nature of the composition of phospholipids that mimic the membrane. However, small differences are observed between different PAMPA models.

Di *et al.* described the use of porcine brain lipids to predict *in vivo* BBB permeation by HTS PAMPA model.[138] Thus, by using Polar Brain Lipids (PBL), Di and co-workers classified 33 marketed drugs in CNS or not depending on the permeability through BBB. They concluded that small differences between employing PBL or PML were observed. Since PAMPA-BBB is a good model to predict *in vivo* BBB permeability, it has been widely applied to evaluate new CNS and non-CNS candidates.[139]

V.3.2.2 PAMPA-BBB for new antioxidant compounds

The permeability by passive diffusion of new antioxidant agents **A-N**, Trolox and CR-6 was assessed by PAMPA-BBB. This model was carried out in the *Design, synthesis and evaluation of peptides and proteins* group in IRB-PCB, in Barcelona, under the supervision of Dra. Meritxell Teixidó.[38]

[138] Di, L.; Kerns, E.H.; Fan, K.; McConnell, O.J.; Carter, G.T. *Eur. J. Med. Chem.* **2003**, *38*, 223-232.
[139] Kansy, M.; Avdeef, A.; Fischer, H. *Drug Discovery Today Tec.* **2004**, *1* (4), 349-355.

The penetration of new antioxidant compounds **A**-**N**, Trolox and CR-6 was evaluated by PAMPA-BBB to measure the passive diffusion of test compounds through an artificial membrane of phospholipids. The polar brain lipids employed were the Pig Brain Lipid Extraction (PBLE) that is composed by 12.6% phosphatidylcholine (PC), 33.1% phosphatidylethanolamine (PE), 18.5% phosphatidylserine (PS), 4.1% phosphatidylinositol (PI), 0.8% phosphatidic acid and 30.9% of other compounds.

Following the experimental procedure, 200 µL of stock solution (10 mM) in buffer of test compound were placed in the donor compartment. 20% 1-Propanol was used as co-solvent to assure the totally dilution of test compound. The acceptor plate was placed into the donor compartment, ensuring that the underside of the membrane was totally in contact with the buffer solution, like in a sandwich (Figure 5.5). Then, the mixture of 20 mg/mL phospholipids (PBLE) in dodecane were placed over each filter followed by the buffer (with 20% 1-propanol) to each acceptor well. The plate was covered and incubated for 4 hours at room temperature in humidified atmosphere under an orbital agitation gutbox to assure an Unstirred Water Layer (UWL) of 25 µm thickness.

Both passively and actively transported compounds may be affected by the so-called Unstirred Water Layer (UWL), which is lining the apical surface of the monolayer. UWL is < 1µm in *in vivo* BBB, but the diffusion across the UWL may become rate-limiting for the transport of highly lipophilic compounds in *in vitro* assays. Therefore, stirring the apical and the basolateral media during the transport experiment is recommended to reduce the thickness of UWL and mimic better the BBB.[38] Hence, all PAMPA plates were placed on an orbital shaker at 100 rpm.

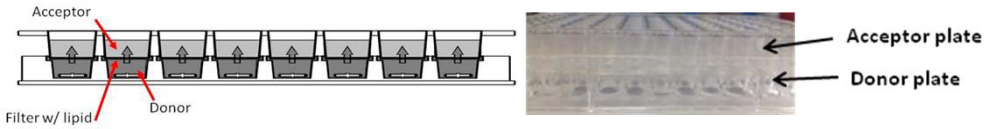

Figure 5.5. *Plate as a "sandwich" for PAMPA model (up) and pictures for 96-well plate of the experiment (down). The donor plate is situated in the lower side, wheras the acceptor is in the upper. The direction of the permeable compound is from the lower to the upper plate. The stirring is required to reduce the UWL, which can affect passive diffusion permeability in in vitro studies.*

When the experiment is finished, aliquots of donor receiver compartments were injected in a HPLC-UV ($\lambda_{max.}$=220 and 290 nm). The transport was also confirmed by UPLC-MS. The area under the curve of determined peak in the chromatogram is proportional to the concentration. Therefore, the rate of permeation was determined by the compound's effective permeability (P_e) following the expression:[38]

$$P_e = \frac{-218.3}{t}\log\left[1-\frac{2\cdot C_A(t)}{C_D(t_0)}\right]\cdot 10^{-6} cm/s$$

where t is time (h), $C_A(t)$ is the compound concentration at the acceptor well at time t, and $C_D(t_0)$ is the concentration at the donor well at initial time.

Results obtained for the screening of test compounds using the PAMPA-BBB model in decreasing order of permeability are shown in Table 5.7. As mentioned before, the pH on a permeability experiment is determinant for the absorption of drug candidates with ionizable groups in the molecule. For gastrointestinal PAMPA assay, it is recommended to use two different pH values, for example 4 and 7.4 due to the variation of pH along the intestine. But in case of PAMPA-BBB, only pH at 7.4 is performed. Owing to the fact that pK_a of carboxylic acid group of some molecules is 3.6 (pH > pK_a), it should be assumed that these test compounds were in their anionic form during the assay.

Table 5.7. *Results obtained for the screening of test compounds using the PAMPA-BBB model of test compounds.*

Antioxidant	P_e (10^{-6} cm/s)	Recovery (%)
Trolox	0.47±0.04	46.4
CR-6	0.25±0.01	1.1
G	1.18±0.4	73.6
L	0.52±0.06	64.4
F	0.50±0.2	36.3
I	0.35±0.04	37.8
A	0.30±0.01	15.8
D	0.16±0.0005	41.4
M	0.07±0.01	*Not comprehensive*
C	0.06±0.04	18.4
E	0.06±0.05	9.1
B	0.03±0.02	28.3
N	0	35.2
K	0	14.7
H	*Not detected*	*Not detected*
J	*Not detected*	*Not detected*

According to data in Table 5.7, all compounds presented poor permeability in PAMPA-BBB model ($P_e \leq 2 \cdot 10^{-6}$ cm/s).[138] Carboxylic acid compounds **B**, **C**, **D**, **E** and **N** showed the poorest permeability through artificial membrane of phospholipids by passive diffusion. In contrast, **F** and **G**, also acids, had a low but better penetration. Indeed, although these two compounds are acid, the presence of an additional aromatic ring (a phenyl group for **F** and an indole group for **G**) might make them more lipophilic and therefore they might be passively diffused easily through the membrane. **A**, **I** and **L** molecules without ionizable groups such as carboxylic acid, exhibited low penetration by passive diffusion, but P_e values better than CR-6. In case of **K**, the glucose ring might make the molecule more hydrophilic and difficult to be delivered by transcelullar passive diffusion. Compound **M** was not considered in the analysis due to its misapprehended recovery value. Comparing the results with references CR-6 and Trolox, in general, new test antioxidants are less permeable. The higher lipophilicity of the references might be the cause of their better penetration by passive diffusion, even though Trolox has a free carboxylic acid group.

Lipophilicity (expressed normally as logP or logD values) plays a major role in passive diffusion. An adequate lipophilicity is required for a permeable compound to travel across the phospholipid membrane. However, it was demonstrated by Balimane *et al.* that there is no a good correlation between lipophilicity and PAMPA permeability, due to the fact that permeability also depends on other factors like

polar surface area, molecular volume and hydrogen bonding.[52] Therefore, models such as PAMPA and Caco-2 cells can only be used as one-way screening since compounds with high permeability might be typically well absorbed in humans, but low permeable compounds cannot be ruled out as poorly absorbed.

V.3.3 Bovine Brain Capillary Endothelial Cells (BBCECs) *in vitro* model

Following the studies of passive diffusion and efflux pump interaction using *in vitro* models, the permeability of new antioxidant agents **A-N**, Trolox and CR-6 was assessed by bovine brain capillary endothelial cells (BBCECs). This model was asayed in the *Laboratoire de la Barrière Hémato-encéphalique (LBHE)* at the *Unversité d'Artois* (Lens, France), under the supervision of Prof. Romeo Cecchelli and Dr. Maxime Culot, and the assistance of Emmanuel Sevin and Lucie Dehouck, during a short stay of three months.[32]

V.3.3.1 Literature research of BBCEC in vitro models

Bovine brain microvessel endothelial cells have been isolated and grown in culture to monolayers on porous supports.[30] These *in vitro* models allowed the study of drug transcellular transport through the brain endothelial cell monolayers. However, Pardridge *et al.* showed that the permeability values measured *in vitro* overestimated BBB permeability *in vivo*. These results were expected, since endothelial cells isolated from their environment can rapidly loose some of their characteristics.[30] In order to re-induce some of these properties, Rubin *et al.* studied the effect of astrocyte-conditioned medium on the electrical resistance of endothelial cell monolayer. In this case, the value increased and they demonstrated that the conditioned medium with astrocytes allowed the re-inducing of some BBB *in vivo* properties. However, other characteristics such as specific enzymes are not always present or are lost during the growth.[32]

Other *in vitro* models have been developed consisting of human, rat or bovine endothelial cells in the presence of astrocytes from different species. Although all these models exhibited endothelium characteristics, most of them have not been characterized to the same extent and thus are not really validated.[32] In 1999, Cecchelli *et al.* described an *in vitro* model in BBCECs that closely mimics the *in vivo* situation and serves to evaluate the drug transport in BBB by co-culturing brain capillary endothelial cells and astrocytes on different sides of a filter.[32]

V.3.3.2 Method to study BBB transport

V.3.3.2.1 Brain capillary endothelial cells primary culture

Several procedures and many modifications have been used to obtain endothelial cell primary cultures. The species and sources of cerebral microvessels vary from one laboratory to another, but usually all the procedures use mechanicals means to disperse brain tissue.[30,32] However, different approaches are used to collect and grow the disrupted capillaries.

The most critical part is the filtration and separation of microvessels from other brain constituents to get a pure capillary endothelial cell cultures. Different from other laboratories that employed enzymatic digestion, Cecchelli *et al.* preferred the cloning of endothelial cells. Hence, after the isolation by mechanical homogenization from one bovine cerebral hemisphere, microvessels are seeded onto dishes and coated with extracellular matrix secreted by bovine corneal endothelial cells. Only capillary cells remain adhered to the extracellular matrix; therefore, other brain constituents (such as arterioles and venules) that can contaminate the colonies of capillary cells, are easily removed. After two trypsination processes and cultures in appropriate medium[140] the subculture bovine cells consist only of pure capillary endothelial cells. After 6-8 days of culture, they reach the right confluent at the split ratio of 1:20. Then, cells are stored in liquid nitrogen until transport experiments.[30,32] Cecchelli and co-workers found an obvious advantage of the use of cloned endothelial cells emerging from identified capillaries against enzymatic digestion: the culture is not contaminated by endothelial cells of arteriolar and venular origin.[32] Moreover, after the cells are rapidly thawed at 37ºC and seeded on a 60-mm diameter plate gelatin coated for the experiments, cells are subcultured up to passage eight. Therefore, the subculture technique avoids the limitations of primary cultures and provides large quantities of these monolayers.[30,32]

V.3.3.2.2 Co-culture of bovine brain capillary endothelial cells with astrocytes

Primary or low-passage cell cultures retain many of the morphological and biochemical properties that characterized the BBB *in vivo*, including endothelial transporters, receptors, expression of enzymes and complex tight junctions. However, as mentioned before, there is strong evidence that glial cells dynamically interact with the BBB to regulate these properties and thus, the microenvironment of the brain. There are various approaches that mimic the glial influences, but the co-culture of the brain endothelium on permeable supports together with primary astrocytes of glial cells (astrocytes, oligodendrocytes and microglia) is the most valuable approach.[30,32] As shown in Figure 5.6, the brain endothelial cells are cultured over a permeable membrane coated with collagen that separates the compartment where the glial cells are grown. Culture medium is shared by both compartments, allowing

[140] Dubelco's modified Eagle's medium supplemented with 15% calf serum, 2 mM glutamine, 50 µg/mL gentamycin, 2.5 µg/mL amphotericib B and 1 ng/mL basic fibroblast growth factor every other day.

humoral interchange without direct cell contact. Following the co-culture procedure the *in vitro* BBB model mimics the *in vivo* situation.

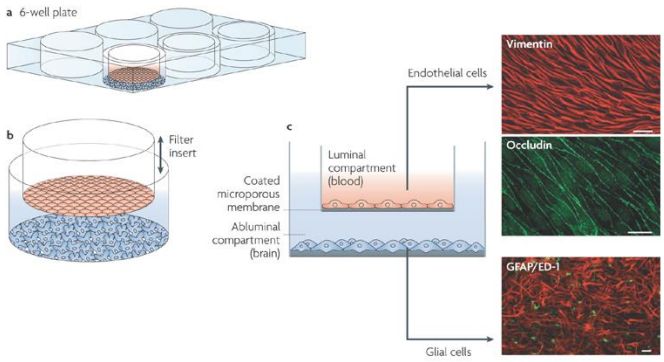

Figure 5.6. *In vitro BBB model based on the co-culture of endothelial cells with astrocytes in two different compartments separated by a collagen coated membrane.* ***a)*** *Illustration of a 6-well plate where the model is performed. The co-culture can be performed in 6-, 12- or 24-well plate.* ***b)*** *Brain endothelial cells are grown on filter inserts together with the astrocytes in the other compartment or well.* ***c)*** *Illustration of a typical experimental design which allows a co-culture of endothelial cells with astrocytes or glial cells. Vimentin immunostaining shows a confluent brain endothelial cell monolayer (top right picture); the tight junction protein occluding reflects the tightness of the barrier (middle right picture); and the staining of glial cells with glial fibrillary acidic protein (GFAP) shows the astrocytes as red colored (bottom right picture). Extracted from Cecchelli et al.*[30]

The development of a cell culture system that mimics a biological barrier requires the establishment of the culture of endothelial cells on microporous supports. In order to reconstruct some of the cellular environment complexities that exist *in vivo*, Cecchelli *et al.* developed an *in vitro* model of co-culture. At this stage, they studied the influence of different matrix on the microporous membrane.[30]

V.3.3.2.3 Study of matrix on microporous membrane

In order to select the matrix on microporous membrane which will support cell attachment, growth and differentiation, different Biocoat cell culture inserts (0.45 µm pore size and 30-mm diameter) commercially prepared and in-house made membranes coated with rat tail collagen were tested for brain capillary endothelial cell culture. The Biocoat cell culture inserts were coated with different matrixes: matrigel, human fibronectin, mouse laminin or commercial rat tail collagen I. For the in-house membranes, some Millicell-CM filters were coated with in-house rat tail collagen solution. In parallel, all supports were evaluated after 1 hour at 37ºC and rinsing with water and PSB-CMF. The results demonstrated that in experiments with in-house rat tail collagen, the endothelial cells formed an organized confluent monolayer with typical tight junctions.[32]

V.3.3.2.4 Tight junctions, electrical resistance and expression of transcellular transporters

Electron microscopy and inmunostaining experiments were employed by Cecchelli *et al.* to study the formation of tight junctions between brain capillary endothelial cells. The results demonstrated very tight and complex junctions that sealed the cells. In these conditions, the electrical resistance of the monolayer reached to 800 $\Omega \cdot cm^2$.[30,32] The formation of the tight junctions is very important to generate the chemical and electrical gradients across the cell monolayer that are required to form the different cell membrane sides (apical and basolateral) and the directional transport processes.

Moreover, Cecchelli *et al.* demonstrated the presence of typical transporters and receptor, and efflux pumps in established *in vitro* model compared to BBB *in vivo*.[32] Indeed, Tatsuta *et al.* had shown that the level of P-gp and some transporters expression in brain capillary endothelium is regulated by a tissue specific factor in the brain matrix.[141] Cecchelli *et al.* suggested that this factor is segregated by the astrocytes and, then trapped within the brain matrix where the endothelial cells grow. All their results demonstrated the necessity of the co-culture with astrocytes to re-induce all the BBB *in vivo* morphological properties lost during the homogenization of the brain to form the primary culture.[30,32]

*V.3.3.3 Transendothelial transports studies for synthesized antioxidants **A-N**, Trolox and CR-6*

As mentioned above, the BBB permeability of compounds Trolox, CR-6 and derivatives **A-N** (except for **H**, **K** and **M**) was evaluated in the Cecchelli's group following their set up procedure BBCEC *in vitro* model. The established microporous support membrane coated with in-house rat tail collagen should be readily permeable to hydrophilic and hydrophobic solutes and to both low and high molecular weight molecules. For this reason, before conducting transport studies with cell cultures, it is essential to do the experiments using the microporous membrane coated only with collagen, that is without cells. These results will assure that the solute is freely permeable and that the diffusion barrier is only provided by the cell monolayer. In addition, these results can also provide information about their potential binding to the plastic devices.

Transport studies were performed in the same way with and without cell cultures. The day of experiments, solutions of 10 µM test antioxidant in RH were prepared from 10 mM solutions in DMSO (final concentration of DMSO 0.01%) and 50 µL of 10 mM Lucifer Yellow was added to each solution. Then, for cell culture experiments, the cells were equilibrated for 20 minutes at 37ºC with RH solution. During the same time, the solutions were also warmed to 37ºC. After the temperature and pH equilibration, 1.5 mL RH was added to each lower compartment of a 12-well plate. One filter was then transferred into the first well of the 12-well plate containing RH and 0.5 mL of test solution with LY in RH

[141] Tatsuta, T.; Naito, M.; Mikami, K.; Tsuoro, T. *Cell Growth Differ.* **1994**, *5*, 1145-1152.

were added in the upper compartment. Incubations were performed on a rocking platform at 37ºC for 60 minutes (the time measurement is important in permeation studies). Indeed, as happened in PAMPA model, shaking minimizes the thickness of UWL on the cell monolayer surface and it can influence on the permeability of lipophilic solutes. When the incubation was completed, aliquots of each compartment (lower and upper) and also initial test solution were taken and the amount of drug in each one was measured by UPLC-MS. In the chromatograms, each solute was analyzed by the m/z of $[M+H]^+$ signal and the corresponding peak was integrated.

Permeability calculations were performed as described by Siflinger-Birnboim *et al*. To obtain a concentration-independent transport parameter, the clearance principle was used. The total cleared volume at 60 minutes was calculated by the following expression:[142]

$$Clearance(mL) = \frac{X}{C_d}$$

where *X* is the amount of drug in the receptor chamber (the area under the peak of the chromatogram) after 60 minutes and C_d is the donor chamber concentration at initial time. The average volume cleared between the three replicates was plotted versus time (0 and 60 minutes) and the slope was estimated from the linear regression analysis. This slope corresponds to PS_t for experiments with cultured cells and PS_f for experiments with coated collagen only, where the PS (in cm^3/min) corresponds to the multiplication of the permeability and the surface area (S = 1.12 cm^2). From PS_t and PS_f, the PS_e or absolute PS-value for the endothelial monolayer was calculated using the following expression:[32]

$$\frac{1}{PS_e} = \frac{1}{PS_t} - \frac{1}{PS_f}$$

to generate the absolute P_e-value (permeability of endothelial cell monolayer) in 10^{-3} cm/min units, PS_e-value was divided by the surface area of the microporous membrane.

For all test compounds, the P_e-values (presented as mean±SD) and the mass balances from the BBCECs *in vitro* model after 60 minutes are shown in Table 5.8. In addition, Figure 5.15 shows the illustration of different permeability in BBCEC *in vitro* model for test compounds. Following Astrazeneca criteria, the compounds can be classified as high, medium and low BBB rate permeation depending on the P_e-value: high for $P_e > 2{\cdot}10^{-3}$ cm/min, medium for $1{\cdot}10^{-3} < P_e \leq 2{\cdot}10^{-3}$ cm/min and low for $P_e \leq 1{\cdot}10^{-3}$ cm/min.

According to Table 5.8, compounds **B**, and **I** can be considered as high permeable because of Pe > $2{\cdot}10^{-3}$ cm/min. Compounds **C** and **G** exhibited moderate rate of permeation ($P_e \geq 1{\cdot}10^{-3}$ cm/min) of bovine brain cellular monolayer. Unfortunately, compound **B** had a non-reliable result due to the high value of

[142] Siflinger-Birnboim, A.; Del Becchio, P.J.; Cooper, J.A.; Blumenstock, F.A.; Shepart, J.N.; Malik, A.B. *J. Cell. Physiol.* **1987**, *132*, 111-117.

Recovery (227%) for the experiment with cells. Compounds **D**, **E**, **F** and **J** showed low permeability through BBB ($P_e < 1 \cdot 10^{-3}$ cm/min) whereas Trolox and compound **L** did not exhibit any transport ($P_e = 0$ cm/min). Due to detection problems with UPLC-MS, compounds **A**, **N** and CR-6 were not detected neither in donor solution at initial time nor in the receiver.

Table 5.8. *Results for BBCECs in vitro model. Experiments with and without cells.*

Antioxidant	P_e ($\cdot 10^{-3}$ cm/min)[a,b]	Recovery with cells (%)	Recovery without cells (%)
Trolox	0	110	92
CR-6	*Not detected*	-	-
A	*Not detected*	-	-
B	2.16±0.40	227	119
C	1.09±0.48	77	129
D	0.72±0.19	71	92
E	0.47±0.10	68	75
F	0.57±0.19	68	74
G	1.44±0.71	87	77
H	*Not analyzed*	-	-
I	3.62±1.63	28	58
J	-0.72±0.06[c]	67	40
K	*Not analyzed*	-	-
L	0	8	129
M	*Not analyzed*	-	-
N	*Not detected*	-	-

[a] The results are expressed as mean±SD of triplicates.
[b] PS_t and PS_f values are shown in the Supporting Information (CD).
[c] A negative P_e value corresponds to a $PS_f < PS_t$.

As in PAMPA and Caco-2 assay, the *Recovery* (%) value was also calculated to assure the total recovery of the compound and the confidence on the results. In general, most values are higher than 50%, except for **L** (8%) and **I** (28%) in the experiments with cells, and **J** (40%) in the experiments without cells. A low *Recovery* (%) could be due to a high attachment to cells, plastic devices or filter, or to enzymatic metabolism. Indeed, the *Recovery* for compounds **C**, **D**, **E**, **F**, **I** and **L** in experiments with cells was lower than experiments without cells. Therefore, they might have a high affinity to cell or they might be metabolized. For other compounds, the *Recovery* was practically the same (Trolox and **G**). Only for compound **J**, the *Recovery* for experiments without cells was lower than with cells; 40% front of 67%.

Figure 5.7 illustrates the results explained above. The $P_e > 2 \cdot 10^{-3}$ cm/min values correspond to compounds with high permeability in BBCEC model whereas compounds with Pe between 1 and $2 \cdot 10^{-3}$ cm/min are considered as moderate permeable.

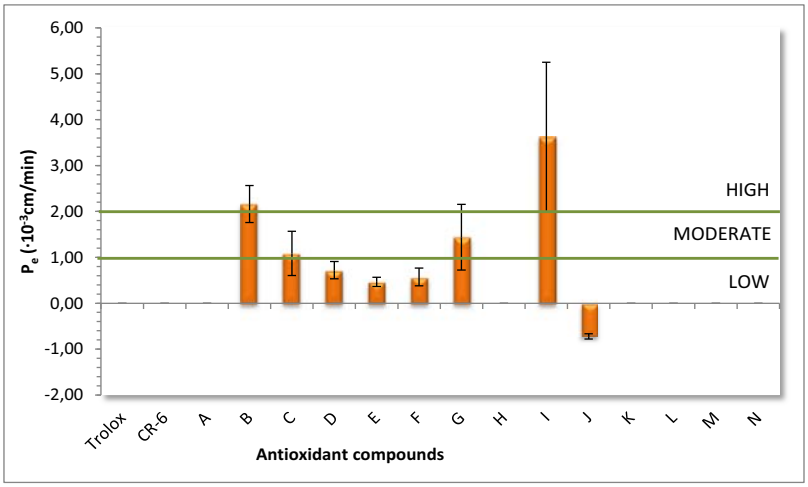

Figure 5.7. *Representation of permeability P_e for all test compounds (Trolox, CR-6 and* ***A-N*** *compounds) in BBCEC in vitro model. The values of P_e represent the mean of triplicates and the standard deviation (SD). The green lines classifies the compounds on low, moderate and high rate of permeation.*

With the aim of extracting a better interpretation of the results, comparisons of *in vitro* models have been studied.

V.3.4 Comparison within the *in vitro* assays

V.3.4.1 PAMPA and Caco-2 assays

V.3.4.1.1 PAMPA and Caco-2 cell model: Synergies

PAMPA and Caco-2 cell models are often used in combination to evaluate the permeability properties of a large number of compounds at the early stage of drug discovery. PAMPA captures the transcellular passive permeability across lipid membrane barrier without the contribution from pores or drug transporters, whereas Caco-2 cell model is capable of incorporating not only the transcellular passive permeability, but also the transport-mediated, efflux or influx, and the paracellular component of transport.

In 2004, Kerns and co-workers showed a correlation of PAMPA and Caco-2 cellular assay for different set of drugs.[134] They found that compounds with passive diffusion presented correlation between PAMPA and Caco-2 cell models. For compounds below the correlation line, with PAMPA P_e values higher than Caco-2, a secretory transport (efflux) existed. But there was an absorptive transport (active transport or paracellular passive diffusion) for compounds above the line, whose PAMPA P_e values were lower than Caco-2. Hence, they extracted the following general conclusions:

- Passive diffusion for compounds with PAMPA = Caco-2
- Absorptive transport for compounds with PAMPA << Caco-2
- Secretory transport for compounds with PAMPA >> Caco-2

The combination of PAMPA-BBB and Caco-2 models provided us more information about the permeability of compounds in a HTS cost-effective manner. Following this interpretation, the results of new antioxidants compounds (**A**-**N**), Trolox and CR-6 for PAMPA-BBB and Caco-2 cellular models were compared. Table 5.9 presents the combined results.

Table 5.9. *Comparison of results obtained for PAMPA-BBB and Caco-2 (A→B) cell model assays.*

Antioxidant	PAMPA-BBB P_e ($\cdot 10^{-6}$ cm/s)	Caco-2 $P_{app(A\rightarrow B)}$ ($\cdot 10^{-6}$ cm/s)
Trolox	0.47±0.04	0
CR-6	0.25±0.01	*Not detected*
A	0.30±0.01	*Not detected*
B	0.03±0.02	27.6[a]
C	0.06±0.04	0
D	0.16±0.0005	10.9±2.9
E	0.06±0.05	3.4±0.6
F	0.50±0.2	6.7[a]
G	1.18±0.4	0
H	*Not detected*	*Not analyzed*
I	0.35±0.04	330±0.7
J	*Not detected*	62.1±0.4
K	0	*Not analyzed*
L	0.52±0.06	449[a]
M	0.07±0.01	*Not analyzed*
N	0	*Not detected*

[a] The results are expressed as mean±SD, but in case of compounds **B**, **F** and **L** the SD is not valid because they expressed $P_{app(A\rightarrow B)}$ = 0 in two of three replicates.

Figure 5.8 illustrates the comparison results obtained for Caco-2 cell assay and PAMPA. It was inspired in Balimane *et al.* correlations.[52]

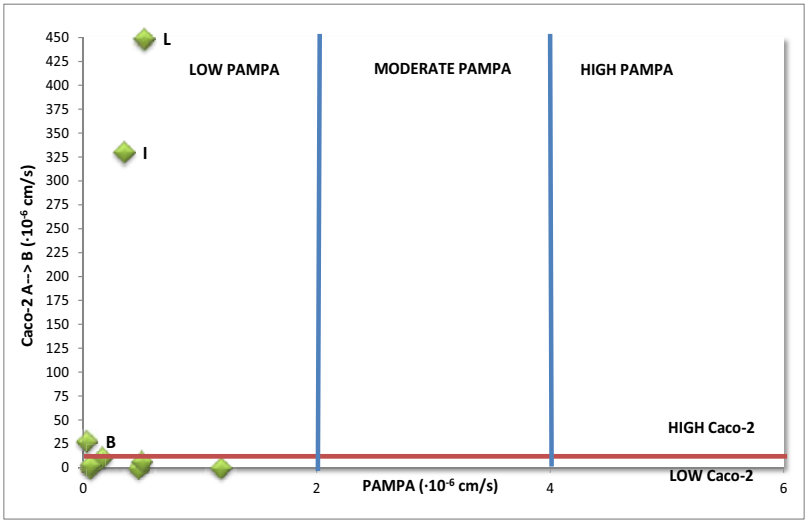

Figure 5.8. *PAMPA-BBB and Caco-2 cell models comparison. Red and blue lines represent the cutoffs for both models: $10 \cdot 10^{-6}$ cm/s for Caco-2 cellular assay and 2 and $4 \cdot 10^{-6}$ cm/s for PAMPA model, respectively, that classify the molecules in low, moderate or high permeability for Caco-2 and PAMPA models. This figure is inspired in Balimane et al. correlations.*[125]

According to these data, all studied compounds had low permeability for PAMPA-BBB model ($P_e \leq 2 \cdot 10^{-6}$ cm/s). However, for Caco-2 from A→B model assay, compounds **B**, **D**, **I** and **L** presented high permeability ($P_{app} > 10 \cdot 10^{-6}$ cm/s) whereas Trolox, **C**, **E**, **F** and **G** showed low permeability ($P_{app} < 10 \cdot 10^{-6}$ cm/s). As PAMPA values are lower than Caco-2, compounds **B**, **D**, **I** and **L** might take part into an active influx transport. Compound **G** is the only one with PAMPA P_e-value >> $P_{app(A \rightarrow B)}$ in Caco-2 assay, but below than cutoff at $P_e \leq 2 \cdot 10^{-6}$ cm/s; hence, this compound might be an efflux pump substrate. These results were consistent with Caco-2 cellular experiments.

V.3.4.2 Comparison of PAMPA-BBB and Caco-2 results with BBCEC in vitro model

In this section the results obtained for PAMPA-BBB, Caco-2 and BBCEC model assays are compared. Regarding these data and the nature of the three different models, the classification of test compounds depending on the transcellular transport mechanism that they might use to cross through the BBB is suggested. This classification derives from an interpretation of the results, but they must be confirmed by complementary assays. Joining all results in Table 5.10 preliminary suggestions were extracted: *In* for influx transport active or facilitated (CMT or RMT), *Ex* for compounds with an efflux pump interaction, *Pass* for passive diffusion, *Met* for metabolism of compound in both cellular assays, and *Bmet* and *Cmet* for metabolism in BBCEC or Caco-2 cells, respectively.

P_e in BBCEC assay and $P_{app(A \rightarrow B)}$ in Caco-2 assay for compounds from **B** to **G** might suggest the presence of an active or facilitated influx mechanism in BBB due to a free carboxylic acid group. This mechanism might be a specific transporter for monocarboxylic acid, such as MCT1, or maybe the amino acid transporter (LAT-1). Remarkably, compounds with carboxylic acid group (**B**, **C**, **D**, **E**, **F** and **G**) are negatively charged at pH 7.4; therefore, they did not pass, in general, the phospholipid barrier in PAMPA-BBB model. However, they exhibited a permeation of the BBB in BBCEC model due to the presence of CMTs.

In previous section, it was mentioned that compound **G** is an efflux pump substrate due to the fact that $P_{app(A \rightarrow B)}$ in Caco-2 cells was equal to 0, but higher in the other direction (B→A). Also, it was commented that it might have a passive diffusion when any active transporter is expressed, like it happened in a PAMPA-BBB model ($P_e = 1.18 \cdot 10^{-6}$ cm/s). In BBCEC model, the P_{app} was higher than P_e PAMPA-BBB; hence, as in case of the other free carboxylic acid derivatives, a monocarboxylic acid might be involved in the transport.

Table 5.12. *Comparison of BBCEC in vitro model with PAMPA-BBB and Caco-2 assays.*

Antioxidant	PAMPA-BBB P_e ($\cdot 10^{-6}$ cm/s)	Caco-2 $P_{app(A\rightarrow B)}$ ($\cdot 10^{-6}$ cm/s)	BBCEC P_e ($\cdot 10^{-3}$ cm/min)	Preliminary conclusions
Trolox	0.47±0.04	0	0	*Pass*[a] and *Met*[b]
CR-6	0.25±0.01	*Not detected*	*Not detected*	-
A	0.30±0.01	*Not detected*	*Not detected*	-
B	0.03±0.02	27.6[g]	2.16±0.40	*In*[c]
C	0.06±0.04	0	1.09±0.48	*In* and *Cmet*[d]
D	0.16±0.0005	10.9±2.9	0.72±0.19	*In*
E	0.06±0.05	3.4±0.6	0.47±0.10	*In*
F	0.50±0.2	6.7[g]	0.57±0.19	*In*
G	1.18±0.4	0	1.44±0.71	*Ex*[e] and *Pass*
H	*Not detected*	*Not analyzed*	*Not analyzed*	-
I	0.35±0.04	330±0.7	3.62±1.63	*In*
J	*Not detected*	62.1±0.4	-0.72±0.06	*In*
K	0	*Not analyzed*	*Not analyzed*	-
L	0.52±0.06	449[g]	0	*In* and *Bmet*[d]
M	0.07±0.01	*Not analyzed*	*Not analyzed*	-
N	0	*Not detected*	*Not detected*	-

[a] *Pass* means Passive transcellular diffusion
[b] *Met* represents any enzymatic metabolism or a common metabolism in both cell types: BBCEC and Caco-2
[c] *In* corresponds to an active influx (such as LAT-1, GLUT-1, MCT1, etc.)
[d] *Cmet* corresponds to Caco-2 cells specific enzymatic metabolism; for those molecules that are only metabolized in Caco-2
[e] *Ex* represents an active efflux (for example, P-gp)
[f] *Bmet* corresponds to BBCEC specific enzymatic metabolism; for those molecules that are only metabolized in BBCEC
[g] The results are expressed as mean±SD for triplicates, but for compounds **B**, **F** and **L** for BBCEC models it was not possible to calculate the SD.

Compounds **I** and **L** exhibited high P_{app}-values in Caco-2 assay, which might suggest that there is an active or facilitated transport for low hindered amides. But compound **L** has not exhibited a transport in BBCEC.

In case of **J**, due to its high size, it might be transported by transcytosis. For this reason it presented a transport in Caco-2 and also in BBCEC model. In the last case, the value is negative due to in the experiments with cells it was much more transported than without cells.

Regarding the enzymatic metabolism, Compound **D** might be degraded by some specific enzymes presented in Caco-2 cells. It is, maybe, rather metabolized than the rest of compounds with similar structures due to the accessibility of the amido-acid carboxylic moiety. Trolox, in contrast, is degraded by some common enzyme in both cells: Caco-2 cell and BBCEC. In addition, the Pe = 0 in BBCEC for compound **L** suggests its matebolization only in these cells.

In this analysis, CR-6 and compounds **A**, **H**, **K**, **M** and **N** are not considered because they were not analyzed or not detected for more than one assay.

Comparing these results and the structural-prediction table at the beginning of this chapter (Table 5.1, page 131), only compounds **B**, **C**, **D**, **E**, **F** and **J** seem to have a behavior similar to the predicted. In case of compounds **G**, **I** and **L** the final results were different to the previous predictions.

In conslusion, the introduction of variability at position C_2 of the CR-6 molecule with known carriers seems to be positive for the bioavailability into the brain by crossing the BBB for some of the new analogues. Compounds B and I exhibited high permeation through gastrointestinal barrier and BBB in Caco-2 and BBCEC models. Although the final results could not be compared to references CR-6 and Trolox, there was observed a penetration into the brain for some of these analogues. Nevertheless, new compounds **H**, **K** and **M** must be evaluated and complementary assays should be performed to assess the facilitated or active influx of these new antioxidant agents, such as the inhibition of these mechanisms and the comparison with our results.

VI. Evaluation of toxicity

VI.1 TOXICITY

Cellular toxicity by candidate drugs can occur through a diverse range of mechanisms that disrupt cellular integrity. Membrane-soluble or pore-forming compounds may act directly on the cytoplasmatic cell membrane and prevent the cell homeostatic integrity, thus leading to necrosis. Other compounds may act indirectly to disrupt the cell's biochemical, synthetic or signalling integrity leading to apoptosis. We can have compounds that act directly or indirectly to damage the cell's genetic integrity, resulting in inheritable mutation, disruption, proliferation integrity, or apoptosis.

The toxicity of new antioxidant compounds A, B, C, D, E, F, G, H, I, J, K, L, M and N was evaluated in MDA-MB-468, MDA-MB-231, Caco-2 and BBCE cells. The toxicity evaluation let us to know the cell viability in the presence of these compounds, and hence it provides a confidence on cellular antioxidant activity evaluation, and Caco-2 and BBCE cells permeation assay results.

VI.1.1 Toxicity in MDA-MB-468 and MDA-MB-231 cell line

VI.1.1.1. A brief introduction to the MTT-assay

Traditionally, several approaches have been used to determine the cell growth by counting viable cells after staining them with a vital dye. Trypan blue staining is a simple way to evaluate cell membrane integrity (assuming cell proliferation or death), but the method is not sensitive and cannot be adapted for high throughput screening (HTS). Measuring the uptake of radioactive substances, usually tritium-labeled thymidine, is accurate but it is also time-consuming and involves handling of radioactive material.[143]

Multi-well scanning spectrophotometers ELISA-like readers can evaluate a large number of samples at the same time with a high degree of precision.[144] Ideally, a colorimetric assay should utilize a colourless substrate that is modified to give a coloured product in living cells, but not when they are dead. Tetrazolium salts could be good candidates due to the fact they are intensively coloured by the action of various dehydrogenase enzymes in the active living cells mitochondria. In 1983, Mosnann investigated the yellow reagent MTT (3-(4,5-dimethylthiazol-2-yl)-2,5-diphenyltetrazolium bromide, a tetrazole) as a good HTS of living cells measurement.[144] The reduction of MTT to purple formazan (Figure 6.1) takes place in the mitochondria of viable cells by dehydrogenase enzymes; therefore, the conversion is directly related to the number of living cells.

[143] van de Loosdrecht, A.A.; Beelen, R.H.J.; Ossenkoppele, G.J.; Broekhoven, M.G.; Langenhuijsen, M.M.A.C. *J. Immunol. Methods* **1994**, *174*, 311-320.
[144] Mosmann, T. *J. Immunol. Methods* **1983**, *65*, 55-63.

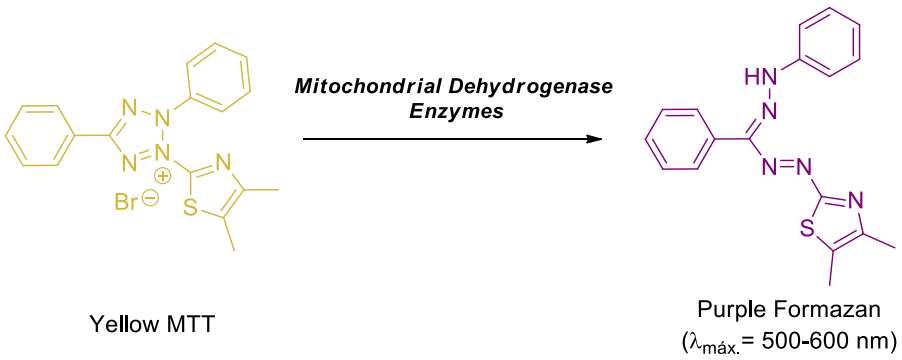

Figure 6.1. *Transformation of yellow MTT reagent into purple formazan by the opening of the tretrazole ring in the presence of mitochondrial reductase enzymes.*

The absorbance of this colored solution can be measured and quantified at a certain wavelength (500-600 nm) (Figure 6.1).[143] The maximum absorption is dependent on the solvent employed. Mitochondrial dehydrogenase enzymes of viable cells cleave the tetrazolium ring, yielding purple MTT formazan crystals, which are insoluble in aqueous solutions.[143] These crystals can give problems in the determination and they must be dissolved in acidified isopropyl alcohol. The effectiveness of an agent (known or unknown) in causing death of cells can be elicited by comparing the amount of purple formazan produced by cells treated with the agent and the amount of formazan produced by untreated control cells, in a linear dose-response curve.[144] A growth in cell number results in an increase of the amount of MTT formazan produced by enzymatic reaction and then the absorbance also increased.

The use of the MTT method has some limitations influenced by the physiological state of cells and the variance in mitochondrial dehydrogenase activity in different cell types. Nevertheless, the MTT method of cell determination is useful for the measurement of cell growth in response to mitogens, antigens stimuli, growth factors and other cell growth promoting reagents, cytotoxicity studies, and in the deviation of cell growth curves.[143]

Mosnann *et al.* studied different variables in MTT assay to optimize conditions.[144] They tested some tetrazolium salts in different alcohol solutions and cell lines and their best results for MTT reagent were obtained in acidic isopropyl alcohol solution, as the most suitable solvent. They also confirmed that the absorbance is directly proportional to the number of cells, extending the linearity over almost the entire range of cells tested, from 200 to 50 000 cells/well. Therefore, the MTT assay is a rapid, versatile, sensitive and quantifiable assay to measure cell viability. This MTT method of cell determination is particularly useful when cultures are prepared in multi-well plates. Each test should include a blank containing complete culture medium without cells.[144]

VI.1.1.2. Determination of cell viability of test compounds by MTT-assay in MDA-MB-468 and MDA-MB-231 cell line

The toxicity of compounds **A**, **B**, **C**, **D**, **E**, **F**, **G**, **H**, **I**, **J**, **K**, **L**, **M** and **N**, Trolox and CR-6 in human breast adenocarcinoma cell lines MDA-MB-231 and MDA-MB-468 was evaluated. First of all, MDA-MB-231 or MDA-MB-468 cells were incubated overnight in two different 96-well plates in humidified atmosphere with 5% CO_2 at 37ºC. Then, cells were treated with test antioxidant compounds at different concentrations from 0 to 100 µM in DMSO. DMSO was used as a vehicle for these experiments to dissolve the test compound and also the crystals of formazan generated during the process. After 24 hours, the MTT reagent in PBS was added to each well. Blanks and controls were assayed by treating cells with DMSO and MTT, and only with MTT, respectively. The formation of formazan compound for test compounds and controls was evaluated spectrophotometrically at $\lambda_{max.}$= 570 nm, and the living cells or viability was calculated as percentage (%) using following expression:

$$\%Viability = \frac{A_{test}}{A_{control}} \cdot 100$$

where A_{test} and $A_{control}$ represent the absorbance for test antioxidant compounds and control (MTT only), respectively, at $\lambda_{max.}$= 570 nm.

The results of %Viability for MBA-MB-231 and MBA-MB-468 cells, respectively, were plotted *versus* the concentration of test new antioxidant compound from 0 – 100 µM and compared to the control DMSO as vehicle, (see Figures 6.2 and 6.3), using the GraphPad Prism 5 software for Windows. Figure 6.2 shows the results of the toxicity assay MTT for MDA-MB-231 cells in presence of test antioxidants. According to these data, all compounds did not exhibit toxicity in concentrations from 0 to 100 µM; no one compound, except for **J** and **A**, showed a cell viability (percentage of living cells) lower than 50%. In general, at 100 µM, compounds exhibited a cell survival above 60-70%; but derivatives **J** and **A** showed cell viability lower than 50% and different from vehicle DMSO. At some concentrations, cell viability is higher than that elicited by vehicle DMSO, which might mean that these antioxidants restore the deleterious effects of DMSO on cells.

MDA-MB-231

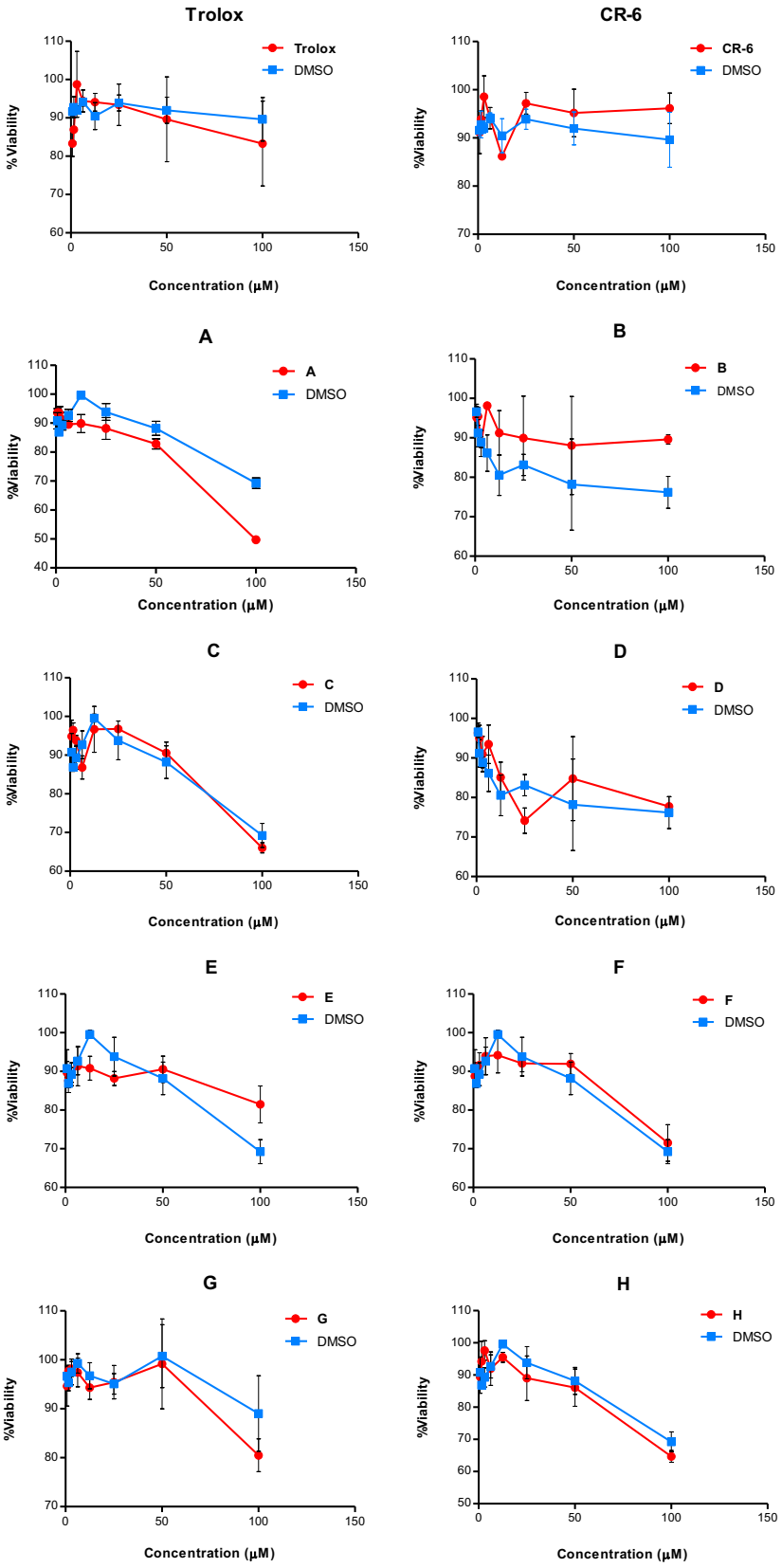
Trolox
Trolox
DMSO
%Viability
Concentration (µM)
CR-6
CR-6
DMSO
%Viability
Concentration (µM)
A
A
DMSO
%Viability
Concentration (µM)
B
B
DMSO
%Viability
Concentration (µM)
C
C
DMSO
%Viability
Concentration (µM)
D
D
DMSO
%Viability
Concentration (µM)
E
E
DMSO
%Viability
Concentration (µM)
F
F
DMSO
%Viability
Concentration (µM)
G
G
DMSO
%Viability
Concentration (µM)
H
H
DMSO
%Viability
Concentration (µM)

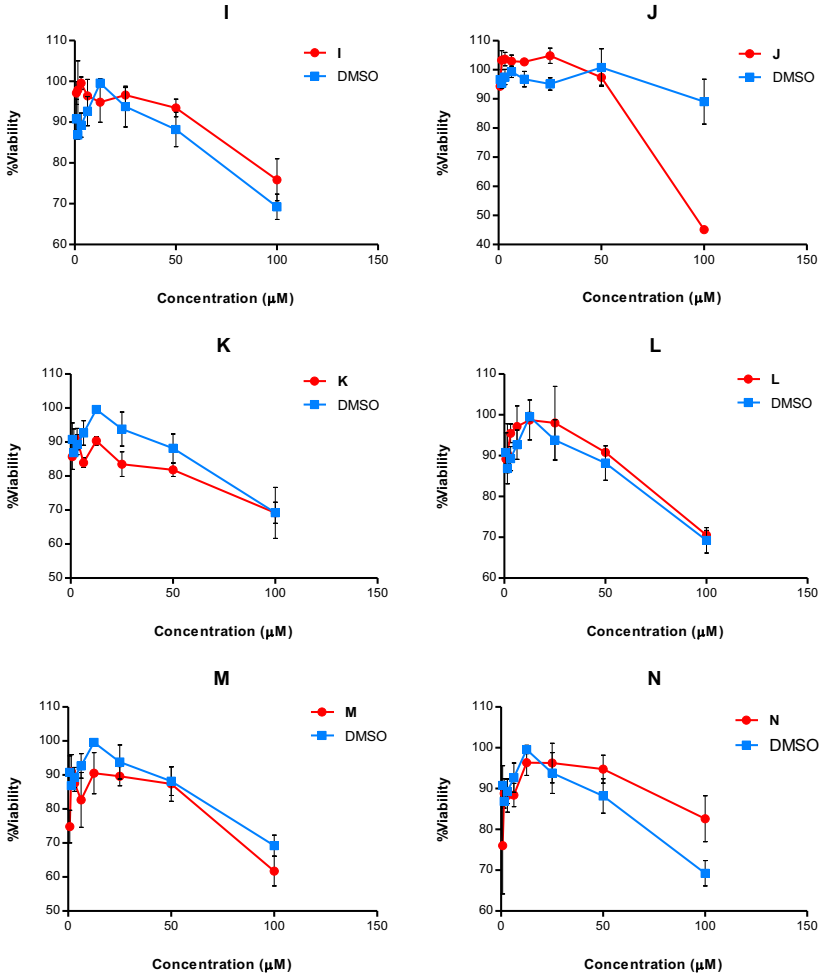

Figure 6.2. Plots of %Viability of cells - concentration (µM) curves for test compounds and the vehicle (DMSO) for MDA-MB-231 cell line in MTT toxicity assay. In red, the test antioxidant compound and in blue cells treated only with DMSO.

Figure 6.3 shows the results for toxicity assay MTT of test compounds in MDA-MB-468 cell line. According to these results, all compounds, except antioxidant **J**, presented similar or better viability of MDA-MB-468 cells than cells treated only with the DMSO at concentrations below 100 µM. They had %Viability higher than 50%, meaning that only less than 50% of cells died as consequence of the treatment of these test antioxidant compounds at concentrations lower than 100 µM. At 100 µM, more test compounds (for instance **A**, **J**, **M** and **N**) showed less viability of cells treated with the antioxidant than only with the vehicle. Moreover, in general, treatment with the antioxidant showed higher cell survival (higher viability) than controls, which might mean that these antioxidants suppress the deleterious effects of DMSO on cells.

MDA-MB-468

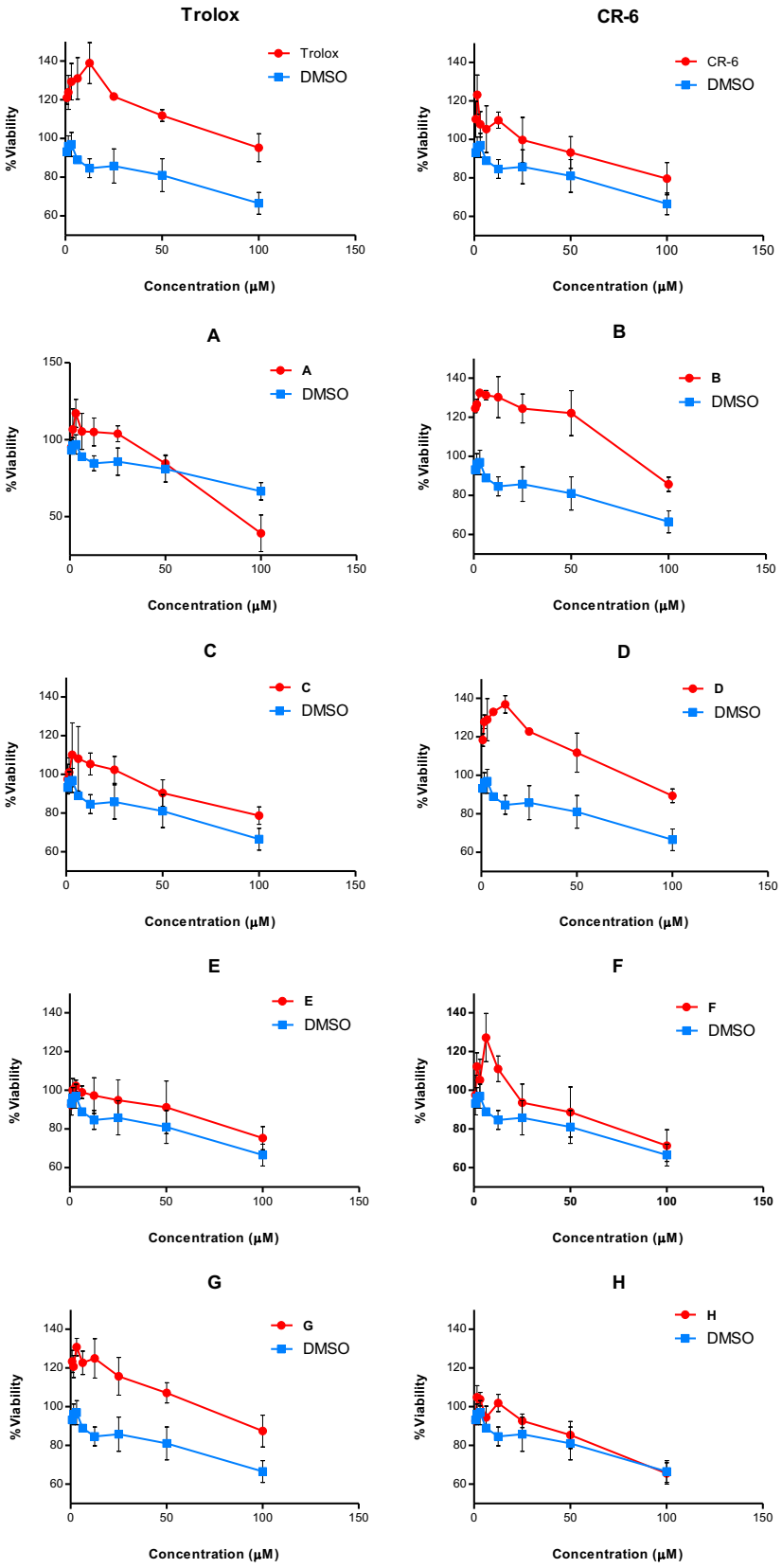
Trolox
Trolox
DMSO
% Viability
Concentration (µM)
CR-6
CR-6
DMSO
% Viability
Concentration (µM)
A
A
DMSO
% Viability
Concentration (µM)
B
B
DMSO
% Viability
Concentration (µM)
C
C
DMSO
% Viability
Concentration (µM)
D
D
DMSO
% Viability
Concentration (µM)
E
E
DMSO
% Viability
Concentration (µM)
F
F
DMSO
% Viability
Concentration (µM)
G
G
DMSO
% Viability
Concentration (µM)
H
H
DMSO
% Viability
Concentration (µM)

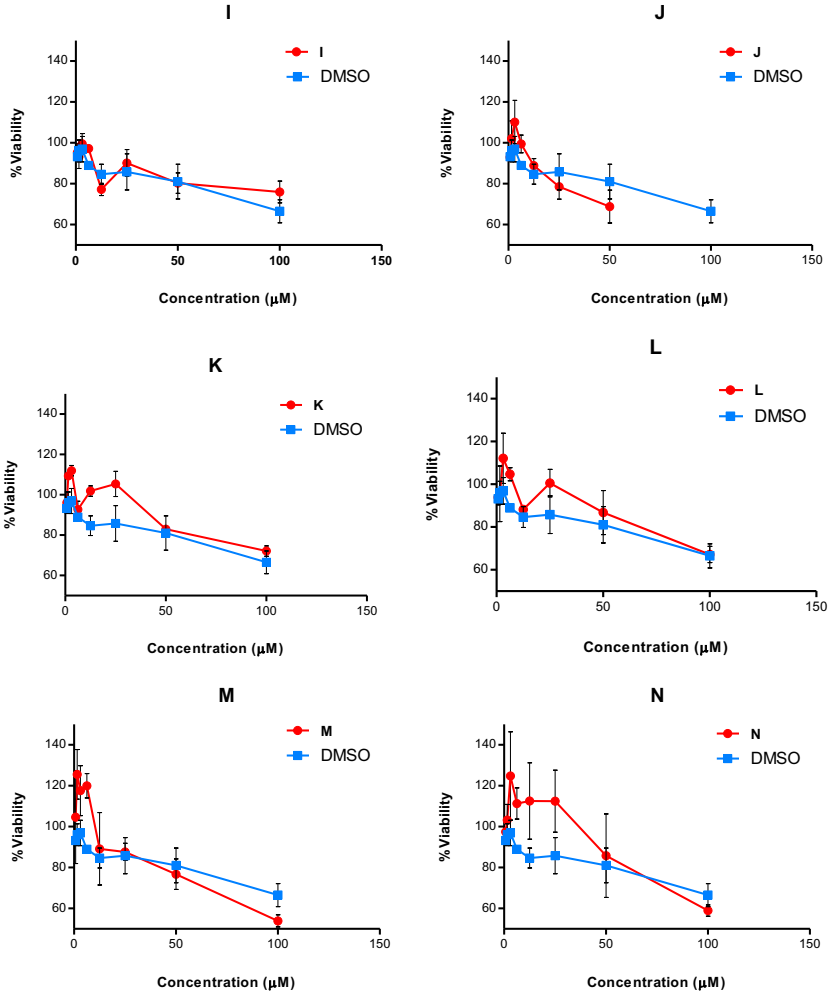

Figure 6.3. *Plots of %Viability of cells - concentration (µM) curves for test compounds and the vehicle (DMSO) for MDA-MB-458 cell line in MTT toxicity assay. In red, the test antioxidant compound and in blue cells treated only with DMSO.*

VI.1.2 Toxicity in Caco-2 cells

VI.1.2.1 Lucifer Yellow staining

Dyes have been widely used for determining cell monolayer integrity by the observation of cells in a microscope or by using a fluorescent impermeable staining or capable of being attached to the cell membrane. Dyes employed for labelling cells to evaluate overall cell architecture should exhibit the following properties: visible, immediately or after chemical reaction; remain in the injected cell (due to a lack cell membrane permeation or strong bound to the cytoplasm), no toxic; stable and not break down to give products with different properties, and withstands histological processing.

Lucifer Yellow (LY, Figure 6.4) is a low molecular weight (MW 444.25 g/mol) water-soluble and cell membrane-low-permeable marker used in transport experiments across endocytic and endothelial cell membranes. It is the most popular fluorescent compound for determining overall cellular architecture by fluorescence technique. LY has low permeability and so travels across cell (such as Caco-2 or BBCEC)

monolayers only by passive paracellular diffusion (between cells). It is not toxic and does not break down into other products. LY struggles to pass from the apical to basolateral compartment; therefore, only the cell membrane disruption makes possible the presence of a high quantity of LY in the basolateral side. The different fluorescence in both sides of cell monolayer is used to evaluate the cell-membrane integrity and thus the cell viability. LY has an excitation and emission maxima at 430 and 540 nm, respectively; and its fluorescence is constant from pH 2-12.[145] Normally, for usage, LY is presented as carbohydrazide (CH) and it is prepared as a lithium salt, as in Figure 6.5.

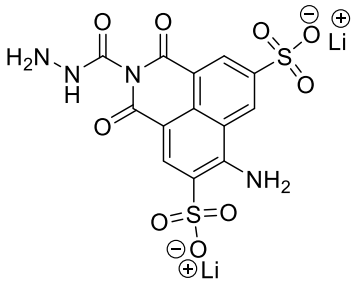

Figure 6.5. *Structure of the lithium salt of Lucifer Yellow carbohydrazide.*

V.1.2.2. Determination of toxicity of test compounds using Lucifer Yellow in the Caco-2 cellular assay

For transport studies and for toxicity experiments, the integrity of Caco-2 cell monolayer was monitored with the LY marker. Hence, the toxicity of our antioxidant compounds (**A**, **B**, **C**, **D**, **E**, **F**, **G**, **I**, **J**, **L** and **N**), Trolox and CR-6 in Caco-2 cell was evaluated. Compounds **H**, **K** and **M** have not been yet analyzed.

For A → B experiments, 10 mM fluorescent LY solution was added to the test antioxidant solution ($[LY]_{final}$ = 100 µM). Then, the absorption assay Caco-2 took place: 200 µL of each mixture were added in the apical compartment and 800 µL on each basolateral. For B → A experiments, a 100 µM LY solution was prepared in Ringer-Hepes' buffer, without antioxidant, and 200 µL of this solution were added in the apical compartment. In each basolateral compartment 800 µL of test antioxidant solution was added. Figure 6.6 shows the experimental procedure for experiments A→B and vice versa. In Caco-2 assay the concentration of the test antioxidant was 25 µM.

In these experiments DMSO was used as co-solvent. To avoid unwanted toxicological effects the solvent concentration in the test solutions was limited to maximum 0.25%. Once the experiment finished, an aliquot of 200 µL of each basolateral compartment in both experiments was placed in a black plate, for optimal sensitivity in fluorescence equipment, and fluorescence was measured ($\lambda_{excitation}$ = 432 nm and $\lambda_{emission}$ = 538 nm). The apparent permeability (P_{app}) for LY was calculated as in section V.3.1.3.1, page 142,

[145] Stewart, W.W. *Cell* **1978**, *14*, 741-759.

taking into account the fluorescence results in basolateral compartments and the fluorescence at initial 100 µM LY solution.

Figure 6.6. *Illustration of experiments A→B and B→A in Caco-2 assay. In both experiments the Lucifer Yellow was added in the apical compartment, even though the antioxidant test solution addition was different. The test antioxidant travelled from the apical to basolateral compartment in experiment A→B, and from the basolateral to apical compartment in experiment B→A; in contrast, LY travelled from A→B in both experiments.*

Table 6.2 shows the results for the P_{app} LY obtained for test antioxidant compounds in experiments A→B and vice versa.

Table 6.2. *Results of toxicity in Caco-2 cell monolayer: P_{app} LY for A→B and vice versa experiments.*

Antioxidant	P_{app} LY (A→B) ($\cdot 10^{-6}$ cm/s)[a]	P_{app} LY (B→A) ($\cdot 10^{-6}$ cm/s)[a]
Trolox	0.06±0.01	0.10±0.03
CR-6	0.09±0.03	0.13±0.01
A	0.08±0.01	0.09±0.02
B	0.08±0.02	0.14±0.01
C	0.08±0.02	0.12±0.01
D	0.08±0.02	0.11±0.03
E	0.11±0.05	0.11±0.02
F	0.08±0.03	0.11±0.06
G	0.13±0.10	0.20±0.13
H	*not analyzed*	*not analyzed*
I	0.09±0.03	0.59±0.30
J	0.09±0.03	0.38±0.24
K	*not analyzed*	*not analyzed*
L	0.08±0.03	0.13±0.03
M	*not analyzed*	*not analyzed*
N	0.12±0.04	0.16±0.10

[a] Results are expressed as mean±SD for triplicates.

A compound was considered toxic for the cell when the P_{app} LY was above $1 \cdot 10^{-6}$ cm/s. Figure 6.5 illustrates the results for the P_{app} LY obtained for test antioxidant compounds, Trolox and CR-6 in experiments from A→B and B→A.

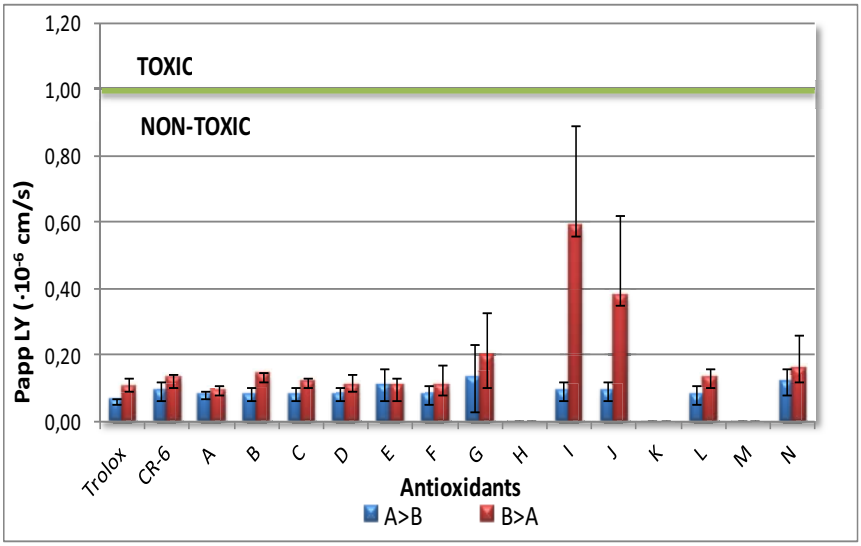

Figure 6.5. *Examination of toxicity and cell viability for test antioxidant compounds at 25 µM for experiments A→B and B→A in Caco-2 cellular assay. The red line points out the cufoff at P_{app} = 1·10^{-6} cm/s. Compounds with a P_{app} LY > 1·10^{-6} cm/s are toxic, whereas compounds with P_{app} LY ≤ 1·10^{-6} cm/s are not.*

According to these results, all test compounds (Trolox, CR-6, **A**, **B**, **C**, **D**, **E**, **F**, **G**, **I**, **J**, **L** and **N**) presented P_{app} values for marker LY lower than 1·10^{-6} cm/s and very similar for most of compounds in both experiments directions. Only compounds **I** and **J** showed higher P_{app} values for B→A experiment than for A→B. Taken together, the integrity and architecture of Caco-2 cell monolayer is not damaged and hence these compounds do not present toxicity to Caco-2 cells at evaluated concentration (25 µM).

VI.1.3 Toxicity in BBCEC

VI.1.3.1 Determination of toxicity of test compounds using Lucifer Yellow in BBCECs

Following the same procedure as in Caco-2 cellular assay, LY was used as marker to evaluate the toxicity of our antioxidant collection of compounds (**A**, **B**, **C**, **D**, **E**, **F**, **G**, **I**, **J**, **L** and **N**), Trolox and CR-6 in BBCEC. Once again, compounds **H**, **K** and **M** were not analyzed.

Table 6.3. *Results for P_e LY for toxicity in BBCEC assay.*

Antioxidant	P_e ($\cdot 10^{-3}$ cm/min)[a]
Trolox	0.11±0.02
CR-6	0.08±0.03
A	0.12±0.03
B	0.08±0.01
C	0.11±0.03
D	0.10±0.03
E	0.33±0.10
F	0.10±0.02
G	0.13±0.04
H	*not analyzed*
I	0.20±0.10
J	0.14±0.04
K	*not analyzed*
L	0.22±0.13
M	*not analyzed*
N	0.09±0.02

[a] Results are expressed as mean±SD for triplicates.

As in the Caco-2 cellular assay, the transport through BBCEC and toxicity were evaluated simultaneously. In this case, due to the different morphology of BBCEC with respect to Caco-2 cells, the final concentration of LY solution was 50 µM. A solution of 10 mM LY was added to the apical side compartment of BBCEC assay with the test solution (the concentration of test antioxidant was 10 µM with 0.10% of DMSO) and cells were incubated for 60 minutes at 37ºC. After this time, 200 µL-aliquot fluorescence of each basolateral compartment was measured ($\lambda_{excitation}$ = 432 nm and $\lambda_{emission}$ = 538 nm) in a black plate. The endothelial permeability (P_e) for marker LY was calculated as expression used in section V.3.3.3, page 153, taking into account the fluorescence results in basolateral compartments and the fluorescence at initial 50 µM LY solution. Table 6.3 shows the results for the P_e LY obtained for test antioxidant compounds in BBCEC assay for the toxicity evaluation.

A compound was considered toxic for the BBCECs when the P_e LY was above $1 \cdot 10^{-3}$ cm/s. Figure 6.6 illustrates the results for the P_e LY obtained for our antioxidant compounds, Trolox and CR-6 in BBCEC assay.

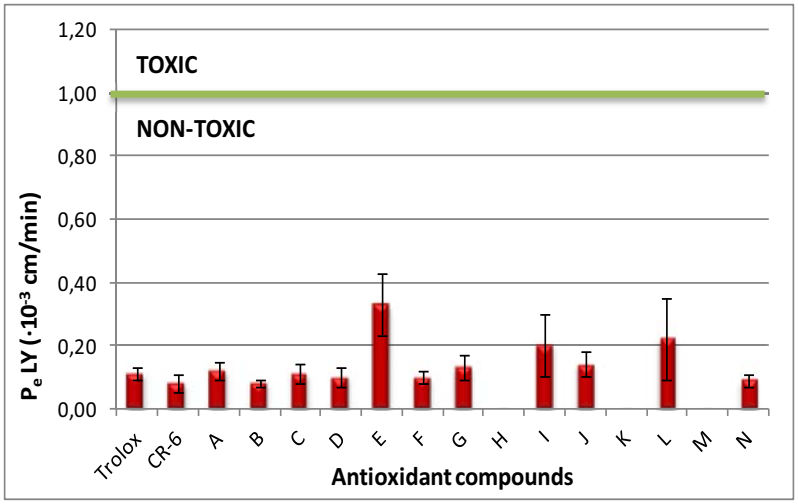

Figure 6.6. *Examination of toxicity and cell viability for test antioxidant compounds at 10 µM. The red line points out the cufoff at P_e = 1·10^{-3} cm/min. Compounds with a P_e LY > 1·10^{-3} cm/min are toxic, whereas compounds with P_e LY ≤ 1·10^{-3} cm/min are not.*

According to these results, all test compounds (Trolox, CR-6, **A**, **B**, **C**, **D**, **E**, **F**, **G**, **I**, **J**, **L** and **N**) showed P_e for marker LY lower than 1·10^{-3} cm/s and very similar for most of them. Compounds **E**, **I** and **L** exhibited the highest values. According to P_e-values, the integrity and architecture of BBCECs monolayer is not damaged, which indicates that these compounds are not toxic to BBCECs at evaluated concentration (10 µM).

VII. Conclusions

From the work of the present Doctoral Thesis and the results obtained, the following conclusions have been extracted:

1. Fourteen CR-6 analogues (**A**-**N**) have been synthesized optimizing short synthetic route to improve the BBB bioavailability of the present CR-6 molecule. The CR-6 scaffold was coupled to different essential nutrients to the brain or retina (amino acids, glucose, retinol, etc.). The synthetic pathway consisted in the formation of peptidic bond with acid **6** and commercially available amines, and amine **18** and commercially available acids.

2. Regarding the stereogenic center at C_2, the stereoselective preparation of compounds has been studied. The chiral chromatographic separation of **1**, as a key intermediate for all CR-6 analogues, was evaluated. Thus, the two enantiomers were efficiently separated in most of the columns tested. Overall, taking under consideration selectivity (α) and resolution (Rs) factors, column Chiralpak IA was selected as the best one.

3. The effect on the antioxidant activity by the introduction of variability into the CR-6 scaffold at C_2 has been studied using two different *in vitro* assays.

   In the DPPH assay, most of compounds exhibited an antioxidant capacity not statistically different ($p > 0.05$) from CR-6 and Trolox. These results indicate that the antioxidant activity is retained by the introduction of variability at C_2. Some compounds (**A**, **N** and **I**) neutralized more molecules of free radical DPPH· (3-4) than CR-6 (2), which suggests that some functional groups present on the side-chain or the electronic distribution of analogues may improve their antioxidant activity.

4. On the other hand, the antioxidant activity was evaluated in a cellular environment using breast cancer cells MDA-MB-231 and -468. In this assay, in general, test compounds were statistically different ($p > 0.05$) from CR-6. However, taking into account IC_{50} values, several compounds exhibited a comparable activity with that of CR-6: **A**, **L**, **N**, **I** and Trolox in MDA-MB-231 cells; and derivatives **A**, **F**, **N**, **L** and Trolox in MDA-MB-468 cells. In contrast, compounds **J** and **G** exhibited the weakest activity. All this suggests that the biological environment affects to the final antioxidant activity: not all compounds are permeable to the lipid bilayer of cells or some of them can be metabolized.

5. The permeability by passive diffusion of the library of CR-6 analogues was evaluated using *in silico* analysis. Regarding the physicochemical properties (pK_a, HBD, clogD, clogP and TPSA), the passive diffusion was studied using the CNS MPO score. CR-6 Analogues showed CNS MPO values below 4.5, except for Trolox and analogue **N** that it was 4.5. These results suggest that CR-6 analogues are not able to be delivered through BBB by passive diffusion, even they might exhibit poor ADME and safety properties *in vivo*. However, these predictions are not always necessarily true in an *in vivo* situation.

6. Complementarily, Caco-2 assay, PAMPA and BBCEC assay were performed to evaluate the *in vitro* BBB permeability and to predict drug *in vivo* absorption. Comparing the results from the three assays it can be concluded that in general CR-6 analogues presented good permeability through BBB by means of some facilitated or active influx mechanism. These results also suggest that they do not interact with efflux pumps, with the exception of derivative **G**, which exhibited a better transport from B→A (P_{app} > $10 \cdot 10^{-6}$ cm/s) than A→B. In addition, these compounds expressed weak passive diffusion in PAMPA assay ($P_e < 2 \cdot 10^{-6}$ cm/s), although analogues **A**, **F**, **G**, **I** and **L** exhibited better results than CR-6. The free carboxylic acid (negatively charged at pH 7.4) present in most of compounds might be the responsible for the low passive diffusion in PAMPA. Furthermore, compounds **I** and **L** might have a facilitated or active influx transporter in Caco-2, and **B** and **I** in BBCEC.

7. The recovery values in the *in vitro* BBB permeability assays were good for most of compounds (higher than 50%). Derivatives with low recovery may remain attached to cells or in the filter or plastic devices and could not be totally recovered. In addition, metabolism effects may play a role in decreasing this percentage recovery value.

8. The toxicity and cell viability of test antioxidants in MDA-MB-231 and -468 cells, and Caco-2 and BBCE cells were studied using the MTT assay and the Lucifer Yellow (LY) marker. The MTT assay for MDA-MB-231 and -468 cells showed that all compounds were not toxic (cell viability was higher than 50% from 50-100 μM). Furthermore, at most concentrations, CR-6 analogues exhibited better cell viability than vehicle DMSO, which might be due to an antioxidant effect of compounds on side effects of DMSO on cells. In addition, measures with cell marker LY showed that tested antioxidants do not elicit toxicity in Caco-2 and BBCE cells.

For future work, the analysis of aliquots from *in vitro* BBB permeability assays by UPLC-MS should be improved to permit the comparison of results with CR-6. In addition, derivatives **H**, **K** and **M** should be assayed in Caco-2 and BBCEC assays. Moreover, to improve the permeability of some compounds in Family 1, analogues containing free amino acid group should be prepared and studied. Regarding the low passive diffusion of these compounds, some of them should be prepared with less HBD or lower TPSA to observe the effect on the BBB permeability. In addition, it should be studied some analogues with the phenol protected. It is feasible that these molecules could be more able to cross BBB and then the protecting group should be easily enzymatically released inside the brain to elicit its antioxidant activity.

Taken all together, and regarding on BBB permeability, analogues **B** and **I** could be identified as the best neuroprotectants of that series of compounds and might be evaluated in an *in vivo* model.

VIII. Experimental part

VIII.1 SYNTHESIS OF NEW ANTIOXIDANTS

VIII.1.1 General

All reagents were obtained from commercial sources and used without further purification. Methoxyhydroquinone, trimethyl orthoformiate, sulfuric acid 98%, methyl vinylketone, sodium hydride (NaH), benzyl bromide (BnBr), trimethyl phosphonoacetate, lithium aluminium tetrahydride ($LiAlH_4$), sodium cyanide (NaCN), ammonium chloride (NH_4Cl), dried magnesium sulfate ($MgSO_4$), 7 M NH_3 solution in methanol, *N*-(3-dimethylaminopropyl)-*N'*-ethylcarbodiimide hydrochloride (EDC·HCl), dicyclohexylcarbodiimide (DCC), 1-hydroxybenzotriazole hydrate (HOBt), diisopropilethylamine (DiPEA), dopamine hydrochloride salt, L-tyrosine methyl ester hydrochloride, L-alanine methyl ester hydrochloride, L-valine methyl ester hydrochloride, L-proline benzyl ester hydrochloride, L-phenylalanine benzyl ester hydrochloride, L-tryptophan methyl ester hydrochloride, L-glutamine methylester hydrochloride, 0.5 M NH_3 solution in dioxane, palladium on carbon 10 wt. % (Pd/C), pyridine, p-toluenesulfonyl chloride (TsCl), sodium azide (NaN_3), triphenylphosphine (PPh_3), triethylamine (NEt_3) and acetyl chloride were purchased from Sigma-Aldrich. 2-Iodoxybenzoic acid (IBX) was prepared from the 2-iodobenzoic acid and Oxone®, also purchased from Sigma-Aldrich. TsCl was purified by dissolving in CH_2Cl_2 and washing with saturated solution of $NaHCO_3$. Retinoic acid was purchased from Alfa Aesar.

Anhydrous solvents were obtained from PureSolv M (Solvent Purification System), except for anhydrous DMF which was purchased from Sigma-Aldrich at 99.8% of purity.

Reaction monitoring was carried out using SiO_2-coated TLC plates eluting with mixtures of EtOAc:Hexane. Alternatively, analytical RP-HPLC was performed with a Hewlett-Packard Series 1100 (UV detector 1315A) modular system using a reverse-phase Kromasil 100 C_{18} (150 mm x 4.6 mm, 5 µm) column. CH_3CN-H_2O mixtures containing 0.1% TFA at 1 mL/min were used as mobile phase and monitoring wavelength was set at 220 and 254 nm. A gradient method from 20% to 100% of CH_3CN in 20 minutes was used.

For purifications, a Biotage chromatography system in normal or reverse phase was usually used. For this purpose columns of C_{18} or silica from Biotage (Uppsala, Sweden) were employed. When considered convenient, conventional flash chromatography purifications were carried out.

Nuclear Magnetic Ressonance spectra (NMR) have been recorded in the *Servei de Ressonància Magnètica* in *Institut de Química Avançada de Catalunya*. The ^{1}H- and ^{13}C-NMR spectra were recorded with a VMRS 400 spectrometer with an OneNMR ProTune in $CDCl_3$ or CD_3OD with TMS as internal standard. The chemical shifts are given in δ (ppm), using the residual non-deuterated solvent as reference (at 7.26 ppm for $CDCl_3$ and at 3.31 ppm for CD_3OD). The abbreviations used to describe the signal multiplicities are: s (singlet), $s_{exch.}$ (siglet exchange, broad singlet), d (doublet), t (triplet), q (quadruplet), p (quintuplet), dd (double doublet), ddd (double double doublet), dt (double triplet), ddt (double double

triplet), dq (double quadruplet), td (triple doublet) m (multiplet), and *J* (in Hz) to indicate the coupling constant. Although diastereomers of some compounds were not prepared separately, diastereotopic peaks were observed. Therefore, the ^{1}H- and ^{13}C-NMR signals were assigned as far as possible to so-called diastereomer A and diastereomer B.

High Resolution Mass Spectra (HRMS) have been registered in the *Servei d'Espectrometria de Masses* in *Institut de Disagnòstic Ambiental i Estudis de l'Aigua* with an LCT premier UPLC/MS Q-TOF (Waters) using electrospray ionization (EI) detector and leucine as reference (m/z = 557.3812).

Infrared Spectra (IR) have been registered in a Nicolet Avatar 360 FT-IR spectrophotometer using a KBr pellet.

Elemental analyses were carried out in Thermofinnigan elemental microanalyzer (A7) Flash 2000 series model for the C, H, N and S determinations, at the *Servei de Microanàlisi Orgànica* in *Institut de Química Avançada de Catalunya*.

Melting points were determined on a Büchi Melting Point B-545 (Büchi, Switzerland) hot stage apparatus.

The HPLC, HRMS, NMR and IR data for all the synthesized compounds from which the characterization has been carried out are available in the Supporting Information.

VIII.1.2 Synthesis of intermediates 1 and 2

3,4-Dihydro-6-hydroxy-2-methyl-2,7-dimethoxy-1-(2H)-benzopyran, 3

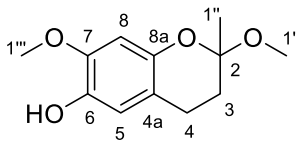

3

To a solution of methoxyhydroquinone (25.3 g, 0.18 mol) in anhydrous MeOH (100 mL) trimethyl orthoformate was added (27 mL, 0.25 mol), under N_2 atmosphere. After cooling the solution to 0ºC with an ice-water bath, sulfuric acid 98% (0.45 mL) was added followed by methyl vinylketone (34 mL, 0.42 mol). The mixture was stirred for 48 hours at room temperature (TLC monitoring, 3:2 hexane:EtOAc) and then neutralised by adding 1 M NaOH (20 mL) dropwise. After removal of the solvent under vacuum, the residue was extracted with *tert*-butyl methyl ether and the combined organic layer was washed with brine, dried over anhydrous $MgSO_4$ and the solvent was evaporated under vacuum. The residue was

purified by flash chromatography on silica gel (gradient, from 95:5 hexane:EtOAc to EtOAc) to give the compound **3** (31.9 g, 80%) as a greenish oil.

Elemental analysis $C_{12}H_{16}O_4$: calculated: C 64.27%, H 7.19% and O 28.54%; found: C 64.08%, H 7.40% and O 28.52% (± 0.3%). **^{1}H-NMR ($CDCl_3$, 400 MHz):** δ: 6.61 (s, $1H_8$), 6.40 (s, $1H_5$), 5.16 (s exch., $1H_{OH}$), 3.83 (s, J = 3.9 Hz, $3H_{1'''}$), 3.28 (s, J = 2.2 Hz, $3H_{1'}$), 2.89 (dddd, J = 16.1, 12.9, 6.3 Hz, $1H_4$), 2.49 (ddd, J = 15.9, 5.8 Hz, $1H_4$), 2.04 (ddd, J = 13.4 , 6.2, 2.1 Hz, $1H_3$), 1.78 (ddt, J = 13.4, 6.1, 1.1 Hz,, $1H_3$), 1.52 (s, J = 3.3 Hz, $1H_{1'}$). **^{13}C-NMR ($CDCl_3$, 100 MHz):** δ: 145.99 (C_{8a}), 145.87 (C_7), 140.05 (C_6), 114.64 (C_8), 114.59 (C_{4a}), 100.79 (C_5), 98.61 (C_2), 56.52 ($C_{1'''}$), 49.47 ($C_{1'}$), 32.42 (C_4), 23.66 ($C_{1''}$), 21.47 (C_4).

6-Benzyloxy-3,4-dihydro-2-hydroxy-2-methyl-7-methoxy-1-(2H)-benzopyran, 5

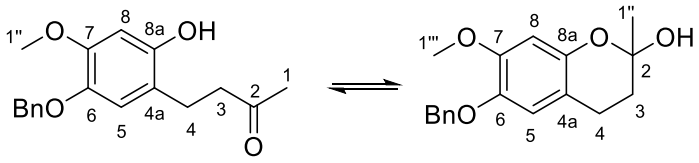

5a **5b**

To a suspension of NaH (642 mg, 16.1 mmol, 60% in mineral residue), previously washed with hexanes, in anhydrous THF (15 mL) and cooled to 0ºC in an ice-water bath, a solution of **3** (2.7 g, 11.9 mmol) in anhydrous THF (15 mL) was added dropwise, followed by the addition of benzyl bromide (1.5 mL, 12.7 mmol). The mixture was stirred for 14 hours at room temperature (TLC monitoring , 3:2 hexane:EtOAc). The mixture was treated with water dropwise and once bubbling stopped, acetone (20 mL) was added followed by a solution of 1 M HCl (20 mL). The reaction was stirred at room temperature for 4 hours (TLC monitoring TLC, 3:2 hexane:EtOAc); then the solvent was removed under vacuum. The residue was extracted with *tert*-butyl methyl ether and washed with brine. The combined organic layers were dried over anhydrous $MgSO_4$ and the solvent evaporated under vacuum. The residue was purified by flash chromatography on silica gel (gradient, from 95:5 hexane:EtOAc to EtOAc) to give the hemiacetal **5** (3.1 g, 88%) as a brownish oil.

HRMS for $C_{18}H_{21}O_4$: calculated: 301.1440 ($[M+H]^+$); found: 301.1448. **^{1}H-NMR ($CDCl_3$, 400 MHz):** δ: 7.71 (s, $1H^A_{OH}$), 7.48 – 7.39 (m, $2H^A_{Bn}$ + $2H^B_{Bn}$), 7.39 – 7.32 (m, $2H^A_{Bn}$ + $2H^B_{Bn}$), 7.32 – 7.27 (m, $1H^A_{Bn}$ + $1H^B_{Bn}$), 6.64 (s, $1H^B_8$), 6.56 (s, $1H^A_8$), 6.53 (s, $1H^A_5$), 6.41 (s, $1H^B_5$), 5.05 (s, $2H^B_{Bn}$), 5.03 (s, $2H^A_{Bn}$), 3.81 (s, $3H^B_{1'''}$), 3.80 (s, $3H^A_{1''}$), 2.87 (ddd, J = 6.1, 12.7, 22.3 Hz, $1H^B_4$), 2.79 (dd, J = 5.2, 6.2 Hz, $1H^A_4$ + $1H^A_3$), 2.66 (dd, J = 4.2, 6.3 Hz, $1H^A_4$ + $1H^A_3$), 2.55 (ddd, J = 16.1, 5.9, 2.9 Hz, $1H^B_4$), 2.13 (s, $3H^A_1$), 2.03 (ddd, J = 13.4, 6.1, 3.0 Hz, $1H^B_3$), 1.87 – 1.76 (m, $1H^B_3$), 1.61 (s, $3H^B_{1''}$). **^{13}C-NMR ($CDCl_3$, 100 MHz):** δ: 212.00 ($C_2{}^A$), 149.81 ($C_{8a}{}^B$), 149.37 ($C_7{}^A$), 149.19 ($C_7{}^B$), 146.88 ($C_{8a}{}^A$), 142.36 ($C_6{}^B$), 141.89 ($C_6{}^A$), 137.61 ($C_{Bn}{}^A$), 137.58 ($C_{Bn}{}^B$), 128.43 (C_{Bn}), 128.38 (C_{Bn}), 128.37 (C_{Bn}), 127.71 (C_{Bn}), 127.60 (C_{Bn}), 127.59 (C_{Bn}), 127.42 (C_{Bn}), 118.32 ($C_{4a}{}^A$), 117.87 ($C_5{}^A$), 115.63 ($C_5{}^B$), 112.09 ($C_{4a}{}^B$), 102.54 ($C_8{}^A$), 101.59 ($C_8{}^B$), 96.19 ($C_2{}^B$), 72.56 ($C_{Bn}{}^A$), 72.16 ($C_{Bn}{}^B$), 55.96 ($C_{1'''}{}^B$), 55.89 ($C_{1''}{}^A$), 45.46 ($C_3{}^A$), 31.59 ($C_3{}^B$), 29.71 ($C_1{}^A$), 28.59 ($C_{1''}{}^B$), 22.63 ($C_4{}^A$), 21.12 ($C_4{}^B$).

6-Benzyloxy-3,4-dihydro-2-methyl-7-methoxy-2-methoxycarbonylmethyl-1-(2H)-benzopyran, 1

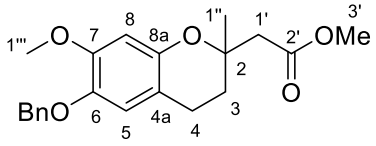

1

To a suspension of NaH (871 mg, 21.8 mmol, 60% mineral residue), previously washed with hexanes, in anhydrous THF (15 mL), under N_2 atmosphere and cooled to 0ºC in an ice-water bath, trimethyl phosphonoacetate (3.5 mL, 21.8 mmol) was added portionwise. The resulting white foam was stirred for 1 hour at room temperature. Then, a solution of hemiacetal **2** (3.3 g, 10.9 mmol) in anhydrous THF (15 mL) was added and stirred for another 1 hour. Then, the mixture was stirred for 30 minutes under reflux and (TLC monitoring, 3:2 hexane:EtOAc). The mixture was cooled to room temperature and treated with a cold solution of NH_4Cl. The mixture was concentrated under vacuum and the residue was extracted with *tert*-butyl methyl ether and washed with brine. The combined organic layer was dried with anhydrous $MgSO_4$ and the solvent was removed under vacuum. The resulting residue was purified by flash chromatography on silical gel (gradient, from 98:2 hexane:EtOAc to EtOAc) to give product **1** (3.0 g, 76%) as an orangish oil.

HRMS for $C_{21}H_{25}O_5$: calculated: 357.1702 ($[M+H]^+$); found: 357.1718. **^{1}H-NMR ($CDCl_3$, 400 MHz):** δ: 7.48 – 7.40 (m, $2H_{Bn}$), 7.39 – 7.33 (m, $2H_{Bn}$), 7.32 – 7.27 (m, $1H_{Bn}$), 6.59 (s, $1H_8$), 6.38 (s, $1H_5$), 5.05 (s, $2H_{Bn}$), 3.81 (s, $3H_{1'''}$), 3.69 (s, $3H_{3'}$), 2.71 – 2.57 (m, $2H_4$ + $2H_{1'}$), 1.99 (dt, J = 13.1, 6.4 Hz, $1H_3$), 1.92 – 1.78 (m, $1H_3$), 1.43 (s, $3H_{1''}$). **^{13}C-NMR ($CDCl_3$, 100 MHz):** δ: 170.87 ($C_{2'}$), 149.45 (C_{8a}), 147.52 (C_7), 142.10 (C_6), 137.60 (C_{Bn}), 128.39 (C_{Bn}), 127.65 (C_{Bn}), 127.37 (C_{Bn}), 115.71 (C_5), 111.26 (C_{4a}), 101.62 (C_8), 74.40 (C_2), 72.15 (C_{Bn}), 55.88 ($C_{1'''}$), 51.59 ($C_{3'}$), 43.55 ($C_{1'}$), 30.85 (C_3), 24.82 ($C_{1''}$), 21.48 (C_4). **IR (KBr):** ν (cm^{-1}): 2950, 1735, 1512.

6-Benzyloxy-3,4-dihydro-2-(2'-hydroxyethyl)-2-methyl-7-methoxy-1-(2H)-benzopyran, 2

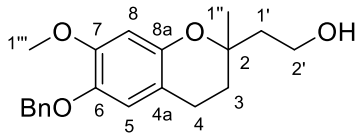

2

To a suspension of $LiAlH_4$ (147 mg, 3.9 mmol) in anhydrous THF (8 mL), at 0ºC with an ice-water bath, under N_2 atmosphere, a solution of ester **1** (683 mg, 2.0 mmol) in anhydrous THF (4 mL) was added dropwise, and the mixture was stirred for 1 hour at room temperature (TLC monitoring, 3:2 hexane:EtOAc).Then the crude reaction mixture was cooled to 0ºC and water was carefully added. The mixture was filtered through Celite® and the residue was extracted with Et_2O and washed with brine. The combined organic layer was dried with anhydrous $MgSO_4$ and the solvent was removed under vacuum to give compound **2** (611 mg, 97%) as a white solid.

HRMS for $C_{20}H_{25}O_4$: calculated: 329.1753 ($[M+H]^+$); found: 329.1739.**^{1}H-NMR ($CDCl_3$, 400 MHz):** δ: 7.46 – 7.41 (m, $2H_{Bn}$), 7.39 – 7.33 (m, $2H_{Bn}$), 7.32 – 7.26 (m, $1H_{Bn}$), 6.59 (s, $1H_5$), 6.35 (s, $1H_8$), 5.04 (s, $2H_{Bn}$), 3.92

(ddd, J = 12.5, 7.4, 5.1 Hz, $1H_{2'}$), 3.88 – 3.82 (m, $1H_{2'}$), 3.81 (s, $3H_{1'''}$), 2.74 – 2.58 (m, $2H_4$), 2.05 – 1.90 (m, $2H_{1'}$), 1.73 (dt, J = 13.8, 5.8 Hz, $2H_3$), 1.31 (s, $3H_{1''}$). **^{13}C-NMR ($CDCl_3$, 100 MHz):** δ: 149.71 (C_{8a}), 147.89 (C_7), 142.24 (C_6), 137.79 (C_{Bn}), 128.53 (C_{Bn}), 127.81 (C_{Bn}), 127.55 (C_{Bn}), 116.03 (C_5), 111.53 (C_{4a}), 101.53 (C_8), 76.04 (C_2), 71.99 (C_{Bn}), 58.54 ($C_{2'}$), 55.55 ($C_{1'''}$), 41.40 ($C_{1'}$), 31.22 (C_3), 23.10 ($C_{1''}$), 20.89 (C_4). **IR (KBr):** ν (cm^{-1}): 3418, 2935, 1951, 1619.

VIII.1.3 Synthesis of CR-6 derivatives from intermediate 1. Family 1

6-Benzyloxy-2-hydroxycarbonylmethyl-3,4-dihydro-2-methyl-7-methoxy-1-(2H)-benzopyran, 6

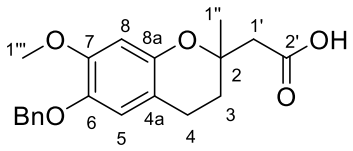

6

To a solution of ester **1** (1.8 g, 4.9 mmol) in dioxane (25 mL) a solution of 4 M NaOH (25 mL) was added and the mixture was heated under reflux for 4 hours (HPLC-UV monitoring). When the reaction was completed, the mixture was cooled to room temperature and acidified with 2 M HCl. The residue was extracted with CH_2Cl_2 and washed with brine. The combined organic layers were dried with anhydrous $MgSO_4$ and the solvent was evaporated under vacuum to give acid **6** (1.6 g, 99 %) as a cream-colored solid.

HRMS for $C_{20}H_{23}O_5$: calculated: 343.1545 ($[M+H]^+$); found: 343.1552. **^{1}H-NMR ($CDCl_3$, 400 MHz):** δ: 7.41 (dd, J = 7.9, 1.0 Hz, $2H_{Bn}$), 7.37 – 7.31 (m, $2H_{Bn}$), 7.31 – 7.25 (m, $1H_{Bn}$), 6.58 (s, $1H_5$), 6.38 (s, $1H_8$), 5.03 (s, $2H_{Bn}$), 3.80 (s, $3H_{1'''}$), 2.67 (s, $2H_{1'}$), 2.64 (t, J = 6.7 Hz, $2H_4$), 1.99 (dt, J = 13.7, 4.3 Hz, $1H_3$), 1.85 (dt, J = 13.6, 6.7 Hz, $1H_3$), 1.42 (s, $3H_{1''}$). **^{13}C-NMR ($CDCl_3$, 125 MHz):** δ: 172.83 ($C_{2'}$), 149.58 (C_{8a}), 146.88 (C_7), 142.48 (C_6), 137.51 (C_{Bn}), 128.45 (C_{Bn}), 127.73 (C_{Bn}), 127.40 (C_{Bn}), 115.69 (C_5), 111.24 (C_{4a}), 101.63 (C_8), 74.49 (C_2), 72.13 (C_{Bn}), 55.96 ($C_{1'''}$), 43.73 ($C_{1'}$), 30.96 (C_3), 24.38 ($C_{1''}$), 21.37 (C_4). **IR (KBr):** ν (cm^{-1}): 3471, 3409, 1707.

6-Benzyloxy-2-[5'-(9',10'-dihydroxyphenyl)ethylaminocarbonylmethyl]-3,4-dihydro -2-methyl-7-methoxy-1-(2H)-benzopyran, 7

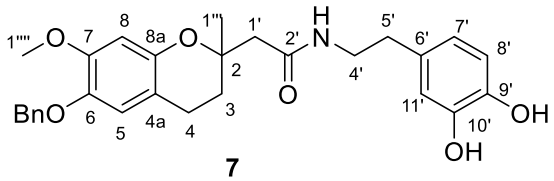

7

To a solution of acid **6** (406 mg, 1.19 mmol) in anhydrous CH_2Cl_2 (10 mL) EDC·HCl (296 mg, 1.54 mmol), HOBt (217 mg, 1.61 mmol) and DIPEA (2.3 mL, 13.2 mmol) were added, under N_2 atmosphere. The mixture was stirred for 30 minutes at room temperature. After this time, dopamine hydrochloride salt (250 mg, 1.32 mmol) was added, and the stirring was prolonged for 48 hours (HPLC-UV monitoring). Then, the mixture was washed with 1 M HCl and with a saturated solution of $NaHCO_3$. The combined

organic layer was dried with anhydrous $MgSO_4$ and the solvent was evaporated under vacuum. The residue was purified by chromatography in reverse phase (gradient, from 9:1 H_2O:CH_3CN to CH_3CN) to give amide **7** (309 mg, 54%).

HRMS for $C_{28}H_{32}NO_6$: calculated: 478.2230 ([M+H]$^+$); found: 478.2264. **^{1}H-NMR ($CDCl_3$, 400 MHz):** δ: 7.47 – 7.40 (m, 2H_{Bn}), 7.39 – 7.34 (m, 2H_{Bn}), 7.33 – 7.28 (m, 1H_{Bn}), 6.69 (d, J = 2.0 Hz, 1$H_{6''}$), 6.65 (d, J = 8.0 Hz, 1$H_{3''}$), 6.60 (s, 1H_5), 6.48 (dd, J = 8.0, 2.0 Hz, 1$H_{2''}$), 6.37 (t, J = 5.7 Hz, 1H_{NH}), 6.20 (s, 1H_8), 5.05 (s, 2H_{Bn}), 3.81 (s, 3$H_{1''''}$), 3.53 (m, 2$H_{1'}$), 2.77 – 2.42 (m, 2H_4 + 2$H_{4'}$ + 2$H_{5'}$), 1.78 – 1.68 (m, 2H_3), 1.29 (s, 1$H_{1'''}$). **^{13}C-NMR ($CDCl_3$, 100 MHz):** δ: 170.68 ($C_{2'}$), 149.27 (C_{8a}), 146.69 (C_7), 144.07 ($C_{5''/4''}$), 142.64 ($C_{5''/4''}$), 142.33 (C_6), 137.22 (C_{Bn}), 130.62 ($C_{1''}$), 128.36 (C_{Bn}), 127.72 (C_{Bn}), 127.34 (C_{Bn}), 120.37 ($C_{2''}$), 115.71 (C_5), 115.20 ($C_{6''/3''}$), 115.14 ($C_{6''/3''}$), 111.59 (C_{4a}), 101.61 (C_8), 74.59 (C_2), 72.00 (C_{Bn}), 56.11 ($C_{1''''}$), 46.60 ($C_{1'}$), 40.36 ($C_{4'}$), 34.70 ($C_{5'}$), 30.83 (C_3), 23.72 ($C_{1'''}$), 21.18 (C_4).

6-Benzyloxy-3,4-dihydro-2-methyl-2-((S)-4'-(9'-hydroxyphenylmethyl)-4'-methoxycarbonyl)amino carbonylmethyl)-7-methoxy-1-(2H)-benzopyran, 8

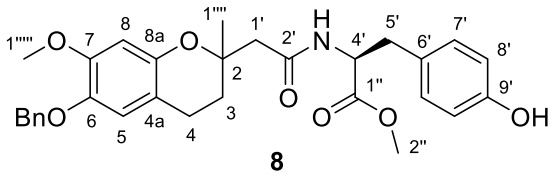

8

Following the above procedure, 404 mg (1.18 mmol) of acid **6**, 304 mg (1.58 mmol) of EDC·HCl, 208 mg (1.54 mmol) of HOBt, 2.3 mL (13.2 mmol) of DIPEA and 314 mg (1.36 mmol) of L-tyrosine methyl ester hydrochloride salt in CH_2Cl_2 (10 mL), afforded, after 20 hours, the desired amide **8** (311 mg, 51%).

HRMS for $C_{30}H_{34}NO_7$: calculated: 520.2335 ([M+H]$^+$); found: 520.2379. **^{1}H-NMR ($CDCl_3$, 400 MHz):** δ: (diastereomer A and diastereomer B) 7.49 – 7.27 (m, 5H^A_{Bn} + 5H^B_{Bn}), 7.01 (d, J = 8.53 Hz, 2$H^A_{7'}$), 6.83 – 6.69 (m, 1H^A_{NH} + 1H^A_{NH} + 2$H^B_{7'}$ + 2$H^A_{8'}$), 6.60 (s, 1H^A_5), 6.58 (s, 1H^B_5), 6.41 (d, J = 8.53 Hz, 2$H^B_{8'}$), 6.30 (s, 1H^A_8), 6.27 (s, 1H^B_8), 5.09 (m, 2H^A_{Bn} + 2H^B_{Bn}), 4.94 – 4.84 (m, 1$H^A_{4'}$ + 1$H^B_{4'}$), 3.78 (s, 3$H^A_{1''''}$), 3.76 (s, 3$H^B_{1''''}$), 3.75 (s, 3$H^A_{2''}$), 3.61 (s, 3$H^B_{2''}$), 3.13 – 3.01 (m, 2$H^A_{5'}$ + 1$H^B_{5'}$), 2.87 (dd, J = 14.2, 7.1 Hz, 1$H^B_{5'}$), 2.70 – 2.40 (m, 2H^A_4 + 2H^B_4 + 2$H^A_{1'}$ + 2$H^B_{1'}$), 1.93 – 1.82 (m, 1H^A_3), 1.82 – 1.72 (m, 1H^A_3), 1.72 – 1.48 (m, 2H^B_3), 1.30 (s, 3$H^A_{1'''}$), 1.29 (s, 3$H^B_{1'''}$). **^{13}C-NMR ($CDCl_3$, 100 MHz):** δ: 172.70 ($C_{1''}{}^A$), 172.48 ($C_{1''}{}^B$), 170.37($C_{2'}{}^A$ + $C_{2'}{}^B$), 155.48 ($C_{9'}{}^A$), 155.26 ($C_{9'}{}^B$), 149.91 ($C_{8a}{}^A$ + $C_{8a}{}^B$), 147.41 ($C_7{}^A$), 147.25 ($C_7{}^B$), 142.83 ($C_6{}^A$), 142.59 ($C_6{}^B$), 137.85 ($C_{Bn}{}^A$ + $C_{Bn}{}^B$), 130.78 ($C_{2''}{}^A$), 130.35 ($C_{2''}{}^B$), 128.88 ($C_{6'}{}^A$), 128.77 ($C_{6'}{}^B$), 128.23 (C_{Bn}), 128.07 (C_{Bn}), 128.00 (C_{Bn}), 127.85 (C_{Bn}), 127.74 (C_{Bn}), 127.65 (C_{Bn}), 116.04 ($C_5{}^A$), 115.91 ($C_5{}^B$), 115.73 ($C_{8'}{}^A$), 115.65 ($C_{8'}{}^B$), 111.80 ($C_{4a}{}^A$), 111.67 ($C_{4a}{}^B$), 101.97 ($C_8{}^A$ + $C_8{}^B$), 74.61 ($C_2{}^A$), 74.60 ($C_2{}^B$), 72.05 ($C_{Bn}{}^A$), 72.03 ($C_{Bn}{}^B$), 55.93 ($C_{1''''}{}^A$), 55.84 ($C_{1''''}{}^B$), 53.13 ($C_{4'}{}^A$), 52.80 ($C_{4'}{}^B$), 52.12 ($C_{2''}{}^A$), 51.98 ($C_{2''}{}^B$), 46.53 ($C_{1'}{}^A$), 46.03 ($C_{1'}{}^A$), 37.16 ($C_{5'}{}^A$), 36.85 ($C_{5'}{}^B$), 31.08 ($C_3{}^A$), 30.31 ($C_3{}^B$), 23.68 ($C_{1'''}{}^A$), 23.46 ($C_{1'''}{}^B$), 21.01 ($C_4{}^A$ + $C_4{}^B$).

6-Benzyloxy-3,4-dihydro-2-methyl-2-((S)-4'-methyl-4'-methoxycarbonyl]aminocarbonylethyl)-7-methoxy-1-(2H)-benzopyran, 9

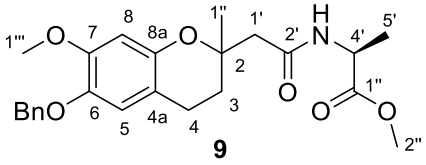

9

Following the above procedure, 389 mg (1.14 mmol) of acid **6**, 288 mg (1.50 mmol) of EDC·HCl, 204 mg (1.51 mmol) of HOBt, 2.2 mL (12.6 mmol) of DIPEA and 379 mg (1.38 mmol) of L-alanine methyl ester hydrogenchloride salt in CH_2Cl_2 (10 mL) afforded, after 20 hours, the desired amide **9** (319 mg, 66%).

HRMS for $C_{24}H_{30}NO_6$: calculated: 428.2073 ([M+H]$^+$); found: 428.2093. **^{1}H-NMR ($CDCl_3$, 400 MHz):** δ: (diastereomer A and diastereomer B) 7.47 – 7.41 (m, $2H^A_{Bn}$ + $2H^B_{Bn}$), 7.36 (dd, J = 10.0, 4.7 Hz, $2H^A_{Bn}$ + $2H^B_{Bn}$), 7.33 – 7.27 (m, $1H^A_{Bn}$ + $1H^B_{Bn}$), 6.89 (d, J = 7.0 Hz, $1H^A_{NH}$ + $1H^B_{NH}$), 6.61 (s, $1H^A_5$ + $1H^B_5$), 6.50 (s, $1H^A_8$), 6.49 (s, $1H^B_8$), 5.05 (s, $2H^A_{Bn}$ + $2H^B_{Bn}$), 4.59 (qd, J = 7.1, 2.8 Hz, $1H^A_{4'}$ + $1H^B_{4'}$), 3.85 (s, $3H^A_{1''''}$), 3.84 (s, $3H^B_{1''''}$), 3.76 (s, $3H^A_{2''}$), 3.68 (s, $3H^B_{2''}$), 2.73 – 2.57 (m, $2H^A_{1'}$ + $2H^A_4$ + $2H^B_4$), 2.45 (d, J = 2.3 Hz, $1H^B_{1'}$), 2.41 (d, J = 2.1 Hz, $1H^B_{1'}$), 1.97 – 1.76 (m, $2H^A_3$ + $2H^B_3$), 1.44 (d, J = 7.1 Hz, $3H^A_{5'}$), 1.39 (s, $3H^A_{1'''}$ + $3H^B_{1'''}$), 1.38 (d, J = 5.2 Hz, $3H^B_{5'}$). **^{13}C-NMR ($CDCl_3$, 100 MHz):** δ: 173.42 ($C_{1''}{}^A$), 173.28 ($C_{1''}{}^B$), 169.57 ($C_{2'}{}^A$), 169.43 ($C_{2'}{}^B$), 149.54 ($C_{8a}{}^A$ + $C_{8a}{}^B$), 146.88 ($C_7{}^A$), 146.84 ($C_7{}^B$), 142.45 ($C_6{}^A$ + $C_6{}^B$), 137.50 ($C_{Bn}{}^A$ + $C_{Bn}{}^B$), 128.42 ($C_{Bn}{}^A$), 128.40 ($C_{Bn}{}^B$), 127.70 ($C_{Bn}{}^A$ + $C_{Bn}{}^B$), 127.37 ($C_{Bn}{}^A$), 127.36 ($C_{Bn}{}^B$), 115.72 ($C_5{}^A$ + $C_5{}^B$), 111.42 ($C_{4a}{}^A$ + $C_{4a}{}^B$), 101.64 ($C_8{}^A$), 101.56 ($C_8{}^B$), 74.69 ($C_2{}^A$), 74.64 ($C_2{}^B$), 72.07 ($C_{Bn}{}^A$ + $C_{Bn}{}^B$), 55.93 ($C_{1''''}{}^A$), 55.92 ($C_{1''''}{}^B$), 52.33 ($C_{2''}{}^A$), 52.28 ($C_{2''}{}^B$), 48.04 ($C_{4'}{}^A$), 47.93 ($C_{4'}{}^B$), 46.27 ($C_{1'}{}^A$), 45.96 ($C_{1'}{}^B$), 31.77 ($C_3{}^A$), 31.52 ($C_3{}^B$), 24.09 ($C_{1'''}{}^A$), 23.77 ($C_{1'''}{}^B$), 21.38 ($C_4{}^A$), 21.36 ($C_4{}^B$), 18.52 ($C_{5'}{}^A$), 18.49 ($C_{5'}{}^B$).

6-Benzyloxy-3,4-dihydro-2-methyl-2((S)-4'-isopropyl-4'-methoxycarbonyl)aminocarbonylethyl-7-methoxy-1-(2H)-benzopyran, 10

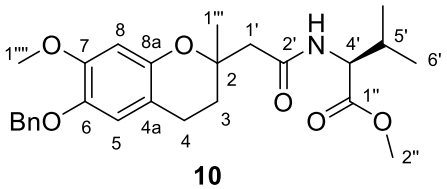

10

Following the above procedure, 389 mg (1.14 mmol) of acid **6**, 283 mg (1.48 mmol) of EDC·HCl, 201 mg (1.49 mmol) of HOBt, 2.2 mL (12.6 mmol) of DIPEA and 228 mg (1.36 mmol) of L-valine methyl ester hydrochloride in CH_2Cl_2 (10 mL) afforded, after 20 hours, the desired amide **10** (140 mg, 27%).

HRMS for $C_{26}H_{34}NO_6$: calculated: 456.2386 ([M+H]$^+$); found: 456.2405. **^{1}H-NMR ($CDCl_3$, 400 MHz):** δ: (diastereomer A and diastereomer B) 7.46 – 7.41 (m, $2H^A_{Bn}$ + $2H^B_{Bn}$), 7.36 (tt, J = 8.0, 1.7 Hz, $2H^A_{Bn}$ + $2H^B_{Bn}$), 7.33 – 7.27 (m, $1H^A_{Bn}$ + $1H^B_{Bn}$), 6.87 (d, J = 8.6 Hz, $1H^A_{NH}$), 6.81 (d, J = 8.7 Hz, $1H^B_{NH}$), 6.61 (s, $1H^A_5$ + $1H^B_5$), 6.47 (s, $1H^A_8$), 6.45 (s, $1H^B_8$), 5.06 (s, $2H^A_{Bn}$ + $2H^B_{Bn}$), 4.57 (q, J = 4.4 Hz, $1H^A_{4'}$ + $1H^B_{4'}$), 3.83 (s, $3H^A_{1''''}$), 3.82 (s, $3H^B_{1''''}$), 3.75 (s, $3H^A_{2''}$), 3.65 (s, $3H^B_{2''}$), 2.75 – 2.58 (m, $2H^A_{1'}$ + $2H^A_4$ + $2H^B_4$), 2.49 (d, J = 2.3 Hz, $1H^B_{1'}$), 2.45 (d, J = 2.1 Hz, $1H^B_{1'}$), 2.28 – 2.12 (m, $1H^A_{5'}$ + $1H^B_{5'}$), 1.97 – 1.76 (m, $2H^A_3$ + $2H^B_3$), 1.40 (s, $3H^A_{1'''}$ + $3H^B_{1'''}$), 1.01 (s, $3H^A_{6''}$), 0.96 (d, J = 5.2 Hz, $3H^B_{6''}$), 0.90 (s, $3H^A_{6''}$), 0.88 (d, J = 5.2 Hz, $3H^B_{6''}$). **^{13}C-NMR ($CDCl_3$, 100 MHz):** δ: 172.86 ($C_{1''}{}^A$), 172.65 ($C_{1''}{}^B$), 170.51 ($C_{2'}{}^A$), 170.25 ($C_{2'}{}^B$), 149.87 ($C_{8a}{}^A$), 149.84 ($C_{8a}{}^B$), 147.14 ($C_7{}^A$), 147.13 ($C_7{}^B$), 142.73 ($C_6{}^A$), 142.71 ($C_6{}^B$), 137.73 ($C_{Bn}{}^A$), 137.72 ($C_{Bn}{}^B$), 128.62 ($C_{Bn}{}^A$ + $C_{Bn}{}^B$), 127.91 ($C_{Bn}{}^A$ + $C_{Bn}{}^B$), 127.59 ($C_{Bn}{}^A$), 127.57 ($C_{Bn}{}^B$), 115.90 ($C_5{}^A$), 115.88 ($C_5{}^B$), 111.52 ($C_{4a}{}^A$), 111.47 ($C_{4a}{}^B$), 101.57 ($C_8{}^A$), 101.51 ($C_8{}^B$), 74.66 ($C_2{}^A$), 74.61 ($C_2{}^B$), 71.93 ($C_{Bn}{}^A$), 71.91 ($C_{Bn}{}^B$), 56.79 ($C_{4'}{}^A$), 56.67 ($C_{4'}{}^B$), 55.62 ($C_{1''''}{}^A$), 55.61 ($C_{1''''}{}^B$), 51.73 ($C_{2''}{}^A$), 51.66 ($C_{2''}{}^B$), 46.15 ($C_{1'}{}^A$), 46.09 ($C_{1'}{}^B$), 31.31 ($C_3{}^A$), 31.28 ($C_3{}^B$), 30.75 ($C_{5'}{}^A$), 30.57 ($C_{5'}{}^B$), 23.45 ($C_{1'''}{}^A$), 23.27 ($C_{1'''}{}^B$), 20.90 ($C_4{}^A$ + $C_4{}^B$), 18.59 ($C_{6'}{}^A$), 18.49 ($C_{6'}{}^B$), 17.33 ($C_{6'}{}^A$), 17.17 ($C_{6'}{}^B$).

6-Benzyloxy-3,4-dihydro-2-methyl-2-[2'-((S)-4'-benzyloxycarbonyl)pyrrolidinyl]carbonylethyl-7-methoxy-1-(2H)-benzopyran, 11

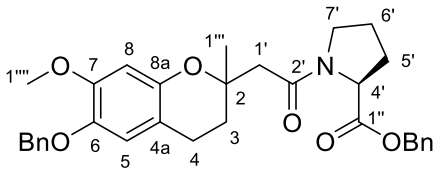

11

Following the above procedure, 400 mg (1.17 mmol) of acid **6**, 314 mg (1.64 mmol) of EDC·HCl, 213 mg (1.58 mmol) of HOBt, 2.2 mL (12.6 mmol) of DIPEA and 379 mg (1.38 mmol) of L-proline benzyl ester hydrogenchloride salt in CH_2Cl_2 (10 mL) afforded, after 20 hours, the desired amide **11** (215 mg, 41%).

HRMS for $C_{32}H_{36}NO_6$: calculated: 530.2543 ([M+H]$^+$); found: 530.2545. **^{1}H-NMR ($CDCl_3$, 400 MHz):** δ: (diastereomer A and diastereomer B) 7.47 – 7.40 (m, 2H$^A_{Bn}$), 7.39 – 7.27 (m, 3H$^A_{Bn}$ + 5H$^B_{Bn}$), 6.60 (s, 1H$^A_5$), 6.59 (s, 1H$^B_5$), 6.35 (s, 1H$^A_8$), 6.35 (s, 1H$^B_8$), 5.26 – 5.00 (m, 2H$^A_{Bn}$ + 2H$^B_{Bn}$), 4.55 (td, J = 8.3, 4.0 Hz, 1H$^A_{4'}$ + 1H$^B_{4'}$), 3.81 (s, 3H$^A_{1''''}$), 3.80 (s, 3H$^A_{1''''}$), 3.72 – 3.46 (m, 2H$^A_{7'}$ + 2H$^B_{7'}$), 2.73 – 2.53 (m, 2H$^A_4$ + 2H$^B_4$ + 2H$^A_{1'}$ + 2H$^B_{1'}$), 2.24 – 1.82 (m, 2H$^A_{5'}$ + 2H$^B_{5'}$ + 2H$^A_{6'}$ + 2H$^B_{6'}$ + 2H$^A_3$ + 2H$^B_3$), 1.46 (s, 3H$^A_{1'''}$), 1.43 (s, 3H$^B_{1'''}$). **^{13}C -NMR ($CDCl_3$, 100 MHz):** δ: 172.65 (C$_{1''}^A$), 172.62 (C$_{1''}^B$), 169.41 (C$_{2'}^A$), 169.36 (C$_{2'}^B$), 149.83 (C$_{8a}^A$), 149.80 (C$_{8a}^B$), 148.10 (C$_7^A$), 148.05 (C$_7^B$), 142.40 (C$_6^A$), 142.38 (C$_6^B$), 137.97 (C$_{Bn}$), 136.08 (C$_{Bn}$), 129.01 (C$_{Bn}$), 128.92 (C$_{Bn}$), 128.82 (C$_{Bn}$), 128.81 (C$_{Bn}$), 128.73 (C$_{Bn}$), 128.72 (C$_{Bn}$), 128.57 (C$_{Bn}$), 128.50 (C$_{Bn}$), 128.49 (C$_{Bn}$), 128.43 (C$_{Bn}$), 128.38 (C$_{Bn}$), 127.99 (C$_{Bn}$), 127.98 (C$_{Bn}$), 127.72 (C$_{Bn}$), 127.70 (C$_{Bn}$), 127.68 (C$_{Bn}$), 116.13 (C$_5^A$), 116.10 (C$_5^B$), 112.09 (C$_{4a}^A$), 112.05 (C$_{4a}^B$), 101.71 (C$_8^A$), 101.66 (C$_8^B$), 75.96 (C$_2^A$), 75.86 (C$_2^B$), 72.11 (C$_{Bn}^A$ + C$_{Bn}^B$), 66.69 (C$_{Bn}^A$), 66.67 (C$_{Bn}^B$), 58.74 (C$_{4'}^A$), 58.73 (C$_{4'}^B$), 55.79 (C$_{1''''}^A$), 47.67 (C$_{1''''}^B$), 47.52 (C$_{1'''}^A$), 42.86 (C$_{7'}^A$), 42.77 (C$_{7'}^B$), 30.60 (C$_{1'}^A$), 28.91 (C$_{1'}^B$), 24.59 (C$_{6'}^A$), 24.55 (C$_{6'}^B$), 24.47 (C$_{1'''}^A$), 24.44 (C$_{1'''}^B$), 21.27 (C$_4^A$), 21.21 (C$_4^B$).

6-Benzyloxy-3,4-dihydro-2-((S)-4'-benzyl-4'-benzyloxycarbonyl)aminocarbonylethyl-2-methyl-7-methoxy-1-(2H)-benzopyran, 12

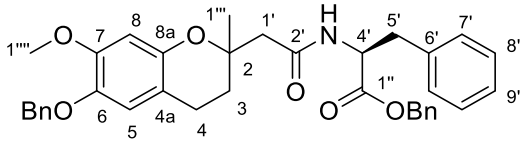

12

Following the above procedure, 408 mg (1.19 mmol) of acid **6**, 295 mg (1.54 mmol) of EDC·HCl, 206 mg (1.53 mmol) of HOBt, 2.2 mL (12.6 mmol) of DIPEA and 407 mg (1.38 mmol) of L-phenylalanine benzyl ester hydrochloride in CH_2Cl_2 (10 mL) afforded, after 20 hours, the desired amide **12** (430 mg, 62%).

HRMS for $C_{36}H_{38}NO_6$: calculated: 580.2699 ([M+H]$^+$); found: 580.2700. **^{1}H-NMR ($CDCl_3$, 400 MHz):** δ: (diastereomer A and diastereomer B) 7.49 – 7.42 (m, 2H$^A_{Bn}$ + 2H$^B_{Bn}$), 7.40 – 7.27 (m, 7H$^A_{Bn}$ + 7H$^B_{Bn}$), 7.25 – 7.18 (m, 1H$^A_{Bn}$ + 1H$^B_{Bn}$ + 2H$^A_{8'}$ + 1H$^A_{9'}$), 7.12 – 7.07 (m, 2H$^B_{8'}$ + 1H$^B_{9'}$), 7.03 (dd, J = 11.0, 4.2 Hz, 2H$^A_{7'}$), 6.91 (d, J = 7.8 Hz, 2H$^B_{7'}$), 6.82 (d, J = 7.9 Hz, 1H$^A_{NH}$), 6.78 (d, J = 7.5 Hz, 1H$^B_{NH}$), 6.59 (s, 1H$^A_5$), 6.57 (s, 1H$^B_5$), 6.28 (s, 1H$^A_8$), 6.26 (s, 1H$^B_8$), 5.22 – 5.12 (m, 2H$^A_{Bn}$), 5.11 – 5.03 (m, 2H$^A_{Bn}$ + 4H$^B_{Bn}$), 4.98 (dq, J = 13.5, 6.1 Hz, 1H$^A_{4'}$ + 1H$^B_{4'}$), 3.77 (s, 3H$^A_{1''''}$), 3.76 (s, 3H$^B_{1''''}$), 3.18 – 3.11 (m, 2H$^A_{5'}$ + 1H$^B_{5'}$), 3.01 (dd, 1H$^B_{5'}$), 2.67 – 2.41 (m, 2H$^A_{1'}$ + 2H$^B_{1'}$ + 2H$^A_4$ + 2H$^B_4$), 1.88 (dt, J = 13.8, 6.8 Hz, 1H$^A_3$), 1.75 (dt, J = 18.7, 6.0 Hz, 1H$^A_3$), 1.71 – 1.60 (m, 2H$^B_3$), 1.30 (s, 3H$^A_{1'''}$), 1.30 (s, 3H$^B_{1'''}$). **^{13}C-NMR ($CDCl_3$, 100 MHz):** δ: 171.96 (C$_{1''}^A$), 171.82 (C$_{1''}^B$), 170.13 (C$_{2'}^A$ + C$_{2'}^B$), 149.92 (C$_{8a}^A$), 149.87 (C$_{8a}^B$), 147.29 (C$_7^A$), 147.22 (C$_7^B$), 142.80 (C$_6^A$), 142.72 (C$_6^B$), 137.91 (C$_{Bn}$), 137.88 (C$_{Bn}$), 136.19 (C$_{Bn}$), 136.02 (C$_{Bn}$), 135.47 (C$_{6'}^A$), 135.42 (C$_{6'}^B$), 129.68 (C$_{7'}^A$), 129.40 (C$_{7'}^B$), 128.86 (C$_{8'}^A$), 128.82 (C$_{8'}^B$), 128.81 (C$_{Bn}$), 128.80 (C$_{Bn}$), 128.75 (C$_{Bn}$), 128.74 (C$_{Bn}$), 128.73 (C$_{Bn}$), 128.71 (C$_{Bn}$), 128.65 (C$_{Bn}$), 128.03 (C$_{Bn}$), 128.00 (C$_{Bn}$), 127.66 (C$_{Bn}$), 127.65 (C$_{Bn}$), 127.27 (C$_{9'}^A$), 127.08 (C$_{9'}^B$),

115.95 (C_5^A), 115.83 (C_5^B), 111.57 (C_{4a}^A + C_{4a}^B), 101.77 (C_8^A + C_8^B), 74.58 (C_2^A), 74.55 (C_2^B), 72.00 (C_{Bn}), 71.98 (C_{Bn}), 67.07 (C_{Bn}), 66.98 (C_{Bn}), 55.79 ($C_{1''''}^A$), 55.79 ($C_{1''''}^B$), 52.99 ($C_{4'}^A$), 52.76 ($C_{4'}^B$), 46.62 ($C_{1'}^A$), 45.91 ($C_{1'}^B$), 37.74 ($C_{5'}^A$), 37.68 ($C_{5'}^B$), 31.10 (C_3^A), 30.65 (C_3^B), 23.68 ($C_{1''}^A$), 23.22 ($C_{1''}^B$), 20.99 (C_4^A), 20.90 (C_4^B).

6-Benzyloxy-3,4-dihydro-2-methyl-2-((S)-4'-indolylmethyl-4'-methoxycarbonyl)aminocarbonylmethyl-7-methoxy-1-(2H)-benzopyran, 13

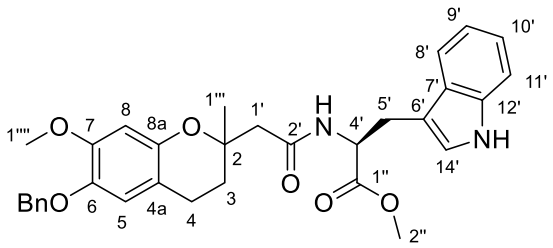

13

Following the above procedure, 401 mg (1.17 mmol) of acid **6**, 288 mg (1.50 mmol) of EDC·HCl, 232 mg (1.71 mmol) of HOBt, 2.2 mL (12.6 mmol) of DIPEA and 301 mg (1.30 mmol) of L-tryptophan methyl ester hydrochloride in CH_2Cl_2 (10 mL) afforded, after 20 hours, the desired amide **13** (486 mg, 80%).

HRMS for $C_{32}H_{35}N_2O_6$: calculated: 543.2495 ([M+H]$^+$); found: 543.2520. **^{1}H-NMR ($CDCl_3$, 400 MHz):** δ: (diastereomer A and diastereomer B) 8.38 (d, J = 12.0 Hz, $1H^A_{NH}$), 7.83 (d, J = 11.6 Hz, $1H^B_{NH}$), 7.55 (t, J = 6.7 Hz, $1H^A_{8'}$), 7.52 – 7.46 (m, $1H^B_{8'}$ + $2H_{Bn}$), 7.42 (dq, J = 2.7, 1.6 Hz, $3H_{Bn}$), 7.40 – 7.35 (m, $3H_{Bn}$), 7.35 – 7.27 (m, $2H_{Bn}$ + $1H^A_{9'}$ +), 7.20 – 7.08 (m, $1H^B_{9'}$ + $1H^A_{10'}$ + $1H^A_{11'}$ + $1H^B_{11'}$), 7.08 – 7.01 (m, $1H^B_{10'}$), 7.00 (d, J = 2.2 Hz, $1H^A_{13}$), 6.91 (d, J = 7.5 Hz, $1H^A_{NH}$), 6.86 (d, J = 7.8 Hz, $1H^B_{NH}$), 6.67 – 6.63 (m, $1H^B_{13}$), 6.58 (s, $1H^A_5$ + $1H^B_5$), 6.23 (s, $1H^A_8$), 6.10 (s, $1H^B_8$), 5.11 (c, J = 12.3 Hz, $2H^A_{Bn}$), 5.04 (s, $2H^B_{Bn}$), 5.02 – 4.93 (m, $1H^A_{4'}$ + $1H^B_{4'}$), 3.70 (s, $3H^A_{1''''}$), 3.65 (s, $3H^A_{1'''}$), 3.60 (s, $3H^B_{2''}$), 3.55 (s, $3H^B_{2''}$), 3.37 – 3.18 (m, $2H^A_{5'}$ + $2H^B_{5'}$), 2.64 – 2.34 (m, $2H^A_{1'}$ + $2H^B_{1'}$ + $2H^A_4$ + $2H^B_4$), 1.91 (dt, J = 13.8, 6.9 Hz, $1H^A_3$), 1.81 – 1.71 (m, $1H^A_3$), 1.59 (ddt, J = 21.7, 14.1, 7.1 Hz, $2H^B_3$), 1.32 (s, $3H^A_{1'''}$), 1.31 (s, $3H^B_{1'''}$). **^{13}C-NMR ($CDCl_3$, 100 MHz):** δ: 172.42 ($C_{1''}^A$ + $C_{1''}^B$), 169.71 ($C_{2'}^A$), 169.65 ($C_{2'}^B$), 149.32 (C_{8a}^A), 149.29 (C_{8a}^B), 146.81 (C_7^A + C_7^B), 142.21 (C_6^A), 142.01 (C_6^B), 137.46 (C_{Bn}), 137.39 (C_{Bn}), 136.05 ($C_{12'}^A$), 135.93 ($C_{12'}^B$), 128.49(C_{Bn}), 128.37 (C_{Bn}), 127.83 (C_{Bn}), 127.69 (C_{Bn}), 127.44 ($C_{7'}^A$ + $C_{7'}^B$), 127.34 (C_{Bn}), 122.89 ($C_{14'}^A$), 122.76 ($C_{14'}^B$), 122.05 ($C_{10'}^A$), 121.95 ($C_{10'}^B$), 119.45 ($C_{9'}^A$), 119.34 ($C_{9'}^B$), 118.52 ($C_{8'}^A$), 118.38 ($C_{8'}^B$), 115.58 ($C_{5'}^A$ + $C_{5'}^B$), 111.54 (C_{4a}^A), 111.36 (C_{4a}^B), 111.13 ($C_{11'}^A$), 111.07 ($C_{11'}^B$), 109.75 ($C_{6'}^A$), 109.48 ($C_{6'}^A$), 101.73 (C_8^A), 101.53 (C_8^B), 74.60 (C_2^A), 74.60 (C_2^B), 71.95 (C_{Bn}), 71.80 (C_{Bn}), 55.87 ($C_{1''''}^A$), 55.75 ($C_{1''''}^A$), 52.61 ($C_{4'}^A$), 52.28 ($C_{4'}^B$), 52.21 ($C_{2''}^A$), 52.09 ($C_{2''}^B$), 46.46 ($C_{1'}^A$), 46.06 ($C_{1'}^B$), 31.05 (C_3^A), 30.69 (C_3^B), 27.72 ($C_{5'}^A$), 27.60 ($C_{5'}^B$), 24.14 ($C_{1''}^A$), 23.69 ($C_{1''}^B$), 21.27 (C_4^A), 21.20 (C_4^B).

6-Benzyloxy-3,4-dihydro-2-methyl-2-((S)-4'-aminocarbonylpropyl-4'-methoxycarbonyl)aminocarbonyl ethyl-7-methoxy-1-(2H)-benzopyran, 14

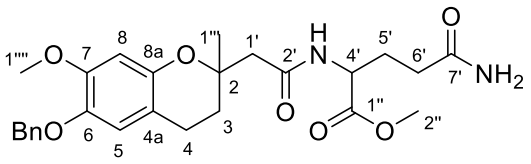

14

To a solution of acid **6** (250 mg, 0.73 mmol) in anhydrous CH_2Cl_2 (10 mL), DCC (196 mg, 0.95 mmol) and DMAP (161 mg, 1.32 mmol) were added, under N_2 atmosphere. The reaction mixture was stirred for 30 minutes. Then, the L-glutamine methyl ester hydrochloride (128 mg, 0.65 mmol) was added and the mixture was stirred for 48 hours at room temperature (HPLC-UV monitoring). Then, the mixture was filtered through Celite® and the solvent was removed under vacuum. The resulting residue was purified by chromatography in reverse phase (gradient, from 9:1 H_2O:CH_3CN to CH_3CN) to give amide **14** (140 mg, 40%).

HRMS for $C_{26}H_{33}N_2O_7$: calculated: 485.2288 ($[M+H]^+$); found: 485.2295. **^{1}H-NMR ($CDCl_3$, 400 MHz):** δ: (diastereomer A and diastereomer B) 7.42 (d, J = 7.2 Hz, $2H_{Bn}$), 7.35 (t, J = 7.6 Hz, $2H_{Bn}$), 7.29 (dd, J = 10.2, 3.7 Hz, $1H_{Bn}$), 7.18 (d, J = 7.6 Hz, $1H^A_{NH}$ + $1H^B_{NH}$), 6.59 (s, $1H^A_5$ + $1H^B_5$), 6.52 (s, $1H^A_8$), 6.48 (d, J = 2.3 Hz, $1H^B_8$), 6.36 ($s_{exch.}$, $1H_{NH}$), 6.09 ($s_{exch.}$, $1H_{NH}$), 5.77 ($s_{exch.}$, $1H_{NH}$), 5.65 ($s_{exch.}$, $1H_{NH}$), 5.02 (s, $2H_{Bn}$), 4.58 (tdd, J = 15.1, 9.8, 5.4 Hz, $1H^A_{4'}$ + $1H^B_{4'}$), 3.82 (s, $3H^A_{1'''}$ + $3H^B_{1'''}$), 3.74 (s, $3H^A_{2''}$), 3.63 (s, $3H^B_{2''}$), 2.71 – 2.54 (m, $2H^A_4$ + $2H^B_4$ + $1H^A_{1'}$ + $1H^B_{1'}$), 2.46 (dd, J = 14.5, 3.9 Hz, $1H^A_{1'}$ + $1H^B_{1'}$), 2.33 (q, J = 6.4 Hz, $2H^A_{6'}$), 2.24 – 2.13 (m, $2H^A_{5'}$ + $2H^B_{5'}$ + $2H^B_{6'}$), 2.05 – 1.74 (m, $2H^A_3$ + $2H^B_3$), 1.38 (s, $3H^A_{1'''}$), 1.35 (s, $3H^B_{1'''}$). **^{13}C-NMR ($CDCl_3$, 100 MHz):** δ: (diastereomer A and diastereomer B) 174.55 ($C_{1''}{}^A$), 174.43 ($C_{1''}{}^B$), 172.37 ($C_{7'}{}^A$), 172.18 ($C_{7'}{}^B$), 170.47 ($C_{2'}{}^A$), 170.43 ($C_{2'}{}^B$), 149.65 ($C_{8a}{}^A$), 149.61 ($C_{8a}{}^B$), 147.05 ($C_7{}^A$), 147.02 ($C_7{}^B$), 142.44 ($C_6{}^A$ + $C_6{}^B$), 137.55 ($C_{Bn}{}^A$), 137.53 ($C_{Bn}{}^B$), 128.52 ($C_{Bn}{}^A$), 128.51 ($C_{Bn}{}^B$), 127.85 ($C_{Bn}{}^A$), 127.82 ($C_{Bn}{}^B$), 127.51 ($C_{Bn}{}^A$ + $C_{Bn}{}^B$), 115.81 ($C_5{}^A$ + $C_5{}^B$), 111.48 ($C_{4a}{}^A$), 111.42 ($C_{4a}{}^B$), 101.79 ($C_8{}^A$), 101.78 ($C_8{}^B$), 74.77 ($C_2{}^A$), 74.74 ($C_2{}^B$), 72.15 ($C_{Bn}{}^A$ + $C_{Bn}{}^B$), 56.06 ($C_{1''''}{}^A$), 56.04 ($C_{1''''}{}^B$), 52.54 ($C_{2''}{}^A$), 52.46 ($C_{2''}{}^B$), 51.88 ($C_{4'}{}^A$), 51.77 ($C_{4'}{}^B$), 46.66 ($C_{1'}{}^A$), 46.18 ($C_{1'}{}^B$), 31.92 ($C_{6'}{}^A$), 31.62 ($C_{3'}{}^A$ + $C_{3'}{}^B$), 31.46 ($C_{6'}{}^B$), 28.61 ($C_{5'}{}^A$), 28.43 ($C_{5'}{}^B$), 24.34 ($C_{1'''}{}^A$), 23.77 ($C_{1'''}{}^B$), 21.44 ($C_4{}^A$ + $C_4{}^B$).

2-Aminocarbonylethyl-6-benzyloxy-3,4-dihydro-2-methyl-7-methoxy-1-(2H)-benzopyran, 16

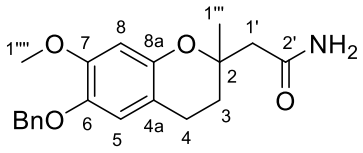

16

To a solution of acid **6** (100 mg, 0.29 mmol) in the minimum amount of anhydrous CH_2Cl_2 (0.6 mL), DIPEA (110 µL, 0.57 mmol) was added followed by EDC·HCl (59 mg, 0.31 mmol), under N_2 atmosphere, and the mixture was stirred for 30 minutes at room temperature. Then, a solution of 0.5 M NH_3 in dioxane (15.4 mL, 7.71 mmol) was added to the mixture at 0ºC and the mixture was stirred for 24 hours (HPLC-UV monitoring). Then, the solvent was removed, and the residue was diluted with CH_2Cl_2 and washed with a solution of 1 M HCl. The organic layer was dried with anhydrous $MgSO_4$ and the solvent was evaporated under vacuum. The residue was purified by chromatography on silica gel (gradient, from 9:1 hexane:EtOAc to EtOAc) to give product **16** (54 mg, 54%) as a brownish oil.

HRMS for $C_{20}H_{24}NO_4$: calculated: 342.1705 ($[M+H]^+$); found: 342.1699. **^{1}H-NMR ($CDCl_3$, 400 MHz):** δ: 7.45 – 7.40 (m, $2H_{Bn}$), 7.40 – 7.32 (m, $2H_{Bn}$), 7.32 – 7.27 (m, $1H_{Bn}$), 6.61 (s, $1H_5$), 6.37 (s, $1H_8$), 6.23 ($s_{exch.}$, $1H_{NH}$), 5.67 ($s_{exch.}$, $1H_{NH}$), 5.05 (s, $2H_{Bn}$), 3.82 (s, $3H_{1'''}$), 2.74 – 2.44 (m, $2H_4$ + $2H_{1'}$), 1.98 – 1.87 (m, $1H_3$), 1.81 (dt, J = 13.7, 6.2 Hz, $1H_3$), 1.38 (s, $3H_{1''}$). **^{13}C-NMR ($CDCl_3$, 100 MHz):** δ: 172.61 ($C_{2'}$), 149.54 (C_{8a}), 146.85 (C_7), 142.47 (C_6), 137.43 (C_{Bn}), 128.44 (C_{Bn}), 127.74 (C_{Bn}), 127.40 (C_{Bn}), 115.82 (C_5), 111.46 (C_{4a}), 101.40 (C_8), 74.53 (C_2), 72.09 (C_{Bn}), 55.97 ($C_{1'''}$), 46.62 ($C_{1'}$), 31.33 (C_3), 23.66 ($C_{1''}$), 21.36 (C_4).

3,4-Dihydro-6-hydroxy-2-[(S)-N-(4'',5''-dihidroxyphenylethyl)aminocarbonylmethyl]-2-methyl-7-methoxy-1-(2H)-benzopyran, A

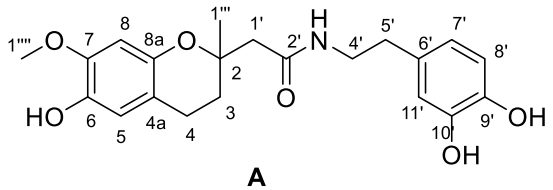

A

A solution of the amide **7** (134 mg, 0.28 mmol) in EtOH (2 mL), previously degassed with a N_2 flow, was added over a suspension of Pd/C (20 mg, 10% w/w) in EtOH (3 mL). The mixture was allowed to react under 1.2 atmospheres of H_2 for 6 hours and, then, filtered through Celite® (using ethanol as eluent). The solvent was evaporated under vacuum to give derivative **A** (107 mg, 98%).

m.p.: 73.4 – 74.5 ºC. **HRMS for $C_{21}H_{26}NO_6$:** calculated: 388.1760 ($[M+H]^+$); found: 388.1768. **^{1}H-NMR (CD_3OD, 400 MHz):** δ: 6.68 – 6.64 (m, $1H_{6'}$ + $1H_{3'}$), 6.54 (dd, J = 8.0, 1.9 Hz, $1H_{2'}$), 6.50 (s, $1H_5$), 6.28 (s, $1H_8$), 3.77 (s, $3H_{1''''}$), 3.41 (q, J = 6.8 Hz, $2H_{1'}$), 2.69 – 2.60 (m, $2H_4$ + $2H_{5'}$), 2.46 (s, $2H_{4'}$), 1.84 (dd, J = 13.7, 6.8 Hz, $1H_3$), 1.75 (dd, J = 13.4, 6.6 Hz, $1H_3$), 1.31 (s, $3H_{1'''}$). **^{13}C-NMR (CD_3OD, 100 MHz):** δ: 173.26 ($C_{2'}$), 148.93 (C_{8a}), 147.86 (C_7), 146.87 ($C_{9'/10'}$), 145.35 ($C_{9'/10'}$), 141.57 (C_6), 132.36 ($C_{6'}$), 121.50 ($C_{7'}$), 117.17 (C_5), 116.72 ($C_{8'/11'}$), 116.46 ($C_{8'/11'}$), 113.80 (C_{4a}), 102.50 (C_8), 75.71 (C_2), 56.41 ($C_{1''''}$), 47.02 ($C_{1'}$), 41.89 ($C_{4'}$), 35.73 ($C_{5'}$), 32.21 (C_3), 24.39 ($C_{1'''}$), 22.16 (C_4).

3,4-Dihydro-6-hydroxy-2-[[(S)-4'-hydroxycarbonyl-4'-(9'-hydroxyphenylmethyl)]aminocarbonylmethyl]-2-methyl-7-methoxy-1-(2H)-benzopyran, B

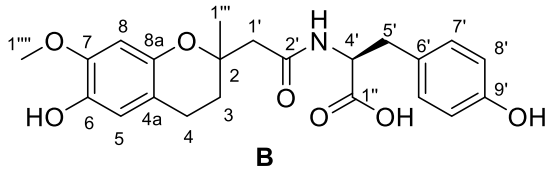

B

To a solution of ester protected amide **8** (145 mg, 0.28 mmol) in dioxane (2 mL), 4 M NaOH (2 mL, 8.0) was added and the mixture was stirred at room temperature for 6 hours. Then, the mixture was acidified with 1 M HCl and the residue was extracted with CH_2Cl_2 to obtain the free acid (87 mg, 61%).

Following the same procedure as **A**, 87 mg (0.17 mmol) of the above acid and 11 mg of 10% w/w Pd/C in EtOH (4 mL) afforded, after 6 hours, the derivative **B** (70 mg, 99%).

m.p.: 78.1 – 79.8 ºC. **HRMS for $C_{22}H_{26}NO_7$:** calculated: 416.1709 ($[M+H]^+$); found: 416.1730. **^{1}H-NMR (CD_3OD, 400 MHz):** (diastereomer A and diastereomer B) 7.10 – 7.05 (m, $1H^A_{8'}$ + $1H^B_{8'}$), 6.97 – 6.92 (m, $1H^A_{8'}$ + $1H^B_{8'}$), 6.72 – 6.66 (m, $1H^A_{7'}$ + $1H^B_{7'}$), 6.61 – 6.57 (m, $1H^A_{7'}$ + $1H^B_{7'}$), 6.50 (s, $1H^A_5$), 6.48 (s, $1H^B_5$), 6.32 (s, $1H^A_8$), 6.24 (s, $1H^B_8$), 4.68 (dt, J = 8.1, 4.9 Hz, $1H^A_{4'}$ + $1H^B_{4'}$), 3.74 (s, $3H^A_{1''''}$), 3.73 (s, $3H^B_{1''''}$), 3.12 (dt, J = 14.0, 4.4 Hz, $2H^A_{5'}$), 2.93 (dd, J = 43.1, 8.2 Hz, $1H^B_{5'}$), 2.89 (dd, J = 43.1, 8.1 Hz, $1H^B_{5'}$), 2.69 – 2.39 (m, $2H^A_{1'}$ + $2H^B_{1'}$ + $2H^A_4$ + $2H^B_4$), 1.84 (dt, J = 13.5, 6.8 Hz, $1H^A_3$), 1.66 (dddd, J = 24.1, 20.0, 13.5, 6.5 Hz, $1H^A_3$ + $2H^B_3$), 1.27 (s, $3H^A_{1'''}$), 1.23 (s, $3H^B_{1'''}$). **^{13}C-NMR (CD_3OD, 100 MHz):** (diastereomer A and diastereomer B) 174.66 ($C^A_{1''}$), 174.62 ($C^B_{1''}$), 172.41 ($C^A_{2'}$), 172.36 ($C^B_{2'}$), 157.43 ($C^A_{9'}$), 157.29 ($C^B_{9'}$), 148.36 (C^A_{8a} + C^B_{8a}), 147.10 (C^A_7+C^B_7), 141.12 (C^A_6+C^B_6), 131.45 ($C^A_{8'}$), 131.24 ($C^B_{8'}$), 128.76 ($C^A_{6'}$ + $C^B_{6'}$), 116.24 (C^A_5), 116.18 (C^B_5), 116.10 ($C^A_{7'}$), 116.03 ($C^B_{7'}$), 113.49 (C^A_{4a}), 113.43 (C^B_{4a}), 102.35 (C^A_8), 102.31 (C^B_8),

75.61 (C_2^A), 75.57 (C_2^B), 56.36 ($C_{1''''}^A$), 56.34 ($C_{1''''}^B$), 54.98 ($C_{4'}^A$), 54.91 ($C_{4'}^B$), 47.02 ($C_{1'}^A$), 46.40 ($C_{1'}^B$), 37.66 ($C_{5'}^A$), 37.58 ($C_{5'}^B$), 32.58 (C_3^A), 32.00 (C_3^B), 24.51 ($C_{1''}^A$), 24.25 ($C_{1''}^B$), 22.31 (C_4^A+C_4^B).

3,4-Dihydro-6-hydroxy-2-methyl-2-[[(S)-4'-hydroxycarbonyl-4'-methyl]aminocarbonylmethyl]-7-methoxy-1-(2H)-benzopyran, C

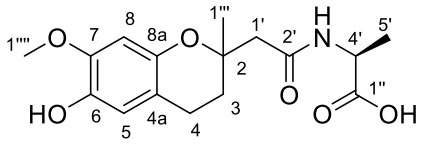

C

Following the same procedure as **B**, 133 mg (0.31 mmol) of amide **9** and 1 mL (4.0 mmol) of 4 M NaOH in dioxane (1 mL) afforded, after 15 hours, the desired acid (119 mg, 93%).

Following the same procedure as **A**, 119 mg (0.29 mmol) of the above acid and 12 mg of 10% w/w Pd/C in EtOH (5 mL) afforded, after 6 hours, the derivative **C** (84 mg, 90%).

m.p.: 61.7 – 63.4ºC. **HRMS for $C_{16}H_{22}NO_6$:** calculated: 324.1447 ($[M+H]^+$); found: 324.1458. **^{1}H-NMR ($CDCl_3$, 400 MHz):** δ: (diastereomer A and diastereomer B) 7.04 (d, J = 6.7 Hz, $1H^A_{NH}$), 6.99 (d, J = 7.0 Hz, $1H^B_{NH}$), 6.63 (s, $1H^A_5$), 6.62 (s, $1H^B_5$), 6.41 (s, $1H^A_8$ + $1H^B_8$), 4.59 (p, J = 7.1 Hz, $1H^A_{4'}$ + $1H^B_{4'}$), 3.83 (s, $3H^A_{1''''}$ + $3H^B_{1''''}$), 2.75 – 2.61 (m, $2H^A_{1'}$ + $2H^B_{1'}$ + $2H^A_4$), 2.48 (d, J = 2.7 Hz, $1H^B_4$), 2.45 (d, J = 3.0 Hz, $1H^B_4$), 1.87 (dtt, J = 20.2, 13.5, 6.6 Hz, $2H^A_3$ + $2H^B_3$), 1.51 (d, J = 7.1 Hz, $3H^A_{5'}$), 1.44 (d, J = 7.2 Hz, $3H^B_{5'}$), 1.39 (s, $3H^A_{1'''}$), 1.38 (s, $3H^B_{1'''}$). **^{13}C-NMR (CD_3Cl_3, 100 MHz):** δ: (diastereomer A and diastereomer B) 175.94 ($C_{1''}^A$), 175.88 ($C_{1''}^B$), 171.02 ($C_{2'}^A$), 170.86 ($C_{2'}^B$), 146.10 (C_{8a}^A + C_{8a}^B), 145.50 (C_7^A), 145.45 (C_7^B), 139.93 (C_6^A), 139.91 (C_6^B), 114.48 (C_5^A), 114.45 (C_5^B), 112.60 (C_{4a}^A + C_{4a}^B), 100.54 (C_8^A), 100.45 (C_8^B), 74.77 (C_2^A), 74.69 (C_2^B), 56.09 ($C_{1''''}^A$), 56.08 ($C_{1''''}^B$), 48.48 ($C_{4'}^A$), 48.40 ($C_{4'}^B$), 46.22 ($C_{1'}^A$), 45.87 ($C_{1'}^B$), 31.98 (C_3^A), 31.86 (C_3^B), 24.06 ($C_{1'''}^A$), 23.78 ($C_{1'''}^B$), 21.45 (C_4^A), 21.42 (C_4^B), 18.23 ($C_{5'}^A$), 18.15 ($C_{5'}^B$).

3,4-Dihydro-6-hydroxy-2[[(S)-4'-hydroxycarbonyl-4'-isopropyl]aminocarbonylmethyl]-2-methyl-7-methoxy-1-(2H)-benzopyran, D

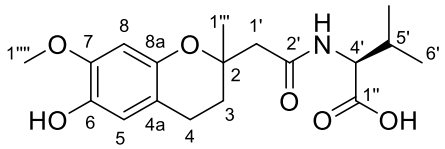

D

Following the same procedure as **B**, 71 mg (0.21 mmol) of amide **10** and 1 mL (4.0 mmol) of 4 M NaOH in dioxane (1 mL) afforded, after 6 hours, the desired acid (57 mg, 61%).

Following the same procedure as **A**, 57 mg (0.14 mmol) of the above acid and 12 mg of 10% w/w Pd/C in EtOH (3 mL) afforded, after 6 hours, the derivative **D** (34 mg, 69%).

m.p.: 63.5 – 65.3ºC. **HRMS for $C_{18}H_{26}NO_6$:** calculated: 352.1760 ($[M+H]^+$); found: 352.1763. **^{1}H-NMR ($CDCl_3$, 400 MHz):** δ: (diastereomer A and diastereomer B) 7.01 – 6.93 (m, $1H^A_{NH}$ + $1H^B_{NH}$), 6.64 (s, $1H^A_5$), 6.63 (s, $1H^B_5$), 6.40 (s, $1H^A_8$), 6.38 (s, $1H^B_8$), 4.57 (ddd, J = 8.3, 5.5, 4.6 Hz, $1H^A_{4'}$ + $1H^B_{4'}$), 3.81 (s, $3H^A_{1''''}$ + $3H^B_{1''''}$), 2.78 – 2.62 (m, $2H^A_{1'}$ + $2H^B_{1'}$ + $2H^A_4$), 2.52 (d, J = 5.1 Hz, $1H^B_4$), 2.48 (d, J = 5.2 Hz, $1H^B_4$), 2.36 – 2.19 (m,

$1H^{A}_{5'}$ + $1H^{B}_{5'}$), 1.97 – 1.75 (m, $2H^{A}_{3}$ + $2H^{B}_{3}$), 1.40 (d, J = 3.4 Hz, $3H^{A}_{1'''}$), 1.39 (s, $3H^{B}_{1'''}$), 1.07 (d, J = 6.9 Hz, $3H^{A}_{6'}$), 1.03 (d, J = 6.9 Hz, $3H^{B}_{6'}$), 0.95 (d, J = 6.9 Hz, $3H^{B}_{6'}$ + $3H^{B}_{6'}$). **^{13}C-NMR ($CDCl_3$, 100 MHz):** δ: (diastereomer A and diastereomer B) 175.08 ($C_{1''}^{A}$), 174.94 ($C_{1''}^{B}$), 170.77 ($C_{2'}^{A}$ + $C_{2'}^{B}$), 145.90 (C_{8a}^{A} + C_{8a}^{B}), 145.34 (C_{7}^{A}), 145.31 (C_{7}^{B}), 139.74 (C_{6}^{A}), 139.71 (C_{6}^{B}), 114.37 (C_{5}^{A}), 114.34 (C_{5}^{B}), 112.48 (C_{4a}^{A}), 112.42 (C_{4a}^{B}), 100.30 (C_{8}^{A} + C_{8}^{B}), 74.75 (C_{2}^{A}), 74.66 (C_{2}^{B}), 57.16 ($C_{4'}^{A}$), 57.05 ($C_{4'}^{B}$), 55.87 ($C_{1''''}^{A}$), 55.86 ($C_{1''''}^{B}$), 46.31 ($C_{1'}^{A}$), 46.23 ($C_{1'}^{B}$), 31.87 (C_{3}^{A}), 31.74 (C_{3}^{B}), 30.77 ($C_{5'}^{A}$), 30.62 ($C_{5'}^{B}$), 23.74 ($C_{1'''}^{A}$), 23.56 ($C_{1'''}^{B}$), 21.29 (C_{4}^{A} + C_{4}^{B}), 19.17 ($C_{6'}^{A}$), 19.06 ($C_{6'}^{A}$), 17.73 ($C_{6'}^{B}$), 17.57 ($C_{6'}^{B}$).

3,4-Dihydro-6-hydroxy-2-methyl-2-[2'-((S)-4'-hydroxycarbonyl)pyrrolidinyl]carbonylmethyl-7-metoxy-1-(2H)-benzopyran, E

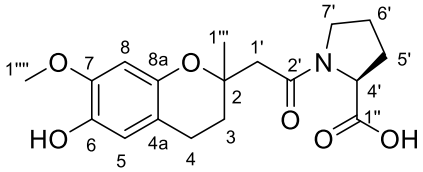

E

Following the same procedure as **A**, 72 mg (0.16 mmol) of amide **11** and 10 mg of 10% w/w Pd/C in EtOH (3 mL) afforded, after 6 hours, the derivative **E** (40 mg, 69%).

m.p.: 73.3 – 75.8ºC. **HRMS for $C_{18}H_{24}NO_6$:** calculated: 350.1604 ($[M+H]^+$); found: 350.1593. **^{1}H-NMR ($CDCl_3$, 400 MHz):** δ: (diastereomer A and diastereomer B) 6.62 (d, J = 1.4 Hz, $1H^{A}_{5}$ + $1H^{B}_{5}$), 6.29 (d, J = 2.0 Hz, $1H^{A}_{8}$ + $1H^{B}_{8}$), 4.67 – 4.61 (m, $1H^{A}_{4'}$ + $1H^{B}_{4'}$), 3.82 (s, $3H^{A}_{1''''}$ + $3H^{B}_{1''''}$), 3.60 (dt, J = 18.6, 9.0 Hz, $1H^{A}_{1'}$), 3.55 – 3.43 (m, $1H^{A}_{1'}$ + $2H^{B}_{1'}$), 2.80 – 2.57 (m, $2H^{A}_{7'}$ + $2H^{B}_{7'}$ + $2H^{A}_{4}$ + $2H^{A}_{4}$), 2.50 (dd, J = 22.1, 9.0 Hz, $2H^{A}_{5'}$), 2.11 – 1.83 (m, $2H^{A}_{6'}$ + $2H^{B}_{6'}$ + $2H^{B}_{5'}$ + $2H^{A}_{3}$ + $2H^{B}_{3}$), 1.48 (s, $3H^{A}_{1'''}$), 1.47 (s, $3H^{B}_{1'''}$). **^{13}C-NMR ($CDCl_3$, 100 MHz):** δ: (diastereomer A and diastereomer B) 172.77 ($C_{1''}^{A}$), 172.54 ($C_{1''}^{B}$), 172.13 ($C_{2'}^{A}$), 171.97 ($C_{2'}^{B}$), 146.23 (C_{8a}^{A}), 146.16 (C_{8a}^{B}) 146.02 (C_{7}^{A}), 145.98 (C_{7}^{B}), 139.60 (C_{6}^{A}), 139.58 (C_{6}^{B}), 114.38 (C_{5}^{A}), 114.25 (C_{5}^{B}), 112.66 (C_{4a}^{A}), 112.45 (C_{4a}^{B}), 100.49 (C_{8}^{A}), 100.46 (C_{8}^{B}), 75.69 (C_{2}^{A}), 75.67 (C_{2}^{B}), 60.21 ($C_{4'}^{A}$), 60.20 ($C_{4'}^{B}$), 56.13 ($C_{1''''}^{A}$), 56.12 ($C_{1''''}^{B}$), 48.90 ($C_{1'}^{A}$), 48.81 ($C_{1'}^{B}$), 43.69 ($C_{7'}^{A}$), 43.36 ($C_{7'}^{B}$), 31.82 (C_{3}^{A}), 31.52 (C_{3}^{B}), 27.51 ($C_{5'}^{A}$), 27.30 ($C_{5'}^{B}$), 25.05 ($C_{6'}^{A}$), 25.01 ($C_{6'}^{B}$), 24.96 ($C_{1'''}^{A}$), 24.78 ($C_{1'''}^{B}$), 21.61 (C_{4}^{A}), 21.57 (C_{4}^{B}).

3,4-Dihydro-6-hydroxy-2-((S)-4'-benzyl-4'-hydroxycarbonyl)aminocarbonylmetyl-2-methyl-7-methoxy-1-(2H)-benzopyran, F

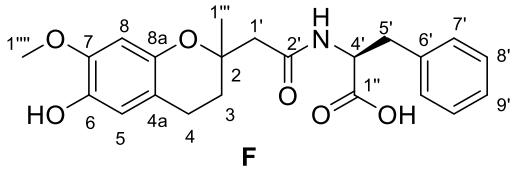

F

Following the same procedure as **A**, 214 mg (0.37 mmol) of amide **12** and 25 mg of 10% w/w Pd/C in EtOH (5 mL) afforded, after 6 hours at 2 atm of H_2, the derivative **F** (135 mg, 91%).

m.p.: 76.8 – 78.1ºC. **HRMS for $C_{22}H_{26}NO_6$:** calculated: 400.1760 ($[M+H]^+$); found: 400.1766. **^{1}H-NMR ($CDCl_3$, 400 MHz):** δ: (diastereomer A and diastereomer B) 7.32 – 7.20 (m, $2H^{A}_{7'}$ + $2H^{A}_{8'}$ + $1H^{A}_{9'}$), 7.13 (dt, J = 18.2, 6.9 Hz, $2H^{B}_{8'}$ + $1H^{B}_{9'}$), 7.03 (d, J = 6.8 Hz, $2H^{B}_{7'}$), 6.89 (t, J = 6.8 Hz, $1H^{A}_{NH}$ + $1H^{B}_{NH}$), 6.60 (s, $1H^{A}_{5}$), 6.58 (s, $1H^{B}_{5}$), 6.21 (s, $1H^{A}_{8}$), 6.14 (s, $1H^{B}_{8}$), 4.91 (dt, J = 16.8, 7.1 Hz, $1H^{A}_{4'}$ + $1H^{B}_{4'}$), 3.74 (s, $3H^{A}_{1'''}$), 3.73 (s, $3H^{B}_{1'''}$), 3.31 – 3.19 (m, $2H^{A}_{1'}$), 3.15 (dd, J = 14.2, 6.7 Hz, $1H^{B}_{1'}$), 3.01 (dd, J = 14.2, 7.3 Hz, $1H^{B}_{1'}$), 2.72 – 2.39 (m, $2H^{A}_{4}$ + $2H^{B}_{4}$ + $2H^{A}_{5'}$ + $2H^{B}_{5'}$), 1.85 (dt, J = 13.7, 6.7 Hz, $2H^{A}_{3}$), 1.80 – 1.71 (m, $1H^{A}_{3}$), 1.71 – 1.55 (m, $1H^{A}_{3}$),

1.28 (s, $3H^{A}_{1''}$), 1.25 (s, $3H^{B}_{1''}$). **^{13}C-NMR ($CDCl_3$, 100 MHz):** δ: (diastereomer A and diastereomer B) 174.74 ($C_{1''}^{A}$), 174.62 ($C_{1''}^{B}$), 171.04 ($C_{2'}^{A}$), 171.00 ($C_{2'}^{B}$), 146.00 (C_{8a}^{A}), 145.98 (C_{8a}^{B}), 145.51 (C_{7}^{A}), 145.44 (C_{7}^{B}), 139.89 (C_{6}^{A}), 139.84 (C_{6}^{B}), 135.91 ($C_{6'}^{A}$), 135.71 ($C_{6'}^{B}$), 129.56 ($C_{7'}^{A}$), 129.22 ($C_{7'}^{B}$), 128.82 ($C_{8'}^{A}$), 128.67 ($C_{8'}^{B}$), 127.35 ($C_{9'}^{A}$), 127.13 ($C_{9'}^{B}$), 114.41 (C_{5}^{A}), 114.35 (C_{5}^{B}), 112.59 (C_{4a}^{A}), 112.56 (C_{4a}^{B}), 100.59 (C_{8}^{A}), 100.56 (C_{8}^{B}), 74.69 (C_{2}^{A}), 74.61 (C_{2}^{B}), 56.12 ($C_{1''''}^{A}$), 56.08 ($C_{1''''}^{B}$), 53.50 ($C_{4'}^{A}$), 53.30 ($C_{4'}^{B}$), 46.81 ($C_{1'}^{A}$), 46.02 ($C_{1'}^{B}$), 37.57 ($C_{5'}^{A}$), 37.53 ($C_{5'}^{B}$), 31.73 (C_{3}^{A}), 31.02 (C_{3}^{B}), 23.98 ($C_{1'''}^{B}$), 23.58 ($C_{1'''}^{A}$), 21.44 (C_{4}^{A}), 21.40 (C_{4}^{B}).

3,4-Dihydro-6-hydroxy-2-methyl-2-((S)-4'-hydroxycarbonyl-4'-indolylmethyl)aminocarbonylmethyl-7-methoxy-1-(2H)-benzopyran, G

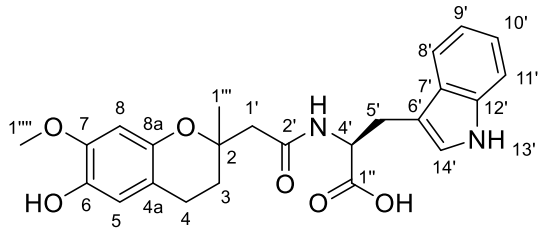

Following the same procedure as **B**, 279 mg (0.51 mmol) of amide **13** and 1 mL (4.0 mmol) of 4 M NaOH in dioxane (1 mL) afforded, after 15 hours, the desired acid (165 mg, 61%).

Following the same procedure as **A**, 128 mg (0.24 mmol) of the above acid and 15 mg of 10% w/w Pd/C in EtOH (5 mL) afforded, after 6 hours, the derivative **G** (101 mg, 96%).

m.p.: 87.5 – 88.9ºC. **HRMS for $C_{24}H_{27}N_2O_6$:** calculated: 439.1869 ($[M+H]^+$); found: 439.1864. **^{1}H-NMR (CD_3OD, 400 MHz):** δ: (diastereomer A and diastereomer B) 10.34 (s, $1H^{A}_{NH}$), 10.18 (s, $1H^{B}_{NH}$), 7.80 (d, J = 7.7 Hz, $1H^{A}_{NH}$ + $1H^{B}_{NH}$), 7.57 (t, J = 9.5 Hz, $1H^{A}_{8'}$), 7.50 (d, J = 7.9 Hz, $1H^{B}_{8'}$), 7.36 – 7.27 (m, $1H^{A}_{11'}$ + $1H^{B}_{11'}$), 7.14 (s, $1H^{A}_{14'}$), 7.07 (dt, J = 12.2, 7.5 Hz, $1H^{A}_{10'}$ + $1H^{B}_{10'}$), 6.98 (dt, J = 16.0, 7.4 Hz, $1H^{A}_{9'}$ + $1H^{B}_{9'}$ + $1H^{B}_{14'}$), 6.45 (d, J = 3.8 Hz, $1H^{A}_{5}$ + $1H^{B}_{5}$), 6.19 (s, $1H^{A}_{8}$), 6.10 (s, $1H^{B}_{8}$), 4.85 – 4.76 (m, $1H^{A}_{4'}$ + $1H^{B}_{4'}$), 3.62 (s, $3H^{A}_{1''''}$), 3.59 (s, $3H^{A}_{1''''}$), 3.41 – 3.36 (m, $1H^{A}_{5'}$), 3.35 (t, J = 4.0 Hz, $1H^{A}_{5'}$), 3.26 (dd, J = 14.9, 7.5 Hz, $1H^{B}_{5'}$), 3.17 (dd, J = 14.8, 7.8 Hz, $1H^{B}_{5'}$), 2.64 – 2.36 (m, $2H^{A}_{1'}$ + $2H^{A}_{1'}$ + $2H^{A}_{4}$ + $2H^{B}_{4}$), 1.82 (dt, J = 13.5, 6.6 Hz, $1H^{A}_{3}$), 1.73 – 1.51 (m, $1H^{A}_{3}$ + $2H^{B}_{3}$), 1.26 (s, $3H^{A}_{1'''}$), 1.19 (s, $3H^{B}_{1'''}$). **^{13}C-NMR (CD_3OD, 100 MHz):** δ: (diastereomer A and diastereomer B) 175.91 ($C_{1''}^{A}$), 175.86 ($C_{1''}^{B}$), 173.23 ($C_{2'}^{A}$ + $C_{2'}^{B}$), 148.91 (C_{8a}^{A}), 148.88 (C_{8a}^{B}), 147.61 (C_{7}^{A}), 147.52 (C_{7}^{B}), 141.66 (C_{6}^{A} + C_{6}^{B}), 138.61 ($C_{12'}^{A}$), 138.54 ($C_{12'}^{B}$), 129.37 ($C_{7'}^{A}$), 129.28 ($C_{7'}^{B}$), 125.11 ($C_{14'}^{A}$), 124.80 ($C_{14'}^{B}$), 122.89 ($C_{10'}^{A}$), 122.86 ($C_{10'}^{B}$), 120.27 ($C_{9'}^{A}$), 120.21 ($C_{9'}^{B}$), 119.85 ($C_{8'}^{A}$), 119.64 ($C_{8'}^{B}$), 116.43 (C_{5}^{A}), 116.40 (C_{5}^{B}), 113.78 ($C_{11'}^{A}$), 113.76 ($C_{11'}^{B}$), 112.64 ($C_{6'}^{A}$ + $C_{6'}^{B}$) , 111.12 (C_{4a}^{A}), 111.08 (C_{4a}^{B}), 102.58 (C_{8}^{A}), 102.48 (C_{8}^{B}), 75.72 (C_{2}^{A} + C_{2}^{B}), 56.29 ($C_{1''''}^{A}$ + $C_{1''''}^{B}$), 54.30 ($C_{4'}^{A}$ + $C_{4'}^{B}$), 46.61 ($C_{1'}^{A}$), 46.32 ($C_{1'}^{B}$), 32.46 (C_{3}^{A}), 32.19 (C_{3}^{B}), 28.40 ($C_{5'}^{A}$), 28.36 ($C_{5'}^{B}$), 24.34 ($C_{1'''}^{A}$), 24.18 ($C_{1'''}^{B}$), 22.10 (C_{4}^{A}), 22.02 (C_{4}^{B}).

3,4-Dihydro-6-hydroxy-2-methyl-2-((S)-4'-hydroxycarbonyl-4'-hydroxycarbonylpropyl]aminocarbonylethyl-7-methoxy-1-(2H)-benzopyran, H

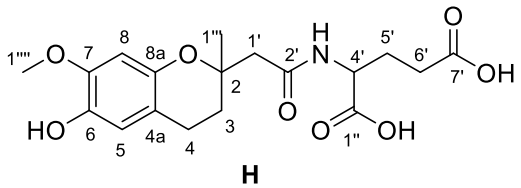

Following the same procedure as **B**, 140 mg (0.29 mmol) of amide **14** and 1.4 mL (5.8 mmol) of 4 M NaOH in dioxane (1.5 mL) afforded, after 4 hours, the desired acid (92 mg, 83%).

Following the same procedure as **A**, 92 mg (0.20 mmol) of the above acid and 9.2 mg of 10% w/w Pd/C in EtOH (4 mL) afforded, after 5 hours, the derivative **H** (72 mg, 95%).

m.p.: 74.2 – 84.6ºC. **HRMS for $C_{18}H_{24}N_2O_7$:** calculated: 382.1502 ([M+H]$^+$); found: 382.1521. **^{1}H-NMR (CD_3OD, 400 MHz):** δ: (diastereomer A and diastereomer B) 6.51 (s, $1H^A_5$ + $1H^B_5$), 6.42 (s, $1H^A_8$), 6.39 (s, $1H^B_8$), 4.51 – 4.40 (m, $1H^A_{4'}$ + $1H^B_{4'}$), 3.73 (s, $3H^A_{1'''}$ + $3H^B_{1'''}$), 2.69 – 2.63 (m, $2H^A_4$ + $2H^B_4$), 2.62 – 2.42 (m, $2H^A_{1'}$ + $2H^B_{1'}$ + $2H^A_{6'}$), 2.42 – 2.34 (m, $2H^B_{6'}$), 2.25 – 2.14 (m, $2H^A_{5'}$), 2.00 – 1.88 (m, $2H^B_{5'}$ + $2H^A_3$), 1.85 - 1.76 (m, $2H^B_3$), 1.37 (s, $3H^A_{1''}$), 1.36 (s, $3H^B_{1''}$). **^{13}C-NMR (CD_3OD, 100 MHz):** δ: (diastereomer A and diastereomer B) 176.32 ($C_{1''}{}^A$ + $C_{1''}{}^B$), 174.96 ($C_{7'}{}^A$ + $C_{7'}{}^B$), 172.66 ($C_{2'}{}^A$), 172.56 ($C_{2'}{}^B$), 148.32 ($C_{8a}{}^A$ + $C_{8a}{}^B$), 147.23 ($C_7{}^A$ + $C_7{}^B$), 140.01 ($C_6{}^A$ + $C_6{}^B$), 116.07 ($C_5{}^A$ + $C_5{}^B$), 113.36 ($C_{4a}{}^A$ + $C_{4a}{}^B$), 102.79 ($C_8{}^A$), 101.79 ($C_8{}^B$), 75.64 ($C_2{}^A$ + $C_2{}^B$), 56.32 ($C_{1'''}{}^A$ + $C_{1'''}{}^B$), 53.07 ($C_{4'}{}^A$ + $C_{4'}{}^B$), 46.89 ($C_{1'}{}^A$), 46.73 ($C_{1'}{}^B$), 32.85 ($C_3{}^A$), 31.94 ($C_3{}^B$), 31.23 ($C_{6'}{}^A$), 31.1 ($C_{6'}{}^B$), 28.00 ($C_{5'}{}^A$), 27.95 ($C_{5'}{}^B$), 24.45 ($C_{1''}{}^A$), 24.31 ($C_{1''}{}^B$), 22.34 ($C_4{}^A$ + $C_4{}^B$).

2-Aminocarbonylmethyl-3,4-dihydro-6-hydroxy-2-methyl-7-methoxy-1-(2H)-benzopyran, I

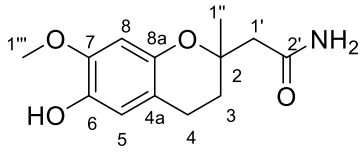

I

Following the same procedure as **A**, 54 mg (0.16 mmol) of amide **16** and 6 mg of 10% w/w Pd/C in EtOAc (4 mL) afforded, after 4 hours, the desired amide **I** (20 mg, 50%).

m.p.: 128.5 – 134.5ºC. **HRMS for $C_{13}H_{18}NO_4$:** calculated: 252.1236 ([M+H]$^+$); found: 252.1207. **^{1}H-NMR ($CDCl_3$, 400 MHz):** δ: 6.62 (s, $1H_5$), 6.33 (s, $1H_8$), 6.28 ($s_{exch.}$, $1H_{NH}$), 5.77 ($s_{exch.}$, $1H_{NH}$), 3.82 (s, $3H_{1'''}$), 2.76 – 2.44 (m, $2H_{1'}$ + $2H_4$), 1.96 – 1.86 (m, $1H_3$), 1.81 (dt, J = 13.6, 6.2 Hz, $1H_3$), 1.37 (s, $3H_{1''}$). **^{13}C-NMR ($CDCl_3$, 100 MHz):** δ: 173.44 ($C_{2'}$), 146.35 (C_{8a}), 145.88 (C_7), 140.07 (C_6), 114.62 (C_5), 112.67 (C_{4a}), 100.40 (C_8), 74.37 (C_2), 55.81 ($C_{1'''}$), 46.33 ($C_{1'}$), 31.11 (C_3), 23.26 ($C_{1''}$), 20.94 (C_4).

VIII.1.4. Synthesis of derivatives from intermediate 2. Family 2

6-Benzyloxy-3,4-dihydro-2-methyl-2-[2'-(p-methylphenylsulfonyloxy)]ethyl-7-methoxy-1-(2H)-benzopyran, 20

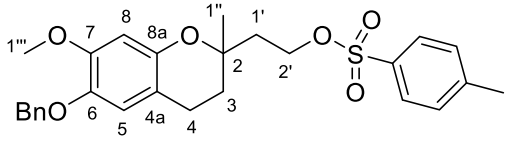

20

To a solution of alcohol **2** (5.0 g, 15.07 mmol) in the minimum amount of anhydrous CH_2Cl_2 (10 mL), pyridine (7 mL) and TsCl (8.0 g, 41.96 mmol) were added under N_2 atmosphere. The mixture was stirred for 4 hours at room temperature (TLC monitoring, 3:2 hexane:EtOAc). Then, the mixture was washed with

a 1 M HCl solution, the organic layer was dried with anhydrous $MgSO_4$ and the solvent was evaporated under vacuum. The resulting crude compound was purified by chromatography on silica gel (gradient, from 98:2 hexane:EtOAc to EtOAc) to give tosylate **20** (6.1 g, 83%).

HRMS for $C_{27}H_{31}O_6S$: calculated: 483.1841 ($[M+H]^+$); found: 483.1803. **^{1}H-NMR ($CDCl_3$, 400 MHz):** δ: 7.82 – 7.74 (m, $2H_{TsO}$), 7.46 – 7.40 (m, $2H_{Bn}$), 7.39 – 7.28 (m, $2H_{TsO}$ + $3H_{Bn}$), 6.56 (s, $1H_8$), 6.29 (s, $1H_5$), 5.04 (s, $1H_{Bn}$), 4.24 (m, $2H_{2'}$), 3.80 (s, $3H_{1'''}$), 2.67 – 2.48 (m, $2H_4$), 2.43 (s, $3H_{TsO}$), 2.07 – 1.88 (m, $2H_{1'}$), 1.76 – 1.69 (m, $2H_{2'}$), 1.24 (s, $3H_{1''}$). **^{13}C-NMR ($CDCl_3$, 100 MHz):** δ: 149.32 (C_{8a}), 147.45 (C_7), 144.61 (C_{Ts}), 141.92 (C_6), 137.46 (C_{Bn}), 132.93 (C_{Ts}), 129.68 (C_{Ts}), 128.30 (C_{Bn}), 127.72 (C_{Ts}), 127.57(C_{Bn}), 127.27 (C_{Bn}), 115.63 (C_5), 111.00 (C_{4a}), 101.39 (C_8), 74.04 (C_2), 72.05 (C_{Bn}), 66.58 ($C_{2'}$), 55.76 ($C_{1'''}$), 38.08 (C_3), 31.39 ($C_{1'}$), 23.98 ($C_{1''}$), 21.49 (C_{Ts}), 21.18 (C_4). **IR (KBr):** ν (cm^{-1}): 2933, 1598, 1512.

6-Benzyloxy-2-(2'-azido)ethyl-3,4-dihydro-2-methyl-7-methoxy-1-(2H)-benzopyran, 21

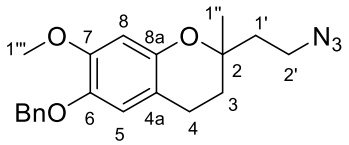

21

To a solution of **20** (538 mg, 1.11 mmol) in anhydrous DMF (8.5 mL), NaN_3 (362 mg, 5.57 mmol) was added under N_2 atmosphere. The mixture was stirred for 22 hours at room temperature (TLC monitoring, 3:2 hexane:EtOAc). Then, the mixture was diluted with CH_2Cl_2, and washed with a saturated solution of $NaHCO_3$. The combined organic layer was dried with anhydrous $MgSO_4$ and the solvent was evaporated under vacuum to give azide **21** (355 mg, 90%).

HRMS for $C_{20}H_{24}N_3O_3$: calculated: 354.1818 ($[M+H]^+$); found: 354.1814. **^{1}H-NMR ($CDCl_3$, 400 MHz):** δ: 7.46 – 7.41 (m, $2H_{Bn}$), 7.36 (tt, J = 8.0, 1.6 Hz, $2H_{Bn}$), 7.33 – 7.27 (m, $1H_{Bn}$), 6.59 (s, $1H_8$), 6.38 (s, $1H_5$), 5.04 (s, $2H_{Bn}$), 3.82 (s, $3H_{1'''}$), 3.47 (ddd, J = 8.3, 4.9, 1.4 Hz, $2H_{2'}$), 2.68 – 2.60 (m, $2H_4$), 2.01 – 1.92 (m, $1H_3$), 1.89 – 1.71 (m, $1H_3$ + $2H_{1'}$), 1.29 (s, $3H_{1''}$). **^{13}C-NMR ($CDCl_3$, 100 MHz):** δ: 149.98 (C_{8a}), 148.22 (C_7), 142.43 (C_6), 138.02 (C_{Bn}), 128.74 (C_{Bn}), 128.00 (C_{Bn}), 127.73 (C_{Bn}), 127.73 (C_{Bn}), 116.11 (C_5), 111.38 (C_{4a}), 101.71 (C_8), 74.37 (C_2), 72.20 (C_{Bn}), 55.78 ($C_{1'''}$), 46.55 ($C_{2'}$), 38.03 (C_3), 31.26 ($C_{1'}$), 23.60 ($C_{1''}$), 21.06 (C_4). **IR (KBr):** ν (cm^{-1}): 2933, 2097, 1616, 1512.

6-Benzyloxy-2-(2'-amino)ethyl-3,4-dihydro-2-methyl-7-methoxy-1-(2H)-benzopyran, 18

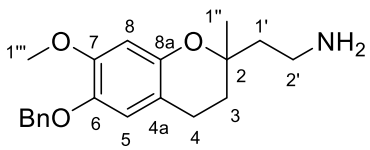

18

To a solution of azide **21** (184 mg, 0.52 mmol) in anhydrous THF (3.5 mL), PPh_3 (215 mg, 0.82 mmol) was added under N_2 atmosphere. The mixture was stirred for 15 hours at room temperature. Then, water (0.5 mL, 13 mmol) was added, and the new mixture was stirred for 3 hours more at room temperature (TLC monitoring, 95:5 CH_2Cl_2:MeOH and 1% NEt_3). The mixture was diluted in CH_2Cl_2 and was washed

with 4 M NaOH solution. The organic layer was dried with anhydrous $MgSO_4$ and the solvent was evaporated under vacuum. The resulting residue was purified by chromatography (gradient, from 95:5 to 85:15 CH_2Cl_2:MeOH and 1% NEt_3) to give amine **18** (140 mg, 82%) as a white solid.

HRMS for $C_{20}H_{26}NO_3$: calculated: 328.1913 ($[M+H]^+$); found: 328.1908. **^{1}H-NMR ($CDCl_3$, 400 MHz):** δ: 7.47 – 7.40 (m, $2H_{Bn}$), 7.35 (dd, J = 10.0, 4.6 Hz, $2H_{Bn}$), 7.31 – 7.23 (m, $1H_{Bn}$), 6.57 (s, $1H_5$), 6.35 (s, $1H_8$), 5.04 (s, $2H_{Bn}$), 3.80 (s, $3H_{1'''}$), 2.88 ($s_{exch.}$, $2H_{NH}$), 2.62 (dd, J = 15.5, 8.5 Hz, $2H_{2'}$), 1.88 – 1.64 (m, $2H_{1'}$ + $2H_4$ + $2H_3$), 1.26 (s, $3H_{1''}$). **^{13}C-NMR ($CDCl_3$, 100 MHz):** δ: 149.45 (C_{8a}), 147.75 (C_7), 141.97 (C_6), 137.64 (C_{Bn}), 128.40 (C_{Bn}), 127.65 (C_{Bn}), 127.40 (C_{Bn}), 115.84 (C_5), 111.16 (C_{4a}), 101.69 (C_8), 75.27 (C_2), 72.20 (C_{Bn}), 55.96 ($C_{1'''}$), 41.33 ($C_{1'}$), 36.74 ($C_{2'}$), 31.53 (C_3), 23.54 ($C_{1''}$), 21.41 (C_4). **IR (KBr):** ν (cm^{-1}): 3365, 3126, 2935, 1616, 1515.

2-(2'-Amino)ethyl-6-hydroxy-3,4-dihydro-2-methyl-7-methoxy-1-(2H)-benzopyran, 22

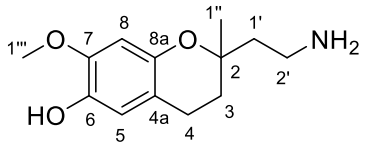

22

Following the same procedure as **A**, 250 mg (0.76 mmol) of amine **18** and 25 mg of 10% w/w Pd/C in EtOH (3 mL) afforded, after 5 hours, the desired amine **22** (104.5 mg, 58%).

HRMS for $C_{13}H_{20}NO_3$: calculated: 238.1443 ($[M+H]^+$); found: 238.1421. **^{1}H-NMR (CD_3OD, 400 MHz):** δ: 6.46 (s, $1H_5$), 6.31 (s, $1H_8$), 3.72 (s, $1H_{1'''}$), 3.01 – 2.85 (m, $2H_{2'}$), 2.69 – 2.53 (m, $2H_4$), 1.88 (ddd, J = 13.7, 8.9, 6.9 Hz, $2H_{1'}$ + $2H_3$), 1.22 (s, $3H_{1''}$). **^{13}C-NMR (CD_3OD, 100 MHz):** δ: 148.35 (C_{8a}), 147.45 (C_7), 141.04 (C_6), 116.14 (C_5), 113.40 (C_{4a}), 102.22 (C_8), 75.81 (C_2), 56.35 ($C_{1'''}$), 40.28 ($C_{1'}$), 37.08 ($C_{2'}$), 32.73 (C_3), 23.78 ($C_{1''}$), 22.25 (C_4).

6-Hydroxy-3,4-dihydro-2-methyl-2[(2',6'-dimethyl-8'(2'',6'',6''-trimethylcyclohex-1''-en)-1E,3E,5E,7E-tetraocten)carbonylaminoethyl]-7-methoxy-1-(2H)-benzopyran, J

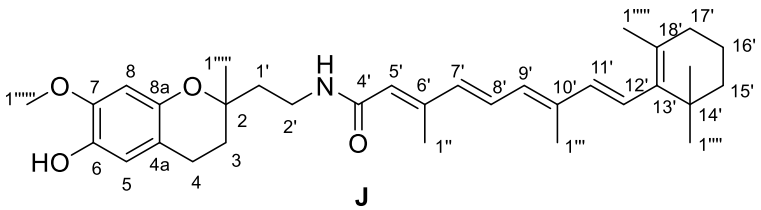

J

To a solution of retinoic acid (139 mg, 0.46 mmol) in the minimum amount of anhydrous CH_2Cl_2 (4 mL), EDC·HCl (162 mg, 0.85 mmol) and DIPEA (250 µL, 1.44 mmol) were added, under N_2 atmosphere and in absence of light, and the mixture was stirred for 30 minutes at room temperature. Then, amine **22** (102 mg, 0.43 mmol) was added and the mixture was stirred for 48 hours (HPLC-UV monitoring). Then, CH_2Cl_2 was added and the resulting solution was washed with 1 M HCl and brine. The organic layer was dried with anhydrous $MgSO_4$ and the solvent was evaporated under vacuum. The bright yellow residue resulting was purified by chromatography on silica gel (gradient, from 95:5 hexane:EtOAc to EtOAc) to give derivative **J** (85 mg, 38%).

m.p.: 80.3 – 81.5ºC. **HRMS for $C_{33}H_{46}NO_4$:** calculated: 520.3427 ([M+H]$^+$); found: 520.3414. **^{1}H-NMR (CD_3OD, 400 MHz):** δ: 6.99 (dd, J = 15.0, 11.3 Hz, $1H_{5'}$), 6.50 (s, $1H_5$), 6.35 (s, $1H_8$), 6.35 – 6.25 (m, $1H_{7'}$ + $1H_{9'}$ + $1H_{11'}$), 6.16 (dd, J = 13.7, 9.0 Hz, $1H_{12'}$ + $1H_{8'}$), 5.81 ($s_{exch.}$, $1H_{NH}$), 3.78 (s, $3H_{1''''''}$), 3.51 – 3.43 (m, $1H_{2'}$), 3.41 – 3.35 (m, $1H_{2'}$), 2.65 (t, J=6.7 Hz, $2H_4$), 2.30 (d, J = 2.4 Hz, $3H_{1''}$), 2.05 (dd, J = 10.3, 5.6 Hz, $2H_{17'}$), 2.01 (d, J = 0.8 Hz, $2H_{1'''}$), 1.97 – 1.74 (m, $2H_3$ + $2H_{1'}$), 1.72 (d, J = 0.8 Hz, $3H_{1''''}$), 1.71 – 1.62 (m, $2H_{16'}$), 1.51 (dt, J = 5.9, 3.3 Hz, $2H_{15'}$), 1.31 (s, $3H_{1''''''}$), 1.05 (s, $6H_{1''''}$). **^{13}C-NMR (CD_3OD, 100 MHz):** δ: 169.70 ($C_{4'}$), 149.14 (C_{8a}), 148.40 ($C_{6'}$), 147.89 (C_7), 140.90 (C_6), 139.50 ($C_{13'}$), 139.18 ($C_{10'}$), 139.13 ($C_{11'}$), 137.13 ($C_{7'}$), 131.15 ($C_{9'}$), 130.76 ($C_{8'}$), 130.58 ($C_{18'}$), 129.07 ($C_{12'}$), 123.07 ($C_{5'}$), 116.19 (C_5), 113.53 (C_{4a}), 102.30 (C_8), 75.94 (C_2), 56.42 ($C_{1''''''}$), 40.86 ($C_{15'}$), 39.48 ($C_{1'}$), 35.84 ($C_{14'}$), 35.34 ($C_{2'}$), 34.07 ($C_{17'}$), 32.84 (C_3), 29.51 ($C_{1''''}$), 24.39 ($C_{1''''''}$), 22.48 (C_4), 22.03 ($C_{1''''}$), 20.42 ($C_{16'}$), 13.93 ($C_{1''}$), 12.92 ($C_{1'''}$).

6-Benzyloxy-3,4-dihydro-2-methyl-2-[((7', 8'R, 9'S, 10'S)-tetra-O-acetoxy-methyl-6'R-pyranyl)carbonylaminoethyl]-7-methoxy-1-(2H)-benzopyran, 23

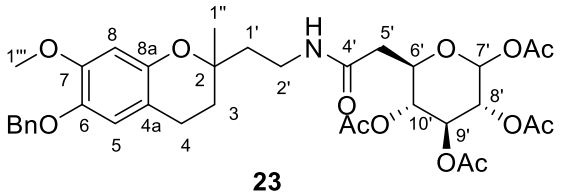

23

1,2,3,4-Tetra-*O*-acetyl-β-D-glucopyranuronic acetic anhydride was prepared following the procedure described by El-Nezhawy *et al*.[146] To a suspension of (3,4,5,6-tetrahydroxy-tetrahydro-pyran-2-yl)acetic acid (71 mg, 0.34 mmol) in Ac_2O (3 mL, 31.8 mmol) at 0ºC, I_2 (11 mg, 0.04 mmol) was added under N_2 atmosphere. The mixture was stirred for 30 minutes at 0ºC and for 2 hours at room temperature. Then, the solvent was evaporated under vacuum and the residue was treated with a 17 mM solution of $Na_2S_2O_3$. The residue was then extracted with CH_2Cl_2. The combined organic layer was dried with anhydrous $MgSO_4$ and the solvent was evaporated under vacuum to give desired reagent **23a** (182 mg, 82%).

To a solution of **23a** (132 mg, 0.31 mmol) in anhydrous CH_2Cl_2 (9 mL), amine **18** (162 mg, 0.49 mmol) was added under N_2 atmosphere. The mixture was stirred for 15 hours at room temperature (TLC monitoring HPLC-UV). Then, the solvent was evaporated under vacuum. The resulting residue was purified by chromatography in reverse phase (gradient, from 9:1 H_2O:CH_3CN to CH_3CN) to give product **23** (119 mg, 55%).

HRMS for $C_{35}H_{44}NO_{13}$: calculated: 686.2813 ([M+H]$^+$); found: 686.2822. **^{1}H-RMN ($CDCl_3$, 400 MHz):** δ: (diastereomer A and diastereomer B) 7.47 – 7.39 (m, $4H_{Bn}$), 7.39 – 7.31 (m, $4H_{Bn}$), 7.28 (d, J = 7.2 Hz, $2H_{Bn}$), 6.58 (s, $1H^A_5$), 6.57 (s, $1H^B_5$), 6.34 (s, $1H^A_8$), 6.33 (s, $1H^B_8$), 6.24 – 6.17 (dd, J = 19.51, 3.74 Hz, $1H^A_{7'}$ + $1H^B_{7'}$), 6.17 – 6.08 (m, $1H_{NH}{}^A$ + $1H_{NH}{}^B$), 5.49 – 5.39 (td, J = 9.77, 2.57 Hz, $1H^A_{8'}$ + $1H^A_{8'}$), 5.03 – 5.01 (m, $4H_{Bn}$), 5.01 – 4.97 (m, $1H_{9'}{}^A$ + $1H_{9'}{}^B$), 4.92 – 4.86 (m, $1H_{10'}{}^A$ + $1H^B_{10'}$), 4.43 – 4.28 (m, $1H^A_{6'}$ + $1H^B_{6'}$), 3.81 (s, $3H^A_{1'''}$ + $3H^B_{1'''}$), 3.52 – 3.40 (m, $2H^A_{2'}$), 3.38 – 3.26 (m, $2H^B_{2'}$), 2.62 (t, J = 6.9 Hz, $2H^A_{5'}$ + $2H^B_{5'}$), 2.41 – 2.31 (m, $2H^A_{1'}$), 2.31 – 2.19 (m, $2H^B_{1'}$), 2.16 (s, $3H_{OAc}$), 2.14 (s, $3H_{OAc}$), 2.13 (s, $3H_{OAc}$), 2.05 – 2.01 (m, $9H_{OAc}$), 2.01 – 1.98 (m, $6H_{OAc}$), 1.86 – 1.66 (m, $2H^A_3$ + $2H^B_3$ + $2H^A_4$ + $2H^B_4$), 1.27 (s, $3H^A_{1''}$), 1.26 (s, $3H^B_{1''}$).**^{13}C-NMR ($CDCl_3$, 100 MHz):** δ: (diastereomer A and diastereomer B) 170.49 ($C_{4'}{}^A$ + $C_{4'}{}^B$), 170.29 (C_{OAc}), 170.26 (C_{OAc}), 170.22 (C_{OAc}), 170.17 (C_{OAc}), 169.61 (C_{OAc}), 169.57 (C_{OAc}), 169.04 (C_{OAc}), 169.04 (C_{OAc}), 149.87 ($C_{8a}{}^A$ + $C_{8a}{}^B$),

[146] El-Nezhawy, A.O.; Adly, F.G.; Eweas, A.F.; Hanna, A.G.; El-Kholy, Y.M.; El-Sayed, S.H.; El-Naggar, T.B. *Arch. Pharm. (Weinhein),* **2011**, *344*, 648-657.

148.06 (C_7^A), 148.04 (C_7^B), 142.37 (C_6^A), 142.34 (C_6^B), 137.93 (C_{Bn}), 137.92 (C_{Bn}), 128.66 (C_{Bn}), 127.92 (C_{Bn}), 127.67 (C_{Bn}), 116.14 (C_5^A), 116.11 (C_5^B), 111.57 (C_{4a}^A), 111.52 (C_{4a}^B), 101.51 (C_8^A + C_8^B), 88.70 ($C_{7'}^A$ + $C_{7'}^B$), 75.28 (C_2^A), 75.27 (C_2^B), 72.08 (C_{Bn}), 72.05 (C_{Bn}), 71.15 ($C_{10'}^A$), 71.08 ($C_{10'}^B$), 69.60 ($C_{8'}^A$ + $C_{8'}^B$), 69.24 ($C_{9'}^A$ + $C_{9'}^B$), 68.44 ($C_{6'}^A$), 68.42 ($C_{6'}^B$), 55.75 ($C_{1'''}^A$), 55.73 ($C_{1'''}^B$), 38.53 ($C_{1'}^A$), 38.44 ($C_{1'}^B$), 38.00 (C_3^A), 37.89 (C_3^B), 34.93 ($C_{2'}^A$ + $C_{2'}^B$), 31.14 (C_4^A), 31.07 (C_4^B), 23.39 ($C_{1''}^A$ + $C_{1''}^B$), 20.97 ($C_{5'}^A$ + $C_{5'}^B$), 20.41 (C_{OAc}), 20.39 (C_{OAc}), 20.20 (C_{OAc}), 20.18 (C_{OAc}), 20.03 (C_{OAc}).

6-Hydroxy-3,4-dihydro-2-methyl-2-[((7', 8'R, 9'S, 10'S)-tetrahydroxy-methyl-6'R-pyranyl)carbonylaminoethyl]-7-methoxy-1-(2H)-benzopyran, K

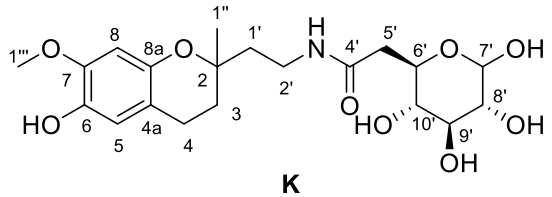

K

To a solution of amide **23** (70 mg, 0.102 mmol) in anhydrous MeOH (1 mL) at 0ºC in an ice-water bath and under N_2 atmosphere, was added a solution of 25% w/w NaOMe in MeOH (10 µL, 0.175 mmol). The mixture was stirred for 5 hours at room temperature (HPLC-UV monitoring). Then, a minimum amount of resin Amberlite 120® H^+ was added to give acidic pH. The resin was filtered off and the solvent was removed under vacuum to get deacetylated product **23b** (36 mg, 69%).

Following the same procedure as **A**, 36 mg (0.07 mmol) of the above deacetylated compound and 15 mg of 10% w/w Pd/C in MeOH (2.5 mL) afforded, after 7.5 hours submitted to 2 atm of H_2, derivative **J** (101 mg, 67%).

m.p.: 75.1 – 84.6ºC. **HRMS for $C_{20}H_{30}NO_9$:** calculated: 428.1921 ($[M+H]^+$); found: 428.1902. **^{1}H-RMN (CD_3OD, 400 MHz):** δ: (diastereomer A and diastereomer B) 6.50 (s, $1H_5^A$ + $1H_5^B$), 6.35 (t, J = 3.2 Hz, $1H_8^A$ + $1H_8^B$), 5.04 (dd, J = 10.1, 3.4 Hz, $1H_{7'}^A$), 4.46 (dd, J = 7.7, 3.2 Hz, $1H_{7'}^B$), 4.19 – 4.08 (m, $1H_{6'}^A$), 3.78 (s, $3H_{1'''}^A$ + $3H_{1'''}^B$), 3.71 – 3.59 (m, $1H_{6'}^B$ + $1H_{10'}^A$), 3.41 (dd, J = 21.3, 11.1 Hz, $2H_{2'}^A$ + $2H_{2'}^B$), 3.35 – 3.22 (m, $1H_{8'}^A$ + $1H_{8'}^B$), 3.17 – 3.03 (m, $1H_{9'}^A$ + $1H_{9'}^B$+ $1H_{10'}^B$), 2.73 (dd, J = 13.6, 6.4 Hz, $2H_{1'}^A$), 2.66 (t, J = 6.7 Hz, $2H_{5'}^A$ + $2H_{5'}^B$), 2.27 (dtd, J = 17.0, 9.4, 5.8 Hz, $2H_{1'}^B$), 1.92 – 1.67 (m, $2H_3^A$ + $2H_3^B$ + $2H_4^A$ + $2H_4^B$), 1.28 (d, J = 5.3 Hz, $3H_{1''}^A$ + $3H_{1''}^B$). **^{13}C-RMN (CD_3OD, 100 MHz):** δ: (diastereomer A and diastereomer B) 174.51 ($C_{4'}^A$), 174.14 ($C_{4'}^B$), 148.92(C_{8a}^A), 148.40 (C_{8a}^B), 148.37 (C_7^A), 148.36 (C_7^B), 141.36 (C_6^A + C_6^B), 116.52 (C_5^A + C_5^B), 113.87 (C_{4a}^A), 113.85 (C_{4a}^B), 102.55 (C_8^A), 102.54 (C_8^B), 98.39 ($C_{7'}^B$), 94.16 ($C_{7'}^A$), 78.20 ($C_{8'}^A$), 76.47 ($C_{9'}^A$), 76.03 ($C_{9'}^B$), 75.92 ($C_{8'}^B$), 75.83 (C_2^A), 75.27 ($C_{10'}^B$), 74.83 ($C_{10'}^A$), 74.35 ($C_{6'}^B$), 74.06 (C_2^B), 69.64 ($C_{6'}^A$), 56.41 ($C_{1'''}^A$), 56.40 ($C_{1'''}^B$), 40.21 ($C_{1'}^A$), 40.02 ($C_{1'}^B$), 39.31 (C_3^A + C_3^B), 35.95 ($C_{2'}^A$ + $C_{2'}^B$), 32.57 (C_4^A + C_4^B), 24.11 ($C_{1''}^A$), 24.04 ($C_{1''}^B$), 22.20 ($C_{5'}^A$ + $C_{5'}^B$).

6-Benzyloxy-3,4-dihydro-2-methyl-2-methylcarbonylaminomethyl-7-methoxy-1-(2H)-benzopyran, 24

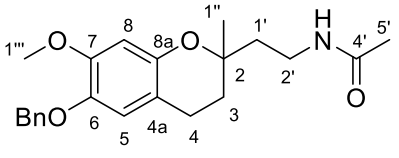

24

A solution of the amine **18** (100 mg, 0.31 mmol) in anhydrous CH_2Cl_2 (2 mL), maintained at 0ºC, was treated with acetyl chloride (30 µL, 0.42 mmol), under N_2 atmosphere, followed by NEt_3 (60 µL, 0.43 mmol). The mixture was stirred for 24 hours at room temperature (HPLC-UV monitoring). Then, after adding a bit of water, the solvent was reduced under vacuum and the residue was extracted with CH_2Cl_2. The combined organic layer was dried with anhydrous $MgSO_4$ and the solvent was evaporated under vacuum. The resulting residue was purified by chromatography in reverse phase (gradient, from 9:1 H_2O:CH_3CN to CH_3CN) to give product **24** (75 mg, 66%).

HRMS for $C_{22}H_{28}NO_4$: calculated: 370.2018 ($[M+H]^+$); found: 370.2048. **^{1}H-NMR ($CDCl_3$, 400 MHz):** δ: 7.45 – 7.40 (m, $2H_{Bn}$), 7.35 (ddd, J = 7.5, 6.3, 1.5 Hz, $2H_{Bn}$), 7.31 – 7.26 (m, $1H_{Bn}$), 6.59 (s, $1H_5$), 6.34 (s, $1H_8$), 5.98 ($s_{exch.}$, $1H_{NH}$), 5.03 (s, $2H_{Bn}$), 3.81 (s, $3H_{1'''}$), 3.52 (cd, J = 13.7, 6.2 Hz, $1H_{2'}$), 3.34 (cd, J = 7.3, 4.8 Hz, $1H_{2'}$), 2.64 (m, $2H_{1'}$), 1.93 (s, $3H_{5'}$), 1.90 – 1.66 (m, $2H_4$ + $2H_3$), 1.28 (s, $3H_{1''}$). **^{13}C-NMR ($CDCl_3$, 100 MHz):** δ: 169.96 ($C_{4'}$), 149.50 (C_9), 147.54 (C_7), 142.15 (C_6), 137.55 (C_{Bn}), 128.43 (C_{Bn}), 127.72 (C_{Bn}), 127.41 (C_{Bn}), 115.97 (C_5), 111.50 (C_{10}), 101.35 (C_8), 75.68 (C_2), 72.18 (C_{Bn}), 55.96 ($C_{1'''}$), 38.12 ($C_{1'}$), 35.30 ($C_{2'}$), 31.56 (C_3), 23.84 ($C_{5'}$), 23.32 ($C_{1''}$), 21.39 (C_4).

3,4-Dihydro-2-methyl-2-methylcarbonylaminoethyl-7-methoxy-1-(2H)-benzopyran, L

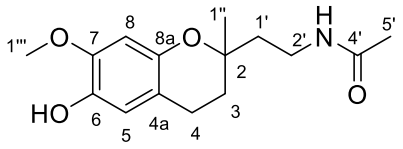

L

Following the same procedure as **A**, 40 mg (0.20 mmol) of amide **24** and 4 mg of 10% w/w Pd/C in EtOH (3 mL) afforded, after 6 hours, desired deprotected amide **L** (52 mg, 95%).

HRMS for $C_{15}H_{22}NO_4$: calculated: 280.1549 ($[M+H]^+$); found: 280.1517. **^{1}H-NMR ($CDCl_3$, 400 MHz):** δ: 6.56 (s, $1H_5$), 6.28 (s, $1H_8$), 5.88 ($s_{exch.}$, $1H_{NH}$), 3.77 (s, $3H_{1'''}$), 3.52 – 3.38 (m, $1H_{2'}$), 3.38 – 3.25 (m, $1H_{2'}$), 2.68 – 2.57 (m, $2H_4$), 1.88 (s, $3H_{5'}$), 1.85 – 1.61 (m, $2H_{1'}$ + $2H_3$), 1.24 (s, $3H_{1''}$). **^{13}C-NMR ($CDCl_3$, 100 MHz):** δ: 169.71 ($C_{4'}$), 146.07 (C_9), 145.71 (C_7), 139.14 (C_6), 114.14 (C_5), 112.37 (C_{10}), 100.11 (C_8), 75.33 (C_2), 55.78 ($C_{1'''}$), 38.03 ($C_{1'}$), 35.06 ($C_{2'}$), 31.45 (C_3), 23.51 ($C_{5'}$), 23.13 ($C_{1''}$), 21.19 (C_4).

VIII.1.5. Synthesis of CR-6 derivatives from precursor 2. Family 3

6-Benzyloxy-2-(2'-formylmethyl)-3,4-dihydro-2-methyl-7-methoxy-1-(2H)-benzopyran, 19

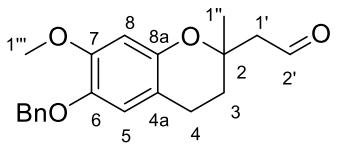

19

A solution of alcohol **2** (2.8 g, 8.5 mmol) in EtOAc (60 mL) was treated with IBX (4.7 g, 19.0 mmol) and heated under reflux for 4 hours (TLC monitoring, 3:2 hexane:EtOAc). After this time, the mixture was

cooled to room temperature, filtered through Celite® and the solvent was evaporated under vacuum to give product **19** (2.8 g, 99%) as an orange oil.

HRMS for $C_{20}H_{23}O_4$: calculated: 327.1596 ([M+H]$^+$); found: 327.1555. **^{1}H-NMR ($CDCl_3$, 400 MHz):** δ: 9.90 (dd, J = 3.1, 2.5 Hz, $1H_{3'}$), 7.46 – 7.41 (m, $2H_{Bn}$), 7.40 – 7.33 (m, $2H_{Bn}$), 7.32 – 7.27 (m, $1H_{Bn}$), 6.60 (s, $1H_8$), 6.40 (s, $1H_5$), 5.05 (s, $2H_{Bn}$), 3.82 (s, $3H_{1'''}$), 2.76 – 2.54 (m, $2H_{1'}$ + $2H_4$), 1.94 – 1.79 (m, $2H_3$), 1.41 (s, $3H_{1''}$). **^{13}C-NMR ($CDCl_3$, 100 MHz):** δ: 201.42 ($C_{2'}$), 149.61 (C_9), 147.38 (C_7), 142.31 (C_6), 137.55 (C_{Bn}), 128.43 (C_{Bn}), 127.71 (C_{Bn}), 127.39 (C_{Bn}), 115.77 (C_5), 110.99 (C_{10}), 101.59 (C_8), 74.40 (C_2), 72.16 (C_{Bn}), 55.92 ($C_{1'''}$), 52.28 ($C_{1'}$), 31.77 (C_3), 24.87 ($C_{1''}$), 21.37 (C_4). **IR (KBr):** ν (cm^{-1}): 2933, 1953, 1721.

6-Benzyloxy-2-(2'-amino-2'-cyano)ethyl-3,4-dihydro-2-methyl-7-methoxy-1-(2H)-benzopyran, 25

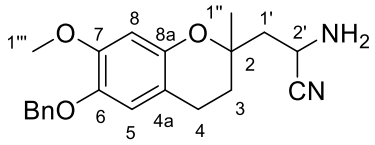

25

A mixture of $MgSO_4$ (233 mg, 1.94 mmol), NH_4Cl (168 mg, 3.14 mmol), NaCN (151 mg, 3.08 mmol) and 7 M NH_3 in methanol (30 mL, 210 mmol) was stirred under N_2 atmosphere for 10 minutes at room temperature. Then, a solution of aldehyde **19** (86 mg, 0.23 mmol) in methanol (0.9 mL) was added and the mixture was stirred for 2 hours and 30 minutes under N_2 atmosphere (HPLC-UV monitoring). After removing the solvent under vacuum, the residue was poured into CH_2Cl_2 and the solution was filtered through Celite®. The solvent was evaporated under vacuum to give the product **25** (900 mg, 96%) as a brownish oil.

HRMS to $C_{21}H_{25}N_2O_3$: calculated: 353.1865 ([M+H]$^+$); found: 353.1882. **^{1}H NMR (500 MHz, $CDCl_3$):** δ: (diastereomer A and diastereomer B) 7.44 (d, J = 7.4 Hz, $2H_{Bn}$), 7.36 (t, J = 7.5 Hz, $2H_{Bn}$), 7.30 (d, J = 6.6 Hz, $1H_{Bn}$), 6.60 (s, $1H^A_5$ + $1H^B_5$), 6.41 (s, $1H^A_8$), 6.38 (s, $1H^B_8$), 5.04 (s, $2H^A_{Bn}$ + $2H^B_{Bn}$), 4.01 (t, J = 6.6 Hz, $1H^A_{2'}$), 3.97 (t, J = 6.6 Hz, $1H^B_{2'}$), 3.80 (s, $3H^A_{1'''}$ + $3H^B_{1'''}$), 2.73 – 2.55 (m, $2H^A_4$ + $2H^B_4$), 2.19 (dd, J = 14.6, 7.2 Hz, $1H^A_{1'}$), 2.13 – 2.00 (m, $2H^B_{1'}$ + $2H_{NH}$), 1.96 – 1.90 (m, $1H^A_{1'}$), 1.90 – 1.80 (m, $2H^A_3$), 1.80 – 1.71 (m, $2H^B_3$), 1.36 (s, $3H^A_{1''}$), 1.34 (s, $3H^B_{1''}$). **^{13}C NMR (125 MHz, $CDCl_3$):** δ: (diastereomer A and diastereomer B) 149.59 ($C_9{}^A$ + $C_9{}^B$), 147.40 ($C_7{}^A$), 147.30 ($C_7{}^B$), 142.22 ($C_6{}^A$ + $C_6{}^B$), 137.59 ($C_{Bn}{}^A$), 137.55 ($C_{Bn}{}^B$), 128.43 (C_{Bn}), 127.74 (C_{Bn}), 127.71 (C_{Bn}), 127.69 (C_{Bn}), 127.40 (C_{Bn}), 122.60 ($C_{CN}{}^A$ + $C_{CN}{}^B$), 115.79 ($C_5{}^A$), 115.71 ($C_5{}^B$), 110.98 ($C_{10}{}^A$), 110.90 ($C_{10}{}^B$), 101.74 ($C_8{}^A$), 101.47 ($C_8{}^B$), 74.34 ($C_2{}^A$), 74.23 ($C_2{}^B$), 72.18 ($C_{Bn}{}^A$), 72.16 ($C_{Bn}{}^B$), 55.93 ($C_{1'''}{}^A$ + $C_{1'''}{}^B$), 45.04 ($C_{1'}{}^A$ + $C_{1'}{}^B$), 39.20 ($C_{2'}{}^A$), 39.09 ($C_{2'}{}^B$), 31.94 ($C_3{}^A$), 31.62 ($C_3{}^B$), 24.09 ($C_{1''}{}^A$), 23.89 ($C_{1''}{}^B$), 21.33 ($C_4{}^A$), 21.25 ($C_4{}^B$). **IR (KBr):** ν (cm^{-1}): 3379, 3313, 2933, 2248, 1619.

2-(2'-Amino-2'-hydroxycarbonyl)ethyl-6-benzyloxy-3,4-dihydro-2-methyl-7-methoxy-1-(2H)-benzopyran, 26

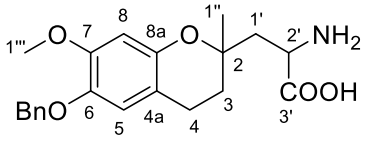

26

A solution of aminonitrile **25** (380 mg, 1.08 mmol) in dioxane (15 mL) was treated with a solution of 1 M NaOH (15 mL, 15.9 mmol). The mixture was heated for 17 hours under reflux (HPLC –UV monitoring). Then, the solution was cooled to room temperature and neutralised with 0.5 M HCl. The residue was isolated by ion exchange flash chromatography using Amberlite 120® H^+ resin (NH_3 and MeOH as eluent solvents) to obtain amino-acid **26** (110.8 mg, 28%).

HRMS for $C_{21}H_{26}NO_5$: calculated: 372.1811 ([M+H]$^+$); found: 372.1800. **^{1}H-NMR (CD_3OD, 500 MHz):** δ: (diastereomer A and diastereomer B) 7.43 (d, J = 7.4 Hz, $2H_{Bn}$), 7.36 (t, J = 7.5 Hz, $2H_{Bn}$), 7.31 (t, J = 7.3 Hz, $1H_{Bn}$), 6.72 (s, $1H^A_5$ + $1H^B_5$), 6.62 (s, $1H^A_8$), 6.55 (s, $1H^B_8$), 5.01 (s, $2H_{Bn}$), 4.39 (dd, J = 10.3, 2.8 Hz, $1H^A_{2'}$), 4.20 (dd, J = 8.6, 3.9 Hz, $1H^B_{2'}$), 3.82 (s, $3H^A_{1'''}$), 3.81 (s, $3H^B_{1'''}$), 2.87 – 2.75 (m, $2H^A_4$), 2.74 – 2.62 (m, $2H^B_4$), 2.39 (ddd, J = 18.0, 15.2, 3.4 Hz, $1H^A_{1'}$ + $1H^B_{1'}$), 2.21 (ddd, J = 25.5, 15.3, 9.4 Hz, $1H^A_{1'}$), 2.07 – 1.98 (m, $1H^A_3$ + $1H^B_{1'}$), 1.94 – 1.76 (m, $2H^B_3$ + $1H^A_3$), 1.39 (s, $3H^A_{1''}$), 1.34 (s, $3H^B_{1''}$). **^{13}C-NMR (CD_3OD, 125 MHz):** δ: (diastereomer A and diastereomer B) 151.65 ($C_{3'}{}^A$), 151.61 ($C_{3'}{}^B$), 149.51 ($C_{4A}{}^a$ + $C_{4a}{}^B$), 149.19 ($C_7{}^A$ + $C_7{}^B$), 144.18 ($C_6{}^A$) , 144.16 ($C_6{}^B$), 139.58 (C_{Bn}), 129.89 (C_{Bn}), 129.88 (C_{Bn}), 129.35 (C_{Bn}), 129.34 (C_{Bn}), 129.33 (C_{Bn}), 118.11 ($C_5{}^A$ + $C_5{}^B$), 113.69 ($C_{4a}{}^A$), 113.66 ($C_{4a}{}^B$), 103.73 ($C_8{}^A$), 103.63 ($C_8{}^B$), 77.52 ($C_2{}^A$), 77.47 ($C_2{}^B$), 73.58 (C_{Bn}), 56.52 ($C_{1'''}{}^A$ + $C_{1'''}{}^B$), 53.29 ($C_{2'}{}^A$ + $C_{2'}{}^B$), 43.44 ($C_{1''}{}^A$) , 42.91 ($C_{1''}{}^B$), 33.96 ($C_3{}^A$), 30.06 ($C_3{}^B$), 23.76 ($C_{1'}{}^A$), 22.19 ($C_4{}^A$), 21.99 ($C_4{}^B$), 21.07 ($C_{1''}{}^B$).

2-(2'-Amino-2'-hydroxycarbonyl)ethyl-6-hydroxy-3,4-dihydro-2-methyl-1-(2H)-benzopyran, M

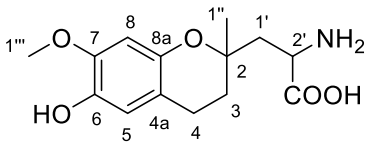

M

Following the same procedure as **A**, 90 mg (0.24 mmol) of amino acid **26** and 9 mg of 10% w/w Pd/C in MeOH (5 mL) afforded, after 5.5 hours, desired deprotected amide **M** (62 mg, 91 %).

m.p.: 163.2 – 165.3ºC. **HRMS for $C_{14}H_{19}NO_5$:** calculated: 282.1341 ([M+H]$^+$); found: 282.1326. **^{1}H-NMR (CD_3OD, 400 MHz):** δ: (diastereomer A and disatereomer B) 6.44 (s, $1H^A_5$), 6.43 – 6.41 (m, $1H^B_5$ + $1H^A_8$), 6.37 (s, $1H^B_8$), 4.15 (d, J = 9.1 Hz, $1H^A_{2'}$), 3.99 (d, J = 5.9 Hz, $1H^B_{2'}$), 3.68 (m, $3H^A_{1'''}$ + $3H^B_{1'''}$), 2.74 – 2.47 (m, $2H^A_4$ + $2H^B_4$), 2.30 (s, $2H^A_{1'}$), 2.16 – 1.97 (m, $2H^B_{1'}$), 1.96 – 1.85 (m, $2H^A_3$), 1.75 (ddd, J = 10.7, 8.7, 5.8 Hz, $2H^B_3$), 1.25 (s, $3H^A_{1''}$), 1.19 (d, J = 5.4 Hz, $3H^B_{1''}$). **^{13}C-NMR (CD_3OD, 100 MHz):** δ: 148.43 ($C_{3'}{}^A$ + $C_{3'}{}^B$), 148.37 ($C_{8a}{}^A$ + $C_{8a}{}^B$), 146.86 ($C_7{}^A$), 146.55 ($C_7{}^B$), 141.52 ($C_6{}^A$), 141.48 ($C_6{}^B$), 116.09 ($C_5{}^A$), 116.03 ($C_5{}^B$), 113.38 ($C_8{}^A$), 113.36 ($C_8{}^B$), 102.66 ($C_{4a}{}^A$), 102.58 ($C_{4a}{}^B$), 76.61 ($C_2{}^A$), 76.47 ($C_2{}^B$), 56.41 ($C_{1'''}{}^A$), 56.39 ($C_{1'''}{}^B$), 42.42 ($C_{1'}{}^A$), 42.16 ($C_{1'}{}^B$), 33.92 ($C_3{}^A$), 30.80 ($C_3{}^B$), 23.69 ($C_{1'}{}^A$), 22.22 ($C_4{}^A$), 22.04 ($C_4{}^B$), 21.26 ($C_{1'}{}^B$).

6-Benzyloxy-2-hydroxycarbonylmethyl-3,4-dihydro-2-methyl-7-methoxy-1-(2H)-benzopyran, N

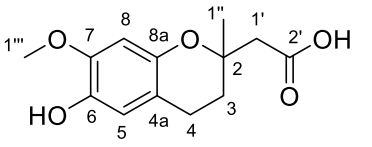

N

Following the same procedure as **A**, 51 mg (0.15 mmol) of the acid **6** and 6 mg of 10% w/w Pd/C in EtOH (4 mL) afforded, after 4 hours, desired acid **N** (38 mg, 99%).

m.p.: 146.6 – 149.9ºC. **HRMS for $C_{13}H_{17}O_5$:** calculated: 253.1076 ([M+H]$^+$); found: 253.1057. **^{1}H-NMR ($CDCl_3$, 400 MHz):** δ: 6.63 (s, 1H_5), 6.38 (s, 1H_8), 3.83 (s, 3$H_{1'''}$), 2.73 – 2.66 (m, 2$H_{1'}$ + 2H_4), 2.06 – 1.94 (m, 1H_3), 1.89 (dt, J = 13.6, 6.7 Hz, 1H_3), 1.46 (s, 3$H_{1''}$). **^{13}C-NMR ($CDCl_3$, 100 MHz):** δ: 175.20 ($C_{2'}$), 145.82 (C_9 + C_7), 139.36 (C_6), 114.12 (C_5), 112.26 (C_{10}), 100.59 (C_8), 74.24 (C_2), 55.90 ($C_{1'''}$), 43.62 ($C_{1'}$), 30.93 (C_3), 24.57 ($C_{1''}$), 21.35 (C_4).

VIII.2 EVALUATION OF ANTIOXIDANT CAPACITY

VIII.2.1 Free radical scavenging activity: DPPH assay

VIII.2.1.1 Materials

2,2-Diphenyl-1-picrylhydrazyl (DPPH) and (±)-6-hydroxy-2,5,7,8-tetramethylchromanee-2-carboxylic acid (TROLOX) were purchased from Sigma-Aldrich; 3,4-dihydro-6-hydroxy-7-methoxy-2,2-dimethyl-1(2H)-benzopyran (CR-6) was kindly provided by Lipotec, S.A. Methanol for the analysis was purchased by Merck, gas chromatography gradient.

VIII.2.1.2 Calibration curve

From a stock solution of 250 µM DPPH in MeOH, previously degassed with a N_2 flow, ten standards at different concentrations from 0 to 110 µM were prepared. The absorbance ($\lambda_{máx}$. 515 nm) for each standard was measured in a Cary300 spectrophotometer and plotted versus the concentration of DPPH.

*VIII.2.1.3 Free radical scavenging assay for new antioxidant compounds **A, B, C, D, E, F, G, H, I, J, K, L, M** and **N***

Free radical scavenging was measured using the absorbance of DPPH at different concentrations of antioxidant. Thus, 2 mL of a solution of antioxidant agent at different concentrations (final concentration from 0 to 30 µM) in methanol, previously degassed, were mixed with 2 mL of a methanolic solution of DPPH (140 µM). The mixture was stirred at room temperature for 60 minutes in the dark. Then, the absorbance of residual DPPH was measured at $\lambda_{máx.}$ = 515 nm. Trolox and CR-6 were used as controls and the absorbance of methanol was measure as blank. Then, the percentage of reduction of DPPH absorbance (%I) was calculated:

$$I(\%) = \frac{A_0 - A_t}{A_0} \cdot 100$$

where A_0 and A_t represent the absorbance of DPPH in absence of antioxidant and at a fixed concentration of antioxidant after 60 minutes of experiment, respectively.

The assay was performed in triplicate, and data values were reported as mean ± SD. The IC_{50} (half maximal inhibitory concentration) values were calculated from the corresponding dose-response curve of plotting the inhibition percentage versus the concentration of antioxidant agent, using the computer software GraphPad Prism 5.03 for Windows (GraphPad Software, San Diego, CA, USA).

VIII.2.1.4 Calculation of other parameters for determining the potential of antioxidant compounds

The ARP (Antiradical Power), the Stochiometric Value and the Number of DPPH Reduced were calculated from the IC_{50} value to determine the mechanistic way during antioxidant procedure. For this, I% was plotted *versus* mol of DPPH/mol of antioxidant compound, and the relative IC_{50} was calculated from the linear regression. Then, these parameters were calculated as follows: *ARP = 1/IC_{50}; Stochiometric Value = 2*IC_{50};* and *Number of DPPH Reduced = 1/ Stochiometric Value*.

VIII.2.2 Determination of intracellular ROS (Reactive Oxigen Species) formation

VIII.2.2.1 Chemicals

2',7'-Dichlorofluorescein diacetate (DCFH-DA), 30% wt H_2O_2 solution and DMSO were purchased from Sigma-Aldrich. Ethanol was purchased from Merck. 10 mM stock solutions of antioxidant compounds in DMSO and 20 mM stock solution of DCFH-DA in EtOH were stored at -20 ºC, and freshly diluted with medium to the appropriate concentrations before being used in the experiments. 100 mM Stock solution of H_2O_2 in H_2O was stored at 4ºC and freshly diluted in EBSS (Sigma) to the appropriate concentration.

VIII.2.2.2 Cell Culture

Two human breast adenocarcinoma cell lines, MDA-MB-231 and MDA-MB-468, were purchased from the America Type Culture Collection (ATCC). Both cancer cell lines were grown as monolayer in 75-cm^2 tissue culture flasks (Sigma) in DMEM media (Sigma) supplemented with 10% v/v foetal bovine serum and 100 ng/mL of penicillin and streptomycin. The cell lines were maintained in a humidified, 5% CO_2 incubator at 37ºC, and sub-cultured once reached confluence (3-4 days) using 0.25% v/v trypsin/EDTA (GIBCO). All experiments were performed using cells in exponential growth phase from passage 10 to 30.

*VIII.2.2.3 ROS Measurement of new antioxidant compounds **A**, **B**, **C**, **D**, **E**, **F**, **G**, **H**, **I**, **J**, **K**, **L**, **M** and **N***

Intracellular formation of ROS was measured using DCFH-DA as substrate, according to the manufacturer's instructions. MDA-MB-231 or MDA-MB-468 cells were seeded at a density of $6x10^4$/well on a 96-well microplate in 100 µL of growth medium/well, and grown overnight at 37ºC and 5% CO_2-water saturated atmosphere. The growth medium was next removed, and wells were treated with 100 µL of test compounds at the indicated concentrations plus 10 µL of a 25 µM H_2DCFDA solution for 1 hour at 37ºC. The medium was next removed, and wells were treated with 100 µL of 125 µM H_2O_2 in EBSS, and incubation continued for 1 hour. Fluorescence intensity ($\lambda_{excitation}$ = 485 nm; $\lambda_{emission}$ = 530 nm) was measured with a Spectramax M5 (Molecular Devices) at 25ºC. Each plate included control and blank wells. Control wells contained cells treated with DCFH-DA and oxidant; blank wells contained cells treated with DCFH-DA and EBSS without oxidant. OS-production (%) was calculated using the following expression:

$$OS - production(\%) = \frac{F_{test}}{F_{control}} \cdot 100$$

where F_{test} and $F_{control}$ represent the fluorescent readings from the drug-treated wells and the control wells, respectively.

VIII.2.2.4 Determination of H_2O_2 concentration

The concentration of oxidant H_2O_2 was determined before the above experiment to find the concentration that allowed the best signal of H_2DCFDA fluorescence. Then, the same experimental procedure as in section VIII.2.4.3 was followed for the two cell lines MDA-MB-231 and MDA-MB-468, without antioxidant compound and at different concentrations of H_2O_2 from 1000 to 7.8 µM.

The determination of H_2O_2 concentration was performed by triplicate, and data values were reported as mean ± SD. The concentration of oxidant (µM) was plotted versus fluorescence to determine the best concentration of H_2O_2, using the computer software Microsolft Excel for Windows.

The assay was performed by triplicate, and data values were reported as mean ± SD. The IC_{50} values were calculated from the corresponding dose-response curves, using the computer software GraphPad Prism 5.03 for Windows (GraphPad Software, San Diego, CA, USA).

VIII.3 BLOOD-BRAIN-BARRIER PENETRATION

VIII.3.1 *In silico* analysis

VIII.3.1.1 Prediction of penetration of BBB. Calculation of CNS MPO

A variant of Harrington's optimization method, using a summation of the individual components to yield a composite desirability score, was developed. Each component of the desirability function is a transformed function, defined by a series of inflection points defining the desirable and undesirable regions of properties (*x* variable) with a certain desirability score (*y* variable), as shown in Figure 8.1. For example, a monotonic decreasing function is defined by a desirable region if the property $x \leq x_1$ and an undesirable region for $x > x_2$ (Figure 8.1). A linear transformation is applied between the two inflection points ($x_1 < x \leq x_2$). Similarly, a hump function is defined by two undesirable regions and one desirable region, with linear transformation between the inflection points (Figure 8.1). In general, when a desirability component is defined by inflection points of (x_1, y_1), (x_2, y_2), … (x_n, y_n), assuming $x_1 < x_2 < \ldots < x_n$ the score at the attribute *x* is determined by piecewise linear function:

$$T(x) = \begin{cases} y_1 & x \leq x_1 \\ y_{i-1} + \dfrac{(y_i - y_{i-1})}{(x_i - x_{i-1})}(x - x_{i-1}) & x_{i-1} < x \leq x_i \\ y_n & x > x_n \end{cases}$$

Once each component function is built, the overall desirability of *M* variables is the sum of each component as defined in the following equation, where w_k is the weighting factor for attribute *k*:

$$D = \sum_{k=1}^{M} w_k T_k(x_k^0)$$

The CNS MPO score was built based on six fundamental physicochemical properties: ClogP, ClogD, MW, TPSA, HBD and pK_a; and a hump function was used for TPSA. All physicochemical properties were weighted equally, with a desirability score ranging from 0.0 to 1.0 for each property. The most desirable and least desirable ranges for each physicochemical property are listed in Table 8.1. Transformed values (T0) of six properties were determined for each compound, and the summation of the transformed component score yielded the final "CNS MPO" desirability score, which can range from zero (0) to six (6). For each physicochemical property, the inflection points that define optimal, less optimal, and undesirable ranges were selected based on the authors' medicinal chemistry experience (Figure 8.1). The inflection point selections were validated using knowledge of property distribution space for CNS drugs highlighted in the preceding publication of Wager *et al.* and other literature scores.[120]

Tabla 8.1. The CNS MPO properties, functions, weights, value range and parameter range.

Properties	Transformation T0	Weight	Desirable range (T0 = 1.0)	Non-desirable range (T0 = 0.0)
ClogD	Monotonic decreasing	1.0	ClogD ≤ 2	ClogD > 4
ClogP	Monotonic decreasing	1.0	ClogP ≤ 3	ClogP > 5
TPSA	Hump function	1.0	40 < TPSA ≤ 90	TPSA ≤ 20; TPSA > 120
MW	Monotonic decreasing	1.0	MW ≤ 360	MW > 500
HBD	Monotonic decreasing	1.0	HBD ≤ 0.5	HBD > 3.5
pKa	Monotonic decreasing	1.0	pKa ≤ 8	pKa > 10

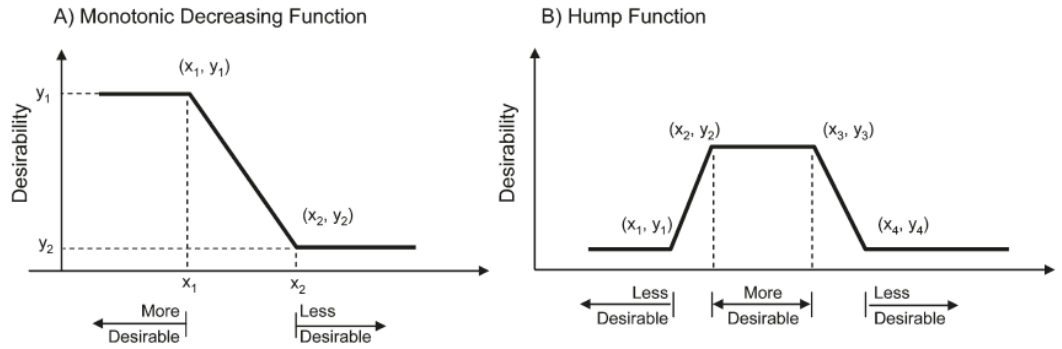

***Figure 8.1**. Monotonic Decreasing Function (left) and Hump Function (right) for the calculation of CNSMPO score.*

For the work herein, calculated physicochemical properties were obtained using standard commercial packages: Chemdraw for ClogP, ACD/Laboratories for ClogD at pH 7.4 and pK_a. For calculation of TPSA, see the protocol follow by Ertl *et al.*[123]

VIII.3.2 *In vitro* BBB analysis

VIII.3.2.1 Caco-2 cellular assay

VIII.3.2.1.1 Materials

All cell culture reagents and medium were obtained from Gibco (Life Technology, SAS Saint Aubin, France), except trypsin-EDTA solution (Biochrom AG, Berlin, Germany). All flasks were obtained from Corning (New York, USA). The Transwell Polycarbonate HTS 24-well plate inserts (0.33 cm^2 of surface area and 0.4 µm pore size) were obtained from Costar (Corning Incorporated, New York, USA).

VIII.3.2.1.2 Cell Culture

$4x10^5$ Caco-2 cells, at passage 026, were seeded on 25 cm^2 plastic flask in complete medium containing Dubelco's Modified Eagle's Medium (DMEM) high glucose (4500 mg/l) with L-glutamine (584 mg/L) supplemented by 10% of Fetal Calf/Bovine Serum, 1% of non-essential amino acids without L-glutamine and 1% of penicillin and streptomycin solution, which was changed every two days. After 3 days of incubation (37ºC and 5% of CO_2), when they cover 80-90% of the flask as a monolayer observed by microscope, the complete medium was removed and Caco-2 cells were rinsed twice with 10 mL of phosphate buffer solution (PBS). Then, Caco-2 cells were trypsinized with 2 mL of Trypsin-EDTA (0.05%) and seeded in a 75 cm^2 flask with a density of $5x10^5$ cells/cm^2 with 25 mL of complete medium.

After 6 days, Caco-2 cells reached high cells density (> $0.5x10^5$ cells/cm^2) and were then trypsinized giving a total volume of 13 mL in complete medium. The cells were seeded into cell HTS 24-well plates with 0.4 µm Polycarbonate membrane inserts at 75 000 cells/well (103 µL/well) in 0.4 mL of complete medium in every apical compartment and 24 mL in the total basolateral compartment. The cells were incubated (37ºC and 5% CO_2) for 21 days and the medium was renewed every two days.

VIII.3.2.1.3 Preparation of the samples

Samples were first dissolved in DMSO at an initial concentration of 10 mM. 12.5 µL of this stock solution were added to 5 mL of Ringer-HEPES (RH, transport buffer, pH 7.4) at 37ºC to give the final concentration of compound (25 µM; 0.25% DMSO). For A → B experiments, 100 µL of fluorescent molecule Lucifer yellow (LY, 10 mM) was added to reach the final concentration of 100 µM. For B → A experiments, a solution of LY 100 µM was prepared in 5 mL of RH buffer. Dissolution of compound **J** required the addition of 12.5 µL of DMSO (0.5% DMSO).and the use of an ultrasonic bath

VIII.3.2.1.4 Analysis of compounds: determination of LOD and LOQ

To measure the LOD and LOQ parameters, all compounds were analysed using tandem mass spectrometry. Instruments that were used included: mass spectrometer, LCT Premier XE (Waters); autosampler, Acquity Sample Manager; UPLC pump, Acquity Binary Solvent Manager (Waters). The following chemicals and reagents were used: ammonium formate (Sigma-Aldrich), methanol TOF gradient (Merck), water TOF gradient (Merck). Samples were stored in a freezer (-20ºC). Then, before the analysis, they were lyophilized and redissolved in 1:1 H_2O:MeOH in 2.5 mM ammonium formate.

For chromatography, the following system was used: analytical column, Acquity UPLC® BEH C_{18} 1.7 µm 2.1x100 mm (Waters); for mobile phase solutions of A 100% MeOH and B 100% H_2O in 5 mM ammonium formate each were prepared; Gradient, 10% A for 1 minute, 10-100% A for 5 minutes, held at 100% A for 1 minute and returned to initial condition in one step; flow rate of 0.3 mL/min; injection

volume of 10 µL (in full loop mode); leucine was used as reference for HRMS (m/z = 557.3812). Detections were performed simultaneously by UV (254 and 290 nm) and mass spectrometry.

*VIII.3.2.1.5 Transport experiment of new antioxidant compounds **A, B, C, D, E, F, G, I, J, L** and **N***

For A → B transport experiment, 0.2 mL of the compound assayed solution was placed on the apical side of the cells and samples were taken from the basolateral compartment. For B → A transport experiment, 0.8 mL of the solution was placed on the basolateral side of the cells and samples were taken from the apical side.

Cells were equilibrated for 20 minutes in transport buffer prior to the transport experiment and incubations with compounds were performed at 37ºC under agitation. After 1 hour aliquots were taken from each compartment (apical and basolateral) separately. The amount of LY was determined using a fluorescence spectrophotometer ($\lambda_{excitation}$ = 428 nm, and $\lambda_{emission}$ = 536 nm) Hitachi (Tokio, Japan) and all the compounds were determined by UPLC-MS in *Servei d'Espectrometria de Masses* in *Institut de Diagnòstic Ambiental i Estudi de l'Aigua (IDAEA-CSIC)* (Barcelona, Spain) following the same protocol than used in section VIII.3.2.1.4.

The apparent permeability coefficient (P_{app}) was determined according to the expression:

$$P_{app}(\cdot 10^{-6} cm/s) = \frac{J}{A \cdot C_0}$$

where *J* is the rate of appearance of the drug in the receiver chamber, C_0 is the initial concentration of the solute in the donor chamber and *A* the surface area of the filter.[131] The results were given with descriptive statistics (n, mean, SD, SEM) which were performed using Microsoft Excel software.

VIII.3.2.3 Passive diffusion penetration. PAMPA assay

VIII.3.2.3.1 Materials

Concentrated buffer solution was obtained from pION. The phospholipid mixture used was a porcine Polar Brain Lipid Extract (PBLE) with a composition of 12.6% phosphatidylcholine (PC), 33.1% phosphatidylethanolamine (PE), 18.5% phosphatidylserine (PS), 4.1% phosphatidylinositol (PI), 0.8% phosphatidic acid and 30.9% of other compounds.

*VIII.3.2.3.2 Evaluation of passive diffusion for of new antioxidant compounds **A, B, C, D, E, F, G, H, I, J, K, L, M, N**, Trolox and CR-6*

The PAMPA assay was used to determine the capacity of compounds to cross the BBB by passive diffusion. The effective permeability of these compounds was measured in triplicate at an initial concentration of 10 mM. The buffer solution was prepared from a concentrated one purchased by pION, following the manufacturer's instructions, and pH was adjusted to 7.4 using a 0.5 M NaOH solution. To dissolve the samples, 20% of 1-propanol was added to the buffer solution. The assayed compounds were dissolved in 1 mL of buffer solution to get the desired concentration (10 mM). The PAMPA sandwich was separated and the donor well was filled with 195 µL of the compound solution to be studied. The acceptor plate was placed into the donor plate, ensuring that the underside of the membrane was totally in contact with buffer. Then, 4 µL of the mixture of phospholipids (20 mg/mL) in dodecane were added to each filter and 200 µL of buffer solution to each acceptor well. The plate was covered and incubated at room temperature in a saturated humidity atmosphere for 4 hours under orbital agitation gutbox (UWL thickness of 25 µm). Then, 150 µL/well of the donor plate and 150 µL/well of the acceptor plate were transferred to HPLC vials. Propanolol was used as a positive control and, Trolox and CR-6 as samples.

100 µL of each sample (donor at initial time, donor and acceptor after 4 hours) were injected in a HPLC reverse phase model HP 1100 (Waters) connected to a C_{18} column KROMASIL 100 (150 mm x 4.6 mm x 5 µm, Scharlau). The transport was also confirmed by UPLC-MS at aliquots of acceptor wells (gradient from 10 to 100% of CH_3CN and water with 20 mM formic acid, at rate flow 0.3 mL/min in Acquity UPLC® BEH C_{18} 1.7 µm 2.1x100 mm analytical column from Waters).

The percentage of transport after 4 hours was calculated as the effective permeability, using the following expression:

$$P_e(cm/s) = \frac{-218.3}{t} \log\left[1 - \frac{2C_A(t)}{C_D(t_0)}\right] x10^{-6}$$

where *t* is time (hours), $C_A(t)$ and $C_D(t_0)$ represent the concentration of compound assayed at the acceptor well at time *t* and at the donor well at time *0*, respectively.[38]

VIII.3.2.4 In vitro BBB bovine co-culture model

VIII.3.2.4.1 Materials

Cell culture medium DMEM supplemented by 10% (v/v) of foetal calf serum (FCS) inactivated and cell culture medium DMEM supplemented by 10% of calf serum inactivated (CS) and 10% of horse serum inactivated (HS) were purchased from se Invitrogen Corporation, UK. 12-well plate of

polycarbonate inserts Transwell for HTS (12 mm of diameter and 0.4 µm of porous size) were obtained from Costar.

VIII.3.2.4.2 Rat glial cell cultures

Primary cultures of glial cells were isolated from new-born rat cerebral cortex. After removal of the meninges, the brain tissue was gently forced through a nylon sieve, as described by Booher and Sensenbrenner.[147] Glial cells were plated onto 12-well plates at a concentration of $1.2x10^5$ cells/mL in 1.5 mL of medium containing DMEM supplemented with 10% (v/v) heat inactivated Fetal Calf Serum (FCS) (Invitrogen corporation, UK), 2 mM L-glutamine and 50 µg/mL gentamicin, which renewed twice per week. Three weeks after plating, glial cells were stabilized and prepared to be used in co-culture with Brain Capillary Endothelial Cells (BCEC). The glial cells were characterized giving the following population: 60% astrocytes/20% oligoendrocytes/20% microglia.

VIII.3.2.4.3 Bovine brain capillary endothelial cells (BBCECs)

BBCECs were isolated and characterized as described by Méresse *et al*. The use of cloned endothelial cells allows us to obtain highly pure endothelial cell population without contaminating pericytes.[148] BBCECs were cultured on gelatine coated Petri dished in DMEM supplemented with 10% of heat inactivated new-born Calf Serum (CS) and 10% heat inactivated Horse Serum (HS) (Invitrogen corporation, UK), 2 mM L-glutamine, 50 µg/mL gentamicin and 1ng/mL basic Fibroplast Growth Factor (bFGF). BCECs were used up to passage 7.

VIII.3.2.4.4 Co-culture of BBCECs and glial cells

BBCECs were cultured on collagen-coated filter inserts (12-wells Transwell Insert 0.4 µm pore size, 12 mm diameter, Costar, Corning Incorporated, New York, USA). The filter inserts were coated on the upper side with rat tail collagen prepared by a modification of the method of Bornstein.[149] Collagen-coated filter inserts were placed into 12-well plates containing glial cell cultures. BBCECs ($4x10^5$ cells/mL) were plated on the upper side of the filter insert. The co-culture medium was DMEM supplemented with 10% (v/v) CS, 10% HS, 2 mM L-glutamine, 50 µg/mL gentamicin and 1 ng/mL bFGF. The medium was changed every two days. After 7 days in co-culture, BCECs reached the confluence, but they were grown another 5 days to form a tight barrier.

[147] Booher, J.; Sensenbrenner, M. *Neurobiol.* **1972**, *2*, 97-105.
[148] Méresse, S.; Dehouck, M.P.; Delorme, P.; Bensaïd, M.; Tauber, J.P.; Delbart, C.; Fruchart, J.-C.; Cecchelli, R. *J. Neurochem*. **1989**, *4*, 1363-1371.
[149] Bornstein, M.B.; Murray, M.R. *J.Biophys. Biochem. Cytol.* **1958**, *4*, 499-504.

VIII.3.2.4.5 Experimental setup

The preparation of stock solution was carried out following the section VIII.3.2.1.3. Then from a concentration of compound of 10 mM in DMSO, 10 mL of solution at 10 µM in the buffer Ringer-HEPES (0.1% DMSO) were prepared. In this experiment, 50 µL of 10 mM LY were added at each sample to have a final concentration of 50 µM.

VIII.3.2.4.6 Transendothelial permeability of BBCEC monolayer

The experiments were carried out in buffered Ringer-HEPE's solution at pH 7.4 on a rocking platform at 37ºC. Prior to the transport experiments, cell monolayers were stabilized with buffered Ringer-HEPES's solution for 20 minutes. At the initiation of the experiment, 1.5 mL of buffer was added into wells of 12-well plate in the receiver compartment. Then, inserts, containing confluent monolayers of BBCEC, were subsequently placed inside these wells and 0.5 mL of solution of compound was added over there as donor compartment. The experiment was repeated in triplicate for each compound. After 60 minutes in rotatory agitation, aliquots were taken from each compartment, donor and receiver. The amount of LY was quantified by fluorescence as an indicator of the integrity of the cell monolayer. The amount of tested compounds was analysed by UPLC-MS following the same conditions as in section VIII.3.2.1.4.

VIII.3.2.4.7 Data analysis and calculations

The cleared volume (µL) was calculated, as described by Siflinger-Birnboim *et al.*, by dividing the amount of compound in the receiver compartment ($C_R \cdot V_R$) by the concentration of compound in the donor compartment (C_D), following the expression:[142]

$$Clearance(\mu L) = \frac{C_R \cdot V_R}{C_D}$$

The average cumulative volume cleared was plotted versus time (0 and 60 min) to give a line where the slope and its standard deviation were estimated by linear regression analysis. The slope of the clearance curve with inserts alone and inserts with BBCEC monolayers is equal to PS_f and PS_t, respectively, where *PS* is the residue between the permeability and the surface area. The units of *PS* and *S* are µL/min and cm^2, respectively. The PS-value for endothelial monolayer (PS_e) was obtained following the expression:

$$\frac{1}{PS_e} = \frac{1}{PS_t} - \frac{1}{PS_f}$$

To obtain the endothelial permeability coefficient, P_e (10^{-3} cm/min), the PS_e-value was divided by the surface area of the insert (1.13 cm^2).

Descriptive statistics (n, means, SD, SEM) and statistical analyses were performed using Microsoft Excel software for Windows.

VIII.4 TOXICITY

VIII.4.1 MTT assay

VIII.4.1.1 Materials

3-[4,5-Dimethylthiazol-2-yl]-2,5-diphenyl tetrazolium bromide (MTT) and DMSO were purchased from Sigma-Aldrich. 10 mM Stock solutions of compounds in DMSO were stored at -20 ºC, and freshly diluted with medium to the appropriate concentrations before use in experiments. 5 mg/mL Stock solution of MTT in PBS (GIBCO) was stored at 4 ºC.

VIII.4.1.2 Cell culture

Two human breast adenocarcinoma cell lines, MDA-MB-231 and MDA-MB-468, were purchased from the America Type Culture Collection (ATCC). Both cancer cell lines were grown as monolayer in 75-cm^2 tissue culture flasks (Sigma) in DMEM media (Sigma) supplemented with 10% v/v foetal bovine serum, and 100 ng/mL each of penicillin and streptomycin. The cell lines were maintained in a humidified, 5% CO_2 incubator at 37ºC, and sub-cultured when reached confluence (3-4 days) using 0.25% v/v trypsin/EDTA (GIBCO). All experiments were performed using cells in exponential growth phase from passage 10 to 30.

*VIII.4.1.3 Assay of MTT Toxicity for new antioxidant compounds **A, B, C, D, E, F, G, H, I, J, K, L, M** and **N** in MBA-MB-231 and MBA-MB-468 cell lines*

MDA-MB-231 or MDA-MB-468 cells were seeded at a density of 104 cells/well on a 96-well microplate in fresh media (100 µL/well), and grown overnight at 37ºC and 5% CO_2-water saturated atmosphere. The growth medium was next removed, and wells were treated with 100 µL of test compounds or DMSO at the indicated concentrations at 37ºC. After 24 hours, 10 µL of 5 mg/mL of MTT solution in PBS were added to each well and incubated at 37 ºC for 3 hours. After removal of the MTT-containing medium, 100 µL of DMSO were added to each well to dissolve the formazan crystals. After 30 min, the absorbance at 570 nm was determined using a Spectramax M5 (Molecular Devices) at 25 ºC. Control wells were included, which contained cells treated with MTT. Live cells (%) were calculated using the following equation: $(A_{test}/A_{control})*100$, where A_{test} and $A_{control}$ represent the absorbance readings from the drug-treated wells and the control wells, respectively.

The assay was performed by triplicate for each condition, and data values were reported as mean ± SD.

IX. Abstract

Oxidative stress is one of the most important factors in degenerative diseases like cancer, Alzheimer or in episodes like ischemia. During these processes, reactive species of oxygen (ROS) and nitrogen (RNS) are generated.[1,4,9] This fact can cause the chemical modification of important biomolecules, in particular lipids and proteins.[6] The strategy that involves the use of antioxidants and neuroprotective agents to fight against the lesive effects of these species stumbles over the blood-brain-barrier (BBB). This barrier protects the brain from the action of a wide variety of organic molecules and drugs.[36,55, 51] Thus, it is important to develop novel antioxidant agents with good delivery through the BBB.

In our group it was discovered the antioxidant agent 3,4-dihydro-2,2-dimethyl-7-metoxy-1-(2*H*)-benzopyran (CR-6),[¡Error! Marcador no definido.] an analogue of α- and γ-tocopherols (Figure 3.1),[15,¡Error! Marcador no definido.] which is currently used in dermopharmacy and it is also in a phase II trials for anticancer treatment (combined with other drugs). In our present project, one of the main goals is the synthesis of a short library of CR-6 analogues that could improve the pass through the BBB.

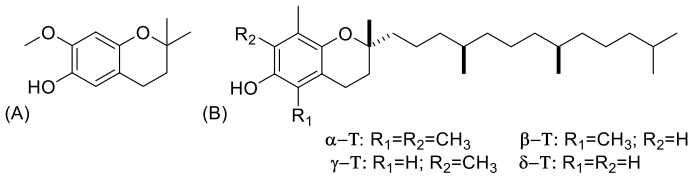

Figure 3.1 *a) Structure of CR-6. b) Structure of natural tocopherols.*

Accordingly, fourteen novel CR-6 analogues have been synthesised. The antioxidant activity of these new derivatives has evaluated by conventional cellular and non-cellular *in vitro* models. Hence, the antioxidant activity did not vary comparing to CR-6 using a non-cellular assay even though the incorporation of different structures at C_2 position. In contrast, in cellular assays, it was observed more variability due to the biological enviroment.

In addition, their permeability through the BBB has been assayed using an *in vitro* bovine model in collaboration with Prof. Romeo Cecchelli's group (University of Artois in Lens, France). It has been demonstrated that some compounds exhibited a moderate BBB permeation. This permeability might be possible to a facilitative or active influx transport.[32] Moreover, the passive diffusion assays in collaboration with Dr. Meritxell Teixidó Tura (Parc Científic de Barcelona) showed that some CR-6 analogues had better transport than CR-6.[38]

X. Spanish summary

X.1 INTRODUCCIÓN

El estrés oxidativo es uno de los factores etiológicos y de progresión más importantes en muchas enfermedades neurodegenerativas como el Alzheimer o el cáncer, y es la consecuencia de lesiones neurológicas en episodios de isquemia cerebral y trombosis, dañando las células y provocando su muerte. Durante el proceso de estrés oxidativo se genera una gran cantidad de especies reactivas de oxígeno (ROS) y de nitrógeno (RNS) que provocan la oxidación de biomoléculas como el ADN, las proteínas y los lípidos dando lugar a la oxidación de nucleótidos, a la modificación en la estructura terciaria de las proteínas y alteraciones en su función, o bien a la degradación de membranas lipídicas. Alguna de estas especies reactivas son subproductos habituales en reacciones fisiológicas celulares, como la producción del radical superóxido ($O_2^{\cdot-}$) durante el proceso de respiración celular, y que, a baja concentración, desarrollan funciones en la señalización celular y en la transducción de la señal. En estado normal, existen varios sistemas de defensa que actúan para reducir la sobreproducción de ROS y RNS. Pero una alteración en el sistema puede llevar a la acumulación de estas especies reactivas.[5,6,8]

El término de ROS engloba especies radicalarias como el radical superóxido ($O_2^{\cdot-}$), el hidroxilo ($^{\cdot}OH$), el peróxido ($RO_2^{\cdot}$) y el alcóxido ($RO^{\cdot}$), pero también ciertas especies no radicalarias con carácter oxidante como el peróxido de hidrógeno (H_2O_2), el ozono (O_3), el oxígeno singlete ($^1O_2$) y el ácido hipocloroso (HOCl). De la misma manera, RNS incluye diversos radicales de óxido de nitrógeno ($NO^{\cdot}$ y $NO_2^{\cdot}$) y el anión peroxinitrito ($ONOO^-$), entre otros (Figura 10.1). De todas estas especies reactivas, H_2O_2, $NO^{\cdot}$ y $O_2^{\cdot-}$ reaccionan rápidamente con determinadas moléculas; por el contrario, el radical $^{\cdot}OH$, reacciona rápidamente con casi cualquier molécula. El resto de radicales libre tienen una velocidad de reacción intermedia. El radical hidroxilo ($^{\cdot}OH$) está considerado el radical libre más reactivo.

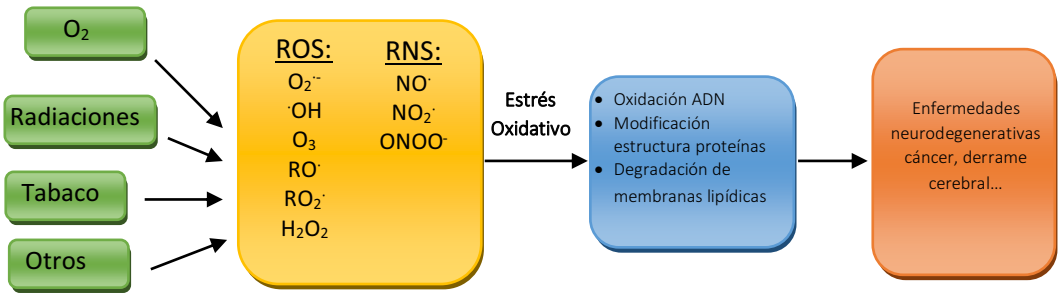

Figura 10.1. *Esquema del proceso de generación de especies reactivas de oxígeno (ROS) y de nitrógeno (RNS), el estrés oxidativo causado por acumulación de estas especies y la aparición de enfermedades debido a este proceso.*

Procesos bioquímicos o mecanismos endógenos que se dan en el propio organismo pueden dar lugar a la generación de las especies reactivas (Figura 10.1). El proceso de respiración cellular, como se mencionó anteriormente, y la autooxidación de algunas moléculas (neurotransmisores como la dopamina y la adrenalina) en presencia de oxígeno, son ejemplos de procesos bioquímicos que generan el radical

$O_2^{\cdot-}$. De hecho, se ha estimado que entre 1-3% del oxígeno molecular que se respire se convierte en radical superóxido, lo que significa generar más de 2 kg de $O_2^{\cdot-}$ al año.

No obstante, no solamente existe la producción de radicales libres mediante mecanismos endógenos o procesos bioquímicos. Una gran variedad de fuentes antropogénicas como radiaciones (rayos X, γ y UV), una dieta rica en grasas y el tabaco, entre otros, generan en el organismo muchas especies reactivas.

La neutralización de ROS y RNS, y la reducción de sus efectos negativos se lleva a cabo mediante mecanismos antioxidantes endógenos o exógenos que se adquieren con una dieta sana. Desafortunadamente, en numerosas ocasiones no es suficiente y puede conllevar a la acumulación de aquellas especies y al estrés oxidativo.

Se conoce que el cerebro, debido a la alta actividad metabólica, necesita grandes cantidades de oxígeno y que su carencia (por ejemplo en un episodio de isquemia), activa un mecanismo en el que se generan grandes cantidades de especies ROS y RNS provocando lesiones neurológicas permanentes. Así, el estrés oxidativo tiene un papel muy importante en la patogénesis de varias enfermedades neurodegenerativas, siendo un factor etiológico de primer orden de las lesiones provocadas durante el proceso de reperfusión, posterior a un estado temporal de isquemia.

Un derrame cerebral, debido a un episodio de isquemia, puede dar lugar a la pérdida importante de función cerebral y la posterior muerte. Este episodio es la causa más importante de pérdida de función en adultos y la segunda causa más importante de muerte en los países occidentales. La hipertensión, la edad, la diabetes, el elevado nivel de colesterol en sangre y el tabaco son factores de riesgo importantes que pueden conllevar a un derrame cerebral.

Muchos agentes antioxidantes han demostrado tener mecanismos de neuroprotección en ensayos experimentales en cerebro isquémico. Estos antioxidantes actúan inhibiendo la producción, neutralizando las especies radicalarias o bien incrementando la velocidad de degradación de ROS y RNS. En estudios preclínicos en procesos de isquemia/reperfusión se ha demostrado que el uso de agentes antioxidantes aporta efectos beneficiosos y que tiene un papel protector de la lesión cerebral neutralizando la acción de los radicales que se generan y así reduciendo las lesiones provocadas durante la reperfusión.

De entre los agentes antioxidantes que neutralizan a las especies reactivas, un grupo importante son los fenoles. Su poder de actuación se debe a la facilidad de transferencia del átomo de hidrógeno fenólico a los radicales libre, como el $^{\cdot}OH$, formando el radical ariloxi estabilizado por resonancia, el cual es cinéticamente incapaz de continuar con la reacción radicalaria en cadena.[8] Este tipo de antioxidantes se pueden dividir en dos grandes grupos:[8] los polifenólicos como los flavonoides, los estilbenos, el resveratrol, la curcumina y las hidroquinonas; y los monofenólicos o fenoles simples como los tocoferoles o vitamina E, los tocotrienoles, el trolox, el 17β-estradiol (estrógeno), 5-hidroxitriptamina (serotonina) y derivados de la tirosina.

La vitamina E es uno de los antioxidantes naturales más potentes.[5] Está constituida mayoritariamente por tocoferoles y tocotrienoles. Los tocoferoles tienen una estructura común de cromano y una cadena lateral hidrocarbonada. La vitamina E está formada por cuatro tocoferoles diferentes: el α-, el β-, el γ- y el δ-tocoferol, dependiendo de los sustituyentes en el anillo aromático de la estructura de cromano (Figure 10.2).

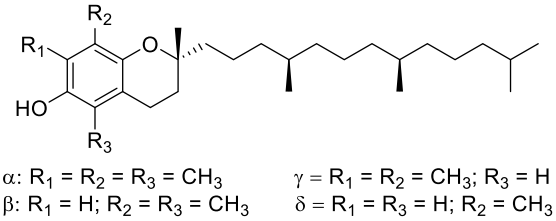

Figura 10.2. *La vitamina E está compuesta por una mezcla de cuatro tocoferoles diferentes (α-, β-, γ- y δ-tocoferol), dependiendo de los sustituyentes en el anillo aromático de cromano.*

En la actualidad, se conocen agentes antioxidantes que podrían actuar como neuroprotectores en el cerebro. Desafortunadamente, los agentes neuroprotectores ensayados no son capaces de demostrar efectos beneficiosos en las fases clínicas II y III aunque sí hayan demostrado buenos resultados preclínicos. Se piensa que el problema se debe a la administración del agente neuroprotector como fármaco en humanos, que en muchas ocasiones requiere la combinación con agentes antitrombolíticos.[12] El tratamiento más efectivo en la actualidad para el derrame cerebral en un cerebro post-isquémico es el activador plasminógeno de tejido recombinante (rtPA). No obstante, este tratamiento es solamente beneficioso hasta las 4.5 horas posteriores del accidente cerebral.

Hace unos años, en nuestro grupo de investigación se desarrolló el 3,4-dihidro-2,2-dimetil-7-metoxi-1-*(2H)*-benzopirano (CR-6), como un agente antioxidante análogo estructural de los tocoferoles, que neutraliza con eficacia las especies ROS y las RNS (Figura 10.3).[16,150] Actualmente, el CR-6 se utiliza en el área de la dermofarmacia y la dermocosmética, y se encuentra en la fase clínica II como medicamento para el tratamiento del cáncer (combinado con otros fármacos).

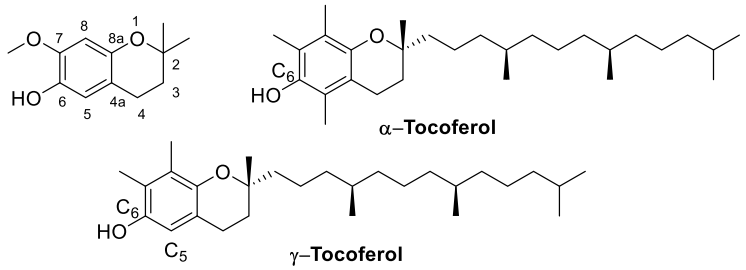

Figura 10.3. *Arriba a la izquierda está el compuesto CR-6 con la numeración de sus carbonos; a la derecha, el α-tocoferol; y en la parte inferior de la figura el γ-tocoferol. En α- y γ- tocoferol están indicados las partes de la molécula que participan en la neutralización de especies reactivas ROS y RNS.*

[150] Casas, J.; Gorchs, G.; Sánchez-Baeza, F.; Teixidó, P.; Messeguer, A. *J. Agric. Food. Chem.* **1992**, 40, 585-590.

Ensayos *in vitro* del CR-6 realizados en células neuronales demostraron que este antioxidante actúa como captador de especies ROS mediante mecanismos radicalarios, por la cesión del hidrogeno fenólico, y como captador de RNS debido a las dos posiciones libres y activadas del anillo aromático (C_8 y C_5), que permiten la reacción con compuestos como el NO. Se han realizado estudios en los que se ha detectado el compuesto CR-6 nitrado en la posición 5, lo que indica que en presencia de NO el CR-6 reacciona regioselectivamente dando lugar a un compuesto estable, y se demuestra su poder captador de especies RNS.[15,59] Por ello el CR-6 se considera un análogo de α- y γ-tocoferol (Figura 10.3).

A partir de la alta actividad del CR-6 se establecieron dos colaboraciones con la Dra. Anna Planas del IIBB-CSIC en Barcelona y con el Prof. Thomas Cotter de la Universidad de Cork en Irlanda, para profundizar en dos aplicaciones potenciales para el CR-6.

Por un lado, con la Dra. Planas se realizaron ensayos *in vivo* en ratón donde se observó que el agente antioxidante sintético CR-6 llega al cerebro aunque de manera poco eficiente. A pesar de ello, proporciona un efecto neuroprotector en los procedimientos de isquemia/reperfusión, pero no en los de isquemia permanente, debido a que inhibe las lesiones provocadas durante el proceso de reperfusión.

Con el Prof. Cotter, se observó que el tratamiento con CR-6 disminuía los efectos negativos provocados por el proceso de estrés oxidativo durante la apoptosis en células 661W (línea celular de fotoreceptores murina), de interés en enfermedades degenerativas oculares. No obstante, pese a que reduce la formación de ROS, CR-6 no previene la activación de la caspasa mediante procesos mitocondriales.

Pese a estas potenciales aplicaciones del CR-6, su actividad en el cerebro no era suficiente. Se pensó que esto se debía a que atravesaba con dificultad la barrera que separa el cerebro del flujo sanguíneo.

La barrera hematoencefálica (BBB),[29,27] a diferencia de las barreras endoteliales de los órganos que se encuentran en la periferia, es una membrana formada por un sistema complejo de capilaridad endotelio-cerebral en el que existen unas proteínas de unión muy estrechas de unión entre las células endoteliales que la forman y una capa posterior que la envuelve, formada por células gliales, como los astrocitos, y por los pericitos. De esta manera, la BBB es una barrera física que restringe la entrada de toxinas y muchas moléculas orgánicas desde el flujo sanguíneo al cerebro y mantiene la homeostasis cerebral. No obstante, es un obstáculo para el transporte efectivo de muchos fármacos al sistema nervioso central (SNC), Figura 10.4.

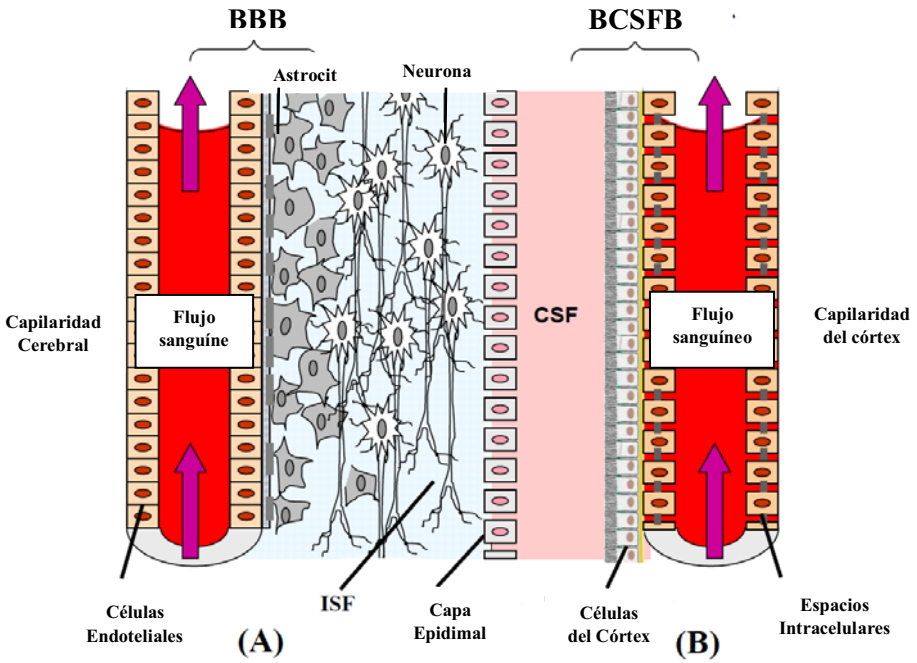

Figura 10.4. La Barrera Hematiencefálica (BBB, (A)) y la Barrera Hemato-fluido cerebroespinal (BCSFCB, (B)). La BBB es una membrana impermeable que ocupa la mayor parte del cerebro y espina dorsal separando el cerebro del flujo sanguíneo. La BBB está constituida por una membrana basal y diferentes tipos de células en el fluido interticial (ISF). En cambio, la BCSFB es mucho más permeable con más separaciones entre las células endoteliales que permite la penetración de más sustancias; pero ocupa un área más pequeña del cerebro. Esta figura se ha extraído de la publicación de Pavan et al

Un bajo porcentaje de moléculas pequeñas e hidrosolubles pueden atravesar por difusión paracelular las uniones estrechas que existen entre las células endoteliales de la BBB. Las demás moléculas, más grandes e/o hidrosolubles, deben atravesar la BBB vía transcelular. Existen diversos mecanismos de transporte transcelular a través de la BBB que se clasifican en transporte pasivo y transporte activo. El transporte pasivo es aquel en el que no se requiere de un aporte energético para realizarlo, simplemente una diferencia de concentración entre los lados de la barrera provoca que las moléculas viajen. Moléculas pequeñas con propiedades lipófilas viajan al interior del cerebro sin necesidad de un mecanismo endógeno mediante difusión pasiva a través de la membrana lipídica. Otras moléculas pequeñas pero más hidrofilias requieren una difusión facilitada por proteínas de membrana . El transporte activo, en cambio, es aquel que requiere de energía.[28,29]

Tanto la difusión facilitada como el transporte activo son mecanismos endógenos de transporte que permiten el intercambio de moléculas orgánicas entre el cerebro y el flujo sanguíneo. La mayor parte de los compuestos no pueden penetrar por difusión pasiva y necesitan de transportadores endógenos para poder atravesar la BBB y llegar al cerebro. Las moléculas de peso molecular bajo utilizan un sistema facilitado por transportadores o “carriers” (CMT). Por otro lado, moléculas grandes (como péptidos o proteínas) penetran al cerebro mediante transcitosis a partir del reconocimiento molecular mediado por receptores (RMT) de membrana o mediante absorción por interacción electrostática con las células cerebrales.[28,29]

Existen también mecanismos activos de eflujo, como las glicoproteínas P (P-gp), que realizan el transporte en sentido contrario desde el interior del cerebro al flujo sanguíneo obstaculizando la penetración de muchas moléculas orgánicas.[28,29]

En la Figura 10.5 se ilustran los mecanismos de transporte más habituales en la BBB: el transporte paracelular que mayoritariamente está restringido, la difusión pasiva, el CMT, el RMT, la absorción mediante transcitosis y las bombas de eflujo.

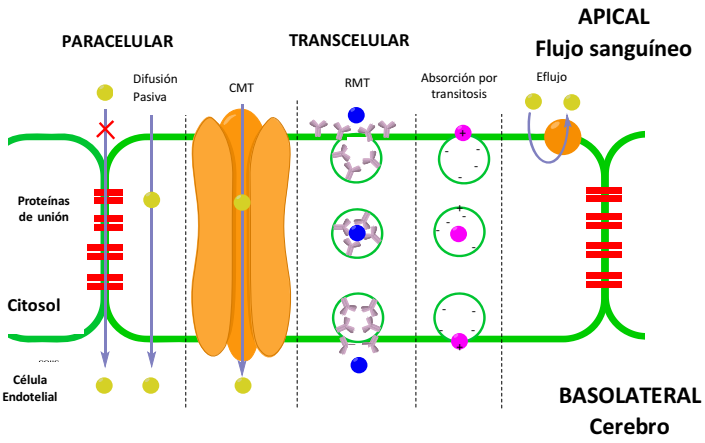

Figura 10.5. *Mecanismos de transporte más habituales en la BBB: el transporte paracelular que mayoritariamente está restringido, la difusión pasiva, el transporte mediado por "carriers" (CMT), el transporte mediado por receptores (RMT), la absorción mediante transcitosis y las bombas de eflujo.*

En la actualidad existen fármacos efectivos para el tratamiento de enfermedades neuronales, pero la mayoría tienen una aplicación limitada debido a la baja distribución en el cerebro o a la incapacidad por cruzar la BBB. Por ello, para poder administrar este tipo de fármacos se han estado utilizando métodos invasivos y lesivos para el órgano y organismo, como la apertura temporal de la BBB o la inyección directa del fármaco en la espina dorsal. Estos inconvenientes han conducido al desarrollo de nuevos métodos menos dañinos.[37]

Aunque inicialmente son métodos muy utilizados en biomedicina, aumentar la lipofilia u obtener fármacos que mimeticen substancias que se conoce que pasan la BBB no han acabado siendo métodos muy efectivos. Por un lado, pueden ser absorbidos por otros órganos diferentes al cerebro siendo necesarias dosis muy altas de fármaco y, por otro lado, pueden disminuir el anclaje al sitio activo debido a la modificación estructural del fármaco original, disminuyendo la actividad biológica.

En este mismo contexto, en los últimos años se ha estudiado el desarrollado de conjugados de compuestos terapéuticos con moléculas que se conoce que penetran la BBB y actúan como transbordadores. En muchos casos, la conjugación también mejora la solubilidad del fármaco en medio fisiológico.[38] Teixidó *et al.* desarrollaron una serie de 2,5-dicetopiperazinas (DKP) capaces de actuar como transbordadores de fármacos por difusión pasiva.[37] Más tarde, Gynther *et al.* sintetizaron conjugados de fármacos sin transporte en la BBB con nutrientes esenciales como la glucosa o amino ácidos y estudiaron

su transporte a través de mecanismos de difusión facilitada.[44] A estos compuestos que ayudan a mejorar la penetración les llamaron "BBB-shuttle".

X.2 OBJETIVOS

Con estos antecedentes bibliográficos y el trabajo previo en el grupo de investigación para la obtención de un agente antioxidante potente, el principal objetivo de la presente tesis era la preparación de conjugados análogos de CR-6 con nutrientes esenciales para mejorar la biodisponibilidad en el cerebro de este compuesto mediante difusión pasiva, facilitada o transporte activo, y que mantengan su capacidad antioxidante.

De esta manera, se quieren aprovechar, entre otros, los transportadores LAT-1 (Transportador 1 de Aminoácidos del tipo L) o el GLUT-1 (Transportador 1 de Glucosa) que son transportadores endógenos de aminoácidos y de glucosa, respectivamente. La variabilidad en el anillo de cromano del CR-6 se introduciría mediante la conjugación con nutrientes esenciales en la posición C_2. Debido a requerimientos sintéticos, todos los compuestos a sintetizar se dividieron en tres familias dependiendo de la ruta sintética que seguían.

En la Figura 10.6 se muestran las estructuras de los 14 compuestos propuestos separados por familias.

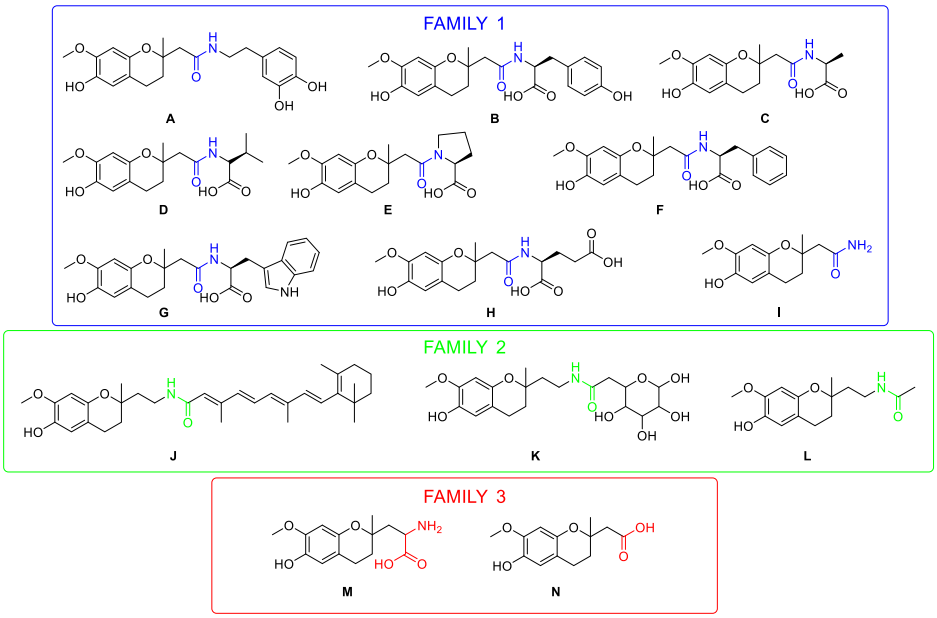

Figura 10.6. *Estructuras de los 14 derivados del CR-6 propuestos para ser sintetizados mediante la estrategia del acoplamiento de nutrientes esenciales para el cerebro en la posición C_2 del anillo de cromano.*

Una vez sintetizados estos compuestos se debería comprobar la actividad antioxidante de los derivados de CR-6 que se mantenga, o mejore.

Por otro lado, la planteó de ensayos *in vitro* para evaluar la penetrabilidad de estos compuestos a través de la BBB.

También, y debido a la presencia de un estereocentro en la posición C_2 común para todos los compuestos a sintetizar, el estudio de la separación de los estereoisómeros de los compuestos con una actividad biológica mayor sería interesante para valorar qué estereoisómero proporciona mejor actividad.

X.3 RESULTADOS Y DISCUSIÓN

X.3.1 Síntesis de análogos del CR-6 y estudio de su preparación estereoselectiva

X.3.1.1 Síntesis de análogos del CR-6·

Una vez evaluada la retrosíntesis de los compuestos se plantearon tres rutas sintéticas diferentes con dos intermedios clave: el éster **1** y el alcohol **2**. A su vez, la preparación del ácido **6** y de la amina **18** eran claves para la formación de los conjugados mediante enlace de acoplamiento peptídico.

Así, la síntesis se inició en dos compuestos comercialmente disponibles: la vinilcetona y la metil hidroxiquinona. La reacción tuvo lugar en presencia de ortoformiato de trimetilo y ácido sulfúrico para dar lugar al acetal **4** con un rendimiento del 79%. La neutralización con una solución NaOH no impediría que se formase el sub-producto hemiacetal **4a**. Seguidamente el fenol se tuvo que proteger para evitar posibles reacciones adversas debido a la basicidad del hidrógeno fenólico (pk_a = 10-11). Se probaron distintos agentes protectores, y la protección en forma de bencilo fue finalmente la seleccionada (Figura 10.7).

La reacción del acetal **4** con bromuro de bencilo en presencia de hidruro de sodio y seguida de hidrólisis ácida, dio lugar al hemiacetal **5** con un rendimiento del 88%. El hemiacetal **5** se encuentra en equilibrio ceto-enólico entre la forma cerrada (**5a**) y la abierta (**5b**), que es más abundante. Posteriormente, la obtención del éster **1** con un 84% de rendimiento se realizó mediante una reacción de Honer-Wadsworth-Emmons (HWE) con fosfonoacetato de trimetilo y NaH. A partir de aquí la ruta se dividió en dos (Figura 10.7).

La síntesis de los compuestos en la Familia 1 se efectuó mediante del acoplamiento del ácido **6** con diversas aminas comerciales (dopamina, metil L-tirosina, metil L-alanina, metil L-valina, bencil L-prolina, bencil L-fenilalanina, metil L-triptofano, metil L-glutamina y amoníaco). Primero la hidrólisis en medio básico del éster **1** facilitó la formación del ácido derivado **6**. A partir de este ácido se sintetizaron los compuestos **7**-**15** con rendimientos entre 27-80% mediante un acoplamiento en presencia de EDC·HCl, HOBt y DiPEA. El compuesto derivado de L-glutamina no dio resultados positivos siguiendo la misma metodología de acoplamiento de enlace peptídico que en los otros casos. Después de probar varias posibilidades, se obtuvo el derivado **14** con un rendimiento del 40% usando DCC y DMAP (Figura 10.7).

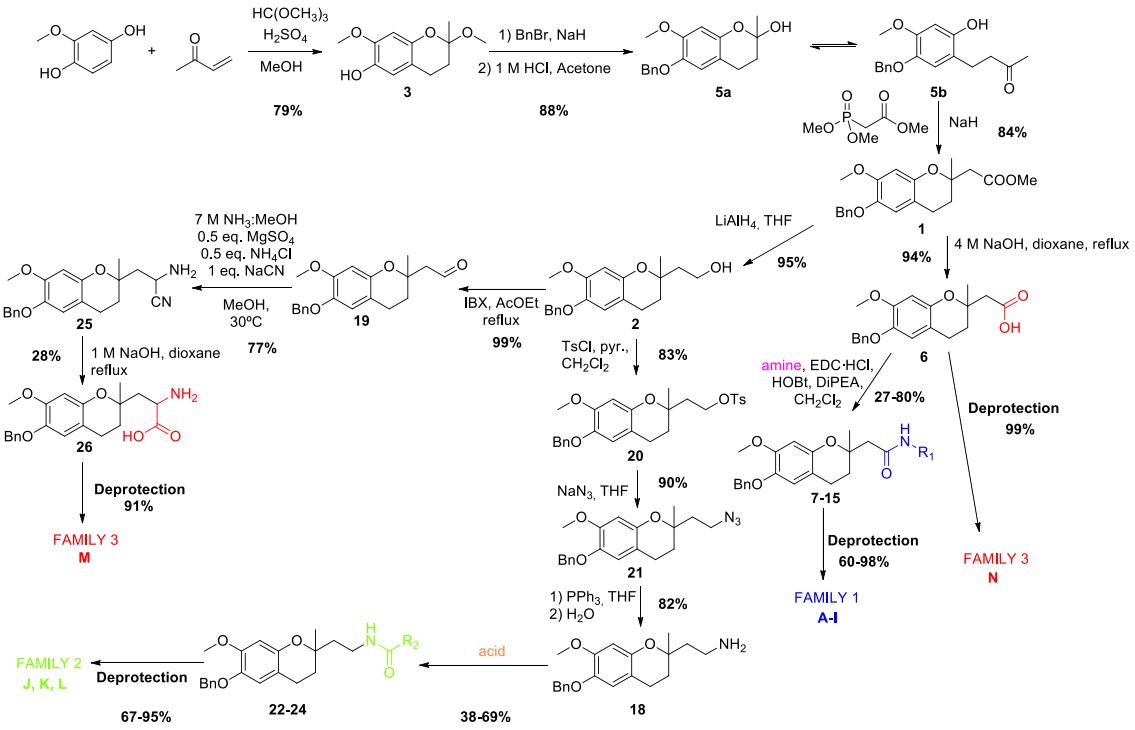

Figura 10.7. *Ruta sintética seguida para síntesis de los 14 derivados del CR-6 propuestos. La ruta se dividió en tres para dar lugar a las tres familias de compuestos. Los compuestos éster **1** y alcohol **2** son intermedios comunes, y el ácido **6** y la amina **18** intermedios clave.*

La desprotección del éster metílico en medio básico y la desprotección del bencilo por hidrogenación a 1-2 atmosferas de H_2 y catalizador de Pd/C al 10% en peso, generaron los compuestos de la Familia 1 (**A**-**I**), con rendimientos del 61-93% para la desprotección del ácido carboxílico, y del 50-99% en la desprotección del bencilo. En este punto se observó que la amida terminal del derivado de L-glutamina se había hidrolizado a ácido carboxílico, posiblemente durante la hidrólisis del ester metílico, siendo ahora el derivado de L-glutamato (**H**). Como el glutamato es uno de los nutrientes esenciales más presente en el cerebro, para los estudios de la permeabilidad de membrana no importaba tener el derivado de L-glutamina o L-glutamato (Figura 10.7).

El éster **1** se redujo a alcohol primario con hidruro de aluminio y litio ($LiAlH_4$) para dar lugar al intermedio **2** con un 95% de rendimiento. A partir del alcohol **2** se sintetizaron los compuestos de la Familia 2. Primero, se protegió el alcohol primario en forma de tosilato con cloruro de tosilo y piridina en CH_2Cl_2, y se obtuvo el tosilato **20** con un rendimiento del 83%. Después, la azida **21** se obtuvo con un rendimento del 93% al reaccionar el tosilato **20** y la azida sódica (NaN_3). Una vez estudiada la manera de obtener la amina **18**, se preparó a partir de la reacción de Staudinger. Primero la azida reaccionó con la trifenil fosfina y pasadas unas horas se le añadió agua para parar la reacción. La amina **18** se obtuvo pura con un rendimiento del 82%. Siguiendo los pasos de la Familia 1, los derivados de la Familia 2 se obtuvieron por acoplamiento mediante el enlace peptídico de la amina **18** con ácidos comerciales. Pero en este caso cada derivado siguió su propia ruta (Figura 10.7).

Por un lado, el derivado de retinol necesariamente necesitaba reaccionar con la amina **18** desprotegida en el bencilo, ya que el retinol, debido a la elevada conjugación de su estructura, no se podía someter a una hidrogenación. Así que se desprotegió la amina **18** por hidrogenación (58%) y se realizó el acoplamiento con el ácido retinóico en presencia de EDC·HCl y DiPEA, para obtener el derivado **J** (38%).

El ácido (3,4,5,6-tetrahidroxi-tetrahidropiran-2-il)acético se utilizó para preparar el derivado de D-glucosa. Debido a la interacción de los hidroxilos del anillo en el acoplamiento con la amina **18**, se tuvo que proteger en forma de acetilo con Ac_2O y I_2, para obtener el intermedio **23a** (82%). Este intermedio tenía un grupo anhídrido y, debido a que por sí solo era suficientemente reactivo para la formación del acoplamiento peptídico, no se requirió de ningún agente acoplante. De este modo, el intermedio **23a** reaccionó con la amina **18** en CH_2Cl_2 para dar lugar al intermedio **23** con un rendimiento del 55%. Seguidamente, se desprotegieron los acetilos con una solución al 25% de metóxido sódico en metanol (NaOMe/MeOH) que dio lugar al intermedio **23b** (69%). Finalmente, el derivado **K** se generó tras la desprotección del bencilo. El compuesto **23b** se sometió a 2 atmósferas de hidrógeno con catalizador de Pd/C al 10% en peso y dio el compuesto **K** con un 67% de rendimiento (Figura 10.7).

El derivado acetilamida **24** se preparó con un rendimiento del 66% a partir de cloruro de acetilo (AcCl) con trietilamina (NEt_3). Posteriormente, se sometió el intermedio **24** a hidrogenación en presencia del catalizador de Pd/C al 10% en peso para obtener el derivado **L** (95%).

La Familia 3, que se compone del derivado amino acido libre **M** y ácido carboxílico **N**, se obtuvieron de forma muy diferente debido a que ninguno tiene enlace amida en su estructura. Partiendo del intermedio alcohol primario **2**, se preparó el aldehído **19** (99%) mediante oxidación con el ácido 2-yodoxibenzóico (IBX) en acetato de etilo (AcOEt). Seguidamente se sometió el aldehído **19** a una reacción de Strecker para la obtención del intermedio aminonitrilo **25**. Así, en presencia de sulfato magnésico ($MgSO_4$), cloruro amónico (NH_4Cl), cianuro sódico (NaCN) y amoníaco (NH_3), el aldehído se transformó en el aminonitrilo **25** con un rendimiento del 96%. La hidrólisis en medio básico proporcionó la formación del derivado amino ácido **26**. Este compuesto debido a la formación de sales y de su zwiterión fue muy difícil extraerlo del medio de reacción, incluso a pH neutro. Una extracción con columna de intercambio iónico permitió obtener el derivado **26** con un 28% de rendimiento. Finalmente, el compuesto **26** se sometió a hidrogenación para desproteger el bencilo y obtener el derivado **M** (91%).

El derivado **N** se preparó con un rendimiento del 99% después de la desprotección del bencilo mediante hidrogenación.

Con la ruta sintética explicada en la Figura 10.7 se obtuvieron los análogos de CR-6 **A**-**N** de forma eficiente y generalmente con buenos rendimientos para todos los pasos de síntesis..

X.3.1.2 Estudio de la preparación estereoselectiva

Puesto que el CR-6 tiene un estereocentro en la posición C_2, resultó interesante estudiar la preparación estereoselectiva de los compuestos finales **A**-**N** con mayor actividad biológica. Para ello se seleccionó el intermedio éster **1** para separar sus enantiómeros. De esta manera, una vez seleccionados los compuestos que penetran mejor la BBB se prepararían por separado sus estereoisómeros a partir de los enantiómeros separados del éster **1** y siguiendo la misma ruta sintética explicada anteriormente.

De este modo se pensó en la hidrólisis estereoselectiva del éster **1** con estereasas de cerdo (PLE), pero no funcionó.[72] También se estudió la resolución de sales diastereoméricas del ácido **6** a partir de diversas aminas enantiopuras, favoreciendo la precipitación de una de las sales formadas.[73] No obstante, el exceso enantiomérico (ee%) obtenido no superó en ningún caso el 40%. Se pensó que el grupo funcional que favorece la separación (el éster en el caso de la hidrólisis con PLE y el ácido en el caso de la resolución) estaban muy lejos del estereocentro C_2.

Se pensaron entonces en alternativas que pudieran separar los enantiómeros del éster **1**. La separación cromatográfica con columnas quirales a nivel semipreparativo nos pareció una buena opción. Se estudió la separación en columnas quirales analíticas con fases estacionarias diferentes: Chiralcel OD, Chiralpak IA, Chiralpak IB, Chiralpak IC y Chiralpak ID, y con la misma fase móvil (isocrático, hexano:alcohol isopropílico 90:10).[74] Los resultados obtenidos se evaluaron considerando factores de resolución (R_s) y selectividad (α) y se llegó a la conclusión que la columna Chiralpak IA era la que mejor separaba los enantiomeros. Pese a que la Chiralcel OD tenía una mayor selectividad (α = 1.52 y R_s = 21.8), la Chirakpak IA proporcionó una mayor resolución (α = 1.32 y R_s = 24.5). La Figura 10.8 muestra el cromatograma obtenido del ester **1** para la columna Chiralpak IA.

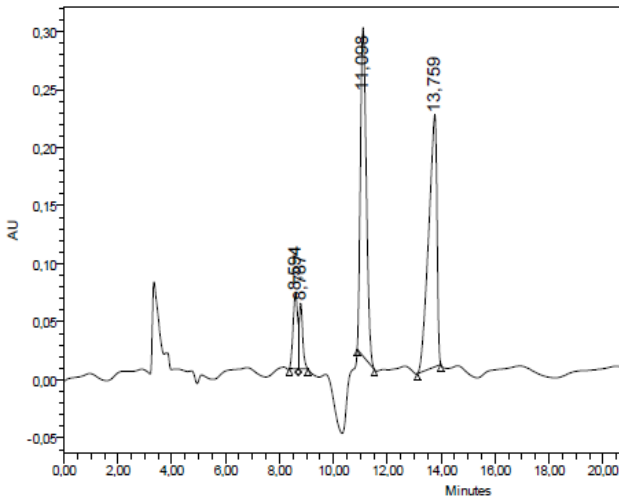

Figure 10.8. *Cromatograma del ester **1** en la columna quiral Chiralpak IA con una fase móvil isocrática de hexano:alcohol isopropílico 90:10.*

X.2.2 Evaluación de la actividad antioxidante

Una vez sintetizados los análogos al CR-6 (**A**-**N**) se quería comprobar si la actividad antioxidante del CR-6 se mantenía al introducir variabilidad en la posición C_2. Para ello, por un lado se evaluó la capacidad antioxidante en solución a partir del ensayo de neutralización del radical libre DPPH·, y también se evaluó en un ambiente celular mediante el ensayo celular de actividad antioxidante (CAA).

X.2.2.1 Ensayo de neutralización del radical libre DPPH·

El DPPH· es un radical libre estabilizado que en disolución tiene una absorción máxima entre 515-520 nm y da una coloración morada muy característica. La presencia de un agente capaz de dar un átomo de hidrógeno, como un compuesto antioxidante, neutraliza el radical DPPH·, la absorción disminuye y el color morado se pierde para dar un amarillo pálido (Esquema 10.1). El antioxidante estabiliza el electrón desaparecido en su estructura y la reacción no avanza (A·).[75,76,79]

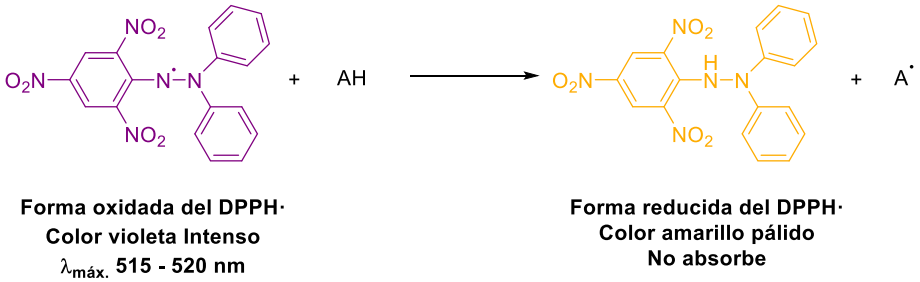

Esquema 10.1. *El radical DPPH· (solución morada intensa) reacciona con un agente dador de átomos de hidrógeno AH para dar lugar a la forma reducida (solución amarillo pálido). La disminución de la absorción del DPPH· nos permite la evaluación de la capacidad antioxidante de los compuestos a ensayar.*

El seguimiento de la disminución de la absorción a diferentes concentraciones de agente antioxidante, nos permite dibujar curvas sigmoidales de inhibición (I%) *versus* log[Antioxidante] para determinar el valor IC_{50} de cada especie. El I% se puede calcular con la expresión siguiente mediante la absorbancia obtenida.

$$I(\%) = \frac{A_0 - A_t}{A_0} \cdot 100$$

donde A_t y A_0 corresponden a las absorbancias a una concentración determinada pasados 60 minutos de experimento y a tiempo cero o concentración inicial, respectivamente. A partir del IC_{50}, se puede determinar el número de DPPH· reducidos por una molécula de antioxidante. Los resultados se pueden ver más abajo en la Tabla 10.1.

De acuerdo con los datos de la Tabla 10.1, los valores de IC_{50} oscilan entre 6.9 y 19.6 µM, donde **A**, **N** e **I** presentan en orden los mejores resultados, comparándolos con las referencia CR-6 (IC_{50} = 15.7 µM) y

Trolox (IC_{50} =14.3 µM). Teniendo en cuenta el número de DPPH· reducidos, la mayoría de los compuestos ensayados reducen dos moléculas de DPPH· por una de antioxidante. Esto se debe a la formación del radical tocoferoxilo que por estabilización del electrón desaparedo en la estructura de cromano permite la liberación de un segundo átomo de hidrogeno capaz de neutralizar una segunda molécula de DPPH· (Esquema 10.2).[79] Los compuestos **A**, **N** e **I**, sin embargo, son capaces de reducir entre 3 y 4 DPPH·.

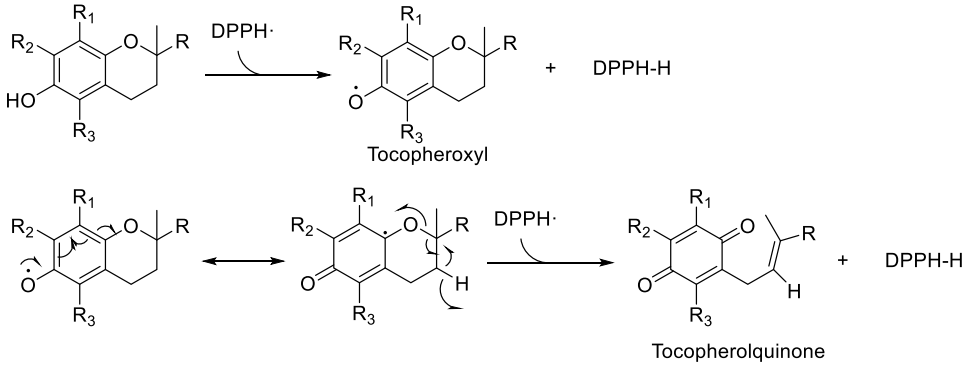

Esquema 10.2. *Curso de la reacción entre un compuesto con estructura de tocoferol y el radical libre DPPH·. Explicación de la reducción de dos moléculas de DPPH· por una molécula de agente antioxidante.*

X.2.2.2 Ensayo de la actividad antioxidante celular (CAA)

La capacidad antioxidante también se estudió en un entorno celular utilizando líneas de adenocarcinoma de mama MDA-MB-231 y MDA-MB-468 mediante el ensayo CAA. En este ensayo se detecta la fluorescencia del diclorofluoresceína (DCF) generado por la oxidación de la diclorofluoresceína reducida (DCFH) en presencia de radicales libres, en el citoplasma celular. La adición de un compuesto antioxidante, reduce el estrés oxidativo, generado en la célula con un oxidante como el peróxido de hidrógeno (H_2O_2), y así disminuye la formación de DCF y la fluorescencia (Figura 10.9).[82]

no inhib

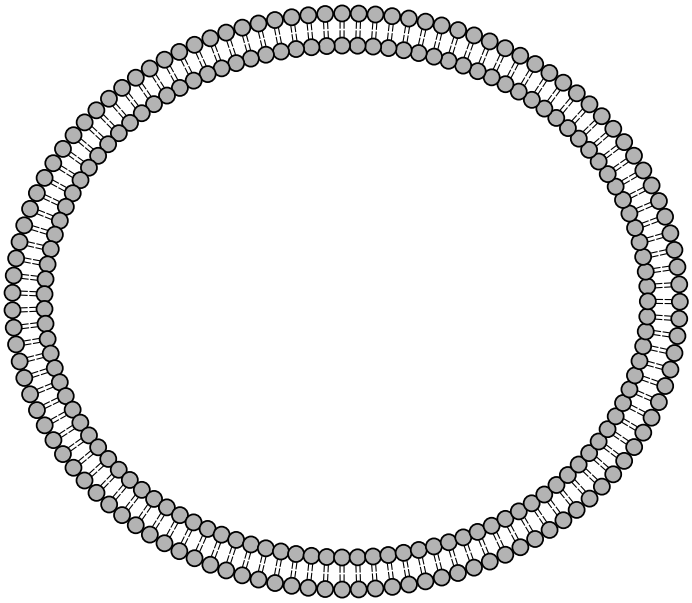

lipídica de las células. En cambio, el compuesto **A** es el que mejor actividad antioxidante muestra para ambas líneas celulares. Incluso, para las células MDA-MB-468 tiene mejores resultados que la referencia CR-6. Por lo tanto, en esta ocasión parece que la variabilidad introducida en C_2 provoca diferencias en la capacidad antioxidante en un entorno celular.

La similitud de los resultados con el CR-6 se ha estudiado mediante métodos estadísticos tanto para el ensayo del DPPH como para CAA, para evaluar si hay diferencias significativas al introducir variabilidad en C_2. Debido a las restricciones de los modelos estadísticos, muy pocos compuestos para el DPPH y ninguno en el CAA daban similitud estadísticamente significativa ($p > 0.05$) con CR-6. Por ello, se han empleado criterios químicos. En el caso del ensayo del DPPH se consideró que aquellos compuestos ensayados con IC_{50} entre 13.2 y 16.2 µM mantienen la capacidad antioxidante del CR-6 (Trolox, **C**, **F**, **G**, **H**, **J**, **K**, **L** y **M** la mantienen). En el ensayo del CAA, se consideró para ambas líneas celulares que los compuestos ensayados con $IC_{50} > 15.8$ µM no mantenían la capacidad antioxidante del CR-6 (Trolox, **A**, **I**, **L** y **N** para MDA-MB-231, y Trolox, **A**, **B**, **D**, **F** y **L** para MDA-MB-468 la mantienen). No obstante, en este último ensayo se tiene que tener en cuenta que la diferencia en la actividad final no depende solo del fenol, sino que procesos biológicos también influyen en el resultado final.

Tabla 10.2. *Capacidad antioxidante obtenida en el ensayo del DPPH y en el CAA para análogos del CR-6* ***A-N****. En rojo y verde se han señalado los compuestos con actividad antioxidante significativamente diferentes (menor o mayor actividad, respectivamente) a CR-6.*

Antioxidante	Ensayo del DPPH		Ensayo CAA	
	IC_{50} (µM)	Número de DPPH· reducido	MDA-MB-231 IC_{50} (µM)	MDA-MB-468 IC_{50} (µM)
Trolox	14.1	2.32	11.61	11.69
CR-6	15.7	2.16	4.54	4.34
A	6.9	4.26	7.73	3.64
B	19.6	1.64	22.08	13.54
C	16.2	1.94	22.89	23.87
D	17.3	1.69	89.09[a]	13.47
E	19.1	1.64	21.52	19.46
F	15.0	1.98	16.40	6.20
G	14.7	2.04	66.30	87.73
H	15.5	1.99	39.71	61.12
I	10.5	2.99	13.50	19.93
J	14.9	2.01	*no inhibición*	*no inhibición*
K	14.1	2.31	36.06	32.45
L	13.1	2.33	8.41	12.52
M	14.3	2.21	46.58	48.93
N	8.4	3.20	9.16	10.73

[a] El experimento para esta molécula se repitió para descartar posibles errores, pero los resultados negativos se confirmaron.

X.2.3 Evaluación penetración de la barrera hematoencefálica (BBB)

Para la evaluación de la penetración a través de la BBB se emplearon analysis *in silico* e *in vitro*. El análisis *in silico* que se utilizó fue el cálculo del algoritmo CNS MPO a partir de

propiedades físico-químicas, y permitió predecir la capacidad de penetrar por difusión pasiva de los compuestos ensayados.[120,121] Los ensayos *in vitro* como el PAMPA o celular como el Caco-2 y el BBCEC permitieron analizar si los compuestos ensayados eran capaces o no de atravesar la BBB.[32,38,131,135]

X.2.3.1 Análisis in silico de difusión pasiva

El análisis *in silico* utilizado está basado en el cálculo del algoritmo CNS MPO que proviene del estudio de seis propiedades fisico-químicas (pK_a, HBD, clogP, clogD, MW y TPSA), importantes en la penetración de la BBB por difusión pasiva, de fármacos capaces de llegar al sistema nervioso central. Este algoritmo, no solo permite la predicción del transporte de la BBB por difusión pasiva, sino que también indica si los compuestos tienen un comportamiento de fármaco, según atributos farmacocinéticos ADME y de toxicidad.

Para el cálculo del CNS MPO cada propiedad físico-química se distribuye en una función de probabilidad deseada construida a partir de las propiedades de fármacos y candidatos cedidas por Pfizer. Las propiedades pK_a, HDB, MW, clogD y clogP se distribuyen según una función monotónica decreciente mientras el TPSA tiene una función en forma de "joroba" (Figura 10.10). Según el valor de la propiedad fisico-química (Tabla 10.3) del compuesto a estudiar, se le da un valor entre 0 y 1: 0 si se encuentra en el área no deseada, 1 si está en l área deseada y entre 0 y 1 si está en la recta que une las dos áreas, dependiendo de la ecuación de la recta. A este valor se le llama T0 y cada propiedad tendrá uno para cada compuesto.

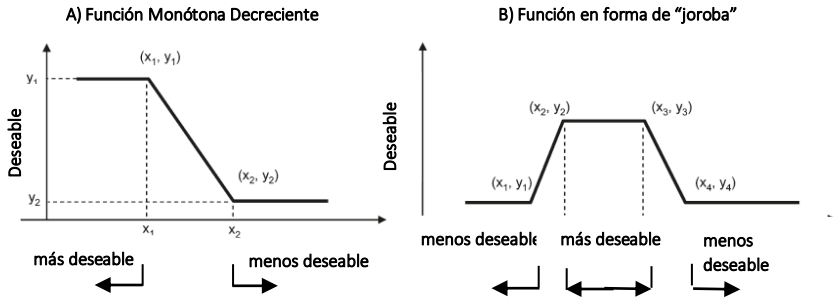

***Figura 10.10**. Funciones Monótona Decreciente (A) y en forma de "joroba" (B) para el cálculo del algoritmo CNS MPO.*

Tabla 10.3. Propiedades físico-químicas para calcular el CNS MPO, las funciones de distribución y, los intervalos deseables y no deseables para cada una de ellas.

Propiedades	Función	Intervalo deseable (T0 = 1.0)	Intervalo no deseable (T0 = 0.0)
clogD	Monotónica decreciente	ClogD ≤ 2	ClogD > 4
clogP	Monotónica decreciente	ClogP ≤ 3	ClogP > 5
TPSA	Forma de "joroba"	40 < TPSA ≤ 90	TPSA ≤ 20; TPSA > 120
MW	Monotónica decreciente	MW ≤ 360	MW > 500
HBD	Monotónica decreciente	HBD ≤ 0.5	HBD > 3.5
pK_a	Monotónica decreciente	$pK_a \leq 8$	$pK_a > 10$

Para obtener el valor de CNS MPO, solamente se suman los diferentes valores de T0 y se obtiene un valor entre 0 y 6. En la tabla 8.4 se muestran los valores de CNS MPO para Trolox, CR-6 y los nuevos antioxidantes **A**-**N**. Un compuesto con CNS MPO ≥ 4.5 tendrá muchas posibilidades de convertirse en un fármaco con atributos farmacocinéticos y de toxicidad adecuados para ser administrado y con capacidad de atravesar la BBB por difusión pasiva. Como se puede ver en la Tabla 10.4, la mayoría de compuestos estudiados tienen un CNS MPO < 4.5, con lo que difícilmente podrán ser distribuidos por el organismo con capacidad de penetrar la BBB mediante difusión pasiva. Solamente el Trolox y el derivado **N** compuestos prometedores. No obstante, este algoritmo es una predicción que puede fallar; por ello otro tipo de ensayos se deben tener en cuenta. Además, este algoritmo solo tiene en cuenta mecanismos de transporte por difusión pasiva, no activa ni facilitada.

Tabla 10.4. Valor del CNS MPO para todos los antioxidantes ensayados.

Antioxidante	CNS MPO
Trolox	4.5
CR-6	4.3
N	4.5
L	4.3
I	4.2
E	4.0
C	3.7
D	3.7
M	3.6
F	3.3
H	2.9
A	2.9
B	2.7
G	2.5
K	2.6
J	1.5

X.2.3.2 Ensayo celular in vitro Caco-2

Este ensayo se realizó con motivo de una estancia en el *Laboratoire de la Barriére Hémato-Encèphalique* (LBHE) de la *Université d'Artois* en Lens (Francia), bajo la supervisión del Prof. Romeo Cecchelli y Dr. Maxime Culot, y la ayuda de Emmanuel Sevin.

Las células Caco-2 son un tipo de células endocíticas polarizadas de adenocarcinoma gastrointestinal de humano. Las células Caco-2 expresan muchos de los mecanismos de transporte existentes en la BBB: transporte vía paracelular a través de las proteínas de unión celular, o vía transcelular mediante difusión pasiva a través de la membrana y "carriers" que faciliten el transporte, o incluso mecanismos que impiden la absorción de compuestos como barreras enzimáticas y bombas de eflujo (Figura 10.11).

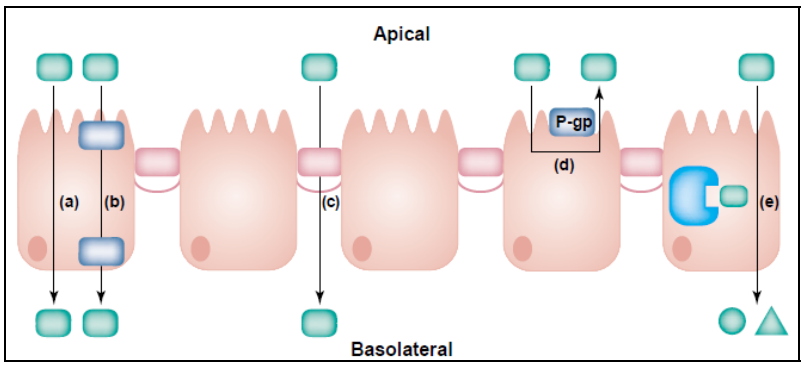

Figura 10.11. *Diferentes vías de transporte para la absorción intestinal de un compuesto:* ***(a)*** *difusión pasiva transcelular,* ***(b)*** *transporte mediado por "carriers" y* ***(c)*** *difusión paracelular a través de las proteínas de unión celular. También existen mecanismos que restringen el paso:* ***(d)*** *bombas de eflujo que expulsan los compuestos, y* ***(e)*** *enzimas que degradan la molécula e impiden que se absorba.*

Por ello, el ensayo *in vitro* de Caco-2 se emplea, por un lado, para estudiar la absorción intestinal y la toxicidad de los compuestos candidatos; pero por el otro lado, debido a que expresan mecanismos de transporte similares en la BBB, se utiliza como un estudio preliminar del transporte a través de la BBB. Las células Caco-2 se cultivan en placas de 24 pocillos en forma de monocapa sobre un filtro de policarbonato que separa el compartimento apical (A) del compartimento basolateral (B), Figura 10.12.

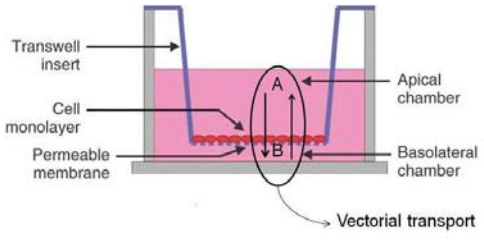

Figura 10.12. *Procedimiento experimental del ensayo Caco-2. Los compartimentos apical y basolateral están separados por un filtro inerte de policarbonato que soporta una membrana constituida por células Caco-2.*

El ensayo se compone de dos experimentos: el primero donde se estudia el transporte del compuesto de A→B y en el segundo se evalúa el sentido contrario, de B→A. De este modo, con el primer experimento podemos observar como son absorbidas las moléculas ensayadas; y con el segundo se

estudia si existe algún mecanismo de eflujo que impida esta absorción. La permeabilidad se representa en forma de permeabilidad aparente (P_{app}) que se calcula con la siguiente fórmula:

$$P_{app} = \frac{dQ}{dt}\frac{1}{A \cdot C_0}$$

donde *dQ/dt* corresponde a la velocidad de desaparición del compuesto (C_t/t, donde C_t es la concentración de compuesto en el compartimento aceptor al final del experimento y *t* es el tiempo experimental en minutos, 60 minutos), *A* es el área del filtro (0.33 cm^2) y C_0 la concentración inicial del compuesto. Los valores de C_t y C_0 se obtuvieron del análisis de alícuotas mediante cromatografía líquida UPLC-MS.

La existencia de interacción con bombas de eflujo se calcula con la relación de eflujo (*ER*):

$$ER = \frac{P_{app(B \rightarrow A)}}{P_{app(A \rightarrow B)}}$$

donde $P_{app(A \rightarrow B)}$ y $P_{app(B \rightarrow A)}$ representan las permeabilidades aparentes para cada experimento. En la Tabla 10.5 se muestran todos los resultados obtenidos.

Tabla 10.5. *Resultados obtenidos en el estudio de la absorción de antioxidantes análogos al CR-6 mediante en ensayo celular in vitro de Caco-2.*

Antioxidante	$P_{app(A \rightarrow B)}$ ($\cdot 10^{-6}$ cm/s)	$P_{app(B \rightarrow A)}$ ($\cdot 10^{-6}$ cm/s)	ER	Interpretación
Trolox	0	0	0	*No penetración*
CR-6	*No detectado*	*No detectado*	-	*No detectado*
A	*No detectado*	*No detectado.*	-	*No detectado*
B	27.6	0	0	*No eflujo*
C	0	0	0	*No penetración*
D	10.9	0	0	*No eflujo*
E	3.8	0	0	*No eflujo*
F	2.3	0	0	*No eflujo*
G	0	3.15	-	*eflujo*
H	*No analizado*	*No analizado*	-	*No analizado*
I	330	123	0.37	*No eflujo*
J	62.1	3.11	0.05	*No eflujo*
K	*No analizado*	*No analizado*	-	*No analizado*
L	449	120	0.27	*No eflujo*
M	*No analizado*	*No analizado*	-	*No analizado.*
N	*No detectado*	*No detectado*	-	*No detectado*

De acuerdo con los datos mostrados en la Tabla 10.5, los derivados **B**, **D**, **I**, **J** y **L** muestran una buena absorción a través de la monocapa de células Caco-2, ya que la $P_{app(A \rightarrow B)} > 10 \cdot 10^{-6}$ cm/s. Además, ninguno de ellos muestra interacción por las bombas de eflujo, ya que pese a que tengan transporte de B→A, el *ER* está por debajo de 2.5. También se puede observar que el $P_{app(A \rightarrow B)}$ en los compuestos **I** y **L** son mucho

mayores que el $P_{app(B\rightarrow A)}$, lo que da a pensar en un posible mecanismo activo o facilitado de penetración. El derivado G es el único que presenta interacción con las bombas de eflujo pese a que ER no se puede calcular, ya que $P_{app(B\rightarrow A)} >> P_{app(A\rightarrow B)}$.

Los compuestos **H**, **K** y **M** no fueron analizados debido a que se sintetizaron con posterioridad a la realización de este ensayo. Los derivados CR-6, **A** y **N** no se detectaron ni siquiera en la solución dadora inicial; suponemos que deben tener dificultad en ionizar durante el análisis por UPLC-MS. Por esto no se ha podido extraer una conclusión de la comparación del transporte de los análogos del CR-6 con el mismo CR-6.

X.2.3.3 Ensayo in vitro PAMPA

El modelo *in vitro* PAMPA se ejecutó con la ayuda de la Dra. Meritxell Teixidó Ribot en el grupo de *Design, Synthesis and Structure of Peptides and Proteins* en el *Parc Científic* de Barcelona.

El ensayo *in vitro* PAMPA, o el ensayo paralelo de permeabilidad en membrana artificial, está basado en el transporte a través de una membrana artificial constituida por fosfolípidos. Este ensayo simula una membrana para evaluar de forma efectiva y a bajo coste el mecanismo de transporte por difusión pasiva de un gran número de muestras de forma simultánea. El ensayo PAMPA sirve para el estudio de membranas intestinales, membranas cutáneas y membranas cerebrales. Se ha demostrado que PAMPA es un buen modelo de predicción *in vivo*.

El ensayo se compone de dos placas de 96 pocillos separadas por un filtro inerte: la placa superior es el aceptor y la inferior el dador. Para simular la BBB al máximo, se utilizan fosfolípidos extraídos de cerebro de cerdo (PBLE). De este modo, el compuesto a ensayar se disuelve en una solución tamponada con un 20% de 1-propanol como co-disolvente y se añade en la placa inferior. La placa aceptor se acopla a la placa dador evitando la formación de burbujas, y se le añaden, sobre el filtro, los fosfolípidos seguido de la solución tamponada (Figura 10.13).

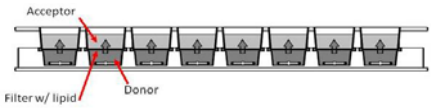

Figura 10.13. *Placa de 96 pocillos para el ensayo del modelo de PAMPA, donde el compartimento superior e inferior están acoplados y separados mediante un filtro inerte.*

Tanto en experimentos *in vivo* como *in vitro* la capa de agua sin agitar que queda cerca de la membrana (UWL) influye en el transporte de los compuestos. Esto es mucho más acusado en los transportes por difusión pasiva. Por ello, la placa inferior tiene un imán agitador para que durante el experimento la disolución inferior se agite y así disminuir el UWL a 25 µm.

Una vez finalizado el experimento, se calcula la permeabilidad efectiva mediante la siguiente fórmula:

$$P_e = \frac{-218.3}{t} \log\left[1 - \frac{2 \cdot C_A(t)}{C_D(t_0)}\right] \cdot 10^{-6} cm/s$$

donde *t* es el tiempo en minutos (240 minutos), y $C_A(t)$ y $C_D(t_0)$ corresponden a la cantidad de soluto en el compartimento aceptor al final del experimento y en el compartimento dador al inicio, respectivamente.

$C_A(t)$ y $C_D(t_0)$ se obtuvieron a partir del análisis de alícuotas por cromatografía líquida HPLC-UV y se confirmaron mediante UPLC-MS.

Los resultados obtenidos se muestran un poco más abajo en la Tabla 8.6. Según los resultados obtenidos, los compuestos Trolox, CR-6 y **A**-**N** tienen baja permeabilidad por difusión pasiva, ya que $P_e < 2 \cdot 10^{-6}$ cm/s en todos los casos. No obstante, se puede observar que Trolox, **G**, **L**, **F**, **I** y **A** muestran una difusión pasiva mejor que el CR-6, siendo **G** el mejor de todos. La baja permeabilidad de la mayoría de compuestos se debe probablemente a la presencia del grupo ácido carboxilo en los compuestos **B**-**H** que en pH 7.4 están cargados negativamente y no pueden atravesar la barrera lipídica de la BBB.

X.2.3.4 Ensayo celular in vitro BBCEC

Igual que el modelo in vitro Caco-2, este ensayo se realizó con motivo de una estancia en el *Laboratoire de la Barriére Hémato-Encèphalique* (LBHE) de la *Université d'Artois* en Lens (Francia), bajo la supervisión del Prof. Romeo Cecchelli y Dr. Maxime Culot, y la ayuda de Emmanuel Sevin.

Las células capilaro-endoteliales de cerebro bovino (BBCEC) se utilizaron en un ensayo *in vitro* para simular la BBB *in vivo*. Durante años se ha estudiado el procedimiento que se debe seguir para el aislamiento de las células endoteliales de cerebro) y el posterior cultivo para conseguir una mayor semejanza con la BBB *in vivo*. Se había visto en el cultivo directo de las BBCEC sobre la placa después de su extracción, estas células no formaban una monocapa con las propiedades de la BBB: no se formaban las proteínas de unión estrechas y, por consiguiente, había más huecos por donde los compuestos podían penetrar. Este sistema causaba que la BBB no se polarizara y, por lo tanto, no desarrollara todos sus mecanismos de transporte y que no fuese tan impermeable como *in vivo*.

En 1990, Cechelli *et al.* desarrollaron un método de cultivo celular basado en el co-cultivo de las BBCEC sobre un filtro de colágeno en un compartimento con una separación a través de una membrana inerte con el compartimento donde se cultivan las células gliales (astrocitos), extraídas de cerebro de rata recién nacida. La presencia de las células gliales, sin estar en contacto directo con las células endoteliales más que por contacto en solución, proporcionaron un ambiente donde las células endoteliales se desarrollan con todos los mecanismos de transporte de la BBB *in vivo* (Figura 10.14).

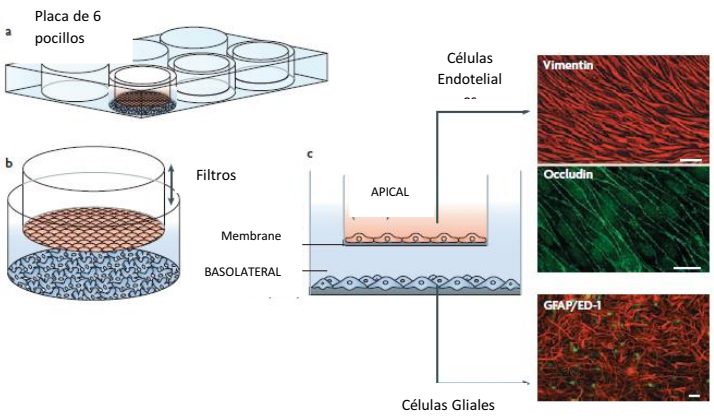

Figura 10.14. *Modelo BBB in vitro basado en el co-cultivo de células endoteliales con los astrocitos en dos compartimentos diferentes separados por una membrana inerte. a) Ilustración de una placa de 6 pocillos donde el modelo in vitro tiene lugar. El co-cultivo se puede llevar a cabo en placas de 6, 12 y 24 pocillos. b) Células endoteliales cerebrales que se están cultivando sobre el filtro en contacto con el compartimento o pocillo donde se cultivan los astrocitos. c) Ilustración de del experimento diseñado que permite el co-cultivo de las células gliales y endoteliales. Las tres imágenes de la derecha muestran: la confluencia de la monocapa de las células endoteliales al teñirlas con vimentina se observan en rojo; la proteína de unión estrecha ocludina refleja en verde la estrechez de la barrera; y las células gliales teñidas con proteína glial fibrilar ácida (GFAP) muestran los astrocitos en color rojo.*

Transcurrido el periodo de co-cultivo, las células endoteliales se someten al experimento de transporte. Los compuestos se disuelven en solución tamponada y se añaden en el compartimento superior (apical). Transcurridos los 60 minutos de incubación a 37ºC, se recogen alícuotas de los compartimentos apical y basolateral y se analizan por cromatografía líquida UPLC-MS. A partir de los valores obtenidos se calcula la permeabilidad efectiva (P_e) teniendo en cuenta la superficie del filtro.

En el modelo *in vitro* BBCEC, puesto a que nos interesa conocer la permeabilidad de la membrana endotelial, se realiza un segundo experimento sin células. Para observar el transporte a través del filtro y demostrar que el filtro no interfiere en la penetración. De este modo, se tiene también en cuenta la permeabilidad del filtro. De los experimentos con células obtenemos PS_t y de los sin células PS_e; aplicando la fórmula siguiente obtenemos PS_e (producto de la P_e con la superficie). Al dividir la PS_e/S, donde S es 1.12 cm^2, se obtiene P_e en unidades de $\cdot 10^{-3}$ cm/s.

$$\frac{1}{PS_e} = \frac{1}{PS_t} - \frac{1}{PS_f}$$

Los resultados obtenidos de P_e se muestran en la Tabla 10.6. De acuerdo con estos resultados, los compuestos **B**, **C**, **D**, **F**, **I** y **J** tienen una buena permeabilidad de la BBB debido a que la $P_e > 10 \cdot 10^{-3}$ cm/s. Igual que pasaba en el modelo *in vitro* de las Caco-2, debido a problemas de detección por UPLC-MS de algunos compuestos ensayados, como el CR-6, los resultados obtenidos no se puedieron comparar con el CR-6. En este caso, los compuestos **H**, **K** y **M** no pudieron ser analizados.

La ejecución de estos tres ensayos in vitro nos permitió extraer las primeras conclusiones preliminares de la penetración a través de la BBB a partir de la comparación de los resultados obtenidos.

Por ejemplo, si un compuesto tiene un P_e en el modelo de PAMPA igual que en el Caco-2 significaría que utiliza un método de penetración por difusión pasiva; si el $P_{app(B\rightarrow A)}$ en Caco-2 fuese mayor al de P_e de PAMPA, existiría una interacción con las bombas de eflujos; pero si por el contrario fuese menor, el compuesto utilizaría un mecanismo activo (Tabla 10.6).

Los compuestos **B**, **C**, **D**, **F**, **I** y **J** podrían tener un componente de influjo activo o facilitado, ya que no se observa difusión pasiva en PAMPA ni una interacción con las bombas de eflujo en Caco-2. De hecho, los derivados B y I tienen una permeabilidad en el modelo de BBCEC alta ($P_e > 2{\cdot}10^{-3}$ cm/min), y F y G moderada ($1 < P_e < 2{\cdot}10^{-3}$ cm/min). No obstante, G podría ser un sustrato de las bombas de eflujo ya que $P_{app(A\rightarrow B)} << P_{app(B\rightarrow A)}$. Es posible que el compuesto **C** se metabolize en el modelo *in vitro* Caco-2, ya que $P_{app} = 0$. El derivado **L** es muy probable que tenga un componente activo o facilitado de influjo, pero parece que se metaboliza en las células endoteliales bovinas. Trolox se podría transportar por difusión pasiva, aunque el valor de P_e en PAMPA es menor a $2{\cdot}10^{-6}$ cm/s, pero parece que se metaboliza.

Pese a estos resultados, se deberían realizar más estudios de la permeabilidad a través de la BBB de los derivados del tocoferol Trolox, CR-6 y **A**-**N**.

Tabla 10.3. *Resultados de los modelos in vitro Caco-2, PAMPA y BBCEC. Comparación y conclusiones preliminares.*

Antioxidant	PAMPA-BBB P_e ($\cdot10^{-6}$ cm/s)	Caco-2 $P_{app(A\rightarrow B)}$ ($\cdot10^{-6}$ cm/s)	BBCEC P_e ($\cdot10^{-3}$ cm/min)	Preliminary conclusions
Trolox	0.47±0.04	0	0	*Pass*[a] and *Met*[b]
CR-6	0.25±0.01	*Not detected*	*Not detected*	-
A	0.30±0.01	*Not detected*	*Not detected*	-
B	0.03±0.02	27.6[a]	2.16±0.40	*In*[c]
C	0.06±0.04	0	1.09±0.48	*In* and *Cmet*[d]
D	0.16±0.0005	10.9±2.9	0.72±0.19	*In*
E	0.06±0.05	3.4±0.6	0.47±0.10	*In*
F	0.50±0.2	6.7[a]	0.57±0.19	*In*
G	1.18±0.4	0	1.44±0.71	*Ex*[e] and *Pass*
H	*Not detected*	*Not analyzed*	*Not analyzed*	-
I	0.35±0.04	330±0.7	3.62±1.63	*In*
J	*Not detected*	62.1±0.4	-0.72±0.06	*In*
K	0	*Not analyzed*	*Not analyzed*	-
L	0.52±0.06	449[a]	0	*In* and *Bmet*[d]
M	0.07±0.01	*Not analyzed*	*Not analyzed*	-
N	0	*Not detected*	*Not detected*	-

[a] *Pass* se refiere a la difusión pasiva transcelular
[b] *Met* respresenta cualquier metabolismo enzimático en BBCEC y/o Caco-2
[c] *In* corresponde al transporte active o facilitado de influjo (como LAT1, GLUT1, MCT1, etc.)
[d] *Cmet* representa el metabolism enzimático por las células Caco-2
[e] *Ex* se refiere al mecanismo active de eflujo (por ejemplo, P-gp)
[f] *Bmet* representa al metabolismo enzimático en las células BBCEC

X.2.4 Toxicidad de los nuevos compuestos antioxidantes

Para finalizar con el trabajo de la presente Tesis, se evaluó la toxicidad de los compuestos Trolox, CR-6 y **A**-**N** en las células de los ensayos que se han utilizado. Para las células utilizadas en la evaluación de la actividad antioxidante (MDA-MB-231 y -468) se ha realizado el ensayo MTT, mientras que para las células Caco-2 y BBCEC se ha utilizado el marcador fluorescente *Lucifer Yellow*.

X.2.4.1 Ensayo de toxicidad MTT

Este ensayo ha sido llevado a cabo por la Dra. María Garrido Martínez de nuestro laboratorio de investigación en el *Institut de Química Avançada de Catalunya* del CSIC, Barcelona.

El ensayo MTT consiste en la incubación de las células con el compuesto antioxidante a ensayar (Trolox, CR-6 y **A**-**N**) y el bromuro de tetrazolio 3-[4,5-dimetiltiazol-2-il]-2,5-difenil (MTT). El anillo de tetrazolio del reactivo MTT se rompe por la acción de las enzimas mitocondriales deshidrogenasas presentes en las células vivas, dando lugar a la formación de Formazano, un compuesto con una coloración intensa violeta y una absorción entre 500-600 nm (Figura 10.15).[144]

Figura 10.15. *Transformación del reactivo MTT de color amarillo a Formazano mediante la acción de las enzimas mitocondriales deshidrogenasas que actúan en las células vivas.*

A partir de la absorbancia obtenida a diferentes concentraciones (0 a 100 µM) del agente antioxidante (A_{test}) y la absorbancia del control con solo DMSO (el vehículo utilizado en el ensayo) y MTT ($A_{control}$), se calculó el porcentaje de viabilidad-celular:

$$\%Viabilidad = \frac{A_{test}}{A_{control}} \cdot 100$$

Los resultados obtenidos demostraron viabilidad de todos los compuestos por encima del 60% para todo el intervalo de concentraciones y para las dos líneas celulares (MDA-MB-231 y -468). Solamente los compuestos **J** (para los dos tipos de células) y **A** (para las MDA-MB-468) disminuyen del 50% de viabilidad celular a concentraciones entre 50-100 µM. Por lo general, la viabilidad celular del antioxidante ensayado

se mantiene a la altura del vehículo DMSO, incluso en varias ocasiones tiene mejor viabilidad que el DMSO.

X.2.4.2 Ensayo del Lucifer Yellow

El ensayo de toxicidad de las células Caco-2 y BBCEC se llevó a cabo con el marcador celular fluorescente *Lucifer Yellow* (LY, Figura 10.16) que es prácticamente impermeable a las membranas de células Caco-2 y BBCEC debido a su carácter hidrosoluble. De este modo, se puede comprobar la integridad y arquitectura de las células con una medida en la fluorescencia de los compartimentos apical y basolateral, y de la solución inicial de LY.

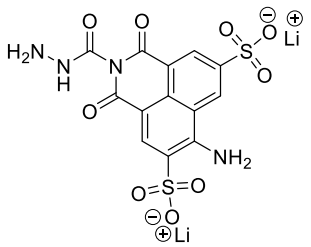

Figura 10.16. *Estructura de la Lucifer Yellow como sal de litio carbohidrazida.*

El LY se añade a la disolución en el compartimento apical de los experimentos de A→B y de B→A en el modelo Caco-2, y en el modelo BBCEC. La integridad de la célula se asegura si la permeabilidad en Caco-2 es P_{app} < 1·10^{-6} cm/s, y en BBCEC es P_e < 1·10^{-3} cm/s. Los resultados obtenidos se muestran en la Tabla 10.4. De acuerdo con los datos de la tabla, se puede observar que todos los compuestos ensayados, tanto en el modelo de Caco-2 como en el de BBCEC no presentan toxicidad a las concentraciones ensayadas (25 y 10 µM, respectivamente) y mantienen la integridad y la arquitectura de la membrana celular ya que el LY mantiene su baja permeabilidad típica (P_{app} < 1·10^{-6} cm/s y P_e < 1·10^{-3} cm/min).

Tabla 10.4. *Resultados de toxicidad en el modelo celular Caco-2 (para los experimentos de A→B y viceversa) y en el modelo BBCEC medido con el marcador fluorescente LY.*

Antioxidante	Modelo Caco-2		Modelo BBCEC
	P_{app} LY (A→B) (·10^{-6} cm/s)[a]	P_{app} LY (B→A) (·10^{-6} cm/s)[a]	P_e LY (·10^{-3} cm/min)[a]
Trolox	0.06±0.01	0.11±0.02	0.10±0.03
CR-6	0.09±0.03	0.08±0.03	0.13±0.01
A	0.08±0.01	0.12±0.03	0.09±0.02
B	0.08±0.02	0.08±0.01	0.14±0.01
C	0.08±0.02	0.11±0.03	0.12±0.01
D	0.08±0.02	0.10±0.03	0.11±0.03
E	0.11±0.05	0.33±0.10	0.11±0.02
F	0.08±0.03	0.10±0.02	0.11±0.06
G	0.13±0.10	0.13±0.04	0.20±0.13
H	*No analizado*	*No analizado*	*No analizado*
I	0.09±0.03	0.20±0.10	0.59±0.30
J	0.09±0.03	0.14±0.04	0.38±0.24
K	*No analizado*	*No analizado*	*No analizado*
L	0.08±0.03	0.22±0.13	0.13±0.03
M	*No analizado*	*No analizado*	*No analizado*
N	0.12±0.04	0.09±0.02	0.16±0.10

[a] Los resultados se expresan como media±SD (Desviación estándard).

X.3 CONCLUSIONES Y TRABAJO FUTURO

A partir del trabajo realizado en la presente Tesis, se han extraído las siguientes conclusiones:

1. Se han sintetizado catorce nuevos análogos al CR-6 para mejorar la biodisponibilidad de estos compuestos en el cerebro. De este modo, se ha seguido la estrategia del "BBB-shuttle", acoplando por un enlace peptídico nutrientes esenciales que tienen transporte a través de la BBB.

2. Se ha estudiado el efecto de la variabilidad en la posición C_2 en la capacidad antioxidante del CR-6. Se ha visto a través del ensayo del DPPH, que la actividad antioxidante no varía significativamente al introducir diferentes nutrientes esenciales en C_2. De hecho, algunos de ellos (**A**, **N** e **I**) la mejoran. No obstante, en el ensayo de la capacidad antioxidante celular (CAA) se ha visto mayores diferencias significativas para ambas líneas celulares. Se piensa que estas diferencias se deben a que en un medio biológico influyen otros factores (permeabilidad de la célula, metabolismo enzimático, etc.) que no existen los ensayos *in vitro* en disolución. Algunos compuestos no han mostrado inhibición del estrés oxidativo, pero otros (**A**) han presentado mejor inhibición que el CR-6.

3. El estudio de la permeabilidad de la BBB en ensayos *in silico* e *in vitro* a mostrado que estos compuestos tienen dificultades para ser transportados mediantes mecanismos de difusión pasiva. No obstante, han mostrado tener algún mecanismo de permeabilidad facilitada o activa a través de la BBB. A su vez, en general no se ha observado interacción con las bombas de eflujo, excepto el compuesto **G**.

4. Los ensayos de toxicidad demuestran que ninguno de los compuestos estudiados presentan toxicidad frente a las células MDA-MB-231, -468, Caco-2 y BBCE.

Por todo lo expuesto se considera que el compuesto **I** y **B** serían los más prometedores. No obstante, se deberían mejorar las técnicas de detección en los ensayos *in vitro* para poder saber la permeabilidad de **A** y **N**, los dos derivados con mayor capacidad antioxidante. También, será interesante completar la evaluación de los compuestos **H**, **K** y **M**.

En un futuro trabajo se ha planteado la síntesis de algunos de los derivados con el grupo amino ácido libre para ser mejor reconocido por el mecanismo LAT-1. Por otra parte, la preparación de estos derivados con el grupo fenol protegido, de manera que pueda liberarse por acción de enzimas metabolizadoras, por ejemplo, esterasas, puede ser otra alternativa viable para optimizar la biodisponibilidad a nivel cerebral de esta familia de antioxidantes.

APPENDIX I. Abbreviations

A→B	From Apical to Basolateral
Ac_2O	Acetic anhidride
ADME	Administration, Distribution, Metabolism and Excretion
ADP	Adenosine diphosphate
AH	Molecule with H donator capacity
AOX	Antioxidant
ARP	Antiradical potential
ATP	Adenosine triphosphate
B→A	Fron Basolateral to Apical
BBB	Blood-brain barrier
BBCEC	Bovine Brain Capillary Endothelial Cells
BCSFB	Blood-cerebrospinalfluid barrier
BMEC	Brain Microcapillary Endothelial Cells
BHT	Butylated hydroxytoluene
BRB	Blood-retinal barrier
CAA	Cellular Antioxidant Activity
CMT	Carrier-mediated transport
CNS	Central Nervous System
CNS MPO	Central Nervous System Multiparameter
CR-6	3,4-dihydro-6-hydroxy-2,2-dimethyl-7-methoxy-1(2*H*)-benzopyran
CSF	Cerebrospinalfluid
δ	Chemical shift
DCC	*N,N'*-Diciclohexyl carbodiimide
DCF	Dichlorofluorescein
DCFH	Dichloro-dihydro-fluorescein
	DCFH-DA
DIC	*N,N'*-Diisopropylcarbodiimide
DiPEA	*N,N*-Diisopropylethylamina
DKP	Diketopiperazine
DMAP	*N,N*-Dimethylaminopyridine
DMEM	Dubelcco's Modified Eagle Medium
DMF	*N,N*-Dimethylformamide
DMSO	Dimethylsulfoxide
DPPH	Di(phenyl)-(2,4,6-trinitrophenyl)iminoazanium
EAAT	Excitory Amino Acid Transporter
EBSS	Earle's Balanced Salt Solution
EDC·HCl	1-Ethyl-3-(3-dimethylaminopropyl)carbodiimide
ee	Enantiomeric excess
EPR	Electron Paramagnetic Ressonance
ER	Efflux Pump
ETC	Electron Trandport Chain
FBS	Fetal Bovine Serum
FTIR	Fourier transport infrared spectroscopy
GLUT-1	Glucose transporter 1
GSH	Glutathione
GSSG	Glutathione peroxidase
H_2DCFDA	2',7'-Dichlorodihydrofluorescein diacetate
HATU	1-[Bis(dimethylamino)methylene]-1H-1,2,3-triazolo[4,5-b]pyridinium 3-oxid hexafluorophosphate
HBA	Hydrogen bond acceptor
HBD	Hydrogen bond donator
HOBt	Hydroxybenzotriazole
HPLC	High Pressure Liquid Chromatography
HRMS	High Resolution Mass Spectroscopy
HTS	Highthroughput Screening
HWE	Horner-Wadsworth-Emmons
IBX	2-Iodoxybenzotriazole

IC_{50}	Half maximal inhibitory concentration
ID	Internal Diameter
IR	Infrared spectroscopy
ISF	Intersticial fluid
LAT-1	Large neutral amino acid transporter 1
LC/MS	Liquid Chromatography/Mass Spectroscopy
LG	Leaving Group
LOD	Limit of Detection
LOQ	Limit of Quantification
LY	Lucifer Yellow
MAO	Monoamino oxidase
MCT1	Monocarboxylic acid transporter
MDCK	Madin-Darby Canine Kidney
MRP-2	Multi-drug Resistance Protein 2
MS	Mass Spectroscopy
MW	Molecular Weight
OS	Oxidant Species
Ox	Oxidant
P_{app}	Apparent permeability
PBL	Pig Brain Lipid
PBLE	Pig Brain Lipid Extract
PBS	Phosphate Buffer Solution
P_e	Efficient permeability
PEA	*N,N*-Propylethylamina
P-gp	P-Glycoprotein
PLE	Pig Lipid Esterase
PML	Polar Membrane Lipid
PSA	Prostatic Specific Antigen
rIC_{50}	Relative half maximal inhibitory concentration
RMT	Receptor-mediated transcystosis
RNS	Reactive Nitrogen Species
RO5	Rule of five
ROS	Reactive Oxygen Species
RP	Reverse phase
rtPA	Recombinat tissue plasminogen activator
RV	Resveratrol
SEM	Standard error of the mean
SNP	Sodium nitroprusside
SOD	Superoxide dismutase
SS	Second Square
T0	Function transformation
TBAF	Tetra-n-butylammonium fluoride
TBDMSH	*tert*-Butyldimethylsilane
TFA	Trifluoroacetic acid
THF	Tetrahydrofurane
TLC	Thin Layer Chromatography
TOF	Time of Flight
TPSA	Topological Polar Surface Area
u.f.	Units of Fluorescence
UPLC	Ultra Pressure Liquid Chromatography
UV	Ultraviolet spectroscopy
UWL	Unstirred Water Layer

APPENDIX II. References

1) Sanvicens, N.; Gómez-Vicente, V.; Messeguer, A.; Cotter, T.G. *J. Neurochem.* 2006, 1-13.

2) Sies, H. In *Oxidative Stress*, Academic Press, London, 1985, 1-8.

3) Warner, D.S.; Sheng, H.; Batinić-Haberle, I. *J. Exp. Biol.* 2004, *207*, 3221-3231.

4) Miranda, M.; Muriach, M.; Almansa, I.; Arnal, E.; Messeguer, A.; Díaz-Llopis, M.; Romero, F.J.; Bosch-Morell, F. *Free Rad. Biol. Med.* 2007, *43*, 1494-1498.

5) Halliwell, B.; Gutteridge, J.M.C. *Free Radicals in Biology and Medicine, 2nd Ed.*, Clarendon Press, Oxford, 1989.

6) Halliwell, B. *Annu. Rev. Nutr.* 1996, *16*, 33-50.

7) Gerschman, R. Gilbert, D.L., Nye, S.W., Dwyer, P., Fenn, W.O. *Science*, 1954, *1119*, 623-626.

8) Behl, C.; Moosmann, B. *Free Rad. Biol. Med*. 2002, *33*, 182-191.

9) Jiménez-Altayó, F.; Caracuel, L.; Pérez-Asensio, F.J.; Martínez-Revelles, S.; Messeguer, A.; Planas, A.M.; Vila, E. *J. Pharmacol. Exp. Ther.* 2009, *331*, 429-436.

10) *Stroke*, or cardiovascular accidents, is the loss of brain function due to a disturbance in the blood supply caused by an ischemia episode.

11) *Hypoxia* is the pathological condition where a region of the body is deprived of and adequate oxygen supply.

12) Amaro, S.; Chamorro, A. *Stroke* 2011, *42*, 1495-1499.

13) Devasagayam, T.P.A.; Boloor, K.K.; Ramasarma, T. *Indian J. Biochem. Biophys.* 2003, *40*, 300-308.

14) Burton, G. W.; Ingold, K.U. *Acc. Chem. Res.* 1986, *19*, 164-201.

15) Montoliu, C.; Sáez, R.; Yenes, S.; Messeguer, A.; Felipo, V. *Biochem. Pharmacol.* 1999, *58*, 255-261.

16) Irurre, J.; Casas, J.; Ramos, I.; Messeguer, A. *Bioorg. Med. Chem.* 1993, *1*, 219-215.

17) Pérez-Asensio, F.J.; de la Rosa, X.; Jiménez-Altayó, F.; Gorina, R.; Martínez, E.; Messeguer, A.; Vila, E.; Chamorro, A.; Planas, A.M. *J. Cerebr. Blood F. Met.* 2009, *30*, 638-652.

18) Sanvicens, N.; Gómez-Vicente, V.; Masip, I.; Messeguer, A.; Cotter, T.G. *J. Biol. Chem.* 2004, *279*, 39268-39278.

19) Bradbury, M.W. *Exp. Physiol.* 1993, *78*, 453-472.

20) Ehrlich, P. *Verlag von August Hischwald* 1885, 1-167.

21) Lewandovsky, M. *Zeitschrift fur klinische Medizin* 1900, *40*, 480-494.

22) a) Goldmann, E.E. *Beiträge Zur Klinischen Chirurgie* 1909, *64*, 192-265. b) Goldmann, E.E. *Beiträge Zur Physio-Pathologie des Plexus Chorioideus und der Hirnhäute*, Verlag de königlichen Akademie der Wissenschaften, 1913, Berlin.

23) Spatz, H. *Archiv. Für Phsychiatrie* 1933, *101*, 267-358.

24) Reese, T.S.; Karnovsky, M.J. *J. Cell Biol.* 1967, *34*, 207-217.

25) Brightman, M.W.; Reese, T.S. *J. Cell Biol.* 1969, *40*, 648-677.

26) Mykko Gynther's Thesis, *Blood-Brain Barrier transporters in CNS Drug Delivery*, 2010, supervised by Proff. Veli-Matti Kosma and Proff. Hannele Turunen, in University of Eastern Finland, Kuopio.

27) Pardridge, W.M. *Fluids Barriers CNS* 2011, *8*, 1-4.

28) Pavan, B.; Dalpiaz, A.; Ciliberti, N.; Biondi, C.; Manfredini, S.; Vertuani, S. *Molecules* 2008, *13*, 1036-1065

29) Pardridge, W.M. *Mol. Biotech.* 2005, *30*, 57-69.

30) Cecchelli, R.; Berezowski, V.; Lundquist, S.; Culot. M.; Renftel, M.; Dehouck, M.-P.; Fenart, L. *Nature* 2007, *6*, 650-661.

31) Abbott, N.J. *J.Anat*. 2000, *200* (6), 629-638.

32) Cecchelli, R.; Dehouck, B.; Descamps, L.; Fenart, L.; Buée-Scherrer, V.; Duhem, C.; Lundquist, S.; Rentfel, M.; Torpier, G.; Dehouck, M.P. *Adv. Drug Deliv. Rev.* 1999, *36*, 165-178.

33) Méresse, S. Dehouck, M.P.; Delorme, P.; Bensaïd, M.; Tauber, J.P.; Delbart, C.; Fruchart, J.C.; Cecchelli, R. *J. Neurochem.* 1989, *55*, 1363-1371.

34) Tilling, T.; Korte, D.; Hoheisel, D.; Galla, H.J. *Brain Res.* 1998, *539*, 247-253.

35) Hynes, R.O. *Cell* 1992, *69*, 11-25.

36) a) Pardridge, W.M. *J. Am. Soc. Exp. NeuroTher.* 2005, *2*, 1-2. b) Pardridge, W.M. *Pharmaceut. Res.* 2007, *24* (9), 1733-1744.

37) Teixidó, M.; Zurita, E.; Malakoutikhah, M.; Tarragó, T.; Giralt, E. *J. Am. Chem. Soc.* 2007, *129*, 11802-11813.

38) Malakoutikhah, M.; Teixidó, M.; Giralt, E. *Angew. Chem. Int. Ed.* 2011, *50*, 7998-8014.

39) Tamai, I.; Tsuji, A. *J. Pharmaceut. Sci.* 2000, *89* (11), 1371-1388.

40) a) Pajouhesh, H.; Lenz, G.R. *NeuroRx.* 2005, *2* (4), 541-553. b) Hitchcock, S.A.; Pennington, L.D. *J. Med. Chem.* 2006, *49* (26), 7559-7583. c) Lipinski, C.A.; Lombardo, F.; Dominy, B.W.; Feeney, P.J. *Adv. Drug Deliv. Rev.* 1997, *23* (1-3), 3-25.

41) Tsuji, A.; Tamai, I. *Adv. Drug. Deliv. Rev.* 1999, *36*, 277-290.

42) Tsuji, A. *J. Am. Soc. Exp. NeuroTher.* 2005, *2*, 54-62.

43) Hawkins, R.A.; O'kane, R.L.; Simpson, I.A.; Viña, J.R. *Am. Soc. Nutr.* 2006, 218S-226S.

44) a) Gynther, M.; Laine, K.; Ropponen, J.; Leppanen, J.; Mannila, A.; Nevalainen, T.; Savolainen, J.; Jarvinen, T.; Raution, J. *J. Med. Chem.* 2008, *51*, 932-936. b) Gynther, M.; Ropponen, J.; Laine, K.; Leppänen, J.; Haapakoski, P.; Peura, L.; Järvinen, T.; Raution, J. *J. Med. Chem.* 2009, *52*, 3348-3353.

45) Mueckler, M.; Makepeace, C. *J. Biol. Chem.* 2008, *283*, 11550-11555.

46) Fernández, C.; Nieto, O.; Rivas, E.; Montenegro, G.; Fontenla, J. A.; Fernández-Mayoralas, A. *Carbohydr. Res.* 2000, *327*, 353-365.

47) a) Occhiutto, M.L.; Freitas, F.R.; Maranhao, R.C.; Costa, V.P. *Pharmaceut.* 2012, *4*, 252-275. b) Kubo, Y.; Shimizu, Y.; Kusagawa, Y.; Akanuma, S.; Hosoya, K. *J. Pharm. Sci.* 2013, *102* (9), 3332-3342.

48) Maeda, A.; Golczak, M.; Chen, Y.; Okano, K.; Kohno, H.; Shiose, S.; Ishikawa, K.; Harte, W.; Palczewska, G.; Maeda, T.; Palczewski, K. *Nat. Chem. Biol.* 2012, *8*, 170-178.

49) Schnaudigel, O. *Graefes Arch. Clin. Exp. Ophthalmol.* 1913, *86*, 93-105.

50) Kubo, Y.; Hosoya, K. *Diabetic Retinopathy, Chapter 5*, book edited by Prof. Mohammad Shamsul Ola, Intech, 2012.

51) Hitchcock, S.A. *J. Med. Chem.* 2012, *55*, 4877-4895.

52) Balimane, P.V.; Han, Y.H.; Chong, S. *Am. Ass. Pharmaceut. Sci. J.* 2006, *8* (1), E1-E13.

53) Deeken, J.F.; Löscher, W. *Clin. Cancer Res.* 2007, *13* (6), 1663-1673.

54) Bradbury, M.W. *Handbook of Experimental Pharmacology*, Vol. 103, Springer-Verlag Berlin Heidelberg, Germany, 1992.

55) Rasheed, A.; Theja, I.; Silparani, G.; Lavanya, Y.; Kumar, C.K.A. *J. Inn. Trends Pharmaceut. Sci.* 2010, *1*(1), 9-18.

56) Van der Waterbeemd, H.; Camenisch, G.; Folkers, G.; Chretien, J.R.; Raevsky, O.A. *J. Drug Target.* 1998, *6*, 151-165.

57) Sun, H.; Kawaguchi, R. *Int. Rev. Cell Mol. Biol.* 2011, *288*, 1-41.

58) Scott, J.W.; Bizarro, F.T.; Parrish, D.R.; Saucy, G. *Helv. Chim. Acta* 1976, *59*, 291-306.

59) Yenes Mínguez, S. *Estudis sobre la preparació, reactivitat i biotransformació d'antioxidants fenòlics estructuralment relacionats amb els tocoferols*, 1999, supervised by Prof. Àngel Messeguer Peypoch.

60) a) Han, S.-Y.; Kim, Y.-A. *Tetrahedron* 2004, *60*, 2447-2467. b) Motalbetti, C.A.G.N.; Falque, V. *Tetrahedron* 2005, *61*, 10827-10852. c) Valeur, E.; Bradley, M. *Chem. Soc. Rev.* 2009, *38*, 606-631. d) Joullié, M.M.; Lassen, K.M. *Arch. Org. Chem.* 2010, *8*, 189-250.

61) a) Hartung, W.H.; Simonoff, R. *Org. React.* 1953, *7*, 263-326. b) Varma, R.S.; Chatterjee, A.K.; Varma, M. *Tetrahedron Lett.* 1993, *34,* 4603-4606. c) Knuchsen, K.R.; Holden, J.; Ley, S.V.; Ladlow, M. *Adv. Synth. Catal.* 2007, *349*, 535-538.

62) Tran, V.H.; Hantharaj, R.; Roufogalis, B.D.-, Duke, C.C. *Eur. J. Org. Chem.* 2006, 2970-2976.

63) Miriyala, B.; Bhattacharyya, S.; Williamson, J.S. *Tetrahedon* 2004, *60*, 1463-1471.

64) a) Khan, S.N.; Bae, S.-Y.; Kim, H.-S. *Tetrahedron Lett.* 2005, *46*, 7675-7678. b) Xu, Y.; Wang, Z.; Tian, Z.-Q.; Li, Y.; Shaw, S.J. *Chem. Med. Chem.* 2006, *1*, 1063-1065. c) Kato, H.; Shibata, I.; Yasaka, Y.; Tsunoi, S.; Yasuda, M.; Baba, A. *Chem. Commun.* 2006, 4189-4192.

65) a) Dangerfield, E.M.; Timmer, M.S.M.; Stocker, B.L. *Org. Lett.* 2009, *11*, 535-538. b) Dangerfield, E.M.; Plunkett, C.H.; Win-Mason, A.L.; Stocker, B.L.; Timmer, M.S.M. *J. Org. Chem*. 2010, *75*, 5470-5471.

66) Lehmann, F.; Scobie, M. *Synthesis* 2008, *11*, 1679-1681.

67) Jacquemard, U.; Bénéteau, V.; Lefoix, M.; Routier, S.; Mérour, J.-Y., Coudert, G. *Tetrahedron*, 2004, *60*, 10039-10047.

68) Tian, W.Q.; Wang, Y.A. *J. Org. Chem.* 2004, *69*, 4299-4308.

69) Lin, F.L.; Hoyt, H.M.; Van Halbeek, H.; Bergman, R.G.; Bertozzi, C.R. *J. Am. Chem. Soc.* 2005, *127*, 2686-2695

70) El-Nezhawy, A.; Adly, F.G.; Eweas, A.F.; Hanna, A.G.; El-Kholy, Y.M.; El-Sayed, S.H.; El-Naggar, T.B.A. *Archiv. Pharm. Chem. Life Sci.* 2011, *344*, 648-646.

71) a) Duthaler, R.O. *Tetrahedron* 1994, *50*, 1539-1650. b) Vincent, S.P.; Schleyer, A.; Wong, Ch.-H. *J. Org. Chem.* 2000, *65*, 4440-4443. c) Yadov, J.S.; Reddy, B.V.S.; Eeshwaraiah, B.; Srinivas, M. *Tetrahedron* 2004, *60*, 1767-1771. d) Cativiela, C.; Díaz-de-Villegas, M.D *Tetrahedron Asymmtr.* 2007, *18*, 569-623. e) Kuethe, J.T.; Gauthier, D.R., Jr.; Beutner, G.L. *J. Org. Chem.* 2007, *72*, 7469-7472. f) Pérez-Fuentes, Y.; Taylos, J.E.; Tickell, D.A.; Mahon, M.F.; Bull, S.D.; James, T.D. *J. Org. Chem.* 2011, *76*, 6038-6047.

72) a) Fadel, A.; Vandromme, L. *Tetrahedron Asymmetr.* 1999, *10*, 1153-1162. b) Arzel, P.; Freida, V.; weber, P.; Fadel, A. *Tetrahedron Asymmetr.* 1999, *10*, 3877-3881.

73) He, Q.; Peng, Y.-F.; Rohani, S. *Chirality* 2010, *22*, 16-23.

74) Rodríguez-Docampo, Z.; Quigley, C.; Tallon, S.; Connon, S.J. *J. Org. Chem.* 2012, *77*, 2407-2414

75) Molyneux, P. *Songklanakarin J. Sci. Tech.*, 2004, *26*, 211-219.

76) Sánchez-Moreno, C. *Food Scientif. Technol. Int.,* 2002, *8*, 121-137.

77) Re, R.; Pellegrini, N.; Proteggente, A.; Pannala, A.; Yang, M.; Rice-Evans, C. *Free Rad. Biol. Med.* 1999, *26*, 1231-1237.

78) Aruoma, O. I. *Mut. Res.* 2003, *523-524*, 9-20.

79) a) Blois, M.S. *Nature*, 1958, *181*, 1199-1200. b) Brand-Williams, W.; Cuvelier, M.E.; Berset, C. *Lebensm.-Wiss. u.-Technol.* 1995, *28*, 25-30.

80) Prior, R.L.; Cao, G. *Free rad. Biol. Med.* 1999, *27*, 1173-1181.

81) Kulisic, T.; Radonic, A.; Katalinic, V.; Milos, M. *Food Chem.* 2004, *85*, 633-640.

82) Liu, R.H.; Finley, J. *J. Agric. Food Chem.* 2005, *53*, 4311-4314.

83) Buenger, J.; Ackermann, H.; Jentzsch, A.; Mehling, A.; Pfitzner, I.; Reiffen, K.-A.; Scheroeder, K.-R.; Wollenweber, U. *Int. J. Cosm. Sci.*, 2006, *28*, 135-146.

84) Magalhães, L.M.; Segundo, M.A.; Reis, S. Lima, J.L.F.C. *Anal. Chim. Acta* 2006, *558*, 310-318.

85) a) Contreras-Guzmán, E.S.; Strong, F.C. *J. Ass. Off. Anal. Chem.* 1982, *65*, 1215-1222. b) Kedare, S.B.; Singh, R.P. *J. Food Sci. Technol.* 2011, *48*, 412-422.

86) a) Yu, L.L. *J. Agric. Food Chem.* 2001, *49,* 3452-3456. b)Parry, J.; Su, L.; Luther, M.; Zhou, K.Q.; Yuraweez, M.P.; Wittaker, P.; Yu, L.L. *J. Agric. Food Chem.* 2005, *53*, 566-573.

87) Prior, R.L.; Wu, X.; Schaich, K. *J. Agric. Food Chem.* 2005, *53*, 4290-4302.

88) Masahiro, N.; Masahiro, K.; Minemitsur, N.; Akio, K.; Yoshimi, N. *Chem. Pharm. Bull*. 2005, *53*, 714-716.

89) Pakrash, A. *Med. Lab. Anal. Prog.* 2001, *19*, 1-6.

90) rIC_{50} represents the relative predicted x-value for $\hat{y}$ = 50 into the adjusted regression line expressed in mol of antioxidant/mol of DPPH·.

91) $\hat{y}$-value corresponds to y-value from the estimated regression line for an specific x-value.

92) Khanduja, K.L.; Bhardwaj, A. *Indian J. Biochem. Biophys.* 2003, *40*, 416-422.

93) *GraphPad Prism Software. Inc, 5.0*; San Diego, CA 92121, 2007.

94) The $logIC_{50}$ from GraphPad Prism 5 calculation corresponds to the inflexion point of the nonlinear sigmoidal fitted curve from the given results. The results were expressed in terms of $logIC_{50}$ due to the symmetric character of the value compared to IC_{50} and because the x-value was expressed in log[antioxidant]. Ultimately, to understand better all these results, they were transformed to IC_{50}.

95) IC_{50} is the half maximal inhibitory concentration in terms of µM.

96) Ratkowsky, D. A. *Handbook of nonlinear regression models*. Dekker: New York, 1990.

97) Motulsky, H.J. *Prism 5 Statistics Guide*, GraphPad Software Inc., San Diego CA, 2007. www.graphpad.com.

98) Gosset, W. S. *"Student's" Collected Papers*. London: Biometrika Office, University College, 1943.

99) StataCorp. Stata: Release 12. Statistical Software. College Station, TX: StataCorp LP, 2011.

100) Kuehl, R. O. *Design of Experiments: Statistical Principles of Research Design and Analysis.* 2nd ed. Belmont, CA: Duxbury, 2000.

101) Coster, D. *Contrast*, *Encyclopedia of Biostatistics*, ed. P. Armitage and T. Colton, 2, 1153-1157. Chichester, UK: Wiley, 2005.

102) Liu, R.H.; Finley, J. *J. Agric. Food Chem.* **2005**, *53*, 4311-4314.

103) Frankel, E.N.; Meyer, A.S. *J. Sci. Food Agric.* **2000**, *80*, 1925-1941.

104) Liu, R.H. *J. Nutr.* **2004**, *134*, 3479S-3485S.

105) Wolfe, K.L.; Liu, R.H. *J. Agric. Food Chem.* **2007**, *55*, 8896-8907.

106) Andreae, W.A. *Nature,* **1952**, *170*, 83-84.

107) Keston, A.S.; Brandt, R. *Anal. Biochem.* **1965**, *11*, 1-5.

108) Wang, H.; Joseph, J.A. *Free Rad. Biol. Med.* **1999**, *27*, 612-616.

109) Sofi, M.S.; Sateesh, M.K.; Bashir, M.; Harish, G.; Lakshmeedha, T.R.; Vedashree, S.; Vedamurthy, A.B. *Cytotechnol.* **2013**, *65*, 407-417.

110) Ling, L.-U.; Tan, K.-B.; Chiu, G.N.C. *Cell Death Dis.* **2011**, *2*, 1-12.

111) Ghose, A. K.; Herberts, T.; Hudkins, R.L.; Dorsey, B.D.; Mallamo, J.P. *ACS Chem. Neurosci.* **2012**, *3* (1), 50-68.

112) Lowe, J.T.; Lee IV, M.D.; Akella, L.B.; Davoine, E.; Donckele, E.J.; Durak, L.; Duvall, J.R.; Gerard, B.; Holson, E.B.; Joliton, A.; Kesavan, S.; Lemercier, B.C.; Liu, H.; Marié, J.-C.; Mulrooney, C.; Muncipinto, G.; Welzel-O'Shea, M.; Panko, L.M.; Rowley, A.; Suh, B.-C.; Thomas, M.; Wagner, F.F.; Wei, J.; Foley, M.A.; Marcaurelle, L.A. *J. Org. Chem.* **2010**, *77*, 7187-7211.

113) a) Overton, E. *Z. Phys. Chem.* **1897**, *22*, 198-209. b) Meyer, H. *Arch. Exp. Pathol. Pharmakol.* **1899**, *42*, 109-118.

114) Hansch, C.; Björkroth, J.P.; Leo, A. *J. Pharm. Sci.* **1987**, *76*, 663-687.

115) Lipinski, C.A. *Drug Discovery Today: Technol.* **2004**, *1*, 337-341.

116) Van de Waterbeemd, H.; Camenisch, G.; Folkers, G.; Chretien, J.R.; Raevsky, O.A. *J. Drug Targeting*, **1998**, *6*, 151-165.

117) Mahar Doan, K.M.; Humphreys, J.E.; Webster, L.O.; Wring, S.A.; Shampine, L.J.; Serabjit-Singh, C.J.; Adkinson, K.K.; Polli, J.W. *J. Pharmacol. Exp. Ther.* **2002**, *303*, 1029-1037.

118) Manallack, D.T. *Perspect. Med. Chem.* **2007**, *1*, 25-38.

119) Hughes, J.D.; Blagg, J.; Price, D.A.; Bailey, S.; DeCrescenzo, G.A.; Devraj, R.V.; Ellsworth, E.; Fobian, Y.M.; Gibbs, M.E.; Gilles, R.W.; Greene, N.; Huang, E.; Krieger-Burke, T.; Loesel, J.; Wager, T.; Whiteley, L.; Zhang, Y. *Bioorg. Med. Chem. Lett.* 2008, *18*, 4872-4875.

120) Wager, T.T.; Hou, X.; Verhoest, P.R.; Villalobos, A. *ACS Chem. Neurosci.* 2010, *1*, 435-449.

121) Wager, T.T., Chandrasekaran, R.Y.; Hou, X.; Troutman, M.D.; Verhoest, P.R., Villalobos, A.; Will, Y. *ACS Chem. Neurosci.* 2010, *1*, 420-434.

122) Harrington, E. C., Jr. *Ind. Qual. Control*, 1965, *21*, 494-498.

123) Erlt, P.; Rohde, B.; Selzer, P. *J. Med. Chem.* 2000, *43*, 3714-3717

124) Himanshu, R.; Jakir, P.; Pradnya, H.; Suneel, P.; Rahul, S. *J. Drug Delivery Therapeut.* 2013, *3* (3), 20-29.

125) Balimane, P.V.; Chong, S. *Drug Dicov. Today.* 2005, *10* (5), 335-343.

126) Balimane, P.V.; Patel, K.; Marino, A.; Chong, S. *Eur. J. Pharmaceut. Biopharmaceut.* 2004, *58*, 99-105.

127) Behrens, I.; Kissel. T. *Eur. J. Pharmaceut. Sci.* 2003, *19*, 433-442.

128) Bohets, H.; Annaert, P.; Mannens, G.; Van Beijsterveldt, L.; Anciaux, K.; Verboven, P.; Meuldermans, W.; Lavrijsen, K. *Curr. Top. Med. Chem.* 2001, *1* (5), 367-383.

129) a) Pade, V.; Stavchansky, S. *J. Pharm. Sci.* 1998, *87* (12), 1604-1607. b) Thomas, S.; Brightman, F.; Gill, H.; Lee, S.; Pufong, B. *J. Pharm. Sci.* 2008, *97* (10), 4557-4574.

130) Cummins, C.L.; Mangravite, L.M.; Benet, L.Z. *Pharm. Res.* 2001, *18* (8), 1102-1109.

131) Lundquist, S.; Renftel, M.; Brillault, J.; Fenart, L.; Cecchelli, R.; Dehouck, M.P. *Pharm. Res.* 2002, *19* (7), 976-

132) Complete medium is composed by Dubelco's Modified Eagle's Medium DMEM, high glucose with L-glutamine supplemented with 10% of Fetal Calf/Bovine Serum, 1% non-essential amino acids and 1% of penicillin and streptomycin solution

133) *%Recovery* = [Final acceptor compartment amount (nmol)/Initial donor compartment amount(nmol)]·100

134) Kerns, E.H.; Di, L.; Petusky, S.; Farris, M.; Ley, R.; Jupp, P. *J. Pharm. Sci.* 2004, *93* (6), 1440-1453.

135) Sevin, E.; Dehouck, L.; Fabulas-da Costa, A.; Cecchelli, R.; Dehouck, M.P.; Lundquist, S.; Culot, M. *J. Pharmacol. Toxicol. Methods*, **2013**, *68*, 334-339.

136) Kansy, M.; Senner, F., Gubernator, K. *J. Med. Chem.* **1998**, *41*, 1007-1010.

137) Avdeef, A. *Eur. J. Pharm. Sci.* **2001**, *14*, 271-280.

138) Di, L.; Kerns, E.H.; Fan, K.; McConnell, O.J.; Carter, G.T. *Eur. J. Med. Chem.* **2003**, *38*, 223-232.

139) Kansy, M.; Avdeef, A.; Fischer, H. *Drug Discovery Today Tec.* **2004**, *1* (4), 349-355.

140) Dubelco's modified Eagle's medium supplemented with 15% calf serum, 2 mM glutamine, 50 µg/mL gentamycin, 2.5 µg/mL amphotericib B and 1 ng/mL basic fibroblast growth factor every other day

141) Tatsuta, T.; Naito, M.; Mikami, K.; Tsuoro, T. *Cell Growth Differ.* **1994**, *5*, 1145-1152.

142) Siflinger-Birnboim, A.; Del Becchio, P.J.; Cooper, J.A.; Blumenstock, F.A.; Shepart, J.N.; Malik, A.B. *J. Cell. Physiol.* **1987**, *132*, 111-117.

143) Mosmann, T. *J. Immunol. Methods* **1983**, *65*, 55-63.

144) van de Loosdrecht, A.A.; Beelen, R.H.J.; Ossenkoppele, G.J.; Broekhoven, M.G.; Langenhuijsen, M.M.A.C. *J. Immunol. Methods* **1994**, *174*, 311-320

145) Stewart, W.W. *Cell* **1978**, *14*, 741-759.

146) El-Nezhawy, A.O.; Adly, F.G.; Eweas, A.F.; Hanna, A.G.; El-Kholy, Y.M.; El-Sayed, S.H.; El-Naggar, T.B. *Arch. Pharm. (Weinhein),* **2011**, *344*, 648-657.

147) Booher, J.; Sensenbrenner, M. *Neurobiol.* **1972**, *2*, 97-105.

148) Bornstein, M.B.; Murray, M.R. *J.Biophys. Biochem. Cytol.* **1958**, *4*, 499-504.

149) Méresse, S.; Dehouck, M.P.; Delorme, P.; Bensaïd, M.; Tauber, J.P.; Delbart, C.; Fruchart, J.-C.; Cecchelli, R. *J. Neurochem*. **1989**, *4*, 1363-1371

150) Casas, J.; Gorchs, G.; Sánchez-Baeza, F.; Teixidó, P.; Messeguer, A. *J. Agric. Food. Chem.* **1992**, 40, 585-590.

APPENDIX III. Supporting information

This Doctoral Thesis also contains supporting information in a CD format. The following material is included:

- Characterization spectres of ^{1}H-NMR, ^{13}C-NMR, HSQC and HRMS for compounds **A**-**N** and all intermediates of synthetic pathway.

- The physicochemical properties values (pK_a, MW, HBD, TPSA, cLogP and cLogD) for compounds **A**-**N**, CR-6 and Trolox.

- The calculation of TPSA for compounds **A**-**N**, CR-6 and Trolox, following the protocol of Ertl *et al.*[123]